ACTIVATION, DESENSITIZATION AND POTENTIATION OF ALPHA7 NICOTINIC ACETYLCHOLINE RECEPTORS: RELEVANCE TO ALPHA7-TARGETED THERAPEUTICS

By

DUSTIN KYLE WILLIAMS

A DISSERTATION PRESENTED TO THE GRADUATE SCHOOL
OF THE UNIVERSITY OF FLORIDA IN PARTIAL FULFILLMENT
OF THE REQUIREMENTS FOR THE DEGREE OF
DOCTOR OF PHILOSOPHY

UNIVERSITY OF FLORIDA

2012

To the most important people in my life: my family

ACKNOWLEDGMENTS

I would like to thank my wife, Julie Williams, and my parents, Kevin and Kathy Williams for their unconditional love and flawless support through the graduate school experience, even when I have had to place work before them.

I would like to thank Dr. Roger Papke for his mentorship over the last five years. I have had more success under his arm than I ever could have expected when I started graduate school. In addition, I am thankful for the many collaborative meetings I participated in with Dr. Nicole Horenstein and Dr. Jingyi Wang. I would like to thank Mathew Kimbrell for his fine work in helping to create the stably transfected cell lines, and for the interactions I have had with all members of the Papke laboratory. I wish to express gratitude to the members of my advisory committee, Dr. Nicole Horenstein, Dr. Brian Cooper, Dr. Michael King, and Dr. Brian Law, for their counsel and guidance.

I am thankful for the financial support I have received from the National Institute on Aging Training Grant T32-AG000196.

TABLE OF CONTENTS

Page

LIST OF TABLES

LIST OF FIGURES

LIST OF ABBREVIATIONS

4OH-GTS-21	3-(4-hydroxy,2-methoxybenzylidene)anabaseine
5-HI	5-hydroxyindole
A-867744	4-(5-(4-chlorophenyl)-2-methyl- 3-propionyl-1*H*-pyrrol-1-yl) benzenesulfonamide
AChBP	acetylcholine binding protein
ACh	acetylcholine
AR-R17779	(-)-Spiro[1-azabicyclo(2.2.2)octane-3,5-oxazolidin-2-one]
BSA	bovine serum albumin
CCMI	N-(4-chlorophenyl)-alpha-[[(4-chloro-phenyl)amino]methylene]-3-methyl-5-isoxazoleacet-amide
D_i	PNU-120596-insensitive desensitization
DMEM	Dulbecco's modified eagle medium
DPBS	Dulbecco's phosphate buffered saline
D_s	PNU-120596-sensitive desensitization
ERK1/2	extracellular signal-related kinase-1 and -2
FBS	fetal bovine serum
GTS-21	3-(2,4-dimethoxybenzylidene)-anabaseine
HBSS	Hank's balanced saline solution
HEK293	human embryonic kidney 293 cell line
I_{max}	maximal current
JNJ-1930942	2-[[4-fluoro-3-(trifluoromethyl)phenyl]amino]-4-(4-pyridinyl)-5-thiazolemethanol
LBD	ligand binding domain
LY-2087101	[2-[(4-Fluorophenyl)amino]-4-methyl -5-thiazolyl]-3-thienylmethanone

MLA	methyllycaconitine
MTSEA	2-aminoethyl methanethiosulfonate
MTSET	[2-(trimethylammonium)ethyl] methanethiosulfonate
N	number of ion channels in a patch
nAChR	nicotinic acetylcholine receptor
NP_{open}	Absolute probability of channel opening
NS-1738	1-(5-chloro-2-hydroxy-phenyl)-3-(2-chloro-5-trifluoromethyl-phenyl)-urea
O*	isolated, short-lived channel opening
O'	relatively long-lived channel opening that primarily occurs in groups or "bursts"
PAM	positive allosteric modulator
PNU-120596	1-(5-chloro-2,4-dimethoxy-phenyl)-3-(5-methyl-isoxazol-3-yl)-urea
PNU-282987	*N*-(3*R*)-1-Azabicyclo[2.2.2]oct-3-yl-4-chlorobenzamide
P_{open}	probability of channel opening
RT-PCR	reverse-transcriptase polymerase chain reaction
SB-206553	3,5-dihydro-5-methyl-N-3-pyridinylbenzo[1,2-b:4,5-b']di pyrrole-1(2H)-carboxamide
SEM	standard error of the mean
t_{crit}	critical duration; burst delimiter value
TQS	3a,4,5,9b-Tetrahydro-4-(1-naphthalenyl)-3*H*-cyclopentan[*c*]quinoline-8-sulfonamide

Abstract of Dissertation Presented to the Graduate School
of the University of Florida in Partial Fulfillment of the
Requirements for the Degree of Doctor of Philosophy

ACTIVATION, DESENSITIZATION AND POTENTIATION OF ALPHA7 NICOTINIC ACETYLCHOLINE RECEPTORS: RELEVANCE TO ALPHA7-TARGETED THERAPEUTICS

By

Dustin Kyle Williams

May 2012

Chair: Roger L. Papke
Major: Medical Sciences

Neuronal nicotinic acetylcholine receptors (nAChRs) are recognized therapeutic targets for cognitive and neurodegenerative disorders. While activation of the ion channel is primarily controlled by the agonist binding sites, it can also be regulated in positive or negative ways by the binding of ligands to other modulatory sites. The functional significance of two highly conserved tryptophan residues located in agonist binding sites are investigated in homomeric α7 and heteromeric α4β2 receptors. The data suggest that tryptophan 149 is critical for activation by diverse agonists, but the tryptophan at position 55 may be important for regulating the ability of benzylidene anabaseine compounds to selectively activate the α7 receptor. A method of conditionally eliminating agonist binding sites is used to investigate the functional significance of multiple binding sites in heteromeric muscle-type and α7 receptors. The results suggest that nAChRs are capable of being effectively activated under conditions of submaximal agonist occupancy. Characterization of the α7 positive allosteric modulator PNU-120596 reveals the existence of two distinct α7 desensitized states that are distinguished by their stability in the presence of PNU-120596. Desensitized states

that are stable in the presence of PNU-120596 are induced by conditions promoting strong ion channel activation and influenced by both agonist and modulator concentrations. Outside-out patch clamp recordings illustrate that PNU-120596 has a profound effect on currents from individual α7 channels. A novel cell line was developed that stably expresses functional human α7 receptors. This cell line was used to investigate the *in vitro* cytotoxicity profile of PNU-120596. In addition, the cell line was used to evaluate the temperature dependence of PNU-120596 potentiating activity that was recently reported. The findings suggest that PNU-120596 can produce concentration-dependent cytotoxic effects and confirm that PNU-120596 potentiation is reduced at physiological temperatures. However, some endogenous factors, such as serum albumins, may partially preserve the ability of PNU-120596 to potentiate α7-mediated responses at 37°C. The work presented in this dissertation will hopefully aid the rational design of therapeutics targeted to the α7 nAChR.

CHAPTER 1
ANIMAL ELECTRICITY: HISTORICAL INTRODUCTION

For many centuries the prevailing theories of neurotransmission had no concept of electricity. “Animal spirits”, an immeasurable force thought to be the source of animation, imagination, reason, and memory, was believed to be contained within the fluid stored in the ventricles and distributed throughout the body via the nerves which acted as conduits of this vital fluid [1, 2]. This fundamental hypothesis was upheld and propagated for more than 1,500 years by many well-known and influential philosophers, physicians, and scientists including Aristotle, Galen, Descartes, Borelli, and Fontanta, each contributing unique variations to the basic idea [2-4]. It was not until the late 18th century that Luigi Galvani discovered electricity as the currency of the nervous system, and even then this important discovery was not readily accepted. Understanding bioelectricity as we do today was truly a multi-national effort that took place over hundreds of years.

Pre-Galvani to Hodgkin & Huxley

By the 1660s, Jan Swammerdam (The Netherlands; 1637-1680) had shown that muscles could contract without any physical connection to the brain, providing perhaps the first evidence against the fallacious animal spirits hypothesis [4]. He devised an isolated nerve-muscle preparation from the frog and showed that mechanical stimulation of the nerve resulted in muscle contraction. His experiments also showed that muscles did not increase in volume (ie by an influx of “animal spirits”) during contraction [3, 4]. He concluded that, “A simple and natural motion or irritation of the nerve alone is necessary to produce muscular motion, whether it has its origin in the brain, or in the marrow, or elsewhere” [5]. However, Swammerdam’s work was unable

to convince the scientific community at large that nervous system function occurred by a mechanism other than animal spirits [4]. In the mid 1700s, Albrecht von Haller (Switzerland; 1708-1777) promoted his “doctrine of irritability”, which was influenced by the work of Swammerdam and Francis Glisson (England; 1599-1677), suggesting that external forces or irritations elicit responses from tissues that are dependent on the tissue’s internal organization [4, 6, 7]. Aware of von Haller’s concept of irritability, Luigi Galvani (Italy; 1737-1798) and his assistants made an observation of profound scientific importance that set into motion the events that changed the definition of “animal spirits” to a physically understandable and measurable force underlying the function of the nervous system. While some claim that Luigi Galvani made his discovery by chance [4], it seems that Galvani sought to test the specific hypothesis that electricity was a source of “irritation” that could evoke muscle contraction based on his experimental set-up and preparation at the time his discovery was made [6, 7]. In Galvani’s time, electricity was still poorly understood, often thought of as a mystical force and often the subject of amusement and speculation. It was well known that frictional or static electricity could be produced by rubbing amber, glass, or rubber. Electrostatic generators, which operate on this principle, had been invented prior to Galvani’s birth in 1737 [3, 8]. In 1746, Pieter van Musschenbroek (The Netherlands; 1692-1761) developed a method for storing electricity produced with electrostatic generators, which could later be used at will, in a type of capacitor known as a Leyden jar [3]. With these two inventions and his own version of Swammerdam’s frog nerve-muscle preparation consisting of the frog’s hind limbs and exposed crural nerves [5, 7], the discovery was made in 1781 when one of Galvani’s assistants, probably either his wife Lucia Galeazzi

Galvani or nephew Giovanni Aldini, touched the exposed nerve with a surgical instrument at the same time that a nearby frictional electricity generator sparked; the nerves had been stimulated by electrostatic induction and the muscles contracted as if the frog legs were alive [7]. Throughout 10 years of experimentation Galvani performed numerous experiments in which he noted a non-linear relationship between stimulus intensity of force of muscle contraction, a refractory period, and muscle contractions evoked by atmospheric electricity. Galvani came to the conclusion that electricity is intrinsic to animal tissue, hypothesizing that a state of electrical disequilibrium exists in muscle and that muscle stores this energy in a way comparable to a Leyden jar [1, 5-7]. Galvani's ideas pre-dated any understanding or demonstration of ions, membranes, and ion channels, but laid the foundation for their discovery.

Galvani's findings quickly became well known throughout Europe; however, they were not immediately accepted and even faced considerable adversity from the physicist Alessandro Volta (Italy; 1745-1827). Volta realized that small currents are produced when two different metals come in contact and this observation led him to question the concept of "animal electricity" based on a small sampling of Galvani's experiments: those in which muscle contractions were observed only if a metallic arc connecting the nerve and muscle was bimetallic and others in which contractions occurred when the preparation was hung on brass hooks, which were suspended from iron gratings, in the absence of atmospheric electricity or other external stimulation. Volta argued that electricity was not produced or stored in animal tissue, but rather that the muscle merely acted as a sensitive detector of electricity produced unknowingly through contact of dissimilar conductors [1, 6]. Although Volta correctly realized that

contact of dissimilar metals could produce an external stimulus sufficient to evoke muscle contraction, he failed to acknowledge Galvani's demonstrations that muscle contractions occur in the complete absence of conducting metals. He also failed to acknowledge the independent confirmation and extension of Galvani's findings to birds, mammals, and reptiles by Alexander von Humboldt (Germany; 1769-1859) [8, 9]. In 1800, Volta's argument became widely accepted when he invented the first battery, the voltaic pile, which was essentially a stack of alternating copper, and zinc discs separated by saline-soaked paper [1]. The voltaic pile was capable of generating a sustained direct current for the first time and when connected to the nerves of a frog leg preparation could evoke muscle contraction. In contrast to Volta, who received great honor and respect for his finding, Galvani lost his position at the University of Bologna and Academy of Sciences when he refused to make an oath of allegiance to Napoleon in the late 1790s just prior to his death [7]. Though not widely accepted scientifically, Galvanism had an important cultural impact throughout much of Europe. The public demonstrations by Giovanni Aldini in which he applied electricity to the brains of recently executed criminals, suggested to many that electricity could revive the dead. In addition, Galvani's discovery provided the inspiration for Mary Shelly's novel "Frankenstein" [7, 10].

At the time, Volta succeeded in convincing the majority of the scientific world that he was correct, however, his very discovery initiated the physical studies of electricity that led to improved equipment and an acceptance of bioelectricity during the next 50 years. In 1820, Hans Oersted (Denmark; 1777-1851) discovered that current moving through a wire deflected the needle of a magnetic compass. The phenomenon of

electromagnetism was soon applied with the invention of the first ammeter, later known as the galvanometer in honor of Galvani, that same year by Johann Schweigger (Germany; 1779-1857)[10]. Leopoldo Nobili (Italy; 1784-1835) created the astatic galvanometer, a refinement of Schweigger's galvanometer, which effectively cancels the Earth's magnetic field allowing for greater instrument sensitivity [10]. Nobili was the first to measure current flow through Galvani's frog preparation in 1828 with his instrument, but he seemed more interested in developing the sensitivity of his galvanometer than in studying the "intrinsic frog current", which he attributed to a thermoelectric effect [7, 10]. In the late 1830s and early 1840s, Carlo Matteucci (Italy; 1811-1868) made several important observations that helped establish the validity of bioelectricity. Matteucci discovered that "injury currents" flow, and could be measured with a Nobili galvanometer, between intact and cut surfaces of denervated muscle. He then stacked several muscles on top of each other, with the injured surface of one muscle in contact with the intact surface of another, and showed that the measured currents were proportional to the number of muscles or elements in series, similar to the voltaic pile [1, 10]. In addition, Matteucci demonstrated that current stops flowing between injured and intact surfaces of muscle upon strychnine-induced tetanus, providing perhaps the first electrophysiological evidence that pharmacological treatment with biologically active compounds manipulates measurable bioelectricity. Further, Matteucci discovered the phenomenon of "induced twitch", in which the contraction of one muscle produces an electrical discharge that is sufficient to induce contraction of another muscle when the only contact between the two muscles is a sciatic nerve [7].

Emil du Bois-Reymond (Germany; 1818-1896) became interested in electrophysiology during the early 1840s as a graduate student after learning about Matteuci's work [1, 10]. Du Bois-Reymond initiated his studies by constructing a very sensitive astatic galvanometer consisting of about one kilometer and thousands of turns of wire [9, 10]. He first used his galvanometer to confirm Matteuci's finding that current flows between intact and injured muscle surfaces and, in addition, extended the finding to nerve [3]. Using his galvanometer to measure currents through a known resistance he used Ohm's law, which was established in 1827 by Georg Ohm (Germany; 1789-1854), to determine that wounded surfaces always had an electrically negative potential relative to uninjured surfaces [7]. Du Bois-Reymond discovered that when electrical stimulation was applied to the positive surface of nerve and muscle, the electrical potential between the injured and uninjured surfaces at that point is reduced, and that the potential of the outer membrane surface actually became negative relative to a distant uninjured surface. He called this reduction in electrical potential "negative variation" and in the mid-late 1840s discovered that the point of reduced potential actually travels along the surface as a wave of "relative negativity", although his instrumentation lacked sufficient time resolution to measure the velocity of the impulse [1, 7, 11]. Nonetheless, Emil du Bois-Reymond was the first to observe and document what would become known as the action potential [1, 7, 10]. Based on his belief that current flowed between the uninjured surface of a muscle and its tendon during muscle contraction not unlike the flow of current observed between injured and intact muscle surfaces [10], du Bois-Reymond formulated one of the earliest hypothesies including polarization, resting electrical potentials, their discharge during activation, and

“electromotive particles” [10] as factors underlying the conduction of bioelectric signals [7]. Although many of the specific details of his hypothesis turned out to be incorrect, his ideas were important as they suggested perhaps the first physical mechanism based on experimental observations, explaining what had been referred to simply as “animal spirits” for hundreds of years.

Although the nerve impulse was beginning to be understood in physical terms, the velocity of bioelectric signal propagation was widely believed to be immeasurable [3]. Hermann von Helmholtz (Germany; 1821-1894) created an apparatus that was capable of measuring the duration between stimulation of a point on a nerve and the resulting muscle contraction. In 1849 he compared the latency of muscle contraction with stimulation at various points along the nerve and determined the impulse velocity in frog nerves to be approximately 27 meters/second, a speed that seemed unexpectedly slow for a purely electrical event [5, 12]. This observation led some to doubt the electrical nature of the nerve impulse, with some suggestions that it was fundamentally a chemical event with outward electrical manifestations, while others viewed the result as consistent with du Bois-Reymond’s hypothesis that nerve conduction of electrical signals involved rearrangements of charged molecules that were more complex than simple passive current flow in a wire [7].

Du Bois-Reymond passed the challenge of measuring the velocity of the “negative variation” to his student Julius Bernstein (Germany; 1839-1917). In 1868, Bernstein succeeded in not only measuring the velocity of the nerve impulse, but also in measuring its time course and in providing its first graphical demonstration using his differential rheotome [1, 11]. Importantly, he showed that the propagation velocity of the

“negative variation” observed by du Bois-Reymond closely matched the speed of the nerve impulse measured by von Helmholtz, reestablishing confidence in the idea that electrical activity underlies nerve activity. Bernstein realized that a reduction in electrical potential between injured and intact nerve surfaces was comparable to that of a propagating nerve signal, or that excitability was associated with a decline in the electrical potential driving currents. Based on this fundamental observation, he hypothesized that the membrane is electrically polarized at rest, with the inside negative relative to the outside, and that the action potential is a self-propagating loss of this polarization. In 1902, Julius Bernstein formulated his “membrane theory” in which he was the first to apply Walther Nernst’s (Germany; 1864-1941) theory of ion diffusion and electric potentials (1889) to biological membranes, correctly suggesting that the origin of membrane polarization was due to a higher concentration of potassium ions inside the cell than outside and a selective resting membrane permeability of potassium. He suggested that a temporary reduction in membrane resistance for all ions occurred during nerve and muscle excitation, during which time ions flowed down their electrochemical gradients leading to a depolarization of the resting membrane potential [7]. During this time, the composition of the cellular membrane was unknown, but as early as 1899 Charles Overton (England; 1865-1933) proposed the concept of a lipid membrane based on his observation that lipid soluble dyes penetrate cells more readily than water-soluble dyes [13, 14]. By 1925, the plasma membrane was proposed to be composed of a lipid bilayer by Evert Gorter (The Netherlands; 1881-1954) and Francois Grendel [5, 15].

Henry Bowditch (USA; 1840-1911), working with Carl Ludwig in Germany, determined that the action potential of frog heart was an all-or-nothing phenomenon in 1871 since contractile response occurred only after a stimulus above threshold intensity, but remained constant even as stimulus intensity increased [7]. However, this phenomenon did not appear to apply to striated muscle since contraction intensity increased proportionately to stimulus intensity regardless of stimulus application through the motor nerve or directly on the muscle. In 1902, Francis Gotch (England; 1853-1913) hypothesized this graded response by striated muscle was due to an increased number of excited fibers rather than an increased response amplitude of individual fibers. Shortly after, Keith Lucas (England; 1879-1916) showed that individual fibers of striated muscle follows the same all-or-nothing phenomenon as cardiac muscle by carefully dissecting the frog dorsal cutaneous muscle of the frog to fewer than 20 active fibers and showing that increased stimulation intensities produced contraction in discrete steps [7]. Edgar Adrian (England; 1889-1977), a former student of Keith Lucas, made the first electrical recordings of individual nerve fibers in 1926 after meticulous dissection [16, 17]. He showed that a stretched muscle sends sensory information through the nerve. He observed that when the load on the muscle was increased only the frequency of action potentials increased while the amplitude, duration, and velocity of each pulse remained constant. Adrian's experiments provided the first direct evidence of the all-or-nothing character of the action potential in nerves [7, 17]. In the early 1920s, Joseph Erlanger (USA; 1874-1965) and Herbert Gasser (USA; 1888-1963) were the first to feed the output of electrical amplifiers into a cathode ray tube oscilloscope in electrophysiological experiments, allowing for the precise display of high

frequency signals in real-time [16, 18]. Recording from peripheral nerves in various animals, Erlanger and Gasser discovered that the shape of the action potential changed as the recording electrode was moved away from the stimulation electrode in a manner that was dependent on axon diameter, with decreased electrical resistance as diameters increased. They discovered that action potentials travel at different speeds; signals in relatively thick motor nerves were conducted much faster than signals in thinner pain nerves.

In 1937, Alan Hodgkin (England; 1914-1998), attempting to measure the decrease in membrane resistance during the action potential that was predicted by Bernstein's membrane theory, instead made the first measurements showing the passive spread of a local electrical response along the nerve fiber- resulting in increased excitability [12, 19]. This finding was consistent with the local circuit theory proposed by Ludimar Hermann (Germany, 1838-1914) in the 1870s [7]. Hodgkin's experiments also showed that conduction velocity of the nerve impulse was dependent on the conductivity of the extracellular solution.

John Zachary Young (England; 1907-1997) discovered the usefulness of giant squid axons in electrophysiology in 1938 [20] and just one year later, Kenneth Cole (USA; 1900-1984) and Howard Curtis used squid axons to experimentally confirm the prediction by Bernstein that a decrease in membrane resistance occurs during the action potential, by making extracellular impedance measurements of a high-frequency sine wave applied during the action potential [5, 21]. Both Hodgkin and Andrew Huxley (England; 1917-present) and Curtis and Cole independently inserted electrodes inside the giant axon and succeeded in directly measuring the transmembrane potential in the

resting state; the interior of the axon was about 50 mV more negative than the electrical potential on the exterior. The existence of the resting membrane polarization hypothesized by Bernstein was confirmed in these studies, however only part of Bernstein's theory was supported. Unexpectedly, the membrane potential overshot the 0 mV level by several tens of mV during excitation, suggesting that a selective membrane permeability, rather than a general permeability decrease, occurred during the action potential. In fact, Bernstein had observed that the amplitude of the action potential exceeded that of the current measured between the intact and injured surfaces of a nerve. This suggested that the action potential may be more than a destruction of the resting electrical condition of the nerve, but Bernstein did not pursue this observation [7, 11].

Hodgkin and Bernard Katz (German, but emigrated to England; 1911-2003) showed that the amplitude of the squid action potential decreased in amplitude when external sodium concentrations were reduced, suggesting that a selective permeability of sodium ions is involved in the action potential [7, 22]. Bernstein's hypothesis was revised to include a selective permeability increase of sodium ions during the action potential, which flowed down their electrochemical gradient into the cell to produce membrane depolarization. Although unknown to them at the time, Charles Overton previously reported that external sodium ions are essential for the nerve impulse and he hypothesized that excitation required the exchange of sodium and potassium ions in the early 1900s shortly after Bernstein proposed his theory [5, 23]. The nature of the action potential precluded study of the relationship between membrane current and membrane voltage since any current large enough to cross threshold also produced changes in

membrane potentials. A method of controlling the membrane voltage was needed and in 1949, Cole and George Marmont developed the voltage clamp. The voltage clamp was used shortly afterwards by Hodgkin and Huxley, in collaboration with Katz, culminating with their famous publication in 1952 that provided final unequivocal evidence that nerve impulses are fundamentally electrical events. The voltage-clamp essentially works by very rapidly determining and applying the feedback current required to keep the transmembrane potential constant during an electrical event; the amount of current injected to maintain the transmembrane potential is of the same magnitude, but opposite polarity of the current actually flowing across the membrane. When Hodgkin and Huxley held membrane potentials at hyperpolarized levels, the recorded currents were inward as expected based on the flow of potassium ions down their electrochemical gradient toward the equilibrium potential. However, when membrane potentials were depolarized, above a threshold, the initial phase of the current was still inward and then followed by an outward current. This observation implied that the membrane properties changed upon depolarization allowing an ion to flow down a pre-existing electrochemical gradient produced by the metabolic activity of the cell. In their experiments, Hodgkin and Huxley altered the external concentrations of sodium and potassium ions allowing them to analyze the membrane current in separate components. The initial inward current was found to be carried by sodium ions, and the delayed outward current by potassium ions. They fit a series of differential equations relating the permeabilites of these two ions to membrane potential and time, which were able to account for most of the properties of the action potential, such as the time

course, all-or-nothing character, refractory period, and the effect of temperature [19, 23, 24].

Chemical Neurotransmission, Receptors, and Ion Channels

First histological identification of neurons with stains occurred in the mid 1800s by Gabriel Gustav Valentin (Switzerland; 1810-1883), Christian Gottfried Ehrenberg (Germany; 1795-1876), Johannes Purkinje (Czech Republic; 1787-1869) and Albert von Kolliker (Switzerland; 1817-1905). These were followed by descriptions of the motor endplate by Wilhelm Kuhn (Germany; 1837-1900) in 1862 and descriptions of processes later known as dendrites and axons that extended from neurons by Otto Dieters (Germany; 1834-1863) in 1865. The silver staining method developed by Camillo Golgi (Italy; 1843-1926) in 1873 greatly enhanced histological and anatomical studies, but did not provide non-disputable evidence whether connections between neurons are continuous or discontinuous. Scientists using the same method came to different conclusions, leading to the development of the neuron doctrine by Santiago Ramon y Cajal (Spain; 1852-1934) and the reticular theory by Golgi [3]. In 1856, Claude Bernard showed that skeletal muscle contractions could not be produced by nerve stimulation of muscle treated with curare, and in 1897, Charles Scott Sherrington (England; 1857-1952) coined the term “synapse” to describe the apparent lack of continuity between the sensory neurons and motor neurons in his studies of reflexes and Wallerian degeneration [3]. Thomas Elliott (England; 1877-1961), a student of John Langley, is probably the earliest to suggest that a chemical is released upon sympathetic nerve stimulation. His studies demonstrated that adrenaline mimicked the effect of nerve stimulation at all smooth muscle and glands innervated by sympathetic nerves. He suggested that “adrenaline might be the chemical stimulant liberated on

each occasion when the impulse arrives at the periphery" [25, 26]. In 1914, Henry Dale (England; 1875-1968) identified nicotinic and muscarinic components of autonomic responses induced by acetylcholine (ACh) through his studies of sympathetic and parasympathetic nerves, but at the time "had no evidence at all that ACh was a constituent of any part of the animal body" [27, 28]. In 1921, Otto Loewi provided the first demonstration of chemical transmission in the peripheral nervous system, between the vagal nerve and heart [17]. His experiment demonstrated that a substance released by the vagal nerve, which he called "vagusstoff", was capable of slowing the heart rate of an isolated heart. Loewi later identified vagusstoff as ACh in 1926 [2]. In 1929 Dale and colleagues isolated ACh from ox and horse spleen [29] and shortly after were able to show that "ACh is liberated" from stimulated nerve endings by demonstrating the presence of ACh in acetylcholinesterase-treated perfusates of muscle tissue and ganglionic synapses [28, 30, 31]. Although chemical transmission in the peripheral nervous system was more or less accepted by the 1930s, electrophysiologists questioned the general applicability of these findings to the central nervous system. The debate went on for a number of years and became known as the war between the "Soups and the Sparks". The issue became resolved when intracellular glass microelectrodes (sharp electrodes) and the amplifiers to deal with the high resistances became available, which allowed for the measurement of transmembrane potentials in muscle fibers and neurons. In 1950, Paul Fatt and Katz's intracellular recording at the motor endplate demonstrated that the change in membrane potential upon stimulation was far larger than expected due to circulating currents [32]. John Eccles (Australia; 1903-1997), at one time a leader of the "Sparks" group, demonstrated that direct

inhibition of the nerve impulse in spinal chord is associated with hyperpolarization of the postsynaptic membrane, and that the hyperpolarization was not induced by external electrical stimulation in 1952. He considered this as evidence in favor of chemical transmission [33]. Eccles and his group continued with their work, which provided descriptions of the ionic basis of inhibitory and excitatory postsynaptic potentials and demonstrations of ACh release in the CNS [34]. Paul Fatt and Bernard Katz, also in 1952, showed that quantal changes in the electrical potential, called miniature endplate potentials, occurred during voltage recordings of the motor endplate (treated with tetrodotoxin to reduce action potentials) and showed statistically that this is described if neurotransmitter is released in quantal events [35, 36]. The development of electron microscopy and its application to biological tissue in the mid 1950s finally provided the definitive evidence in favor of neuron theory and also strong support for chemical neurotransmission [2, 37]. The images clearly showed an extracellular space between two relatively swollen surfaces of distinct neurons with small vesicles in the presynaptic terminal, suggesting that the quantal miniature endplate potentials observed by Fatt and Katz were due to the release of single pre-synaptic vesicles filled with neurotransmitter. In 1965, Katz and Miledi demonstrated that voltage-gated calcium channels open following an action potential invasion of the pre-synaptic terminal, and that calcium is necessary for the vesicular release of neurotransmitter [38].

The concept of a receptor was established much earlier from the independent work of Paul Ehrlich (1854-1915) and John Langley (1852-1925) in the late 1800s [39]. Ehrlich, working with selective histological staining believed that the staining process relied on the chemical interaction of the dye and a substance on the cell, and later, he

developed side-chain theory. He proposed that the cell produces side-chains that bind to toxins and other chemical substances, based on his observations of the immune response [39, 40]. Langley, a pharmacologist, studied a competitive interaction between atropine and pilocarpine on salivary secretion in 1878 [41]. In 1901, he showed that nicotine continued to work on ganglia even after degeneration of the nerve endings and later in 1905 coined the term “receptive substance” in reference to the action of nicotine and curare on muscle tissue [42]. Archibald Vivian Hill (England; 1886-1977), as a student of Langley, studied the relationship between nicotine and curare concentrations and contraction of the frog abdominal muscle and derived the equation that is commonly attributed to Langmuir in 1909 to explain his results [43]. One year later, he refined the equation to include the Hill coefficient, which provided a better fit of his results regarding oxygen binding by hemoglobin in various saline solutions [44]. Alfred Joseph Clark (England; 1885-1941) used Hill’s equations in the 1930s to develop receptor theory, which established principles of receptor-mediated responses, such as saturation, reversibility, stereoselectivity, tissue specificity, and explained the relationship between ligand concentrations versus biological responses in terms of mass-action and receptor occupancy by ligand in a quantitative way [45]. Receptor theory was expanded to include competitive antagonists with the work of John Gaddum (England; 1900-1965) and Heinz Schild (England; 1906-1984) in the 1930s through 1950s [46] [47-49]. This framework was used to classify many pharmacological agents before there was an understanding of how the receptors mediated their response. In 1956, Robert Stephenson proposed his explanation of partial agonism by treating the binding of agonist and the ability to produce a response afterward as

separate steps; he introduced the concepts of affinity and efficacy [50]. One year later del Castillo and Katz proposed the first kinetic mechanism of a receptor mediated response, incorporating an inactive agonist-bound state, to explain their observation that decamethonium can be both “depolarizing and curarizing” [51]. In 1961, Wyman had the initial idea that substrates stabilize specific conformations of an enzyme to which they have greatest affinity; the idea of proteins as allosteric molecules was developed more fully by Monod, Wyman and Changeux in 1965. The allosteric theory was soon applied to the end-plate (nicotinic) receptor as early as 1967 and has been used extensively since [52, 53]. The del Castillo-Katz mechanism and Monod-Wyman-Changeux model of protein allostery have been usefully applied in the study of ligand-gated ion channels, but these concepts were proposed at a time when the existence of the ion channel was still a likely suspicion.

Although Hodgkin and Huxley definitively demonstrated the electrical nature of the nerve impulse, the mechanism of ion permeation across the membrane was unproven. In the early 1950s, the increased membrane permeability of ions during excitation was hypothesized to occur either through aqueous pores in the membrane or via ion carrier molecules [36, 54]. The identification of tetraethlyammonium in 1957 [55] and tetrodotoxin in 1964 [56], which selectively block the sodium and potassium components of the action potential, suggested that separate permeation pathways existed for the two ions. In 1960, Takeuchi and Takeuchi applied the voltage-clamp to the motor endplate and demonstrated that the muscle-type nicotinic receptor expressed there regulates a non-selective permeation pathway for cations [57]. Initial hard evidence for ion channels was obtained from experiments with artificial lipid

membranes. In 1962, Paul Meuller and colleagues reported that the electrical resistance of a lipid bilayer could be reduced by several water-soluble proteins [58]. Hladky and Haydon first directly observed ion channels in artificial lipid bilayers formed by antibiotics in 1970 [59, 60]. Around this time, Bertil Hille (USA; 1940-present) studied the relative permeabilities of over twenty cations with varying physico-chemical properties through voltage-gated sodium channels. He suggested that sodium channels were aqueous pores and that hydrogen bond interactions between spheres of hydration around individual sodium ions are critical for passage through the “selectivity filter” of the ion channel [61, 62].

The first measurements of the currents (mean open times and conductances) through individual ion channels expressed in mammalian cells were performed in the early 1970s by Bernard Katz and Ricardo Miledi through analysis of the noise produced by application of ACh to a voltage-clamped motor endplate [63, 64]. Katz and Miledi suggested that the fluctuations of noise were caused by the “elementary ACh current pulse” and the “ion gate”, meaning in today’s terms the random opening and closing of single ion channels. They estimated a single-channel conductance of 100 pS, a value higher than expected for a charge carrier and which helped confirm that ion permeation was through an aqueous pore in the membrane. The first direct measurement of single ion channels in animal tissue was made from denervated frog muscle fibers in 1976 by Erwin Neher (Germany; 1944-present) and Bert Sakmann (Germany; 1942-present) [65]. Their approach was similar to that which Neher had used previously to record currents from small areas of neuronal cell bodies [66]. They used glass micropipettes with a smooth tip of 3-5 microns in diameter, which allowed them to reduce background

noise by recording from small patches of membrane. The recording circuitry required modification from typical voltage-clamp amplifiers since just one electrode would be used to record the voltage and inject current, while keeping amplifier noise to a minimum. Sakmann and Neher found that upon contacting the surface of muscle fibers (often treated with collagenase and protease) with their micropipette, a seal could be formed with an electrical resistance in the megaOhm range, which provided sufficient electrical isolation of membrane patch to record square-shaped pulses of current with unitary amplitudes of less than 5 pA. At last, the current from an individual ion channel had been observed [67]. The quality of recordings were still limited by noise and patch stability, and a breakthrough was made when it was discovered that very high resistance seals above 10 gigaOhms in resistance could be made by applying light negative pressure to the interior of the micropipette after contact with the cell. The robustness of this seal was found to be sufficiently strong to withstand rupture of the membrane under the micropipette, which allowed for recordings from entire cells and from excised membrane patches. This allowed for control of the transmembrane potential, and in the case of excised patches concentrations, control of saline solutions on both sides of the membrane [68]. The single-channel data collected with this new technique required novel methods for interpretation, most of which were developed by Alan Hawkes and David Colquhoun (England; 1936-present). Using these methods, Colquhoun and Sakmann provided one of the first single-channel kinetic analyses, in which they determined time constants of a plausible kinetic mechanism from recordings of single endplate nicotinic receptors [69, 70]. The patch-clamp method allowed for recording from macroscopic, as well as currents from individual ion channels and very

quickly became one of the preferred electrophysiological methods. The patch-clamp method also allows for electrophysiological recordings to be made from individual neurons, contributing much to our knowledge about properties of neurons: the types of receptors they express and their roles in neuronal circuits.

Since the discovery of ACh as the first neurotransmitter, many others have been discovered, including norepinephrine, serotonin, dopamine, GABA, and glutamate. Most of these were identified in the nervous system throughout the 1950s, but were shown to be neurotransmitters later. The development of radiolabeled ligands has allowed receptors for most of these transmitters to be localized to specific areas of the nervous system. In addition, peptides, adenosine triphosphate, nitric oxide, and others have been discovered to have neurotransmitter activity [2].

The molecular biology revolution of the 1980s led to the cloning of the receptors for these neurotransmitters, as well as many other ion channels gated by voltage and mechanical stimuli, through methods utilizing protein sequencing, homology screens, or functional expression [71, 72]. The ligand-gated ion channels database currently lists over 550 published sequences of subunits from many species belonging to the Cys-loop, glutamatergic, and ATP-gated superfamilies (http://www.ebi.ac.uk/compneur-srv/LGICdb/LGICdb.php).

The first images of an ion channel were of the nAChR in the late 1980s [73]. In 1998, the first high-resolution structure of an ion channel, the potassium KscA channel was published [74]. Since then several structures of other channels have been solved [75, 76]. As a young scientist in the 2000s, it is hard to imagine a time when the nature of the nerve impulse was not considered to be electrical. Even more, it is difficult to

envision a time when ion channels were unknown or unproven. It is easy indeed to take for granted the efforts of many scientists and the knowledge that today seems so common sense.

Two classes of receptors were identified that respond to ACh, distinguished by pharmacological profiles first described by Henry Dale. The agonist nicotine activates one of these receptor classes, whereas the other class is characterized by the ability to be activated by muscarine and inhibited by atropine. Unlike nAChRs, muscarinic ACh receptors are not coupled directly to ion channels, and they mediate their response on the relatively slow time scale of milliseconds to seconds through intracellular signals transduced via G-Proteins, resulting in several possible outcomes which may include the indirect opening of ion channels. I will focus on one of many ion channel families known, the nAChRs, with particular emphasis on the α7 nicotinic receptor subtype.

CHAPTER 2
NICOTINIC ACETYLCHOLINE RECEPTORS: INTRODUCTION

The Cys-Loop Superfamily of Ligand-Gated Ion Channels

The Cys-loop superfamily of ligand-gated ion channels includes receptors that are gated by ACh, GABA, glycine, and serotonin in mammalian cells and all likely evolved from a common ancestor [77]. This superfamily has its name because all the proteins in it have a loop of 13 amino acid residues formed by two disulfide-linked cysteine residues [78]. Although these channels are activated by different agonists and can be permeable to either cations or anions, they share considerable sequence homology and have similar transmembrane topologies and basic functionality. The finding that inhibitory (anion permeable) and excitatory receptors (cation permeable) are structurally related was unexpected [79-81]. All ligand-gated ion channels produce biological signals through their ability to bind an agonist, which translates into receptor motion that gates an aqueous ion channel pore and allows charged ions to move across the cell membrane according to pre-established electrochemical gradients created by the metabolic activity of a living cell. The functional homology of the Cys-loop superfamily was demonstrated through fusion of aspects of the serotonin-gated $5HT_3$ receptor with the α7 nAChR producing functional chimeras [82]. In addition, the α7 nAChR can be converted to an anion-selective channel by substituting as few as three amino acids in the pore domain with those found at the homologous positions in $GABA_A$ or glycine-gated receptors [83). Due to the fact that more is known about nAChRs than any other ligand-gated receptor, they often have been considered as the prototype for studies of other members of the Cys-loop superfamily [84].

nAChRs of muscle and electric organs

The muscle-type nAChR from the electric organs of eels (Electophorus electricus) and rays (Torpedo californica or marmorata) and the neuromuscular junction became the first and most fully characterized neurotransmitter receptor, largely due to the abundance and accessibility of the receptor provided by these tissues. The discovery of cobra and bungarus venom toxins with very high binding affinities enabled these receptors to be the first affinity purified [85, 86]. The purification of the electric organ nAChRs in milligram quantities enabled biochemical studies that determined the receptor is a pentameric complex consisting of distinct protein subunits. These subunits were called α, β, γ, and δ in order or increasing molecular weight, and found in the stoichiometry of $\alpha_2\beta\gamma\delta$ [87, 88]. Receptor purification also led to partial N-terminal protein sequencing of the subunits [89], which was used to derive nucleic acid probes used to clone the receptor subunits [90-92]. The related subunits of the homologous receptor expressed in mammalian tissues were subsequently cloned [93]. An additional subunit known as ε was shown to replace the γ subunit during the development of skeletal muscle, resulting in new biophysical properties such as increased channel conductances and shorter mean open times [94]. The muscle-type nAChR was also the first ligand-gated ion channel to be imaged using electron diffraction techniques due to the high density of receptor expression in electric organ membranes, which can be treated to form two-dimensional crystalline arrays [95, 96].

General Features of nAChR Structure Learned from Muscle-type nAChRs

Early predictions of general subunit structure and orientation in the membrane were based on hydrophobicity analysis of the primary amino acid sequence. These

predictions were tested by numerous experiments using mutagenic, biochemical, immunological, microscopic, and electrophysiological techniques and have turned out to be reasonably accurate [92, 97, 98]. Images of the electric organ nAChR obtained from electron diffraction show that the five subunits of the pentameric complex are arranged in a circular manner to form a central pore. The major elements of a nAChR subunit include a large N-terminal extracellular domain (which accounts for nearly half of the subunit), followed by three closely spaced transmembrane helices, a large cytoplasmic domain, fourth transmembrane domain and a short extracellular C-terminus.

Fitting of voltage-clamp, ion flux, and binding data with predictions from theoretical receptor activation mechanisms suggested that the muscle-type nAChR contained two agonist binding sites [99-102]. Affinity labeling and mutagenesis studies suggested the two agonist binding sites of muscle-type nAChR are located in the extracellular N-terminal domain at the α-δ interface and at the α-γ or -ε interface [103-105]. Studies using affinity labels identified the presence of two adjacent cysteine residues in the α subunit that contribute to agonist binding sites [78]. These cysteines are now known to be part of a loop known as the C-loop, which partially wraps around the outside of the adjacent subunit and constricts over the subunit interface when agonist is bound by the receptor [106]. The agonist binding site is characterized as a hydrophobic pocket of aromatic amino acids that provide an electrically negative surface which stabilizes the agonist-receptor complex through cation-π interactions [107]. In addition to the C-loop, the α subunit contributes the aromatic residues Tyr-93, Trp-149, Tyr-190, and Tyr-198 to form the primary surface of the binding site [108]. The non-α subunit forms the complimentary surface of the binding site, and contains a critical tryptophan residue at

position 57 in the δ subunit and position 55 in the γ and ε subunit. The β1 subunit does not contribute amino acids directly to the agonist binding pocket, but it still influences receptor properties through its contribution to the ion channel pore and by affecting concerted conformational shifts of the pentameric protein [78]. The location of the β1 subunit in the pentamer in relation to the α-δ and α-γ (or ε) pairs is unproven; several studies suggest the γ subunit is located between the two α subunits [109-111], but another study suggests the δ subunit is located between the two α subunits [112]. In addition to the agonist binding sites, the N-terminal domain also contains the characteristic Cys-loop, glycosylation sites, and the main immunogenic region.

Residues from the top third of the first transmembrane helix and entire second transmembrane helix line the ion channel while the third and fourth transmembrane domains form a hydrophobic protein core and interact with the cell membrane. The nAChR ion channel pore is permeable to small monovalent and divalent cations, such as sodium and calcium, which create an excitatory or depolarizing signal to the cell when the ion channel is opened. The intracellular cytoplasmic domain between the third and fourth transmembrane helices is by far the least characterized region of the channel, and shows the least amount of conservation between subunits. Cytoskeletal attachment points, as well as consensus sequences for serine/threonine and tyrosine phosphorylation sites have been found in this region, which appear to provide a mechanism for modulation of channel function [113-117].

The crystallization of the acetylcholine binding protein (AChBP), a soluble protein important in regulating extracellular ACh concentration in freshwater snails, has further confirmed many of the general structural features of nAChR subunits discussed above.

Given that crystallization of membrane-associated proteins remains a challenge, the atomic resolution structures of AChBP in apo-form and bound to various ligands have been used extensively to create homology models of nAChRs [118-121]. The AChBP consists of a homomeric structure with sequence homology to the extracellular N-terminal agonist binding domains of nAChRs, and although the solved structures of AChBP are undeniably valuable, the utility of the AChBP is limited by the facts that the protein lacks transmembrane and intracellular domains of nAChR subunits, and the images are static structures of dynamic proteins.

Neuronal nAChR Subunits

Oligonucleotide probes designed from muscle-type α1 sequence were used to identify the first neuronal nAChR subunit through low stringency screening of a PC12 cell cDNA library [122]. Several other homologous AChR subunits were discovered in short order through similar screening methods of rat and chick cDNA libraries [123]. Although these subunits became known as neuronal nAChR subunits because they were cloned from neuronal-like PC12 cells or cDNA libraries derived from brain tissue [124], it has become clear that some of these subunits are expressed in non-neuronal tissue as well, such as microglia, peripheral macrophages, skin, and lungs [125, 126]. The neuronal nAChR subunits were classified as α if they contained adjacent cysteine residues in the C-loop, homologous to those in the muscle-type α subunit that were shown to be critical elements of agonist binding sites [127], or β subunits if the adjacent cysteines were absent and numbered in the order of discovery. Much of our knowledge of receptor structure, function, and pharmacology has been learned through studies of heterologously expressed receptors, which was made possible with the cloning of the

nAChR subunits. Nine neuronal α nAChR subunits (α2-10) and three β subunits (β2-4) have been cloned to date. The number of possible subunit combinations that can form functional receptors is large, but there appear to be some general rules. The neuronal receptors consist of two general classes, heteromeric receptors or homomeric receptors. Heterologous expression studies have indicated that α2, α3, and α4 subunits require co-expression with β2 or β4 for function. Neuronal heteromeric AChRs contain two agonist binding sites formed by the interface of α- and non-α subunits. Alpha6 subunits usually assemble with β2 and/or β4, but can also assemble with β3 and other α subunits as well. Neuronal β3 and α5 subunits do not appear to form functional agonist binding sites, but rather function as structural or modulatory subunits similar to the β1 subunit of muscle-type nAChR [128]. Although α5 subunits contain the vicinal cysteine residues in the C-loop, they lack other conserved residues in the N-terminal domain that contribute to agonist binding sites. When α5 is assembled into α4β2, α3β2, or α3β4 receptors it can increase agonist sensitivity, calcium permeability, and alter decay rates of macroscopic currents [129, 130]. An additional source of functional and pharmacological diversity comes from the fact that heteromeric receptors consisting of one type of α subunit, and one type of β subunit can exist in multiple stoichiometries, such as $(\alpha4)_2(\beta2)_3$ and $(\alpha4)_3(\beta2)_2$. The $(\alpha4)_2(\beta2)_3$ receptors have high sensitivity to agonists, as defined by the EC_{50} of macroscopic current responses, and relatively low Ca^{2+} permeability while the $(\alpha4)_3(\beta2)_2$ receptors have relatively low sensitivity to agonist and high in Ca^{2+} permeability [131]. The α7, α8, and α9 subunits can assemble into functional homomeric pentamers without β subunits. The α8 subunit was cloned in chickens and has not been identified in mammals to date. The homomeric α7 receptor

is one of the most widely expressed nicotinic receptor subtypes, whereas α8, α9, and α10-containing receptors are expressed in limited areas such as the retina and neuroepithilium of the inner ear [132]. In homomeric receptors, each α subunit contributes both a primary and complementary face to an agonist binding site so that the total number of agonist binding sites is five [133]. Although α7-9 subunits readily form homomeric nAChRs, these subunits can also form heteropentamers such as α7β2 [134-136], α7α8 [137, 138], or α9α10 [139]. Another source of potential diversity comes from realizations that partially duplicated α7 gene and splice variants of α7 exist with varying functional properties [140, 141].

Physiology, Expression, and Functional Roles of Muscle-type nAChRs

The primary function of the muscle-type nAChR at the neuromuscular junction is to depolarize the motor endplate, resulting in activation of a muscle action potential and muscle contraction. In order to perform this task effectively, reliable synaptic transmission must occur with the pre-synaptic motoneuron. The organization of the neuromuscular junction has evolved to allow the muscle-type nAChR to efficiently perform its role. For example, nAChRs are expressed in abundance and highly concentrated at the endplate (~20,000 binding sites per square micron) and in close contact with the pre-synaptic neurotransmitter release sites. This decreases the effects of diffusion and allows local ACh concentrations to reach 1 mM in less than one millisecond. In addition, the extracellular matrix of the synaptic cleft has an abundance of acetylcholinesterase. This enzyme rapidly hydrolyzes ACh to produce choline and an acetate group to ensure the signal produced by ACh release occurs only briefly. Each molecule of ACh that is successful in binding the receptor probably only binds once

before being deactivated by acetylcholinesterase. The rapid rise in agonist concentration, the large population of localized nAChRs, and brief presentation of a strong stimulus all but ensures the efficient transmission of even very high frequency pre-synaptic signals [142]. The abundance of natural toxins that target the muscle-type nAChR at the neuromuscular junction, such as α-bungarotoxin, curare, α-cobratoxin, and anatoxin-a, testifies to the physiological importance of this specialized synapse.

Physiology, Expression, and Functional Roles of Neuronal nAChRs

General Distinguishing Features of Neuronal nAChRs

As early as the 1940s, pharmacological differences of methonium compounds were observed between nicotinic receptors found at the motor endplate and those found at the autonomic ganglia. For example, ganglionic nAChRs are blocked by hexamethonium and pentamethonium, but not decamethonium whereas nAChRs at the motor endplate are first excited, then desensitized by decamethonium [143-145]. The neuronal nAChRs have higher calcium permeabilities than muscle-type nAChR, with relative sodium: calcium permeability ratios of ~2 to 20 (depending on the neuronal nAChR subtype) and ~0.15, respectively [146-149]. In addition, muscle-type receptors conduct current equally well at both hyperpolarized and depolarized potentials (i.e. have a linear current-voltage relationship) while neuronal nAChRs show inward rectification, meaning they conduct current much better at hyperpolarized potentials than at depolarized potentials. This inward rectification is due to intracellular magnesium ions and positively charged polyamines that block the ion channel at positive potentials [150-152]. Differences in non-conserved amino acid residues in or near the channel pore account for the differences between calcium permeability and current rectification. Differences in subunit composition between individual neuronal nAChR subtypes create

pharmacological diversity allowing for reasonably selective activation, inhibition, or potentiation of specific receptor subtypes. Understanding where the diverse neuronal nAChR subtypes are expressed and the functional significance of such diversity continues to be a hot topic of investigation.

Peripheral Neuronal nAChRs

The nAChRs found in the peripheral nervous system primarily mediate excitatory synaptic transmission at the autonomic ganglia and the dominant nicotinic receptor subtype involved in this important function contains the α3 and β4 subunits. Like heteromeric α4β2 receptors, α3β4 receptors can exist in two stoichiometries and can assemble with β2 or α5 [153]. In many cases the exact stoichiometries of neuronal nAChRs expressed on peripheral ganglia are undefined. Single ganglionic neurons can express multiple nAChR subtypes. For example, chick ciliary ganglion neurons express α3-containing nACRs in post-synaptic and peri-synaptic locations and homomeric α7 nAChRs in perisynaptic locations only [154, 155].

Central Neuronal nAChRs

The use of radiolabeled nicotine and α-bungarotoxin ligands enabled the mapping of AChR expression in the central nervous system. This approach led to the realization that at least two major populations of neuronal nAChRs exist and that these receptor populations have mostly non-overlapping expression patterns; those which bind nicotine with high affinity and those which bind α-bungarotoxin with high affinity [156]. Early studies of heterologously expressed α4β2 receptors suggested they are insensitive to inhibition by α-bungarotoxin [157], yet at the same time α-bungarotoxin-sensitive currents in brain tissue were difficult to detect (due to the fact that they desensitize so

rapidly; see below). The neuronal nAChR responsible for α-bungarotoxin binding was elusive, but was eventually cloned in the early 1990s with the aid of affinity purification utilizing α-bungarotoxin and N-terminal protein sequencing [158-160]. It has since been established that the majority of high-affinity binding sites for nicotine in the brain consist of heteromeric β2-containing receptors, while homomeric α7 receptors account for the majority of high-affinity α-bungarotoxin binding sites [154, 156]. Neuronal nAChRs are broadly expressed in many brain regions including the medial habenula, interpeduncular nucleus, retina, lateral and medial geniculate, and cortex.

There are at least three major cholinergic subsystems in the brain, and together they innervate nearly every area of the brain. Cholinergic neurons originating in midbrain tegmental areas innervate the thalamus and key midbrain dopaminergic centers (substantia nigra pars compacta and ventral tegmental area) and also send descending cholinergic projections into the pons and brainstem. Another cholinergic subsystem originates in the basal forebrain nuclei (nucleus basalis, diagonal band of broca, medial septal nuclei) and makes widespread cholinergic innervation to the cortex and hippocampus. The remaining cholinergic system arises from a small group of cholinergic interneurons in the striatum. Together, these cholinergic interneurons make up only approximately 2% of all striatal neurons, but they provide very rich and localized cholinergic signals to specific regions in the striatum and olfactory tubercle [161]. In sharp contrast to cholinergic signaling at the motor endplate and at autonomic ganglia, the majority of cholinergic release sites in the central nervous system release ACh diffusely through volume transmission [162, 163] rather than at focused synaptic sites. One striking example of an area where cholinergic synaptic transmission was expected

to be found, but was not, is a fiber tract running from the medial habenula to interpeduncular nucleus known as the fasciculus retroflexus of Meynert. Despite the fact that this pathway contains a high density of cholinergic fibers and high expression of choline acetyltransferase, excitatory synaptic transmission in this area is glutamatergic, not cholinergic [164-166].

The release of ACh likely occurs in relatively low-frequency (4–10 Hz) theta rhythms and the diffusion of ACh is largely limited by acetylcholinesterase. This enzyme is common in the central nervous system, but does not always match up with ACh release sites [167]. The precise temporal and spatial dynamics of ACh concentrations are still unknown in the brain, and efforts continue to understand this important parameter. Some estimates suggest that steady-state extracellular ACh concentrations in the brain are in the low nM range, but it is very likely that ACh concentrations vary significantly from one microdomain to another [168]. At any rate, the presentation of ACh in the brain appears to be vastly different from that at the neuromuscular junction and autonomic ganglia. There are only a few reports of nAChR-mediated fast synaptic transmission, and in many of these cases the evidence is equivocal [166, 169-171]. The primary mediators of fast synaptic transmission in the central nervous system are glutamatergic and GABAergic systems.

The widespread distribution of nAChRs and observations that they are expressed primarily at somatic, pre-terminal, pre-synaptic, peri-synaptic, and extra-synaptic sites, rather than at post-synaptic sites in the brain is consistent with the observation of diffuse cholinergic release sites [156, 172-175]. It has become widely accepted that nicotinic receptors expressed in the brain play roles in modulation of other neurotransmitter

systems through enhancement of neurotransmitter release, modification of neuronal excitabililty, and influences on synaptic plasticity. Numerous studies with isolated synaptosomes and electrophysiological studies in brain slices have shown that neuronal nAChRs modulate the release of glutamate, dopamine, noradrenaline, and serotonin from brain regions including the medial habenula, interpeduncular nucleus, thalamic nuclei, midbrain limbic regions, cortex, and hippocampus [176-179]. If the application of nicotinic ligands increase the frequency of spontaneous currents in a tetrodotoxin-resistant, calcium-dependent, and nAChR antagonist-sensitive manner, the results are generally interpreted to be mediated by pre-synaptic nAChRs [180, 181]. By taking advantage of the unusually large size of the presynaptic terminals at the developing chick ciliary ganglion, inward currents evoked by nicotine, blocked by α-bungarotoxin, and resistant to tetrodotoxin were recorded directly from the nerve terminal [178].

Neuronal nAChRs influence electrical activity in nearly every area of the brain where they participate in aspects of neuronal signaling involved in attention, learning, memory, and development [182-184]. Disruption of nicotinic signaling mechanisms contributes to Alzheimer's disease, Parkinson's disease, schizophrenia, dementia with Lewy bodies, forms of epilepsy, pain, anxiety, attention deficit disorders, autism, and addiction [185-187]. Research is ongoing to determine functional roles of individual nAChR subtypes and their influence in specific brain regions for these diverse indications. Initial interest in neuronal nAChRs as therapeutic targets came from early observations that nicotine enhances attention and memory performance, combined with observations that a selective loss of cholinergic neurons occurs in Alzheimer's disease. At the behavioral level, the effects of nicotine and other nAChR agonists on cognition

have turned out to be varied. Overall, the data suggest that nAChRs are involved in select forms of memory, such as working memory and episodic memory, and appear to be particularly important when tasks are difficult or when subjects are impaired [188, 189].

High-Affinity Binding Sites

The most widely expressed neuronal nAChR subunit is β2, which accounts for the vast majority (>90%) of high affinity binding sites for nicotine in rodent brain [190]. This finding was confirmed when mice lacking the β2 subunit lost most, but not all, high affinity nicotine binding [191, 192]. The β2 subunit most commonly associates with the α4 subunit in rodent brain, but can assemble with most of the other nAChR subunits as well [193]. The α2 subunit is more widely expressed in the primate brain than it is in rodent brain, and α2β2 receptors may constitute a major nAChR subtype in primate and human brain [194]. Labeling of β2-containing receptors with the monoclonal antibody mAb 270 was highest in the interpeduncular nucleus, thalamic nuclei, superior colliculus, and medial habenula, with more moderate labeling in the presubiculum, cerebral cortex, substantia nigra (pars compacta), and ventral tegmental area [156]. Alpha3-containing receptors are prevalent in autonomic ganglia, but also have limited expression in brain regions such as the medial habenula, pineal gland, spinal cord, and retina [132]. The habenula is a region of diverse and concentrated nAChR expression [195].

The mechanism of nicotine addiction is unknown, but strong evidence suggests that nicotine targets the dopaminergic mesolimbic and nigrostriatal pathways, where it modulates the firing modes, frequencies, and release of dopamine by midbrain

dopaminergic neurons [196-198]. The rewarding influence of nicotine on these pathways is supported by the finding that nicotine administration is reduced when dopamine release is blocked in the nucleus accumbens [199]. Beta2-containing nAChRs with α4 and/or α6 are expressed abundantly in these areas directly on dopaminergic, and also on GABAergic neurons. The net result of nicotine on dopaminergic neurons appears to be increased excitation and decreased inhibition [200]. Desensitization of the heteromeric receptors on inhibitory GABAergic neurons becomes absorbing with a prolonged low-level nicotine stimulus, thus reducing an excitatory drive of the inhibitory neuron to result in less inhibition of the dopaminergic neuron. At the same time, the low-affinity α7 nAChRs on glutamatergic terminals enhance glutamate release onto the dopaminergic neuron [175, 187, 201]. Although heteromeric nAChRs initially open with high probability [202] they accumulate into absorbing high affinity desensitized states that resist further activation more readily at low agonist concentrations than α7 nAChRs [203-205]. It is well established that chronic nicotine upregulates the expression of β2-containing nAChRs [206].

A surprising finding from β2 or β4 knockout mice is that they survive much better than predicted. Beta2 knock-out mice fail to self-administer nicotine and show nicotine-enhanced avoidance learning behavior [191]. In addition, aged mice show impaired learning in the Morris water task, but appear otherwise grossly normal. It is still not clear whether the diversity of nAChR subtypes represents redundancy or a specific functional design. In contrast, knockout of α3 is lethal; likely due to the key role it plays in the autonomic ganglia of the peripheral nervous system.

Low-Affinity Binding Sites: α7 nAChRs

In autoradiographic binding experiments receptors are exposed to ligand for prolonged time periods and accumulate in desensitized states. If the desensitized state shows low-affinity for the ligand, the receptors will lack high affinity binding for agonist and a signal will fail to be produced. This is the case for the homomeric α7 nAChR. In contrast, these receptors bind the antagonist α-bungarotoxin almost irreversibly. Labeling of α7 nAChR with radiolabeled α-bungarotoxin and *in situ* hybridization show high expression in brain regions recognized in cognitive function, including hippocampus (CA1, CA3, dentate gyrus), and cortex (especially layer V), as well as subcortical limbic regions (ventral tegmental area and substantia nigra), hypothalamus, and thalamic nuclei [132, 156, 207]. In addition, α7 nAChR expression occurs in reticular thalamic nuclei in macaques and in human brain tissue [208-210]. The reticular thalamic nuclei are important in mediating attention and sensory gating, processes which are negatively affected in schizophrenia. In the hippocampus, the α7 nAChR is expressed particularly highly on GABAergic interneurons, where it modulates inhibitory/disinhibitory tone onto glutamatergic neurons [211], and to a lesser extent is expressed on glutamatergic terminals.

Distinguishing Functional Characteristics of the homomeric α7 nAChR

The α7 receptor, one of highest expressed nicotinic receptor subtypes in brain and also expressed in non-neuronal cells, is commonly thought to be the ancestor of the other nicotinic genes [212]. One of the most distinguishing functional characteristics of the α7 nAChR is the strong dependence of response kinetics on agonist concentration [213, 214]. At relatively high agonist concentrations peak α7 mediated currents

increase with agonist, but the net charge (area under the response curve) remains relatively unchanged. This is indicative of increased synchronous activity, but not increased overall receptor activation by high agonist concentrations. This phenomenon is clearly demonstrated through comparison of the concentration-response relationships of peak currents versus net charge and is accounted for by a form of desensitization that is readily and rapidly entered in a concentration-dependant manner [213]. Unlike heteromeric nAChRs, the binding sites of α7 appear to cooperate in a negative fashion to produce less channel activation under conditions of high fractional occupancy of the agonist binding sites. The α7 ion channel is characterized by an extremely low probability of being open (P_{open}) during an agonist application. Records of currents mediated by individual α7 receptors show that openings occur rarely, and when they do occur are isolated events usually lasting 100 μseconds or less [215, 216]. A precise measurement of α7 P_{open} has not been possible due to the inability to know the number of functional receptors in a population that contribute to a response, but the open conformation of the α7 receptor appears to be an energetically unfavorable and unstable condition of the protein molecule. Over time, lower agonist concentrations may produce low-level sustained currents that produce more net charge than a response evoked by higher agonist concentrations that quickly favors desensitization. Recovery from desensitization occurs rapidly upon the removal of agonist and receptors readily return to an activatible resting state, consistent with the observation that α7 receptors lack high affinity binding for traditional nicotinic agonists. Desensitization has provided a real challenge in the study of α7 nAChR in native tissues, often making it impossible and at best very difficult to detect contributions of α7 to processes under

study [217]. The ability of α7 nAChR to be activated selectively by choline is another characteristic that sets it apart from other nAChRs and may have important physiological significance. In hypothalamic tuberomammilary neurons, spontaneous firing activity can be modulated by bath-applied choline [218]. Choline, an essential nutrient, is a key component of phospholipids found in the plasma membrane and also a product of acetylcholinesterase activity. Although choline concentrations are typically well below the EC_{50} for activation at 10 μM, this low concentration may provide a tonic signal to α7 nAChRs, potentially producing low-level activation or pre-desensitization. Under conditions of stroke or injury choline concentrations in the brain can increase up to 100 μM [219].

Neuronal nAChRs are known for their relatively high calcium permeability, and this is especially true for the α7 nAChR. The relative permeability of calcium ions is generally reported to be in the range of 10-20 times greater than the permeability of sodium ion [160, 177, 220]. The calcium permeability of the α7 nAChR is often considered comparable to that of the NMDA-type glutamate receptor; this may be of critical importance since α7 nAChRs pass current at resting transmembrane potentials while NMDA-type receptors do not due to the extracellular magnesium block. The high permeability of nAChRs to calcium may allow relatively low numbers of nAChRs to exert significant effects in cellular compartments of small volume, such as in pre-synaptic terminals. The high calcium permeability of α7 has been shown to arise from specific residues on either side of the pore, which can be mutated to eliminate calcium permeability [221]. In addition to directly mediating calcium influx, α7 nAChRs have been shown to induce secondary changes in intracellular calcium through calcium-

induced calcium release from internal stores through ryanodine and/or IP_3 receptors [222-226]. The high calcium permeability has brought a lot of attention to the α7 nAChR, particularly since it has implications for intracellular signaling, gene expression, neurotransmitter release, synaptic plasticity, and cytotoxicity. The calcium signal appears to promote either survival or death, depending on the amplitude and duration of the signal [225, 227, 228]. Relatively weak stimulation was shown to protect differentiated PC12 cells from nerve growth factor and serum deprivation in a manner that depended on protein kinase C and phospolipase C, but high agonist concentrations produced toxicity [223, 227]. The toxicity was attenuated by pre-application, but not post-application, of methyllycaconitine (MLA), whereas protection was only blocked by a 10-minute post-application of MLA. This observation suggests that toxicity is produced through rapid activation of the ion channel, whereas neuroprotection occurs through slower mechanisms, probably involving activation of intracellular signaling pathways [227, 229]. Excitotoxicity produced by excess calcium entry is well known to promote to neuronal death and degeneration [230].

Implications of α7 nAChR in Pathophysiology

Nicotine positively modulates a number of brain functions linked to cognition, such as attention, arousal, learning, and memory functions [182-184]. The importance of the neuronal cholinergic function to learning and memory was first recognized when muscarinic ACh receptor antagonists were found to impair memory in rats [231] and in human young adults [232]. Subsequently, studies of brains from patients with advanced age or Alzheimer's disease consistently found abnormalities in basal forebrain cholinergic neurons that correlated with the level of cognitive decline. Consequently,

the hypothesis that loss of cholinergic function in the central nervous system significantly contributes to the cognitive decline associated with age and AD was developed [233]. Although some debate exists regarding the roles of the cholinergic system in the early stages of Alzheimer's disease [234-238], degeneration of cholinergic neurons in Alzheimer's disease is firmly established. The cholinergic hypothesis of cognitive decline is supported by a considerable amount of evidence which includes: (a) reports that both muscarinic and nicotinic receptor antagonists impair memory performance in a variety of behavioral paradigms in rodents, non-human primates, and humans [234], (b) lesions in animals that damage cholinergic input to the neocortex or hippocampus from the basal forebrain structures diminish performance in the same memory tasks affected by cholinergic blockade [239], (c) ACh synthesis and release is reduced in aged animals [240-243], (d) aged and Alzheimer's patients show high sensitivity to the memory impairing effects of cholinergic antagonists [244-246], and (e) measurements of cholinergic function with *in vivo* imaging methods reveal multiple aspects of the cholinergic system are compromised in Alzheimer's and memory-impaired patients [247-250]. The observation that cholinergic neurons are lost in Alzheimer's disease led to the development of acetycholinesterase inhibitors as a therapy. To this day, acetylcholinesterase inhibitors and memantine (a weak non-competitive blocker of NMDA-type glutamate channels) are the only therapies for Alzheimer's disease approved by the Federal Drug Administration. At best these treatments work temporarily to alleviate symptoms without altering the progression of the disease.

Normal aging, traumatic brain injury, Parkinson's disease, and schizophrenia often have a component of significant cognitive decline [251-256] and therapies aimed at restoring, maintaining, and/or protecting the cholinergic system through nicotinic ligands appear promising and remain under pursuit [257]. While it is true that degeneration of cholinergic pathways is not solely responsible for neurodegenerative disease and that both muscarinic and nicotinic mediated signaling are affected by such degradation, the α7 nicotine receptor is singled out as a therapeutic target due to the substantial body of data suggesting a) that α7 is a primary mediator of nicotine-induced neuroprotection [258-266], b) α7 selective agonists exert a cytoprotective influence against trophic-factor deprivation [227, 265, 267, 268], ethanol toxicity [269, 270], glutamate excitotoxicity [271], amyloid beta(1-42) toxicity [272], and hypoxia [273, 274] on neurons and cultured cells [223, 227, 270, 275-281], (c) α7-selective agonists enhance cognitive function [188, 255, 257, 282-296], and (d) α7 nAChRs do not appear to mediate addiction [297, 298]. A number of reports have indicated that the α7 nAChR interacts with amyloid beta (1-42), the primary component of senile plaques found in the brains of Alzheimer's patients. The data have not always been reproducible or clear, likely due to difficulties in reconstituting active amyloid beta, but do implicate a connection between α7 and the disorder.

In addition to cognitive deficits, α7 nAChRs have been implicated in schizophrenia through sensory gating deficits. Individuals with schizophrenia are significantly more likely to smoke tobacco than non-schizophrenics [299, 300]; this observation has been generally seen as self-medication and has stimulated interest in nAChRs as a therapeutic target in the disease. Schizophrenics often have impaired auditory gating,

as demonstrated by transcranial recordings [301]. In normal individuals, auditory stimuli presented in quick succession are processed such that the response from the second stimulus is greatly attenuated relative to the first. In schizophrenics, there is much less suppression of the response to the second stimulus, which is indicative of failed auditory processing [302, 303]. The implication of this deficit is that hallucinations, delusions, and paranoia may result from integration of unfiltered stimuli by the brain. Genetic linkage studies have mapped sensory gating deficiencies to the chromosomal locus 15q13-q14, which contains the α7 gene [304-306], and may be due to diminished promoter efficacy of the α7 gene [307]. In addition, α7 nAChR expression is often reduced in the hippocampus and thalamus of postmortem brains [305, 308]. Consistent with these observations, a number of α7 agonists and positive allosteric modulators (PAMs) have been shown to improve auditory gating deficits in preclinical models [299], and in humans [303].

Therapeutic Targeting of the α7 nAChR through Positive Allosteric Modulation

The term “allosteric” was first introduced following observations that bacterial enzymes were inhibited by the end product of synthetic pathways, even though the end product had limited structural similarities with the enzyme active site substrate [309]. The inhibition appeared to be non-competitive with substrate, which led to hypotheses that the non-competitive inhibitor produced conformational alterations in the protein [310] and the formulation of the well-known Monod-Wyman-Changeux model of protein allostery [311-313]. The basic concept proposed that proteins are dynamic structures existing in multiple discrete functional states or conformations, all of which are accessible to the protein under resting conditions. Binding of a ligand alters the resting

equilibrium by reversibly stabilizing the protein in the conformation to which the ligand has greatest affinity. The conformation of each subunit was proposed to be constrained by the other subunits, and protein symmetry always conserved. Therefore, the binding of a ligand at one site was predicted to alter the affinity of the other binding sites within the oligomer for the ligands. The model was soon applied to hemoglobin to describe the cooperative nature of oxygen binding, and to proteins involved in signal transduction, including membrane receptors as diverse as G-protein coupled receptors and ligand-gated ion channels including nAChRs [312, 313].

During the last 20 years, intensive effort has been put forth to identify agonists that selectively activate the α7 nAChR. Numerous compounds have been discovered and characterized [314]. Recently an alternative avenue of targeting the α7 nAChR for therapeutic purposes has been appreciated with the discovery of PAMs. This approach may offer the means to overcome some of the factors that limit the efficacy of agonists, such as the low P_{open} and rapid desensitization, potentially with significant benefit for processes that depend on channel activation [291]. In addition, PAMs may synergize and augment natural neurotransmitter-mediated signals rather than oppose or attempt to replace them since a PAM requires the presence of an agonist to function. Further, the binding sites for PAMs are located away from well-conserved agonist binding domains, which may enhance the identification of compounds with desirable subtype selectivity. The sedative-hypnotic drugs, such as the barbiturates and benzodiazepines, which target $GABA_A$ receptors, provide a proven example of allosteric modulator-based therapy, with ion channels from the same superfamily as nAChRs [315].

Positive allosteric modulators selective for α7 share some of the putative therapeutic activities ascribed to α7 agonists, including enhancement of memory-related behavioral performance in the eight-arm radial maze, social recognition, and Morris water maze tasks [316, 317], and normalization of sensory gating deficits [316, 318-321]. The intrinsically low P_{open} of α7 makes it a good candidate for positive allosteric potentiation. However, since α7 is a receptor with high calcium permeability, it must also be considered whether extreme increases in α7 channel activation may lead to unexpected, and potentially undesirable, effects.

The identified α7 PAMs have considerable diversity, ranging from proteins to small molecules [322]. Even the small molecule PAMs vary significantly in structure, as well as in properties and probably mechanisms of the modulation [323, 324]. Gronlien *et al*., 2007 proposed that α7 PAMs be divided into two classes, type I and type II, based on the functional properties of modulation. Following the rapid application of agonists, all PAMs appear to increase receptor sensitivity to agonists, current magnitudes, and empirical Hill coefficients; the type I PAMs (for example 5-HI, NS-1738, or CCMI) do so with little or no effect on the basic onset and decay kinetics, or shape, of the response, while the type II PAMs (for example PNU-120596, TQS, or A-867744) markedly slow response decay kinetics and can even activate receptors that have been desensitized by applications of high agonist concentrations or by application of agonists like GTS-21 that produce residual inhibition or desensitization [316, 318, 325-328]. Since the two classes of α7 modulators were proposed, additional PAMs have been identified that display properties intermediate to the type I and type II classes [320, 321, 329].

Putative allosteric modulator binding sites of $GABA_A$ receptors have been identified in the N-terminal extracellular domains at subunit interfaces not forming orthosteric agonist binding sites (benzodiazepine binding site) and in the transmembrane region (barbiturate, alcohol, neurosteroid, general anesthetic binding sites [330-334]). This information, along with the differing functional profiles of type I and type II PAMs, may be seen as consistent with the hypothesis that multiple allosteric sites also exist on $\alpha 7$. The site where calcium binds to potentiate responses on $\alpha 7$ was localized to the N-terminal extracellular domain [335, 336]. In addition, the crystal structure of galantamine bound to AChBP [337], mutagenesis studies [338], and computer docking simulations [339, 340] provide further evidence for nAChR allosteric sites in the extracellular domain, some of which may be related to benzodiazepine binding sites on $GABA_A$ receptors [337, 341]. Using $\alpha 7$/5-HT_3 chimeras, the N-terminal extracellular domain of $\alpha 7$ has been shown to be sufficient for potentiation by the type I PAMs NS-1738 [342] and 5-HI [343], but not the type II PAM PNU-120596 [342]. In addition, PNU-120596, but not NS-1738, potentiated currents (ACh-evoked) in a reverse 5-HT_3/$\alpha 7$ chimera containing $\alpha 7$ TM regions [342]. These studies also provide evidence that the extracellular $\alpha 7$ M2-M3 loop is implicated in potentiation by genistein and NS-1738 [342, 343].

Other studies using $\alpha 7$/5-HT_3 chimeras suggest that TM1-TM3 regions are critical for potentiation by PNU-120596 and the type I modulators LY-2087101 and ivermectin [344, 345]. Furthermore, mutations at several $\alpha 7$ amino acid residues, which are hypothesized to contribute to an intrasubunit cavity within the four transmembrane domains, significantly reduced potentiation by PNU-120596, LY-2087101 [344], and

ivermectin [345]. Through site-directed mutagenesis, these studies together identify potentially important differences in modulator interactions with the receptors. For example, the A225D mutation reduced potentiation by PNU-120596 significantly more than it reduced potentiation by LY-2087101 [344] and the S276V mutation had no effect on potentiation by PNU-120596 [344], but conferred inhibitory properties to ivermectin [345]. Based on their work with α7/5-HT$_3$ chimeras, mutagenesis studies, blind computer docking simulations, and evidence that an intrasubunit transmembrane site appears to be important for potentiation of glycine and GABA receptors [331, 346-349], Young *et al*., 2008 proposed the intrasubunit cavity is a highly conserved modulatory site of Cys-loop ion channels [344], a hypothesis which has been supported by others [331, 350]. The fact that CCMI was discovered from a library of GABA$_A$ PAMs (that bind away from the benzodiazepine site) provides further support for the existence of conserved allosteric sites and/or mechanisms [316]. The findings that the extracellular domain appears to be sufficient for potentiation by some type I PAMs (NS-1738 and 5-HI), but not others (ivermectin and LY-2087101) suggest that more than one mechanism may produce the type I potentiation profile, and perhaps the same applies to the type II profile.

Positive allosteric modulators have been demonstrated to potentiate many types of α7-mediated responses that may be important within biological systems. For example, ERK1/2 phosphorylation was enhanced in PC12 cells by A-867744 [351] and PNU-120596 [351-353] with several structurally diverse agonists. Several studies have provided evidence that activation of ERK1/2, the prototypical mitogen activated kinase,

is important for α7-mediated protection from death in PC12 cells [223, 352-355] and have implicated ERK1/2 in cognitive functions [355-359].

Several PAMs, including 5-HI, PNU-120596, SB-206553, and A-867744, enhance agonist-evoked α7 responses from hippocampal CA1 stratum radiatum interneurons [318, 320, 326, 360, 361] and glial cells [362] in acute brain slices. Spontaneous and choline- or ACh-induced increases in GABAergic inhibitory post synaptic currents were enhanced by 5-HI [363, 364], PNU-120596 [318], LY-2087101 [365], and A-867744 [326] in hippocampal neurons. JNJ-1930942 increased the amplitude of excitatory post-synaptic potentials in hippocampal dentate gyrus [321]. In cerebellar slices, 5-HI enhanced ACh-induced frequency increases of excitatory post-synaptic currents mediated by glutamate [366]. PNU-120596 (10 μM) potentiated α7 induced increases in [^{3}H]-D-aspartate release from prefrontal cortex synaptosomes, as well as [^{3}H]-dopamine release from prefrontal cortex *in vitro* and *in vivo* [367]. The nicotinic facilitation of long-term potentiation was enhanced by PNU-120596 [368] and JNJ-1930942 [321] in rat dentate gyrus. Physiological concentrations of choline (~10 μM) and 1-5 μM PNU-120596 activated α7-containing receptors in tuberomammillary neurons and hippocampal CA1 pyramidal neurons sufficiently to depolarize a cell and facilitate the firing of action potentials [217, 369].

Supporting the potential therapeutic significance of these *in vitro* assays, NS-1738 [317] and CCMI [316] have been shown to enhance performance in behavioral measures of cognitive function; and CCMI [316], PNU-120596 [318, 319], SB-206553 [320], A-867744 [319], and JNJ-1930942 [321] have been shown to reverse auditory gating deficits in drug-induced or DBA/2 models with systemic administration to rodents,

indicating that these PAMs have sufficient pharmacokinetic properties to modulate brain $\alpha 7$ *in vivo* and that a sufficient level of endogenous agonist is present in relevant brain regions. Pharmacokinetic studies generally suggest that brain concentrations of PAMs are low compared to the EC_{50} for potentiation determined *in vitro* [316, 317, 319, 321]. However, since $\alpha 7$ has an intrinsically low P_{open}, even modest potentiation of $\alpha 7$-mediated signals may be sufficient to produce significant *in vivo* effects. A recent study has provided evidence that simultaneous modulation of $\alpha 5$ $GABA_A$ and $\alpha 7$ nicotinic receptors may function to synergistically enhance long-term potentiation in rodent brain slices and memory-related behavior *in vivo* [370]. This study provides proof-of-concept evidence that molecules engineered to modulate multiple targets might provide an optimized approach for specific therapeutic purposes.

Activation of $\alpha 7$ can have either protective or toxic effects depending on the mode of stimulation [227]. Positive allosteric modulators have been identified which increase the open probability of $\alpha 7$ by several orders of magnitude, inviting the question of whether PAMs may take the activation of this receptor subtype, which has high permeability to the natural catalytic ion calcium, to dangerously high levels. Calcium-mediated toxicity has been reported in SH-SY5Y cells and mice expressing mutant forms of $\alpha 7$ that display dramatically prolonged responses after stimulation [371-373]. *In vivo* toxicity profiles for PAMs are lacking, but there are some *in vitro* experiments that suggest type I and type II PAMs may have different profiles. Ng *et al*., 2007 showed that 24-hour exposure to the type I PAM CCMI did not reduce the viability of SH-SY5Y cells, whereas the type II PAM PNU-120596 did under the same conditions and in a MLA-sensitive manner [316]. Prior to the toxicity assays the authors tested the

cells to verify the presence of functional receptors and successful modulation by PNU-120596 and CCMI. A similar experiment with stable $\alpha 7$-expressing GH4C1 cells showed that the type II PAM PNU-120596 was toxic, while JNJ-1930942 was not toxic in the same paradigm [321]. However, Hu *et al*., 2009 failed to detect toxic effects in undifferentiated PC12 cells and cortical neurons after treatment with the type I PAM CCMI, but they also did not detect any toxic effects with the type II PAMs PNU-120596 or A-867744 [374]. The reason for the contradictory results is unclear, but two shortcomings of this study are that functional $\alpha 7$ expression and potentiation were indirectly evaluated, and only one agonist, PNU-282987, was tested at only one concentration, 10 μM.

CHAPTER 3
METHODS

cDNA Clones

Human nAChR receptor clones were obtained from Dr. Jon Lindstrom (University of Pennsylvania, Philadelphia PA). The human ric3 clone was obtained from Dr. Millet Treinin (Hebrew University, Jerusalem Israel) and co-expressed with $\alpha 7$ to improve the levels and speed of receptor expression [375]. Mouse muscle nAChR $\alpha 1$, $\beta 1$, γ, and δ clones used for receptor expression in *Xenopus* oocytes were obtained from Dr. Jim Boulter (UCLA, Los Angeles, CA), and the mouse ε clone was provided by Dr. Paul Gardner (University of Massachusetts Medical School, Worcester, MA). The mouse muscle cDNA clones in pRBG4 used for transfection of BOSC23 cells were obtained from Dr. Steven Sine (Mayo Clinic, Rochester, MN). The red fluorescent protein clone, pDsRed-N1, was obtained from Clontech (Palo Alto, CA) and used to identify successfully transfected BOSC23 cells.

Chemicals

Solvents and reagents were purchased from Sigma-Aldrich Chemical Company (St. Louis, MO), and Fisher scientific (Pittsburg, PA). 4OH-GTS-21 was obtained from Taiho (Tokyo, Japan). AR-R17779 was provided by Critical Therapeutics, Inc. (Lexington, MA). MTSEA was purchased from Toronto Research Chemicals Inc. (North York, ON, Canada). PNU-120596 was synthesized by Dr. Jingyi Wang as described in [376]. [^{125}I] α-bungarotoxin was kindly provided by Dr. Ralph Loring (Northeastern University, Boston, MA). Unlabeled α-bungarotoxin was purchased from Biotoxins, Inc. (Saint Cloud, FL). Cell culture supplies were purchased from Life Technologies (Grand Island, NY). Fresh ACh and MTSEA stock solutions were made each day of

experimentation. MTSEA stock solutions were made in water, kept on ice, and diluted just before experiments. PNU-120596 stock solutions were prepared in DMSO, stored at -20º C, and used for 30 days. PNU-120596 solutions were prepared fresh each day at the desired concentration from the stock in saline solution.

Site-Directed Mutations

Mutations of selected amino acids were introduced using the QuikChange kit from Stratagene (La Jolla, CA) according to the manufacturer's instructions. Sequences were confirmed with automated fluorescent sequencing at the University of Florida core facility.

Preparation of RNA for Injections into *Xenopus* laevis Oocytes

Subsequent to linearization and purification of cloned cDNAs, cRNA transcripts were prepared *in vitro* using the appropriate mMessage mMachine kit from Ambion Inc. (Austin, TX).

Expression in *Xenopus* laevis Oocytes

Mature (>9 cm) female *Xenopus* laevis African frogs (Nasco, Ft. Atkinson, WI) were used as the source of oocytes. Frogs were maintained in the Animal Care Services facility of the University of Florida, which is fully accredited by the Association for Assessment and Accreditation of Laboratory Animal Care, and the University of Florida Institutional Animal Care and Use Committee approved all procedures. Prior to surgery, frogs were anesthetized by placing the animal in a 1.5 g/L solution of 3-aminobenzoic acid ethyl ester (Sigma, St. Louis, MO) for 30 minutes. Oocytes were removed from an abdominal incision. In order to remove the follicular cell layer, harvested oocytes were treated with 1.25 mg/mL collagenase (Worthington Biochemical Corporation, Freehold, NJ) for 2 hours at room temperature in calcium-free Barth's

solution (88 mM NaCl, 1 mM KCl, 2.38 mM $NaHCO_3$, 0.82 mM $MgSO_4$, 15 mM HEPES (pH 7.6), 12 g/L tetracycline). Subsequently, stage 5 oocytes were isolated and injected with 50 nl (5-20 ng) each of the appropriate subunit cRNAs. Wild type and mutant $\alpha 7$ receptors were routinely co-injected with the cDNA for human ric3, an accessory protein that improves and accelerates $\alpha 7$ expression [377] without affecting the pharmacological properties of the receptors. RNA for $\alpha 4\beta 2$ receptor subunits were injected at an α:β ratio of 1:1. Note that the injection of $\alpha 4$ and $\beta 2$ subunits into the oocytes at a ratio of 1:1 results in a mixture of $(\alpha 4)_2(\beta 2)_3$ and $(\alpha 4)_3(\beta 2)_2$ stoichiometries [378]. Muscle-type receptor cRNAs were injected in the ratio of 2α:1β:1δ:1γ or 1ε. Recordings were made 1 to 10 days after injection.

Two-Electrode Voltage Clamp Electrophysiology

Experiments were conducted using OpusXpress 6000A (Molecular Devices, Union City, CA) [379]. OpusXpress is an integrated system that provides automated impalement and voltage clamp of up to eight oocytes in parallel. Oocytes were perfused with Ringer's solution (115mM NaCl, 2.5mM KCl, 1.8mM $CaCl_2$, 10mM HEPES, 1 μM atropine, pH 7.2), and agonist solutions were delivered from a 96-well plate via disposable tips, which eliminated any possibility of cross-contamination. Drug applications alternated between ACh controls and experimental applications. Perfusion flow rates were set at 2 mL/min for experiments with $\alpha 7$ receptors and 4 mL/min for other subtypes. Unless otherwise indicated, drug applications were 12 s in duration followed by 181 s washout periods with $\alpha 7$ receptors and 6 s with 241 s washout periods for other subtypes. Oocytes were voltage-clamped at a holding potential of -60

mV. Data were collected at 50 Hz and filtered at 20 Hz. Both the voltage and current electrodes were filled with 3 M KCl.

Responses of non-α7 wild type and mutant receptors are reported as peak currents, and responses of α7 wild type and mutant receptors are calculated as net-charge [214]. Each oocyte received two initial control applications of ACh, and thereafter was rechallenged with ACh at the control concentration following each experimental drug application. For experiments with wild type α7 and mutant α7 receptors, the control ACh concentration was 300 μM; except in the case of α7W55Y the ACh control was 30 μM because this mutant could not be activated repeatedly by 300 μM ACh without rundown. For experiments with non- α7 subtypes control applications of ACh were 30 μM; except in the case of α4W149β2 mutants control ACh applications were 100 μM ACh. The peak amplitude and the net charge [214] of experimental responses were calculated relative to the preceding ACh control responses in order to normalize the data, compensating for the varying levels of channel expression among the oocytes. For the experiments in chapter 3, the standard MTSEA treatment in the oocyte experiments was 2 mM applied for 60 s, a treatment that appears to produce a maximal effect on receptors expressed in *Xenopus* oocytes [380].

Means and standard errors were calculated from the normalized responses of at least four oocytes for each experimental concentration. For concentration-response relationships, data were plotted using Kaleidagraph 3.0.2 (Abelbeck Software; Reading, PA), and curves were generated as the best fit of the average values to the Hill equation, Response = $(I_{max}[agonist]^n)/([agonist]^n + (EC_{50})^n)$, where I_{max} denotes the

maximal response for a particular agonist/subunit combination, and n represents the Hill coefficient. I_{max}, n, and the EC_{50} were all unconstrained for the fitting procedures except in the case of the ACh concentration-response curves. Because ACh is the reference full agonist, the data were normalized to the observed ACh maximum, and the I_{max} of the curve fits were constrained to equal 1. Error estimates of the EC_{50} values are the standard errors of the parameters based on the Levenberg-Marquardt algorithm used for the generation of the fits [381]. Although some $\alpha4\beta2$ concentration-response curves were not ideally fit by the single-site Hill equation, presumably because $\alpha4\beta2$ receptors expressed from RNA injected at a $\alpha4$:$\beta2$ ratio of 1:1 resulted in $\alpha4\beta2$ receptors of mixed stoichiometry [378], in most cases the single-site Hill equation provided better concentration-response curve fits than the double-site Hill equation, and so for consistency, single-site fits were generated for all $\alpha4\beta2$ data sets.

Transient Transfection of BOSC23 Cells

BOSC23 cells obtained from American Type Culture Collection (Manassas, VA) were cultured at 37°C, 5% CO_2 in DMEM supplemented with 10% fetal bovine serum (FBS) in the absence of antibiotics. Cells were not used for more than 35 passages. One day prior to transfection, cells were plated onto 12 mm glass coverslips (Fisher Scientific, Pittsburgh, PA) coated with poly-D-lysine (Sigma, St. Louis, MO). Cells were transiently transfected using Fugene 6 (Roche, Indianapolis, IN) according to the manufacturer's instructions. In the transient transfection of the mouse fetal muscle-type receptors, 1 μg of mouse fetal muscle-type receptor cDNA (2α:1β:1γ:1δ) in pRBG4 with 0.8 μg of the cDNA encoding red fluorescent protein in pDsRed (Clontech, Palo Alto, CA) were added to each 35 mm dish containing cells and coverslips. In the transient

transfection of the human α7 nAChR, 1 μg, 0.3 μg, and 0.8 μg of plasmids containing cDNA clones of hα7, hric3, and DsRed, respectively, were added to each 35 mm dish containing cells and coverslips. Experiments were performed 48 to 72 hours after transfection. The red fluorescent protein was used as a marker to identify successfully transfected cells.

Generation of HEK293 Cells Stably Expressing Human α7 and Human ric3

Low passage number HEK293 cells were obtained from ATCC (Manassas, VA). In order to create a HEK293 stably expressing the hα7 nAChR, two rounds of stable transfection were performed. First, cell lines were transfected with either hric3 or hα7 and several (>20) clones that were resistant to 0.15 mg/mL hygromycin (resistance conferred by pcDNA3.1/ric3 vector) or 0.5 mg/mL G418 (resistance conferred by pCiNeo/α7 vector) were isolated using cloning cylinders (Sigma, St Louis, MO) and expanded. The transfections were performed with Fugene HD (Roche, Indianapolis, IN) according to manufacturer's directions. The day before transfection, 125,000 cells were plated in 35 mm dishes. One μg of circular pcDNA3.1 plasmid containing the hric3 gene or 2 μg of circular pCiNeo plasmid containing the human α7 gene were used in transfection. Following the selective period, the hygromycin-resistant cell lines and G418-resistant cell lines were maintained in normal growth media supplemented with 0.15 mg/mL hygromycin and 0.5 mg/mL G418, respectively. Total RNA was extracted using the SV Total RNA Isolation System (Promega, Madison, WI) and the expression of hric3 or α7 mRNA was determined by RT-PCR. The upper and lower primers for hα7, respectively, were TGGACGTGGATGAGAAGAA and TTCCCACTAGGTCCCATTC, resulting in an expected product size of 414 base pairs.

The upper and lower primers for hric3, respectively, were CCGATTTCCACCTATGATG and GGCTGCTTCTGTCTCCTTC, resulting in an expected product size of 346 base pairs. The upper and lower primers for GAPDH, respectively, were ACGGATTTGGTCGTATTGG and TGGCATGGACTGTGGTCAT, resulting in an expected product size of 516 base pairs. None of the antibiotic resistant and PCR-positive clones for ric3 or α7 responded to co-applications of ACh and PNU-120596 in patch-clamp electrophysiology experiments. However, responses from these cells were observed when stably expressing α7 cells were transiently transfected with ric3 only, or vice-versa, when stable ric3 cell lines were transiently transfected with α7 alone (not shown). The process of transfection, selection, cloning, and expansion was repeated using a stable HEK-hric3 expressing cell line as the starting point. The hric3-expressing cell line was transfected with 2 μg of circular pCiNeo/hα7 plasmid. The cells were selected using 0.45 mg/mL G418 and 0.015 mg/mL hygromycin, and thereafter maintained in the same concentration of selective antibiotics. Ten colonies were eventually cloned that were resistant to both hygromycin and G418 and were also positive for both human ric3 and human α7 mRNA by RT-PCR. These cell lines were subsequently screened for functional α7 channel expression through whole-cell patch clamp electrophysiology. The clone (clone 10) that showed highest functional channel expression, and was easiest to patch-clamp, was selected for use in all of the following studies. This cell line will be referred to as HEK-hα7/hric3. For normal passaging, cells were dissociated with a trypsin-free solution containing 0.02% EDTA in calcium- and magnesium-free Hank's balanced saline solution (HBSS) to avoid non-selective damage to the α7 nAChRs expressed on the cell surface. For electrophysiology

experiments, cells were plated on poly-D-lysine-coated cover slips and were used 1-5 days after plating for experiments.

Immunoprecipitation and Western Blot

Three days prior to preparing the sample for western blotting, 50,000 cells were plated in a 12-well plate treated with poly-D-lysine. Cells were washed with ice cold 1% PBS, lysed (lysis buffer, protease inhibitor, and phosphatase inhibitor), scraped off the 12- well plate, and transferred into 1.5 mL tubes. The cells were then sonicated on ice and incubated overnight at 4°C with primary antibody ab848, courtesy of Dr. Cecilia Gotti (University of Milan, Italy). The antigen-antibody complexes were incubated with 50µL of pre-washed protein A magnetic beads (Millipore, Billerica, MA). After washing, immunoprecipitated protein underwent denaturing elution with sample buffer followed by heating to 80°C for 10 minutes. 40 µL were loaded into each well and underwent SDS-polyacrylamide gel electrophoresis using 10% polyacrylamide, using 1µL of MagicMarkXP (Life Technologies, Grand Island, NY).

Protein was transferred overnight at 4°C onto a PVDF membrane. Transfer was confirmed by staining the PVDF membrane with Ponceau-S (Bio-Rad, Hercules, CA) and the gel with coomassie blue. Ponceau-S was removed from the membrane using TBS-T. Membrane was blocked at room temperature with 5% bovine serum albumin (BSA). Overnight incubation at 4°C of the primary antibody ab849 courtesy of Dr. Cecilia Gotti (University of Milan, Italy) was followed by washing the membrane in TBS-T, and incubating it with secondary antibody (Abcam, Cambridge, MA) for one hour at room temperature. After washing again with TBS-T, Super Signal (Thermo Fisher Scientific, Waltham, MA) was added to visualize the protein using the ChemiXRS+ imaging system (Bio-Rad, Hercules, CA).

Fluorescence Microscopy

Untransfected HEK293, HEK-hα7/hric3, HEK-hα7, and HEK-hric3 cells were plated on square glass coverslips (Fisher Scientific, Waltham, MA) coated with poly-D-lysine and incubated at 37%/5% CO_2 in DMEM media with 10% FBS containing the appropriate selective antibiotic for 24 hours prior to imaging. Cells were treated with 1 μg/mL (~125 nM) of Alexa488-α-bungarotoxin (Life Technologies, Grand Island, NY) for 45 minutes at 37C/5% CO_2. For a control, the HEK-hα7/hric3 was also pre-incubated with 1 mM nicotine, and then 1 μg/mL Alexa488-α-bungarotoxin was co-applied with 1 mM nicotine. After the incubation, the cells were carefully rinsed 4 times PBS to remove any excess Alexa488-α-bungarotoxin. The cells were then fixed with 4% (v/v) formaldehyde in PBS for 15 minutes, and washed 3 more times with PBS before being mounted on coverslips for imaging using VectaShield (Vector Laboratories, Burlingame, CA) mounting media containing the nuclear stain DAPI. The slides were imaged immediately using an Olympus DSU-IX81 spinning disc confocal microscope. The images were obtained using a Hamamatsu C4742-80-12AG Monochrome CCD Camera.

Equilibrium Radioligand Binding Assay

Two to three days prior to binding assays cells were plated in poly-D-lysine treated 24-well dishes. Experiments were performed when the cells were ~60-80% confluent. The growth media was removed and cells were washed one time with Dulbecco's phosphate buffered saline (DPBS; Life Technologies, Grand Island, NY). [^{125}I] α-bungarotoxin containing-solutions (0.05 nM-7 nM) were added to the cells and incubated at room temperature for 3 hours. Non-specific binding was determined with

the addition of 1 μM unlabeled α-bungarotoxin in separate wells. After the 3 hour incubation, the radioligand was removed and the cells were washed three times with cold DPBS. The cells were then solubilized with 0.1 M NaOH/0.1% SDS and samples were counted in a gamma counter (Beckman Coulter, Brea, CA). Saturation binding curves were fit to the equation, B_{max}[ligand]/(EC_{50} + [ligand]), with Kaleidagraph 3.0.2 (Abelbeck Software; Reading, PA). Each condition was tested in triplicate in each experiment, and each experiment was repeated three independent times.

Cytotoxicity Experiments

The cells were maintained in normal growth medium, and experiments were completed in HBSS (Life Technologies, Grand Island, NY). One day prior to performing the toxicity studies, two sets of HEK-hα7/hric3 cells from the same passage together with two sets of untransfected HEK293 cells from the same passage were plated in 96-well plates at a density of 15,000 cells per well in normal growth medium grown at 37° C/5% CO_2. Experimental solutions were prepared in HBSS and applied to the cells. One set of HEK-hα7/hric3 cells and untransfected HEK293 cells were placed in an incubator set to 28°C/5% CO_2 and the other set of HEK-hα7/hric3 cells and untransfected HEK293 cells were placed in an incubator set to 37°C/5% CO_2. Incubations with experimental treatments were 2 hours since maximal toxicity occurred within 2 hours, as determined from separate experiments evaluating the onset of toxicity at various time points during 24 hours following treatments. Following the 2 hour treatment period, the experimental solutions were replaced with 100 μL HBSS and 20 μL per well of CellTiter96 solution (Promega, Madison, WI) and incubated for 2-4 hours at 37C with 5% CO_2 after which absorbance readings were made with a microplate

spectrophotomer at 490 nm (BioTek, Winooski, VT). Each condition in an experiment was tested in triplicate and experiments were repeated on at least 3 independent occasions. Background absorbance was measured from cell-free wells and subtracted from all control and experimental test conditions. Absorbance readings from experimental test conditions were normalized to the absorbance values of untreated/DMSO-vehicle controls, which were defined as 100% cell viability. The DMSO was used to dissolve PNU-120596, which is insoluble in water. The highest concentration of DMSO applied with PNU-120596 was limited to 0.3%, and this occurred in the 30 μM PNU-120596 condition. The 20% DMSO and 30 μM thapsigargin conditions were used as positive controls. Cells with fewer than 30 passages since transfection were used in all toxicity experiments.

Outside-out Patch Clamp Electrophysiology

Single-channel currents were recorded in the outside-out patch configuration using an Axopatch 200A amplifier (Molecular Devices, Union City, CA) at room temperature. Cells were bathed in an external solution containing (in mM): NaCl (165), KCl (5), $CaCl_2$ (2), glucose (10), HEPES (5), atropine (0.001), pH adjusted to 7.3 with NaOH. Patch pipettes (Sutter Instruments, Novato, CA) were pulled to a tip diameter of 1-2 μm, fire-polished to 5–10 MΩ, coated with SigmaCote (Sigma, St. Louis, MO), and filled with an internal solution containing (in mM): CsCl (147), $MgCl_2$ (2), $CaCl_2$ (1), EGTA (10), HEPES (10), Mg-ATP (2), pH adjusted to 7.3 with CsOH. No correction was made for the liquid junction potential, which was calculated to be 4.6 mV. Recordings were low-pass filtered to 10 kHz with the built-in amplifier filter (4-pole Bessel) and digitized at 100 kHz with a DigiData 1440 (Molecular Devices, Union City, CA) using Clampex 10

data acquisition software (Molecular Devices, Uniion City, CA). Multiple recordings for each experimental condition were obtained from several transfection and recording dates.

Rapid drug application to outside-out patches was performed in a similar manner as described by [382] and [383]. Theta glass (Sutter Instruments, Novato, CA) was pulled, scored, and then broken by hand to create an application pipette with a diameter of ~120 μM (septum thickness: ~ 10 μM). The application pipette was mounted to a Burleigh piezoelectric stepper (EXFO, Ontario, Canada). The signal sent by Clampex 10 (Molecular Devices, Union City, CA) to the piezoelectric stepper was conditioned by an RC circuit (τ = 2 ms) to reduce oscillations and avoid damage to the crystal [384].

Two solution reservoirs (60 mL Monoject syringes; Sherwood Medical, St. Louis, MO) were connected to each channel of the theta glass application pipette via polyethylene tubing. Flow rates from each reservoir and channel of the drug application pipette were equivalent. Solution exchange times were typically 0.4-0.7 ms (10%-90% rise-times) and were routinely determined by movement of diluted external solution over an open recording pipette. To maintain undisturbed laminar flow from the application pipette and minimize solution mixing, external saline solution was continuously perfused through the recording chamber (Warner Instruments, Hamden, CT) and the application pipette was positioned such that streams flowing from it would directly enter the aspiration port of the chamber. In addition, the tip of the application pipette was kept free of dirt and/or cell debris by periodic cleaning in a hydrochloric acid solution. All solutions were de-gassed under vacuum and passed through a 0.2 μm filter to reduce the probability of particles/air bubbles obstructing solution flow and/or damaging the

outside-out patch. In the experiments with MTSEA and the MTSEA-sensitive mutants (Chapter 5), the chamber was completely emptied and thoroughly rinsed anytime MTSEA entered the chamber, whether the patch survived the entire protocol or not, and the coverslip of cells was replaced. Patches were not treated with MTSEA for the experiments in which 10 nM ACh was applied to $\alpha 1\beta 1\gamma\delta$L121C mutant receptors.

In the case of the experiments with the muscle-type nAChR (Chapter 5), all patch-clamp recordings were processed, idealized, and analyzed with Clampfit 10 (Molecular Devices, Union City, CA). Prior to any analysis, each recording was additionally low-pass filtered to 5 kHz with a software filter simulating an 8-pole Bessel filter, corrected for baseline drift, and any recorded artifacts or spurious noise were removed. The 5 kHz filter frequency was selected as a compromise between reliable event detection and total bandwidth. A resolution limit of 1.3 x filter rise-time was set at 86 μsec and imposed on all recordings [385]. Absolute P_{open} (NP_{open}) values were used as the primary measure of response to ACh for the outside-out patch-clamp experiments, in a manner analogous to the net charge measurements made from responses by receptors expressed in *Xenopus* oocytes. The NP_{open} value was computed for an entire response to ACh, including the non-stationary phase of activation by,

$$\mathrm{NP_{open}} = \frac{1}{iD}\int_0^D I(t)dt$$

where *I* is the recorded current relative to baseline, *t* is time, *i* is the mean single-channel amplitude, and *D* is the duration of the ACh application. No attempt was made to estimate P_{open} for an individual channel since the total number of activatible channels in a patch could not be known with any degree of certainty, and because each patch

served as its own control. Therefore, no kinetic information relating to a single channel is intended by the macroscopic NP_{open} measurement.

Single-channel recordings were idealized with half-amplitude idealization. When simultaneous channel openings occurred, segments of data containing single-channel activity were selected so that non-conducting flanking regions were ≥ 50 ms. Apparent subconductances occurred occasionally, but were ignored since they were not obvious in all traces and since they appeared to occur independently of MTSEA treatment. Data from at least 4 individual patches from each condition were pooled together to obtain sufficient numbers of events for analysis. Burst analysis was conducted with the intention of defining groups of one or more apparent channel openings that arise from an individual channel. Apparent channel openings separated by a closed interval less than the defined t_{crit} of 3.4 ms were called a burst of openings. The t_{crit} value was calculated based on the equation, $e^{-t_{crit}/\tau_{fast}} = 1 - e^{-t_{crit}/\tau_{slow}}$, which misclassifies equal proportions of short and long intervals, from fit time constants of the closed duration histogram of non-MTSEA treated $\alpha 1\beta 1\gamma\delta$L121C receptors [386, 387]. The t_{crit} value determined for wild type $\alpha 1\beta 1\gamma\delta$ receptors was 3.1 ms; small variations in t_{crit} values did not lead to significant changes in burst durations and for consistency the t_{crit} value of 3.4 ms applied to the wild type recordings. The value of t_{crit} for $\alpha 1\beta 1\gamma\delta$L121C patches that received 10 nM ACh was defined as 3.8 ms by the same method.

In the case of experiments performed with the human $\alpha 7$ nAChR (Chapter 6), patch-clamp recordings were analyzed with Clampfit 10 (Molecular Devices, Union City, CA) and QuB (University at Buffalo, Buffalo, NY) software. Sections of data traces with minimal simultaneous openings and flanked by ≥ 100 ms of closed time were selected

for analysis. Following initial periods of multi-channel openings, single-channel bursts potentiated by PNU-120596 occurred in very obvious groups of openings that were separated by long silent periods. This characteristic eliminated the ambiguity that is normally associated with defining a burst delimiter value or t_{crit} used in burst analysis of single-channel recordings [387]. The t_{crit} value used to determine average burst duration intervals was 150 ms; large variations in this value had minimal impact on the outcome of burst analysis. To determine intraburst closure, subconductance, and open durations, a total of 40 protracted bursts were selected at random for careful idealization. Data traces were idealized within QuB using the segmental k-means method [388] and were idealized at a bandwidth of 10 kHz, but the sampling rate was reduced from 100 kHz to 30 kHz to improve the quality of idealization since segmental k-mean idealization is generally optimized at or near the Nyquist frequency (F. Sachs, personal communication via QuB user forum). Following the automated idealization, the fit was manually inspected event-by-event and corrections were made as necessary to the idealization. A temporal resolution limit of 1.3 x filter rise-time was set at 40 μsec and imposed in all analyses.

Whole-cell Patch Clamp Electrophysiology

Whole-cell recordings were recorded using an Axopatch 200 amplifier (Molecular Devices, Union City, CA). In the experiments that involved temperature adjustments, the temperature was controlled with a Warner TC-324B temperature controller (Warner Instruments, Hamden, CT). Cells were bathed in an external solution containing (in mM): NaCl (165), KCl (5), $CaCl_2$ (2), glucose (10), HEPES (5), atropine (0.001), pH adjusted to 7.3 with NaOH. Patch pipettes (Sutter Instruments, Novato, CA) were

pulled to a tip diameter of ~2 μm, fire-polished to approximately 5 MΩ, and filled with an internal solution containing (in mM): CsCl (147), $MgCl_2$ (2), $CaCl_2$ (1), EGTA (10), HEPES (10), Mg-ATP (5), pH adjusted to 7.3 with CsOH. Cells were held at -70 mV. Recordings were low-pass filtered to 5 kHz and digitized at 50 kHz with a DigiData 1440 or DigiData 1322A (Molecular Devices, Union City, CA) using Clampex data acquisition software (Molecular Devices, Union City, CA). A 10 ms test pulse of -10 mV was used to determine access and input resistances prior to each response. For experiments performed at room temperature, whole-cell recordings were analyzed if access resistances were < 40 megaOhms and membrane resistances were >200 megaOhms. On average, the access resistance, membrane resistance, and cell capacitance values were 15.8 ± 0.6 megaOhms, 1.55 ± 0.15 gigaOhms, and 55.2 ± 6.6 pF, respectively. For experiments evaluating the temperature-dependence of PNU-120596, these basic criteria were necessarily relaxed at 37°C. Sweeps with access resistance <40 megaOhms, input resistance >100 megaOhms, holding current < 700 pA were included in the analysis. No attempt was made to compensate for series resistance or for the liquid junction potential, although the liquid junction potential was calculated to be 4.7 mV.

For the ACh concentration-response and MLA inhibition curves in Figure 7-4 drug applications were made using a Burleigh piezoelectric stepper (EXFO, Ontario, Canada) in a similar manner as described above with the outside-out patches, but with a drug application pipette with a diameter of ~350 μm. Solution exchange times were 2.6 ± 0.8 ms as determined by measuring holding current shifts (10-90% rise-times) upon moving diluted external solution over an open recording pipette each day of experimentation.

The open recording pipette was positioned just above the surface of the recording chamber and in a similar arrangement relative to the drug application pipette that occurred during a whole-cell recording. It should be stated that the exchange time estimate measured in this manner is probably only a lower-limit (i.e. fastest time possible) of the solution exchange time achieved to a whole-cell during a recording. Three applications of 300 μM ACh were applied initially followed by 3 test applications of 1 μM - 3 mM ACh with 60 second interstimulus intervals. The responses from the initial 3 responses to 300 μM ACh were averaged, as were the 3 responses from the test concentration of ACh. The averaged response of each cell to the test ACh concentration was normalized to the averaged response to 300 μM ACh, to compensate for varying levels of receptor expression among individual cells. The normalized responses were subsequently adjusted to reflect the response relative to the maximal normalized ACh-evoked response, which was defined as 1, as described above with the oocyte experiments. Both peak current and net-charge responses were measured; net-charge responses were measured as the area under the activation curve during one second of ACh application. Means and standard errors were calculated from the responses of 4-8 cells at each test concentration. The concentration-response relationship was fit to the Hill equation using Kaleidagraph 3.0.2 (Adelbeck Software, Reading, PA) as described above. Experiments for the MLA inhibition curve were performed in a similar manner as the ACh concentration-response curve, with the initial concentration of ACh being 170 μM and test concentrations consisting of 170 μM co-application with 3 nM – 100 μM MLA. No pre-applications of MLA were made. Each data point represents the mean and standard error of 4-6 cells at each test

concentration and the concentration-response relationship was fit to the Hill equation using negative Hill slopes.

In all other whole-cell electrophysiology experiments, local applications of drug were made using single-barrel glass pipettes attached to a picospritzer (General Valve, Fairfield, NJ) with Teflon tubing (11.5-14.5 psi). The application pipette was placed within 10-15 μm of the cell body. Drug applications were 3 seconds in duration and were made every 60 seconds. Drugs applied with this method were determined to be diluted 1.5- fold by the time they reached the cell surface (Williams *et al*., in preparation). In the temperature experiments, 3 baseline responses were recorded at room temperature (23.5°C), after which responses were recorded as the temperature was increased to 37°C. Three responses were recorded at 37°C and then the temperature was returned to 23.5°C. Cells with responses that failed to recover to 50% of the baseline responses upon temperature reduction from 37°C to 23.5°C were excluded from analysis; 15 of 70 total cells failed to meet this criterion. Responses were measured as peak currents. In most cases, the currents recorded at 37°C were normalized to the initial baseline responses recorded at 23.5°C. In comparing the effect of BSA on potentiation by PNU-120596 at 37°C, responses are shown as both normalized currents and the absolute magnitude of evoked currents. To test for the statistical significance of BSA on PNU-120596 potentiation at 37°C, the sweeps obtained from each cell at 37°C were averaged to obtain one mean response from each cell at 37°C. The mean responses from cells recorded at 37°C either in the absence or presence of 30 μM BSA were then compared with a two-tailed student's t-test using Microsoft Excel (Microsoft, Redmond, WA).

CHAPTER 4
DIFFERENTIAL REGULATION OF RECEPTOR ACTIVATION AND AGONIST SELECTIVITY BY HIGHLY CONSERVED TRYPTOPHANS IN THE NICOTINIC ACETYLCHOLINE RECEPTOR BINDING SITE

Introduction

Sequence analysis of receptor subunits within the Cys-loop superfamily, all the way through to prokaryotic ligand-gated ion channels, illustrates remarkable conservation at select sites and implicate great functional significance to aromatic residues localized in the ligand binding domain (LBD) of receptors within the Cys-loop superfamily [389]. In nAChRs, W55 and W149 have been identified amongst other aromatic ring-containing residues as highly conserved throughout evolution and as contributors to the formation of a hydrophobic agonist binding pocket [84,118,390-396].

Several studies have shown that mutation of highly conserved aromatic residues typically results in decreased efficacy and/or potency for ACh and related ammonium compounds [397-400]. However, observations by Horenstein *et al*., 2007 suggest that mutation of conserved aromatic residues may not result in loss of receptor activity for all ligands, and conserved aromatic residues may differentially regulate receptor activation by select agonists. Specifically, the activation of human α7 nAChR by 4OH-GTS-21, an α7-selective agonist, is unaffected by mutation of Y188 to phenylalanine, while ACh potency is drastically reduced in the mutant α7 receptor. The effect of the homologous mutation was qualitatively different in heteromeric α4β2 receptors. While ACh potency was unaffected by the α4Y190F mutation, the efficacy of 4OH-GTS-21 relative to Ach was increased at least 200-fold in α4Y190Fβ2 receptors compared to wild type [401]. These findings suggest the assumption that all conserved residues play comparable roles in all receptor subtypes may be invalid.

The nAChR LBD is localized at the interface of two subunits; W55 and W149 (human α7 numbering) are found on opposing sides of this interface. In heteromeric receptors such as α4β2 and muscle-type receptors, W57 is found on the non-α subunit (complementary face) while W154 is found on the α subunit (primary face) contributing to the binding site. As might be expected, the only subunits in which α7W55 and β2W57 are not conserved are subunits that do not form the complementary face, while the only subunits in which α7W149 and α4W154 are not conserved are subunits that do not contribute to the primary face of an agonist binding site (Figure 4-1A). These tryptophans are both found in α subunits which can form homomeric receptors (α7 - α10) since these α subunits contribute to both the primary and complementary faces of binding sites in the homomeric receptor [402]. The crystal structure of AChBP isolated from *Lymnaea stagnalis*, which is homologous to the extracellular domain of a homomeric receptor [118], suggests the indole ring of the W at position 149 (human α7 numbering) is positioned vertically, deeper and slightly higher in the binding pocket relative to W55, which is positioned horizontally at the mouth of the aromatic pocket (Figure 4-1B).

In this study site-directed mutagenesis and heterologous expression in *Xenopus* oocytes are used to investigate the functional significance of α4W154, β2W57, α7W55, and α7W149 for the activation of homomeric and heteromeric neuronal nAChR by ACh and the structurally diverse α7-selective agonists choline, 4OH-GTS-21, and AR-R17779. The data suggest that nAChR are likely activated in different manners by structurally distinct agonists and provides insight regarding subtype selective activation of nAChR. In particular, some amino acid residues are critical for activation, like α7

W149 (and homologue in other nAChR subtypes), regardless of agonist while others may be involved in regulating subtype selectivity, like α7W55 and α7Y188.

Results

Before the results of this chapter are presented I want to make clear that my contribution to this work was to analyze, interpret, and present the current findings in context of previously published literature. Most of the experiments in this chapter were originally conceived by Dr. Papke and most of the data were collected by OpusXpress technicians of the Papke Laboratory.

Mutation of W55 or W57 of α7 and α4β2 Receptors, respectively, Alters the Pharmacology and Regulates the Selectivity of 4OH-GTS-21

Two general types of effects resulting from mutations in the nAChR LBD were anticipated. First, that there would be changes in the ability of ACh to promote channel activation; and second, that there would be differences in the relative efficacy of α7-selective agonists compared to ACh. Changes in relative efficacy were of particular interest since the primary goal was to test the hypothesis that α7-selective agonists may promote activation through mechanisms that are distinct from the activation mechanism invoked by ACh. While measurements of relative efficacy are readily obtainable from macroscopic currents as long as a reliable reference by which to measure efficacy is employed, effects on the absolute ability of ACh to promote activation are relatively difficult to measure from macroscopic currents since decreases in ACh-evoked responses may result from either decreased ACh activity or decreased receptor expression/assembly. An obstacle in this study for the application of traditional measurements of receptor expression, such as radioligand binding assays, is that mutations of highly conserved LBD residues are arguably equally likely to affect ligand

binding as receptor activation, potentially rendering results of binding experiments uninterpretable. For example, the α7L119C mutation, which is described in chapter 5, disrupts the binding the α-bungarotoxin.

Absolute Efficacy of ACh

With this limitation in mind, the effects of the mutations tested in this study were estimated relative to the absolute effectiveness of ACh to promote channel activation. The comparison was made based on the maximum ACh-induced currents from the mutant receptors to the maximum ACh-induced currents in wild type receptors that were injected the same day from the same harvest of oocytes with RNA of comparable amount and quality, as confirmed on denaturing gels. These measurements of maximal ACh-induced currents then formed the basis from which efficacies of choline, 4OH-GTS-21, and AR-R17779, relative to ACh responses in wild type and mutant receptors, were subsequently determined. Choline and AR-R17779 are considered full agonists of α7, activating α7 as efficaciously as ACh, while 4OH-GTS-21 is a α7-selective partial agonist. None of these drugs produce significant currents in α4β2 receptors (Figure 4-2).

As seen in Figure 4-3A, calculated ACh maximum responses for α7W55A and α7W55 to glycine mutants were approximately 2.5 times larger than for wild type, the α7W55 to valine mutant maximum was approximately equal to wild type, and α7W55Y and α7W55F had ACh maximum net-charge responses approximately one half as large as wild type α7.

Homologous mutations were made in β2. Wild type and β2 mutant subunits were co-expressed (1:1) with α4. As with the α7W55 mutants, the α4β2W57A, G, V, Y and F

mutants gave functional responses to ACh, and $\alpha4\beta2$W57 arginine, serine, and threonine mutants did not (Figure 4-3B and D). However, none of the $\alpha4\beta2$ mutant peak currents were as large as the wild type responses. The calculated maximum ACh responses of the functional mutants were on average approximately one tenth of the wild type calculated maximum ACh peak response (Figure 4-3C). Nonetheless, the ACh potencies were greater for some of the $\alpha4\beta2$W57 mutants than for the wild type (see Figure 4-5).

Relative Efficacy of $\alpha7$ Selective Agonists Compared with ACh

The mutation of $\alpha7$W55 to the non-aromatic amino acids A, G, and V resulted in reduced potencies for all the agonists tested (Figure 4-4A-C, Table 4-1). Although mutation of $\alpha7$W55 to G produced a decrease in the potency of ACh, choline, and AR-R17779 (22-fold, 14-fold, and >92-fold increases in EC_{50} values, respectively, Table 4-1), maximal responses to these agonist were larger than those of wild type receptors. Maximal ACh responses of $\alpha7$W55G mutants were about 2.5-fold higher than maximal ACh responses in wild type receptors (Figure 4-3A). Relative to the maximum ACh-induced currents in wild type and mutant receptors choline efficacy was increased in $\alpha7$W55G mutants (Figure 4-4B). A saturating I_{max} for choline relative to ACh was not possible to achieve due to the low potency of choline for the W55G mutant.

In contrast to the results seen with ACh and choline, $\alpha7$W55G receptors did not produce measurable responses to 4OH-GTS-21 in the concentration range tested. Mutation of $\alpha7$W55 to the other non-aromatic residues, A and V, likewise resulted in decreased agonist potencies, although the effects on potency were not as large as obtained with the mutation to G (Figure 4-4A and C, Table 4-1). 4OH-GTS-21, an $\alpha7$-

selective partial agonist, activated α7W55V mutants as efficaciously as ACh activated the mutant (Figure 4-4C). The relatively conservative mutation of W55 to tyrosine or phenylalanine did not significantly affect ACh potency, as EC_{50} values remained near 30 μM. However, the potencies of choline, 4OH-GTS-21, and AR-R17779 were all altered by these mutations (Table 4-1). Mutation of W55 to phenylalanine caused the EC_{50} of 4OH-GTS-21 to increase 6-fold (Figure 4-4D) and mutation of W55 to tyrosine yielded mutant α7 receptors that did not give detectable responses to 4OH-GTS-21.

The low efficacy of 4OH-GTS-21 for the W55G and W55Y α7 mutants is likely related to desensitization and/or channel block by 4OH-GTS-21. Residual inhibition by 4OH-GTS-21 in wild type α7 receptors was previously characterized [327] and was shown to represent a form of stabilized desensitization that is reversed by the application of the type II PAM PNU-120596. Although 4OH-GTS-21 was relatively ineffective at activating α7 W55G and W55Y mutant receptors, large currents occurred when 4OH-GTS-21 was applied with PNU-120596 (not shown). These observations suggest that 4OH-GTS-21 has access to the binding site in the α7 W55G and W55Y mutants, but that binding promotes PNU-120596- sensitive desensitization much more effectively than activation.

Homologous mutations in the LBD of α4β2 receptors (β2W57) produced qualitatively different results from the mutations made in α7. Mutation to glycine greatly reduced ACh potency in α7 receptors, but increased ACh potency in α4β2W57G mutants. Mutation of W55 to tyrosine in α7 receptors did not affect ACh potency, but ACh was twice as potent for α4β2W57Y mutants as for wild type receptors. ACh also had greater potency for α4β2W57F than for wild type α4β2. However, ACh had

significantly lower potency for α4β2W57A than for wild type α4β2. Neither choline nor AR-R17779 activated any of the α4β2 receptors (Figure 4-5A-E, Table 4-1). However, 4OH-GTS-21 did activate four of the α4β2W57 mutants and provided the most interesting differences amongst these W55 and W57 mutants of the α7-selective agonists tested. Note that maximal ACh responses of the α4β2 mutants were approximately one-tenth of the maximal responses in wild type receptors. While it is true that a selective compromise in ACh-mediated activation would have the tendency to make the relative efficacies of the experimental agonists appear increased, that effect would be manifested in the results of all experimental agonists normalized to the ACh responses. However, the data indicate that the increase in the relative efficacy of 4OH-GTS-21 is many times larger than that of either choline or AR-R17779, which were both immeasurable because currents induced by these drugs were too small to be determined. Therefore, the increased activation of α4β2 mutants by 4OH-GTS-21 is likely to represent a true potentiation of an activation mechanism potentially unique to 4OH-GTS-21 and related compounds. 4OH-GTS-21 activated wild type α4β2 only about 2% and wild type α7 46% as well as ACh (Figure 4-2B and C). 4OH-GTS-21 activated α4β2W57A, glycine, phenylalanine and tyrosine, but not α4β2W57V, arginine, serine, or threonine mutant receptors. Interestingly, 4OH-GTS-21 activated α7W55V mutants as well as ACh did. 4OH-GTS-21 activated α4β2W57A, phenylalanine, and glycine to 60-70% of their ACh maxima, with lowest potency in α4β2W57A and highest potency in α4β2W57Y and α4β2W57F mutants. Importantly, peak responses of α4β2W57Y to 4OH-GTS-21 were 2.5-fold greater than for ACh, while the homologous mutation in α7 decreased the relative efficacy of 4OH-GTS-21 greatly.

Mutation of W149 in Both α7 and α4β2 Receptors Reduced Receptor Activation by Both ACh and α7 Selective Agonists

Responses of α7W149 mutant receptors were significantly lower than those of wild type α7 receptors recorded the same number of days post-injection. Somewhat surprisingly, the relatively conservative mutations of α7W149 to F or Y disrupted receptor responses to ACh to levels below the limits of detection, while the non-conservative mutations to A or G yielded receptors that were capable of producing measurable ACh-induced currents. The α7W149V mutant receptors were also non-responsive to ACh (Figure 4-6A). Of the mutant receptors that were non-responsive to ACh, none were able to produce recordable currents in response to choline, 4OH-GTS-21, or AR-R17779, with the exception of α7W149F mutants, which reproducibly yielded small but measurable currents in response to choline (not shown). The fact that only two of the five α7W149 mutants were sufficiently functional for use in this study suggests that mutation introduced at position 149 may interfere with receptor assembly or with conformational changes linked to channel opening. The mutations introduced at position 149 in α7 resulted in drastically reduced potencies of ACh, choline, and AR-R17779 (Table 4-1). Mutation of α7W149 to glycine had profound effects on receptor activation, resulting in 13-, 20-, and 140-fold increases in EC_{50} values over those seen in wild type receptors for ACh, choline, and AR-R17779, respectively. However, neither α7W149A nor α7W149G mutant receptors had significantly altered potency for 4OH-GTS-21 compared to wild type. Compared to the maximum response of ACh in wild type receptors, the efficacy of choline fell 30% and the efficacy of 4OH-GTS-21 rose 50% in α7W149G mutants (Figure 4-6C and D, Table 4-1).

Alpha4W154β2 mutant receptors produced measurable ACh-induced currents when mutations to A, F or W were introduced, while currents were undetectable when G was introduced at position 149, roughly the opposite of what was observed in α7W149 mutants (Figure 4-7A and B). This observation is suggestive of intrinsic differences between the α7 and α4β2 LBDs. There was no functional expression of α4W154Gβ2 or α4W154Vβ2 mutant receptors detected; these mutants were also non-responsive to choline, 4OH-GTS-21, and AR-R17779 (not shown).

Mutation of α4W154 to A resulted in a 7-fold increase in the EC_{50} for ACh, while mutations to phenylalanine or tyrosine did not greatly alter ACh potency compared to wild type. Of the α4W154β2 mutants tested, none responded to choline, AR-R17779, or 4OH-GTS-21 (Figure 4-7C, D, and E). In general, a loss of receptor function was observed as a result of any mutation introduced at the W149 position, at least for the agonists we tested and mutations we introduced. Taken together, these results suggest the W55 position may better tolerate mutation than W149, and when mutated allows for major alterations in the receptor activation mechanisms, especially in regard to choline and 4OH-GTS-21.

Discussion

Numerous mutational studies of α7W55 and α7W149 (and homologous residues in other nAChR subtypes) and other conserved aromatic residues within the aromatic box of the nAChR LBD generally lead one to believe that mutation of conserved aromatic residues results in reduced receptor functionality. Building on evidence from a previous study, which showed that mutation of Y188 does not necessarily knock down

receptor functionality for all agonists, the functional significance of the conserved α7W55, β2W57, α7W149 and α4W154 residues was investigated.

Using unnatural amino acid substitutions in muscle-type nAChR at positions αW86, αW149, αW184, and γW55/δW57 with W derivatives containing various degrees of predicted cation interaction energies, αW149 has been shown to establish primary interactions with the quaternary ammonium group of ACh [107, 396]. Another implication of the data from Zhong *et al*., 1998 was that W55 may not directly stabilize the quaternary group of ACh through cation-π interactions, and the specific role of this residue in receptor activation remains an open question. In *Torpedo* receptors, mutation of γW55 to leucine reportedly reduced ACh affinity 7,000-fold, while similar mutation of δW57 resulted in only a 20-fold reduction. Double-mutant receptors (γW55L and δW57L) were reported to have reduced binding of many small agonists, including tetramethylammonium. Nicotine binding, however, was unaffected by the double-mutant receptors [400]. W55 was recently proposed to affect desensitization kinetics [403]. However, results of this study are inconclusive since α7 currents were measured as peak responses [214], mutation of W55 affected agonist potency which in turn alters the response waveform [404], and macroscopic currents alone are insufficient to determine kinetics of desensitization [405].

These data suggest that the conserved residues W149 and W55 have different functional significance in α7 nAChR. Mutations at the W55 residue appear to be relatively well tolerated since they provide subtype-dependent effects on channel activation, suggesting they may be important determinants of subtype selective activation by certain agonists. For example, the α7-agonist 4OH-GTS-21 lost efficacy in

α7W55 mutants relative to ACh while the same agonist gained efficacy, up to 300-fold compared to ACh, in some α4β2W57 and α4Y190Fβ2 mutants. The observation that α4β2 receptors gain function with 4OH-GTS-21 when W57 is mutated to smaller residues is consistent with the idea that the wild type receptor has unfavorable steric clashes with this compound. In the case of the α7 receptor, the interactions of 4OH-GTS-21 with W55 may be optimal, such that in general, making this position smaller in size results in less favorable binding and/or function.

In contrast to the variable effects of W55 mutations, W149 seems to serve a role that is universally important for receptor function regardless of agonist or receptor subtype. However, if W149 were solely responsible for stabilizing the ligand, one would expect to see total loss of receptor activity when this residue became incapable of forming cation-π interactions. Clearly this was not the case as non-aromatic α7 W149 mutant receptors still responded to agonists, and mutation to other aromatic residues actually produced receptors that were non-responsive to ACh. Other aromatic residues and non-aromatic residues found within the LBD probably help to stabilize and compensate for lost interactions resulting from mutation, or perhaps form an alternate set of interactions with ACh that are still capable of activating the receptor when the W149 is mutated. It seems likely that residues localized in the vicinity of the LBD may establish interactions with the ligand that place it in a position in which its ability to interact with the receptor and initiate changes in channel gating is regulated by conserved amino acids such as W55, W149, or Y188.

In the current study, 4OH-GTS-21 is the only agonist tested which efficaciously activated certain α4β2 mutants while losing α7 efficacy. Likewise, in the previous study

with Y188F mutants, anabaseine derivatives were the only α7 agonists tested that activated the mutant $\alpha4\beta2$ receptors, with 4OH-GTS-21 being the most efficacious by far [401]. These observations raise questions regarding how 4OH-GTS-21 activates nAChR. While it is possible that 4OH-GTS-21 may fit into the binding site of wild type $\alpha7$ and $\alpha4\beta2$ in different conformations, it is also likely that ligands such as ACh and 4OH-GTS-21 form different types of intermolecular interactions with residues in the protein, and thereby promote receptor activation in different ways. Investigations of AChBP bound with agonists and antagonists have led to the idea that channel opening and, possibly, ligand selectivity may occur through a conformation induced by the ligand which is due to the inherent flexibility of the binding site, allowing it to conform to the structural characteristics of the ligand [106]. A potentially important observation made by Dr. Nicole Horenstein is that ACh, choline, and AR-R17779 all contain sp^3 hybridized ammonium nitrogen atoms while the nitrogen atom thought to be important in 4OH-GTS-21 binding is sp^2 hybridized and flat. The difference in three-dimensional structure between choline, AR-R17779 and 4OH-GTS-21 may underlie some of the unique observations made in this study regarding 4OH-GTS-21.

Adding insight to the results presented here is the report that serotonin activates the highly homologous mouse 5-HT_3 and *C. elegans* MOD-1 receptors through formation of cation-π interactions at different W residues, at the position homologous to W149 in $5HT_3$ and at the position homologous to Y195 in MOD-1. In MOD-1 the residues at the positions homologous to 149 and 195 in α7 are Y and W, respectively [406]. Mutation of these residues suggested that both receptors make specific contacts with serotonin that regulate channel gating, but those specific contacts depend on the

nature of the binding site. These observations could be consistent with either hypothesis discussed above. Evolutionary pressures may have allowed some flexibility in the ability of conserved aromatic residues to act differentially in different receptors, or serotonin may be accommodating to the distinct binding domains, finding alternate ways to establish interactions that lead to receptor activation.

A

```
                                          D Loop                    B Loop
Q15822|ACHA2_HUMAN          EKNQMMTTNVWLKQEWSDYKLR      QQNCKMKFGSWTYDKAKIDLEQ
P32297|ACHA3_HUMAN          EVNQIMETNLWLKQIWNDYKLK      YQNCTMKFGSWSYDKAKIDLVL
P43681|ACHA4_HUMAN          EKNQMMTTNVWVKQEWHDYKLR      QQNCTMKFGSWTYDKAKIDLVN
P30532|ACHA5_HUMAN          EKNQLMTTNVWLKQEWIDVKLR      LQNCSMKFGSWTYDGSQVDIIL
Q15825|ACHA6_HUMAN          EVNQIMETNLWLRHIWNDYKLR      HQNCSLKFGSWTYDKAEIDLLI
P36544|ACHA7_HUMAN          EKNQVLTTNIWLQMSWTDHYLQ      VQHCKLKFGSWSYGGWSLDLQ-
Q9UGM1|ACHA9_HUMAN          ERNQILTAYLWIRQIWHDAYLT      NQQCNLTFGSWTYNGNQVDIFN
Q9GZZ6|ACH10_HUMAN          ERNQVLTLYLWIRQEWTDAYLR      AQHCGLTFGSWTHGGHQLDVRP
P17787|ACHB2_HUMAN          EREQIMTTNVWLTQEWEDYRLT      QQNCTMKFRSWTYDRTEIDLVL
Q05901|ACHB3_HUMAN          EKNQLMTTNVWLKQEWTDHKLR      RQNCSMKFGSWTYDGTMVDLIL
P30926|ACHB4_HUMAN          EREQIMTTNVWLKQEWTDYRLT      QQNCTLKFRSWTYDHTEIDMVL
Y00762|ACHA_HUMAN           EVNQIVTTNVRLKQQWVDYNLK      EQNCSMKLGTWTYDGSVVAINP
P11230|ACHB_HUMAN           EKDEEMSTKVYLDLEWTDYRLS      WQNCTMVFSSYSYDSSEVSLQT
Q07001|ACHD_HUMAN           EVEETLTTNVWIEHGWTDNRLK      WQNCSLKFSSLKYTAKEITLSL
Q04844|ACHE_HUMAN           EKEETLTTSVWIGIDWQDYRLN      WQNCSLIFRSQTYNAEEVEFTF
P07510|ACHG_HUMAN           EREEALTTNVWIEMQWCDYRLR      WQNCSLIFQSQTYSTNEIDLQL
P09482|ACHA4_CHICK          EKNQMMTTNVWVKQEWHDYKLR      QQNCKMKFGSWTYDKAKIDLVS
AJ250362|ACHB2_CHICK        EREQIMTTNVWLTQEWEDYRLT      QQNCTMKFRSWTYDRTEIDLVL
N957513|ACHA7_ZEBRAFISH     EKNQVLTTNIWLQLYWYDYYLQ      LQRCDLKFGSWTYGGWSLDLQ-
F21F3.5|unc-38_C.ELEGANS    EIDQIMTCSVWLKQTWIDRKLS      EQQCHLKFGSWTFSENLLSVEL
T08G11.5|unc-20_C.ELEGANS   EKDQVMHTNVWLTLQWHDFQMK      EQVCTLVFGSWTYNENEIKLEF
P58154|ACHBP_LYMST          EITNEVDVVFWQQTTWSDRTLA      -ATCRIKIGSWTHHSREISVDP
```

B

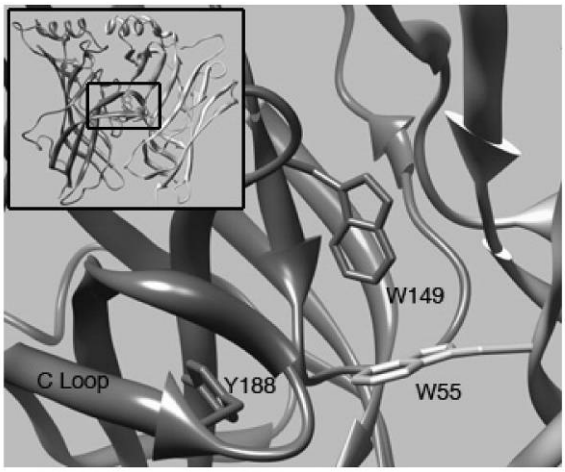

Figure 4-1. Multiple sequence alignment and hypothetical localization of α4W154, β2W57, α7W55, and α7W149. A) Closeup of the LBD from the crystal structure of AChBP isolated from L. stagnalis (PDB ID: 1i9B; [118]). Numbering of residues correspond to human α7 numbering. The image was produced using the UCSF Chimera package from the Resource for Biocomputing, Visualization, and Informatics at the University of California, San Francisco [407]. B) Alignment of human nAChR sequences with sample sequences from chick, C. elegans, and zebrafish show a high degree of conservation at both W residues throughout the nicotinic family and many species. Curiously, these tryptophans are also conserved in the α5 and β3 subunits, which have been proposed to occupy the accessory subunit position and not contribute directly to the agonist binding domain [132]. Sequence alignments were generated using ClustalW at www.ebi.ac.uk/Tools/clustalw2/index.html [408].

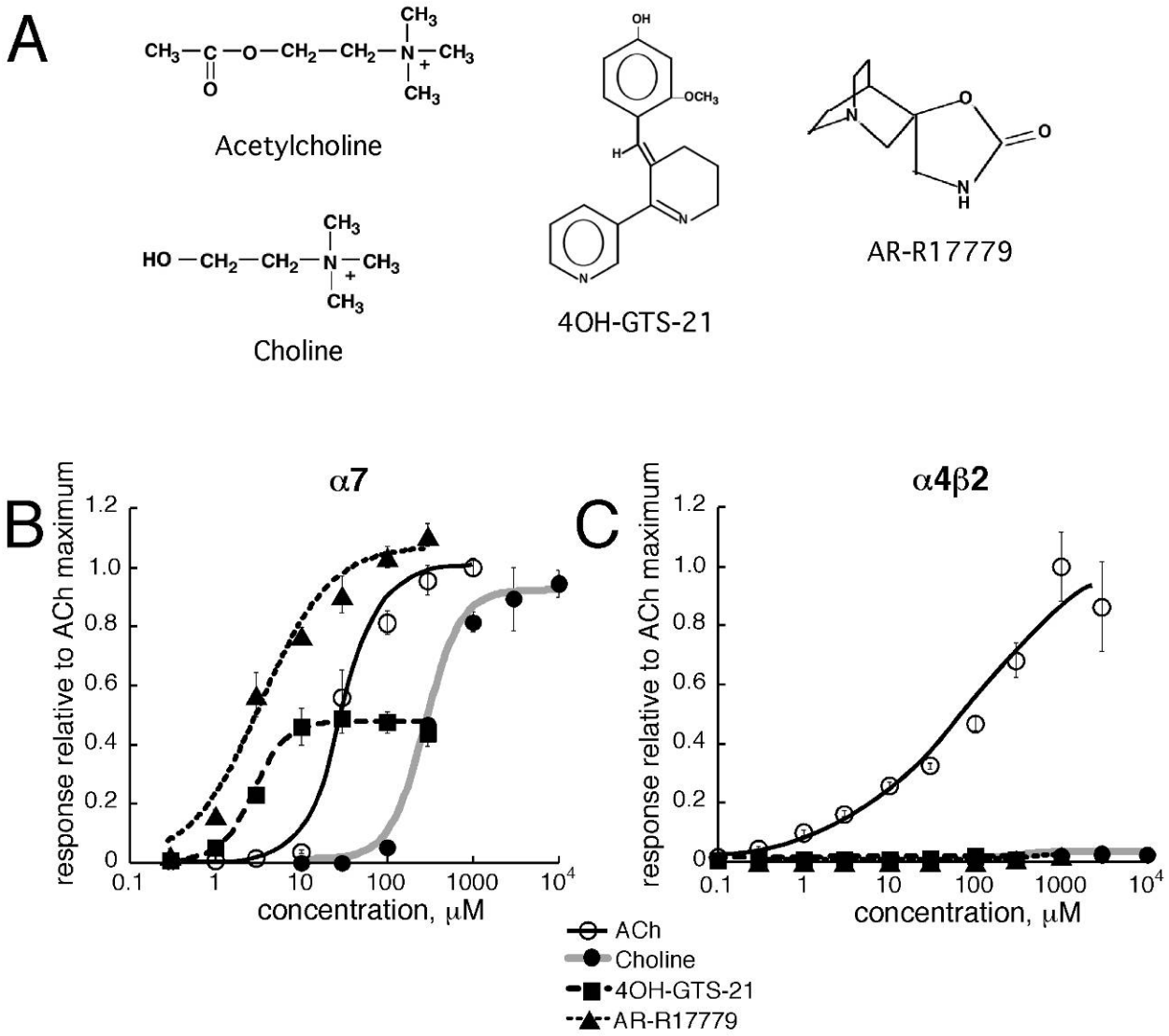

Figure 4-2. Concentration-response relationships of wild type α7 and α4β2 receptors to ACh, choline, 4OH-GTS-21, and AR-R17779. A) Chemical structures of the agonists used in this study. B) Net-charge responses of wild type α7. C) Peak responses of wild type α4β2. Each data point represents the mean ± SEM of at least four oocytes. For consistency the single site hill equation was used to fit the α4β2 curve since the single- site model provided the best fit for most α4β2 mutants in this study. There were no significant differences in chi square or R values between fits by the single-site or biphasic models.

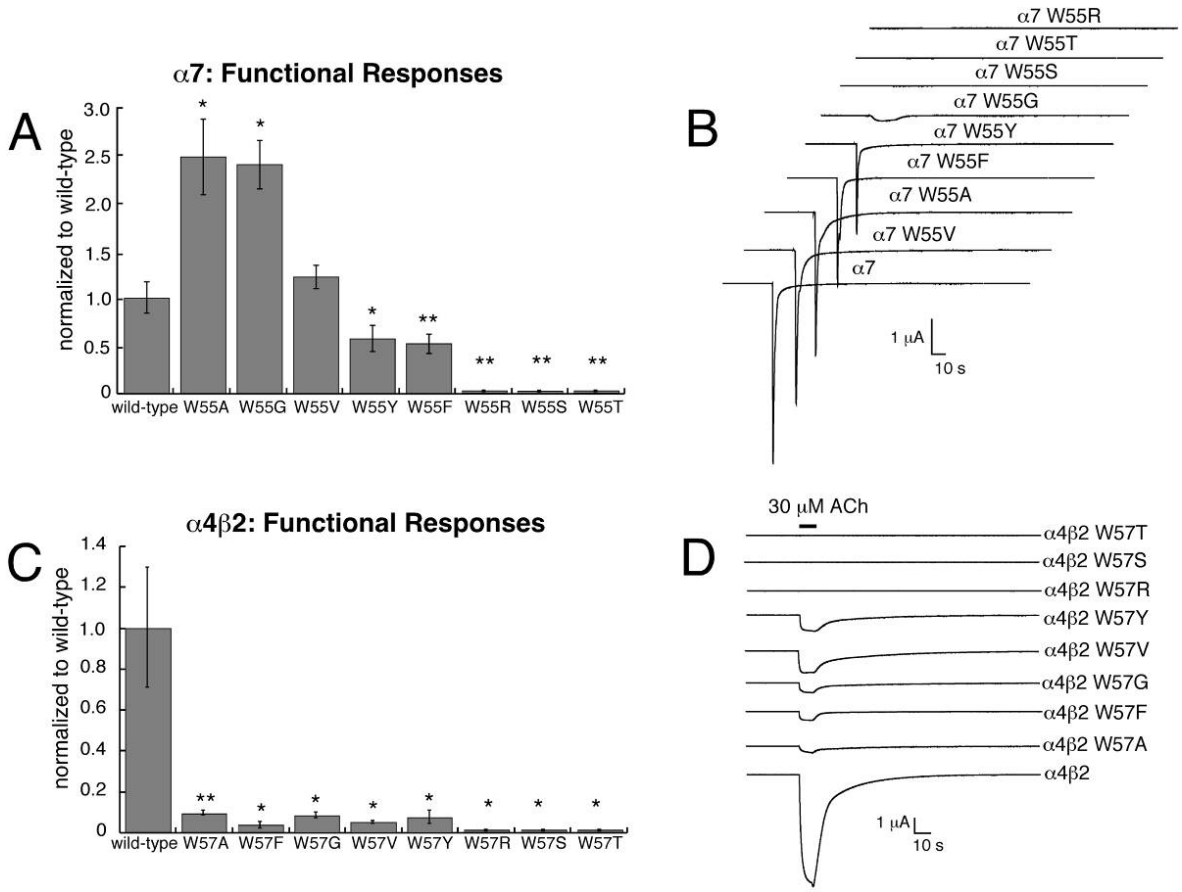

Figure 4-3. Functional responses of human α7W55 and human α4β2W57 mutant receptors relative to ACh-induced maximum responses in wild type. A) Maximum net-charge responses of α7W55 mutant receptors relative to the ACh-induced maximum net-charge response in wild type α7, represented as a value of 1. * and ** denotes statistically significant differences in maximal functional responses between wild type and mutant receptors with $p<0.05$ and $p<0.01$, respectively. B) Representative data traces of responses by α7 wild type and α7W55 mutants to 300μM ACh. C) Maximum peak responses of α4β2W57 mutants relative to the ACh-induced maximum peak response in wild type α4β2, represented as a value of 1. * and ** denotes $p<0.05$ and $p<0.01$, respectively. D) Representative data traces of α4β2W57 mutant receptors in response to 30 μM ACh. Maximum responses for mutant receptors compared to wild type were calculated by averaging responses ± SEM of at least four oocytes to the same concentration of ACh on both wild type and mutant receptors injected the same day, with the same amount of RNA from the same harvest of oocytes. Averaged responses were divided by the percent of ACh maximum for that concentration on a fitted ACh concentration-response curve to find the maximum theoretical response, and then divided by the calculated maximum response for the wild type receptor for the comparison.

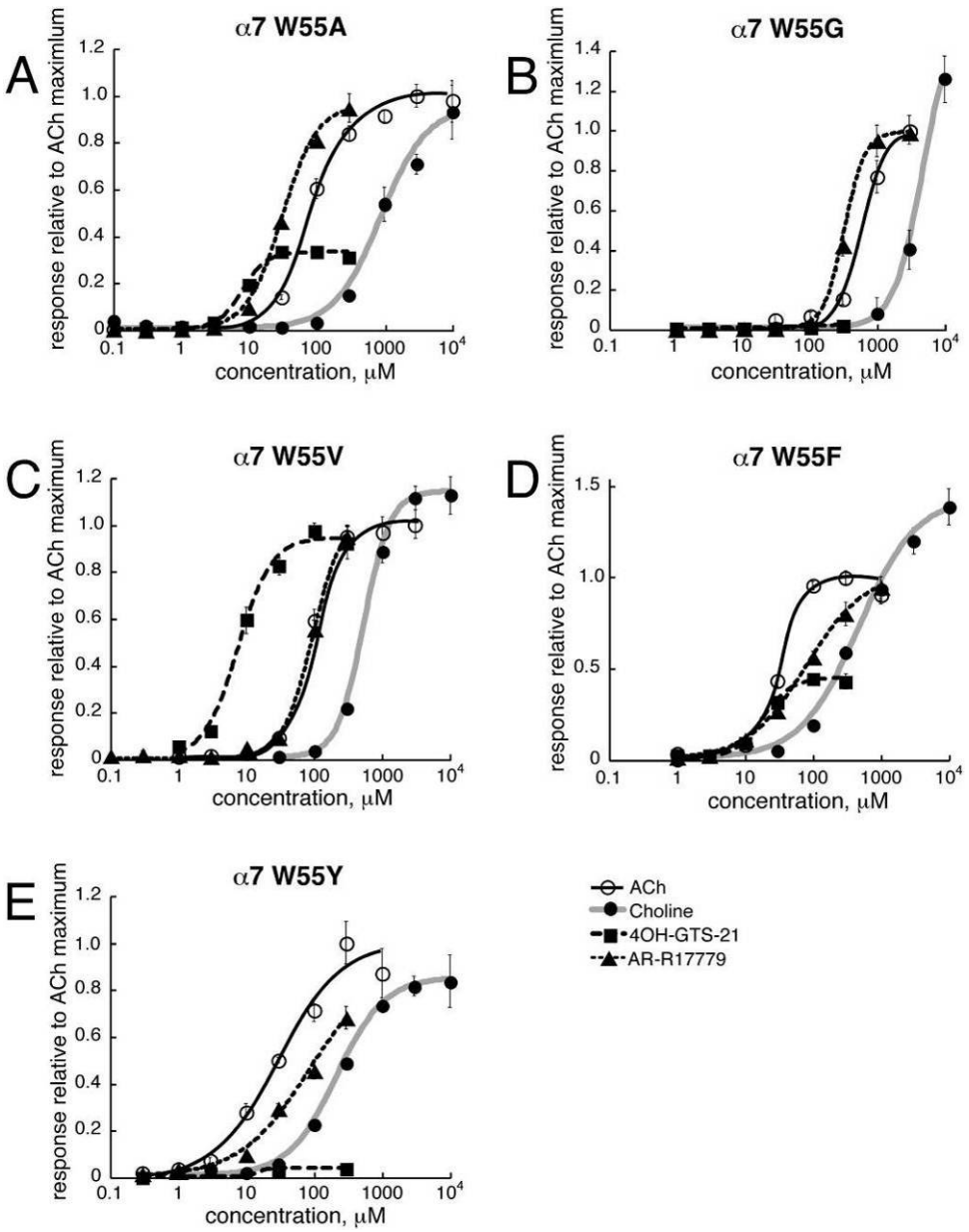

Figure 4-4. Concentration-response relationship of α7W55 mutant receptors to ACh, choline, 4OH-GTS-21, and AR-R17779. A) Net-charge responses of α7W55A mutants. B) Net-charge responses of α7W55G mutants. Note that this mutant did not respond to 4OH-GTS-21 at the concentrations tested. Due to concerns related to channel block and osmotic effects, the highest choline concentration tested was 10 mM. C) Net-charge responses of α7W55V mutants. D) Net-charge responses of α7W55F mutants. E) Net-charge responses of α7W55Y mutants. Note the low efficacy of 4OH-GTS-21. Responses of wild type α7 are presented in Figure 4-2B. Data were measured relative to control ACh responses and then expressed relative to the maximum ACh response for each particular receptor type. Each point represents the mean ± SEM of at least four oocytes.

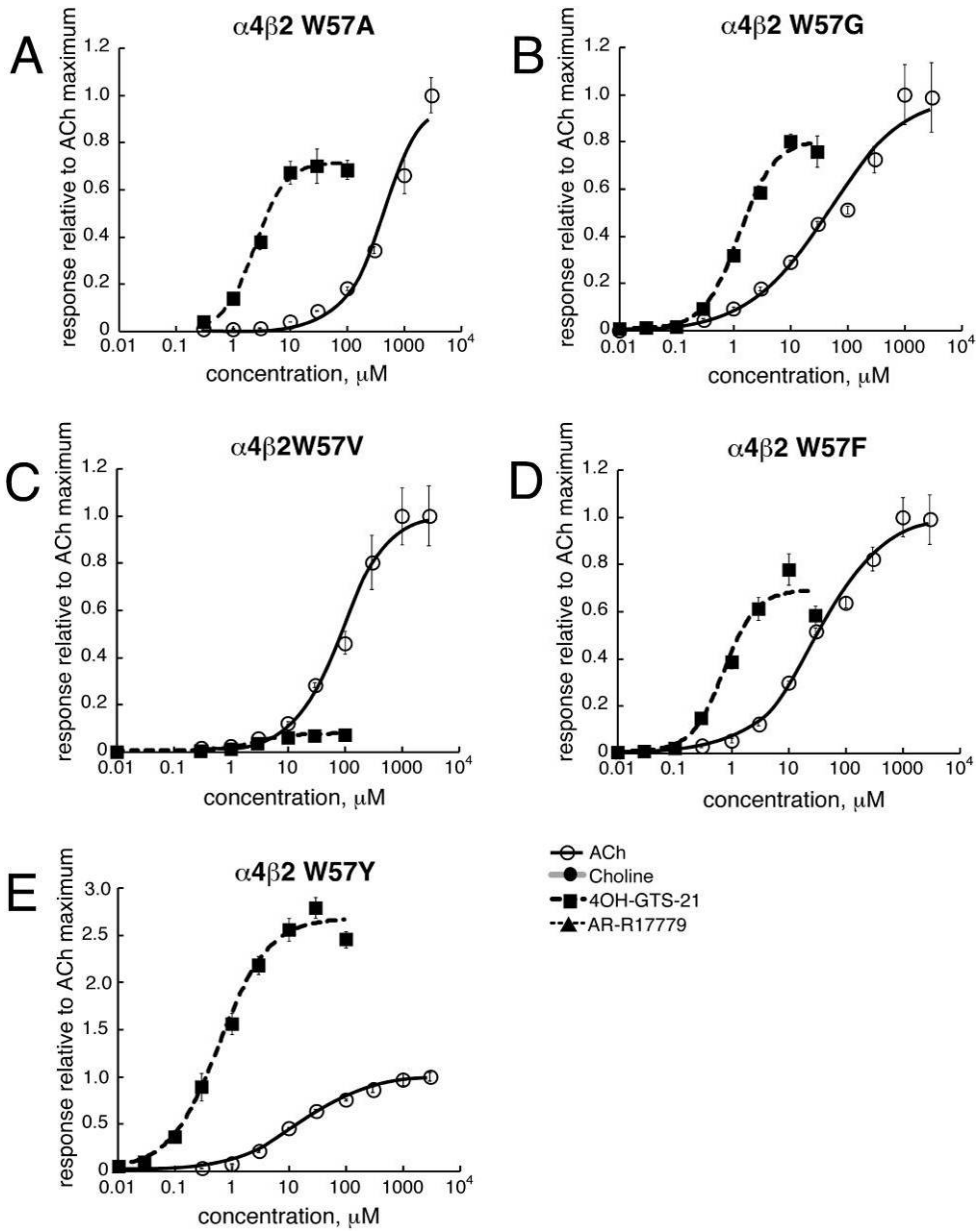

Figure 4-5. Concentration-response relationships of α4β2W57 mutants to ACh, choline, 4OH-GTS-21, and AR-R17779. A) Peak responses of α4β2W57A mutant receptors. B) Peak responses of α4β2W57G mutant receptors. C) Peak responses of α4β2W57V mutant receptors. D) Peak responses of α4β2W57F mutant receptors. E) Peak responses of α4β2W57Y mutant receptors. Note that α4β2W57A, α4β2W57G, α4β2W57F, and α4β2W57Y mutants responded to 4OH-GTS-21. Responses to choline and AR-R17779 were below the limits of detection of all α4β2 receptors. Data were measured relative to control ACh responses and then expressed relative to the maximum ACh response for each particular receptor type. Each point represents the mean ± SEM of at least four oocytes. Peak responses by wild type α4β2 are presented in Figure 4-2C.

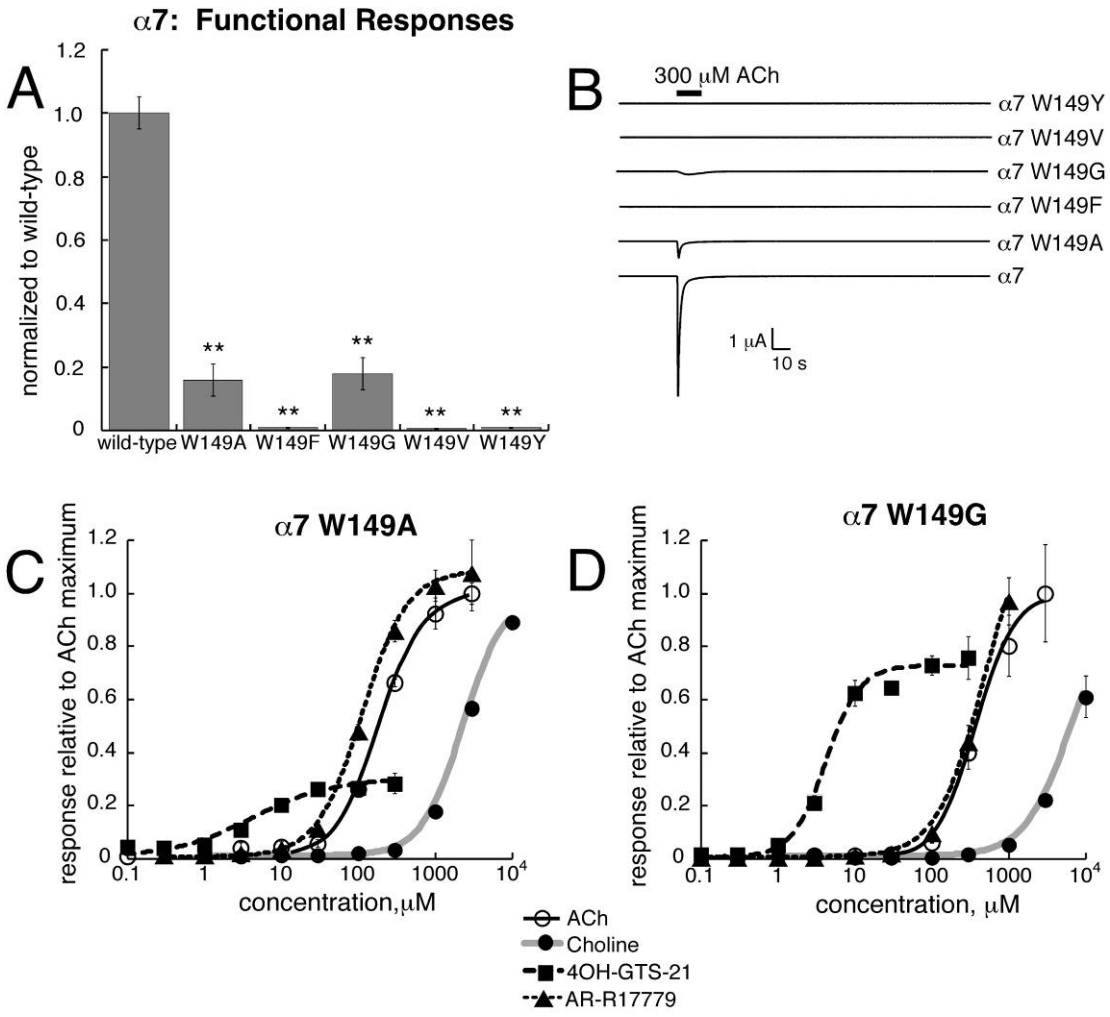

Figure 4-6. Concentration-response relationships of α7W149 mutants to ACh, choline, 4OH-GTS-21, and AR-R17779. A) Maximum ACh-induced net-charge responses of α7W149 mutants compared to maximum net-charge response of ACh in wild type α7. ** denotes $p<0.01$. B) Representative data traces of α7W149 mutants in response to 300 μM ACh. C) Net-charge responses of α7W149A mutant receptors. D) Net-charge responses of α7W149G mutant receptors. Each data point represents the mean ± SEM of at least four oocytes. Responses of wild type α7 to these agonists are presented in Figure 4-2B.

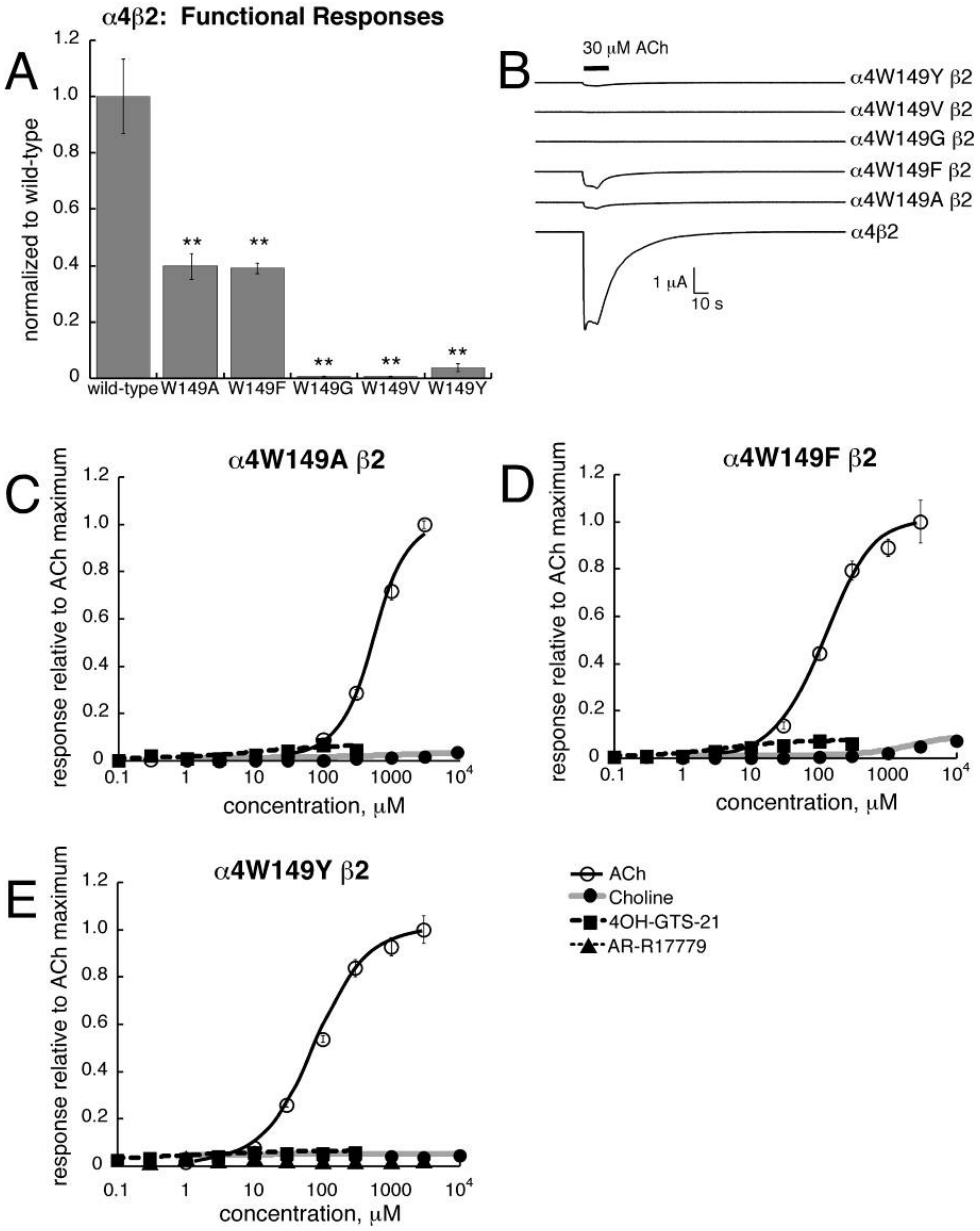

Figure 4-7. Concentration-response relationships of α4W154β2 mutants to ACh, choline, 4OH-GTS-21, and AR-R17779. A) Maximum ACh-induced peak responses of α7W149 mutants compared to the maximum peak response of ACh in wild type α7. ** denotes $p<0.01$. B) Representative data traces of α4W154β2 mutants in response to 30 μM ACh. C) Peak responses of α4W154Aβ2 mutants. D) Peak responses of α4W154Fβ2 mutants. E) Peak responses of α4W154Aβ2 mutants. Each data point represents the mean ± SEM of at least four oocytes. Peak responses by wild type α4β2 are represented in Figure 4-2C.

Table 4-1. EC_{50} and I_{max} values of ACh, Choline, 4OH-GTS-21, and AR-R17779 in wild type and mutant α7 and α4β2 receptors

Drug	Receptor	EC_{50} ± SEM	I_{max} ± SEM relative to ACh maximum	I_{max} ± SEM relative to ACh maximum
ACh	α7	30.6 ± 3.36	1	1
	α7W55A	84.8 ± 5.79	1	2.5 ± 0.40
	α7W55F	32.7 ± 2.70	1	0.52 ± 0.10
	α7W55G	675 ± 6.26	1	2.4 ± 0.25
	α7W55V	84.2 ± 2.53	1	1.2 ± 0.12
	α7W55Y[a]	30.4 ± 5.03	1	0.57 ± 0.13
	α7W149A	194 ± 9.73	1	0.15 ± 0.03
	α7W149G	400 ± 19.3	1	0.17 ± 0.03
	α4β2	76.0 ± 20.2	1	1
	α4β2W57A	468 ± 59.3	1	0.094 ± 0.011
	α4β2W57F	33.3 ± 4.03	1	0.036 ± 0.017
	α4β2W57G	47.4 ± 10.9	1	0.085 ± 0.015
	α4β2W57V	87.0 ± 10.4	1	0.050 ± 0.0073
	α4β2W57Y	16.2 ± 1.60	1	0.076 ± 0.033
	α4W154A β2	526 ± 28.1	1	0.40 ± 0.04
	α4W154F β2	118 ± 6.07	1	0.39 ± 0.06
	α4W154Y β2	81.1 ± 3.44	1	0.04 ± 0.00
Choline	α7	304 ± 21.8	0.90 ± 0.02	0.90 ± 0.02
	α7W55A	949 ± 210	0.95 ± 0.05	2.34 ± 0.12
	α7W55F	502 ± 71.8	1.4 ± 0.07	0.73 ± 0.04
	α7W55G	4120 ± 63.4	3.1 ± 0.03	7.47 ± 0.07
	α7W55V	570 ± 12.4	1.1 ± 0.01	1.38 ± 0.01
	α7W55Y	228 ± 13.2	0.84 ± 0.01	0.48 ± 0.01
	α7W149A	2490 ± 126	0.89 ± 0.03	0.134 ± 0.005
	α7W149G	6870 ± 1440	0.61 ± 0.07	0.104 ± 0.012
4OH-GTS-21	α7	3.00 ± 0.26	0.46 ± 0.01	0.46 ± 0.01
	α7W55A	8.40 ± 0.73	0.33 ± 0.01	0.82 ± 0.02
	α7W55F	18.9 ± 1.93	0.45 ± 0.02	0.23 ± 0.01
	α7W55G	NA[b]	NA[b]	NA[b]
	α7W55V	7.80 ± 0.82	0.94 ± 0.03	0.54 ± 0.02
	α7W55Y	NA[b]	NA[b]	NA[b]
	α7W149A	4.49 ± 1.39	0.28 ± 0.04	0.042 ± 0.006
	α7W149G	4.43 ± 0.50	0.76 ± 0.08	0.130 ± 0.014
	α4β2	NA[b]	0.01 ± 0.00	0.01 ± 0.00
	α4β2W57A	2.56 ± 0.27	0.71 ± 0.02	0.067 ± 0.0019
	α4β2W57F	0.66 ± 0.22	0.62 ± 0.05	0.022 ± 0.0018
	α4β2W57G	1.16 ± 0.20	0.74 ± 0.04	0.063 ± 0.0033
	α4β2W57V	3.00 ± 0.14	0.07 ± 0.01	0.0035 ± 0.0005
	α4β2W57Y	0.65 ± 0.09	2.7 ± 0.08	0.19 ± 0.006
AR-R17779	α7	3.60 ± 0.73	1.05 ± 0.05	1.05 ± 0.05
	α7W55A	32.4 ± 1.69	0.96 ± 0.02	2.36 ± 0.05
	α7W55F	82.3 ± 2.51	1.02 ± 0.01	0.53 ± 0.005
	α7W55G	332 ± 0.68	0.99 ± 0.01	2.36 ± 0.02
	α7W55V	93.9 ± 5.91	1.05 ± 0.04	1.26 ± 0.05
	α7W55Y	86.8 ± 42.1	0.90 ± 0.16	0.51 ± 0.09
	α7W149A	119 ± 3.99	1.07 ± 0.14	0.16 ± 0.021
	α7W149G	506 ± 72.3	0.97 ± 0.09	0.17 ± 0.015

[a]Responses were normalized to 30 μM ACh.
[b]Responses were below the limits of detection.
Note: The average values for each data point was 7 and n values ranged from 4 to 18.

CHAPTER 5
THE EFFECTIVE OPENING OF NICOTINIC ACETYLCHOLINE RECEPTORS WITH SINGLE AGONIST BINDING SITES

Introduction

As explained in Chapter 2, the nAChR LBD is formed by the interface of two protein subunits; the primary surface is formed by an α subunit, which contains several other key elements in addition to the adjacent cysteines of a subdomain identified as the C-loop [108]. The complementary face of an agonist binding site is formed by a non-α subunit in heteromeric nAChRs and by an α subunit in homomeric nAChRs. Subunits like $\alpha7$ are able to contribute to five agonist binding sites at both primary and complementary interface surfaces [133], while heteromeric receptors, which require non-α subunits for the complementary side of the binding site, are limited to two agonist binding sites.

Acetylcholine is a nearly perfect molecule for fast and transient synaptic signaling at sites like the neuromuscular junction, being rapidly released and efficiently hydrolyzed. However, nicotinic signaling appears to be fundamentally different in the brain, where rhythmic ACh release occurs diffusely, rather than at focused synaptic sites, and a primary role of nAChRs in the brain is to modulate neuronal excitability and the release of other neurotransmitters [163, 187]. Due to esterases, extracellular concentrations of diffusely released ACh are expected to be low. While choline is ubiquitous in the brain and body, concentrations are still well below the EC_{50} for acute activation of $\alpha7$ [214], even under conditions of trauma when choline concentrations reach 100 μM [219, 409]. In addition, responses of $\alpha7$ receptors to high ACh concentrations are very limited [214, 229], which raises the question of whether $\alpha7$

nAChR may function effectively under conditions of low fractional occupancy of the agonist binding sites. Single-channel studies of muscle-type nAChR have associated brief openings observed at low agonist concentrations with monoliganded receptors [69, 410-412], supporting the hypothesis that the brief openings characteristic of $\alpha 7$ may also arise from the binding of single agonist molecules.

Here, the functional significance of the multiple agonist binding sites in heteromeric muscle-type and homomeric $\alpha 7$ forms of nAChR is investigated utilizing the L119C mutation ($\alpha 7$ numbering), which is located on the complementary face of the agonist binding site across from the C-loop (see Figure 5-1A), together with sulfhydryl modification at that site to achieve varying levels of conditional binding site modification [128]. Acetylcholine-insensitive $\alpha 7$Y188F subunits [413] co-expressed with wild type $\alpha 7$ subunits in different ratios are also used to provide a complimentary approach. The data are consistent with previous reports that heteromeric muscle-type receptors and homomeric Cys-loop receptors can activate with levels of submaximal agonist occupancy [412, 414-420]. The data offer the additional insight that strong activation of muscle-type and $\alpha 7$ nAChR may be achieved under conditions of agonist saturation at individual binding sites.

Results

The sensitivity of $\alpha 7$L119C mutant receptors was discovered by Dr. Roger Papke and the experiments involving oocytes were performed before I was a member of the lab group. My contributions to this project were the patch-clamp experiments and their integration with the oocyte data, which proved necessary in publishing and understanding this earlier work.

Identification of the α7L119C Mutation as a Tool to Study nAChR Binding Sites

The α7 receptor contains a free cysteine residue at position 116. In order to prevent non-specific modification and/or potential disulfide formations between the single free cysteine at position 116 and the introduced cysteine, a cysteine-null pseudo-wild type C116S background was used. Responses of pseudo-wild type α7C116S receptors to EC_{50} concentrations of ACh, tetramethyl ammonium, quinuclidine, and 4OH-GTS-21 are not significantly different from wild type, and are unaffected by application of MTSEA [128]. A similar pseudo-wild type background was used in other studies that introduced cysteine mutations into α7 [421].

The L119C mutation was identified as an effective tool for the investigation of nAChR binding sites since receptors containing this mutation responded normally to ACh, tetramethyl ammonium, quinuclidine, and 4OH-GTS-21 until treated with MTSEA or any of the three other cationic sulfhydryl reagents applied, after which agonist-induced responses were nearly completely abolished [128]. The near 100% reduction in response to 300 μM ACh that is typical when 2 mM MTSEA is applied for 60 s to α7C116S/L119C mutant receptors expressed in oocytes is shown in Figure 5-1B. The degree of inhibition is not significantly dependent on the ACh concentration used to evoke the responses. In the specific experiment illustrated, net charge responses to 300 μM ACh were reduced by 99.7 ± 0.1%, and responses to 3 mM ACh were reduced to a similar extent (95.9 ± 2.0%, data not shown).

Effects of α7L119C Ratios in Mixed α7 Wild Type/Mutant Heteromers

The purpose of the following experiments was to test the hypothesis that α7 receptors may be activated, even if the receptors have a reduced number of activatible

binding sites. *Xenopus* oocytes were injected with RNA coding for α7C116S (pseudo-wild type) subunits and the MTSEA-sensitive α7C116S/L119C subunits in varying ratios. The possible subunit combinations and likely distributions of those combinations as a probabilistic function of the RNA ratios, assuming equal expression and assembly of the wild type and mutant subunits, are shown in Figure 5-2A. With the highest ratio (5:1) of α7C116S/L119C to α7C116S, less than 4% of the receptors would be predicted to have more than two MTSEA-insensitive binding sites, and 40% would be predicted to be fully MTSEA sensitive. An attempt was made to verify the expression of receptors containing α7L119C mutant subunits by comparison of radiolabeled α-bungarotoxin binding before and after MTSEA treatment. However, the α7C116S and α7L119C mutations appeared to disrupt the binding of the competitive antagonist, and such experiments were not possible to pursue. Comparison of the magnitude of non-normalized functional responses from oocytes to the same concentration of ACh (300 μM) that were injected the same day, with the same amount of RNA from the same harvest of oocytes, revealed equivalent responses among the α7C116S/L119C, 1:1, 3:1, 5:1 groups. The functional responses of the oocytes injected with α7C116S alone were 3-fold greater (data not shown, n ≥ 5 oocytes for each group).

Control responses to 300 μM ACh were recorded for each cell in the three injection sets prior to MTSEA treatment (Figure 5-2B). After treating the oocytes with MTSEA (2 mM, 60s), oocytes were tested with a range of ACh concentrations from 30 μM to 1 mM. The average net charge data are shown in Figure 5-2C (see also Table 5-1), normalized to the 300 μM ACh net charge responses obtained prior to the MTSEA treatment. The most obvious effect of the MTSEA treatment was on the responses to

low ACh concentration in the oocytes injected with the highest fraction of MTSEA-sensitive mutants. In the control (pre-MTSEA) condition, 300 μM ACh was sufficient to produce a maximal net charge response. Responses of the oocytes injected at ratios of 1:1 and 3:1 showed no significant differences in function following MTSEA treatment ($p > 0.05$). Only the oocytes injected at the 5:1 ratio showed a significant decrease in the 300 μM ACh-evoked responses ($p < 0.05$) following MTSEA treatment; however, this average decrease of 33% was less than the percentage of receptors predicted to be fully sensitive to MTSEA (40%, Figure 5-2A). While untreated $\alpha 7$ receptors (not shown) and the treated receptors injected at 1:1 (Figure 5-2C) showed no increase in net charge from 300 μM to 1 mM ACh, the average responses of the 5:1 injected oocytes to 1 mM ACh increased to the extent that responses to 1 mM ACh were not significantly different from the pretreatment 300 μM control responses at the $p < 0.05$ level. One possible explanation is that $\alpha 7$ receptors with one or two functional binding sites may be less affected by the rapid concentration-dependent desensitization that is characteristic of $\alpha 7$ and, therefore, better able to respond to high concentrations of agonist.

Effects of ACh-Insensitive Mutant Ratios in Mixed $\alpha 7$ Wild Type/Mutant Heteromers

A mutation in the primary face of the $\alpha 7$ ACh binding site (Y188F) that produces a 45-fold reduction in ACh potency (ACh EC_{50} shifted from 33 ± 4 μM for wild type to 1500 ± 164 μM for $\alpha 7$Y188F) without any significant effect on the potency of the $\alpha 7$-selective partial agonist 4OH-GTS-21 (4OH-GTS-21 EC_{50} 14 ± 1 μM for wild type and 14 ± 2 μM for $\alpha 7$Y188F) was previously reported [413]. As shown in Figure 5-3A, for wild type $\alpha 7$ the ratio of the 300 μM 4OH-GTS-21-evoked net charge responses to 300 μM ACh-evoked responses were 0.57 ± 0.04. In contrast, for $\alpha 7$Y188F receptors, the ratios of

the 300 μM 4OH-GTS-21-evoked responses to 300 μM ACh-evoked responses were 4.0 ± 0.6. Acetylcholine-sensitive wild type α7 and ACh-insensitive α7Y188F were co-expressed in *Xenopus* oocytes at varying ratios of RNA, similar to what was done with the L119C mutant (Figure 5-2B and C). The response evoked by 4OH-GTS-21 on α7Y188F receptors is consistent with efficient α7Y188F subunit expression and assembly in oocytes [413]. The mutant and wild type subunits responded alike to 300 μM 4OH-GTS-21, but wild type subunits were required to generate responses to 300 μM ACh. However, if only single subunits were required to activate a receptor, then even under the condition when α7Y188F was injected at a 5:1 ratio to wild type α7, the net charge responses to ACh should remain relatively high since 60% of the receptors would have at least one ACh-sensitive wild type subunit. As shown in Figure 5-3B, the sensitivity of the wild type receptor to ACh was retained well, even under the 5:1 injection condition, when it would be predicted that very few of the receptors would have more than 1 or 2 wild type subunits. The shift in 4OH-GTS-21 to ACh response ratios was no more than would have been expected from the prediction that 40% receptors would contain only ACh-insensitive subunits.

Effects of Mutations Homologous to α7L119C in Non-α Subunits of Muscle-Type Receptors

Since modeling of the homomeric α7 subunits places the L119 residue in the complementary face of the agonist binding site (Figure 5-1A), this site is expected to form the specialized domains corresponding to those of the non-α subunits in heteromeric nAChR. Consistent with this prediction, MTSEA treatment reduced responses to high (1 mM) and low (30 μM) ACh concentrations by more than 95% when the mutation homologous to α7L119C was placed in the β2 subunits of α4β2 and α3β2

receptors, while little MTSEA-dependent effects were observed when the homologous mutation was placed in the α subunits [128]. While the placement of the modifiable L119C residue in α7 receptors and the modifiable β2L121C in α4β2 and α3β2 receptors impacts all potential binding sites of these receptors and produces equally profound reduction in function following MTSEA treatment, the effect of the homologous mutation in subunits of heteromeric muscle-type receptors would be expected to depend on the specific subunit(s) in which the mutation was placed since the α1 subunits are paired with different non-α subunits (δ and γ or ε), which contribute different complementary faces to the two agonist binding sites. While MTSEA treatment produced no significant decreases in the ACh-evoked responses of wild type α1β1εδ or α1β1γδ receptors across a range of ACh concentrations from 1 μM to 1 mM (see Figure 5-4 and Table 5-2), receptors with mutations in both ε and δ had large reductions in their responses to both low and high concentrations of ACh (Figure 5-4). Peak current and net charge responses of the double mutants (α1β1εL119CδL121C), to 30 μM ACh were reduced 93 ± 1 and 96 ± 1 %, respectively, and peak current and net charge responses to 1 mM ACh were reduced by 82 ± 6 and 91 ± 3 %, respectively. However, if mutations were placed in only one of the two non-α subunits that contribute to agonist binding sites (α1β1γδL121C, α1β1εL119Cδ, or α1β1εδL121C), MTSEA treatment produced large decreases ($p<0.01$) in the responses evoked by 30 μM ACh with less effect on the 1 mM ACh-evoked peak current responses for either the α1β1γδL121C or α1β1εL119Cδ receptors. Although peak current responses to 1 mM ACh for the α1β1εδL121C receptors were decreased by MTSEA treatment ($p<0.01$), the effect on 1 mM ACh responses (30 ± 7% decrease) was much less ($p<0.0001$) than that on 30 μM ACh

responses (74 ± 4% decrease). Note that although the peak amplitude of the responses evoked from $\alpha 1\beta 1\gamma\delta$L121C and $\alpha 1\beta 1\varepsilon$L119C$\delta$ receptors by 1 mM were not decreased by the MTSEA treatment, the net charge values of the 1 mM ACh-evoked responses on all single-subunit mutants were affected because the MTSEA treatment resulted in currents with significantly ($p<0.05$) faster 90%-10% decay times. This would be consistent with a decreased ability of the treated oocytes to respond to the lower concentrations of ACh during the washout period.

The ACh concentration-response curves for the peak current responses of the muscle-type receptors containing MTSEA-sensitive mutations are shown in Figure 5-5, and the fit I_{max} and EC_{50} values are shown in Table 5-2. In addition to obtaining responses to varying concentrations of ACh, multiple responses to ACh at the control concentration of 30 μM were obtained from each cell before and after MTSEA. These are shown in the right-hand column of plots in Figure 5-5. Note that there was some recovery in the size of the 30 μM control responses after the MTSEA treatments. Given that the MTSEA modification results in a covalent bond, reversibility of the effect seems unlikely. The response reversibility could have represented the insertion of new receptors during the course of the experiment. Muscle-type receptors express better than any other nAChR subtype, and oocytes must be studied immediately on the day after injection or else currents are too large for effective voltage clamping. Another possibility is that the receptors with one unmodified binding site show less of an effect of progressive desensitization with repeated agonist applications.

To further investigate the MTSEA resistant activation of muscle-type receptors with one unperturbed binding site, single-channel patch-clamp experiments were

performed with wild type and mutant $\alpha1\beta1\gamma\delta$ receptors transiently transfected in mammalian BOSC23 cells. The fetal $\alpha1\beta1\gamma\delta$ version of the muscle-type receptor was the focus of these experiments since it is the subject of an extensive literature, due to its expression in BC_3H1 cells (see for example [422-425]. Two main types of analyses were performed on the single-channel data: (1) comparison of post-MTSEA treatment peak current and NP_{open} measurements with the pre-MTSEA measurements obtained from the same patch in response to 1 mM ACh; and (2) fitting of burst-duration histograms from untreated and treated receptors.

At a holding potential of -70 mV, the single-channel amplitudes before and after MTSEA treatment (5 mM, 60 s) of wild type receptors were -2.71 ± 0.02 pA and -2.69 ± 0.01 pA, respectively, of $\alpha1\beta1\gamma\delta$L121C mutant receptors were -2.64 ± 0.05 pA and -2.63 ± 0.03 pA, respectively, and of $\alpha1\beta1\gamma$L119CδL121C double mutant receptors were -2.74 ± 0.05 pA and -2.70 ± 0.06 pA, respectively. The single-channel amplitude with 10 nM ACh concentration at -70 mV was -3.13 ± 0.02 pA. The smaller apparent single-channel amplitude observed with high concentrations of ACh would be consistent with an effect of brief episodes of channel block by agonist, limiting the detection of full amplitude events [426]. The single-channel slope conductance of $\alpha1\beta1\gamma\delta$L121C receptors was 35.5 ± 1.2 pS and the reversal potential was -4.4 ± 2.0 mV (-80 mV to 80 mV, n = 3, data not shown). These values are in agreement with previously published studies on fetal muscle-type nAChR [94, 427, 428].

Figure 5-6A shows traces from outside-out patches under the experimental protocol, which consisted of an ~80 s initial ACh application, followed by either 5 mM MTSEA or external saline application for 60 s, and ended with a follow-up ACh

application. External saline instead of 5 mM MTSEA was applied to some patches expressing $\alpha 1\beta 1\gamma\delta$L121C to allow channel rundown and/or desensitization that may occur independently of any MTSEA-dependent effects to be measured. Figure 5-6B summarizes the post-MTSEA treatment versus pre-MTSEA comparisons of both transient peak currents and NP_{open} with 1 mM ACh, normalized to the average values from 8 rundown/desensitization control patches. Despite consistent experimental setup, the patch-to-patch variability of the peak current and NP_{open} measurements was higher than expected for unknown reasons that probably reflect the unstable and fragile nature of outside-out patches. No attempt was made to identify or eliminate outliers. There were no correlations between post-/pre-MTSEA treatment peak and NP_{open} measurements and transfection dates, recording dates, lower limit of N in the patch, single-channel amplitudes, or 10%-90% rise times. The non-normalized average, SEM, range, and median of values from at least 8 replicates of each condition, including the rundown controls, are reported in Table 5-3. Peak and NP_{open} measurements of wild type receptors were least affected by MTSEA treatment (5 mM, 60 s) with post/pre MTSEA treatment values of 1.1 ± 0.1 and 0.83 ± 0.09, respectively. Receptors with one MTSEA-sensitive binding site had post/pre-treatment peak current and NP_{open} values of 0.74 ± 0.08 and 0.65 ± 0.06, respectively. There was a much greater reduction in both peak and NP_{open} values when receptors contained two MTSEA-sensitive binding sites, with post/pre-treatment values of 0.072 ± 0.003 and 0.14 ± 0.02, respectively.

Figure 5-7 presents single-channel currents obtained from wild type and $\alpha 1\beta 1\gamma\delta$L121C receptors at 1 mM ACh before and after MTSEA treatment, responses from untreated $\alpha 1\beta 1\gamma\delta$L121C receptors at 10 nM ACh, and fit burst-duration histograms

corresponding to each condition. The fit time constants are listed in Table 5-4. Burst-durations, rather than apparent open duration histograms are shown since open channel times are greatly affected by bandwidth limitations, such as missed brief closed intervals and ambiguities associated with idealization, whereas burst-durations are much less affected by these potential confounders and are, therefore, a more reliable measure of channel opening behavior. The burst-durations of wild type $\alpha 1\beta 1\gamma\delta$ receptors were unaffected by MTSEA treatment, while the burst-durations of $\alpha 1\beta 1\gamma\delta$L121C receptors were not different from wild type receptors until treated with MTSEA. The number of components required to generate the best fit of the $\alpha 1\beta 1\gamma\delta$L121C burst-duration histogram after MTSEA increased from two to three, and most bursts consisted of brief, isolated openings, but some longer bursts remained. The proportion of total bursts of duration less than ~ 2 ms increased from 0.26 ± 0.04 before MTSEA treatment to 0.81 ± 0.03 after MTSEA treatment. The longest time constant following MTSEA treatment was equivalent to the long time constant measured on non-treated patches (12.6 ± 0.2 ms versus 12.9 ± 0.05 ms). The frequency (bursts/s) of bursts appeared to increase after MTSEA treatment by a factor of 2.78 ± 0.52. In the case of $\alpha 1\beta 1\gamma\delta$L121C receptors post-MTSEA treatment, "bursts" were usually brief and isolated events. Recordings from $\alpha\beta\gamma\delta$L121 mutants were also obtained without MTSEA treatment at low ACh concentrations (10 nM), where many of the observed openings were likely to arise from singly occupied receptors [69, 412]. The proportion of bursts corresponding to the brief time constant (0.26 ± 0.07 ms) was 0.43 ± 0.02, and the long time constant at 10 nM ACh was more brief than the long time constant at 1 mM ACh (4.66 ± 0.04 ms versus 12.9 ± 0.05 ms).

Discussion

Other studies have investigated the relationship between available binding sites and agonist-evoked responses in muscle-type receptors [100, 416] and in an α7/5-HT3 chimeric receptor [420]. Sine and Taylor 1980 estimated the fractional blockade of binding sites with α-cobratoxin and then measured ion flux in toxin-bound vesicles from BC3H1 cells (fetal receptor). The conclusion was that only receptors with two free agonist binding sites could be activated. However, Groebe *et al*., 1995 reported that application of 500 nM α-conotoxin M1 to BC3H1 cells almost completely inhibits agonist-evoked responses even though the 500 nM concentration of α-conotoxin M1 theoretically results in < 3% occupation of the low affinity binding site (α-γ) by the toxin on the BC3H1 nAChR [429]. In addition, Hansen *et al*., 2005 solved crystal structures for three states in the agonist binding site of the AChBP, one of which was not part of the minimal model for the nAChR (closed, open, and desensitized states). This state was induced by the binding of α-cobratoxin, but not by the binding of relatively small competitive antagonists like MLA. In this state, the C-loop extended in the opposite direction from which it presumably moves during the activation process [106]. Therefore, it is possible that in the original Sine and Taylor 1980 experiments the large conformational change produced by the binding of just one α-cobratoxin molecule was sufficient to render the entire channel unable to gate. Jha and Auerbach 2010 used mutations at position αW149 in adult receptors to produce binding sites with reduced sensitivity to ACh, with the conclusions being that a single agonist binding site can activate the receptor, but with much less efficiency than two binding sites (equilibrium gating constants: $E_1^{ACh} \cong 4.3 \times 10^{-3}$ vs $E_2^{ACh} \cong 28$). However, while expression of

αW149 mutant subunits resulted in receptors with two mutant binding sites and greatly reduced responses to ACh, co-expression of αW149 mutant subunits with wild type α subunits to produce receptors with single functional binding sites resulted in mixed populations of receptors consisting of all wild type subunits, single αW149 mutant subunits, and two mutant αW149 mutant subunits. Rayes *et al*., 2009 used an α7/5-HT_3 receptor chimera with subunits containing α7Y190T and/or α7W55T mutations to reduce ACh sensitivity. In addition, the mutant subunits contained reporter mutations in the 5-HT_3 sequence that altered unitary channel conductance so that receptor subunit combinations could be identified. The conclusions of this study were that α7/5-HT_3 chimeric receptors activated partially when receptors contained fewer than three wild type subunits, or when the three wild type subunits were located at adjacent subunit interfaces. In addition, the authors concluded that receptors with fewer wild type binding sites experienced less desensitization following strong stimulation by ACh. Unfortunately, the α7/5-HT_3 chimera is a "man-made" receptor with a much higher open probability than native α7 nAChR, and so it is unclear to what extent the conclusions of this study may be applied to α7. While the approach used here is not without its own limitations, it provides the significant strength over the loss-of-function mutation approach that responses can be recorded from the same receptor population before and after binding site modification. Notwithstanding the Sine and Taylor 1980 experiments, the general consensus from early single-channel recordings of muscle-type receptors (see below) and experiments utilizing loss-of-function mutations suggest that a single agonist binding site is sufficient to open the nAChR channel, but that openings from a single binding site have a low P_{open} relative to that of openings arising

from multiple binding sites. The results presented here are not inconsistent with this observation given that responses to ACh were reduced at low concentrations after binding site modification.

Early single-channel studies of muscle-type nAChR noted that the component of brief openings at low agonist concentrations behaved as if it arose from monoliganded receptors. The ratio of total events corresponding to brief, isolated openings (fast time constant) versus longer-lived openings (slow time constant) that were attributed to di-liganded receptors was relatively high at low agonist concentrations, but decreased as agonist concentrations increased [69, 410-412, 425, 427]. Interestingly, however, a component of short-lived openings persisted even at high agonist concentrations, accounting for approximately 10% of all apparent channel openings [412, 427]. Prior to performing the patch-clamp experiments, only brief, isolated openings were hypothesized to occur following MTSEA treatment of δL121C receptors, with the frequency of such events increasing as agonist concentration increased. The majority (81 %) of bursts were indeed brief (≤ 2 ms); however, some longer bursts (~12.6 ms) were also observed. This observation, together with previous observations that brief, isolated single-channel openings persist at high agonist concentrations [412], suggest the interesting possibility that both short- and longer-lived channel activations may arise from either mono- or di- liganded receptors, with a single liganded binding site opening with greatest probability to the shorter-lived opening and the diliganded receptor opening to the longer-lived open state with greater probability. In general, the data support the interpretation that conversion to the desensitized state occurs as in relation to the total time spent in the open state. Individual openings from singly liganded

receptors may with higher likelihood be brief; but nonetheless, if entry into desensitized states depends strictly on time in the open state, then such receptors would generate the same net amount of current before desensitizing as diliganded receptors.

Ideally, MTSEA modification occurred to completion at all “L119C” sites, producing binding sites with no affinity for ACh, and with no effect on channel gating itself. The observation that some currents were recorded after MTSEA was applied to the $\alpha 1\beta 1\gamma$L121CδL119C double mutants in both two-electrode voltage clamp and patch-clamp experiments is problematic. Does the MTSEA modification only partially reduce the binding site sensitivity to ACh or were some receptors left unmodified? Unfortunately neither question is straightforward to answer. In a study evaluating residues that contribute to α-bungarotoxin binding in muscle-type receptors, Sine 1997 demonstrated that MTSET modification of receptors containing δL121C, γL119C, or εL119C residues resulted in a 50% decrease in α-bungarotoxin binding, as would be expected if the receptors contained only one modified binding site and modification completely prevented α-bungarotoxin binding. Furthermore, analysis of the binding site-selective antagonists dimethyl-d-tubocurarine and α-conotoxin M1 confirmed that the effect was due to specific modification at the selected binding site. Electrostatic repulsion, rather than effects on channel conformation, was hypothesized to be responsible for the disruption of α-bungarotoxin binding following MTSET modification [430]. In addition, a recently constructed homology model of MTSET modified α7L119C suggests that the modification places a hard positive charge in close proximity to where ACh is expected to bind. Because MTSET differs from MTSEA only in the substitution of methyl groups for hydrogens on the quaternary nitrogen of the sulfhydryl reagent, the

model for MTSEA-modified receptors is expected to be equivalent [128]. From these observations and given that ACh contains a positively charged ammonium group, it seems most likely that the residual current by the double mutants was due to a small fraction of incompletely modified receptors. Could the modification have spared some or all of the binding site affinity for ACh, primarily affecting the ability of the binding site to initiate the gating cascade once ACh bound? Protocols using $\alpha 7$C116S/L119C mutants, MTSEA, and the PAM PNU-120596, which converts some desensitized states into conducting states, suggest that MTSEA modification may stabilize mutant $\alpha 7$ receptors in PNU-120596-sensitive desensitized states since application of PNU-120596 alone following MTSEA modification produces activation. Importantly, MTSEA modified receptors remain insensitive to ACh, even after they have been primed by the powerful allosteric modulator PNU-120596 [380]. However, although the receptor modeling and data favor the position that ACh is excluded from the ligand binding site, the modification by MTSEA could conceivably mimic a permanently bound weak partial agonist, potentially increasing the ability of the unmodified binding site(s) to activate more readily upon binding of the full agonist ACh.

Since the proportion of the total synaptic current from monoliganded muscle-type receptors under normal physiological conditions is likely negligible, the data are arguably most interesting in their possible application to neuronal nAChRs in the brain, where evidence for nicotinic synaptic transmission is slim, and agonist concentrations are expected to be low. In fact, some have wondered whether nAChRs in the brain even see ACh at all [431]. The data show that *Xenopus* oocytes injected with a high percentage of $\alpha 7$L119C mutant RNA, and therefore likely to have a reduced number of

available agonist binding sites following MTSEA treatments, can give responses to high agonist concentrations after MTSEA treatment that are comparable to the responses of receptors with all binding sites intact obtained at lower concentrations of agonist. Likewise, combinations of wild type and α7Y188F receptors likely to have very few ACh-sensitive wild type subunits, nonetheless respond well to ACh.

If submaximal occupancy by agonist is sufficient to activate heteromeric and homomeric receptors, what is the role of the additional binding sites? Especially in the case of α7, the functional consequence of having multiple ACh binding sites may be sensitivity to low levels of agonist, rather than to require high levels of occupancy for activation. High levels of agonist occupancy only appear to promote desensitization, or at least to provide sufficient activation during the process of achieving high levels of agonist site occupancy for the receptors to become desensitized. When challenged with a high concentration of agonist, α7 receptors open with highest probability during the leading edge of the solution exchange, when only a fraction of the agonist binding sites would be occupied [213, 214, 218, 229, 432], after which the receptors are predominantly closed or desensitized. This is true whether recordings are made on a slow time scale in oocytes [213] or on a rapid time scale with dissociated neurons [432], and this is so pronounced that with the normal experimental protocol the time-integrated (i.e. net charge) response to 3 mM ACh shows no significant increase over that evoked by 100 μM ACh. The rapid desensitization of α7 may be a protective mechanism against cytotoxicity induced by excess entry of calcium.

The nature of the desensitized state appears to be rather different for heteromeric and homomeric receptors. For heteromeric receptors, desensitization is associated with

an approximately thousand-fold increase in the apparent affinity of the agonist binding site for ACh, while in $\alpha 7$ receptors there does not appear to be any more than a tenfold increase in agonist affinity with desensitization [432]. The conversion of heteromeric receptors to a high-affinity, desensitized state means they will be likely to retain agonist at the binding sites or rebind agonist even as agonist concentration decreases. This may have the effect of stabilizing the desensitized state and slowing recovery. In contrast, agonist will readily dissociate from homomeric $\alpha 7$ receptors, so that in the presence of low concentrations of agonist, the receptors may easily cycle between activation and desensitization and generate a significant time-integrated calcium signal over a prolonged period of time. This modality of prolonged stimulation by low levels of agonist has been shown to be what is required to achieve cytoprotective effects via $\alpha 7$ receptors [227] and is probably important for other roles played by $\alpha 7$ receptors in the brain [432] and in non-neuronal tissues [126]. Therefore, since it is likely that *in vivo* $\alpha 7$ receptors are exposed to low level stimulation (via tonic choline and diffuse phasic release of ACh), receptor activation, based on partial occupancy of the multiple binding sites, may be an important functional modality mediating the cytoprotective and perhaps also the cognitive effects documented for $\alpha 7$-selective agonists.

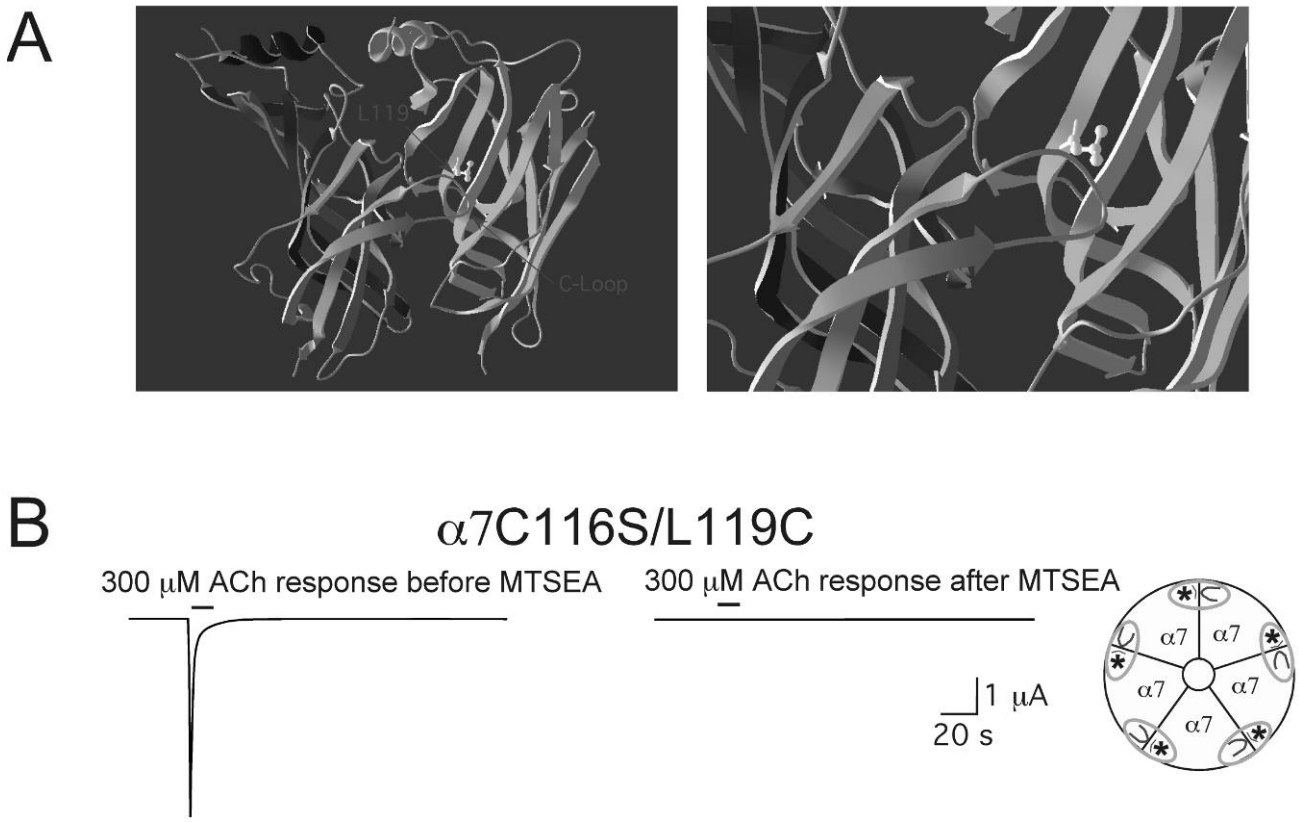

Figure 5-1. Location of the α7L119 residue and the effect of MTSEA on L119C mutant receptors. A) Location of the L119 residue in a homology model of α7 created by Dr. Nicole Horenstein. The images were created in Deep View, Swiss-PdbViewer [433] from the crystal structure model of the AChBP (PDB 1I9B; Brejc *et al*., 2001). B) The effect of MTSEA treatment (2 mM for 60 s) on the ACh-evoked responses of oocytes expressing the α7L119C mutation in a cysteine-null (α7C116S) background. In this experiment, peak current responses to 300 μM ACh were reduced 99.4 ± 0.2%, and net charge was reduced by 99.7 ± 0.1% (n = 4). Responses to 3 mM ACh were reduced to a similar extent, 97.9 ± 0.3% and 95.9 ± 2.0% for peak current and net charge, respectively (n = 4).

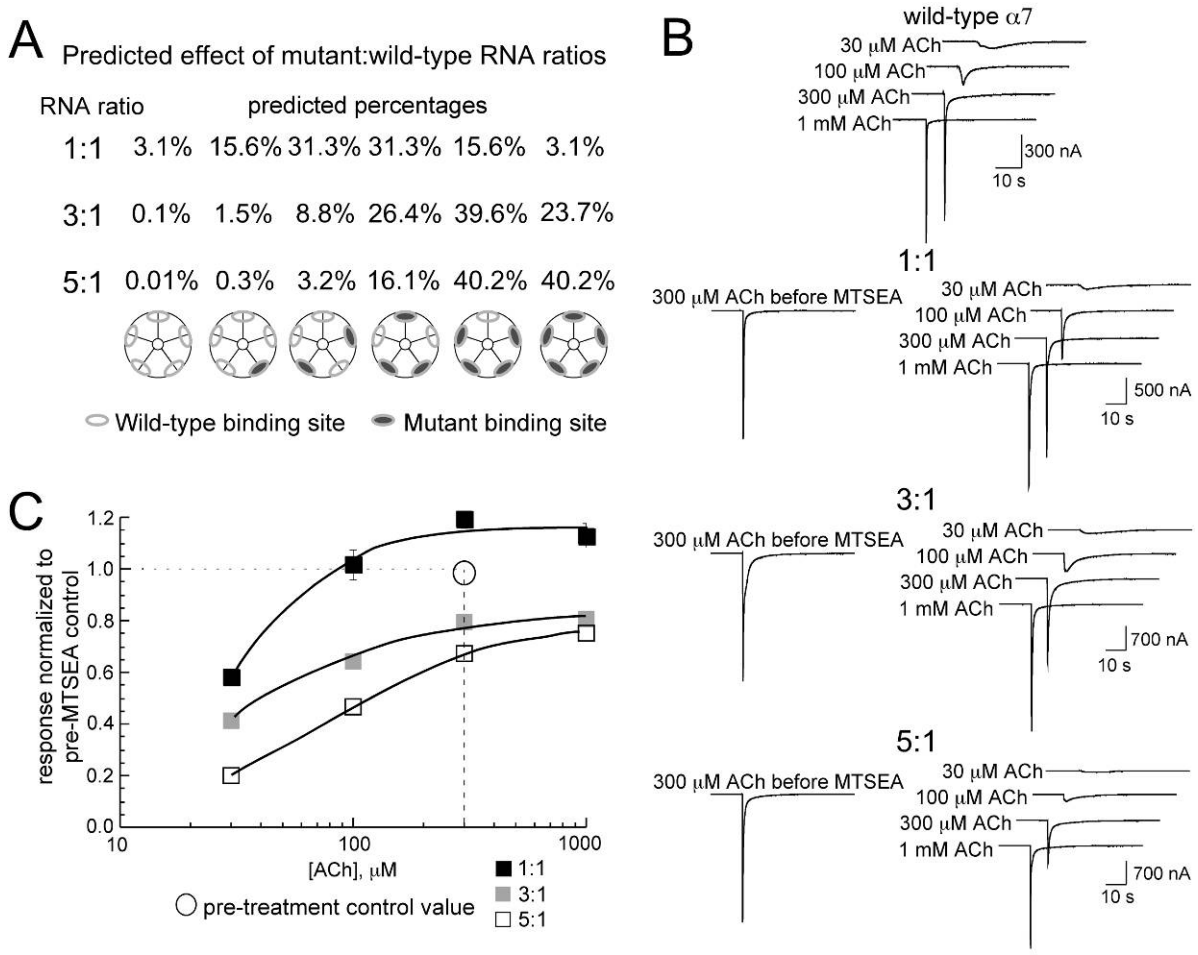

Figure 5-2. Co-Expression of either L119C or Y188F with wild type α7 subunits at varying ratios. A) The probability for the distribution of mutant subunits based on the injected RNA ratios and the binomial theorem. The assumption that receptors are functionally equivalent irrespective of the subunit positions within the pentameric structure is made. B) Data traces obtained from oocytes expressing the α7C116S/L119C MTSEA-sensitive mutant and the α7C116S cysteine-null pseudo wild type at the ratios indicated. The series of traces on on the right are the responses to progressively greater concentrations of ACh obtained after the MTSEA treatment. C) Average net charge values for oocytes expressing the α7C116S/L119C MTSEA-sensitive mutant and α7C116S cysteine-null pseudo wild type at the ratios indicated following treatment with MTSEA normalized to the 300 μM ACh control responses before MTSEA treatment. The data plotted are the means ± SEM for at least 5 oocytes at each of the ratios tested. See Table 5-1 for curve fit values.

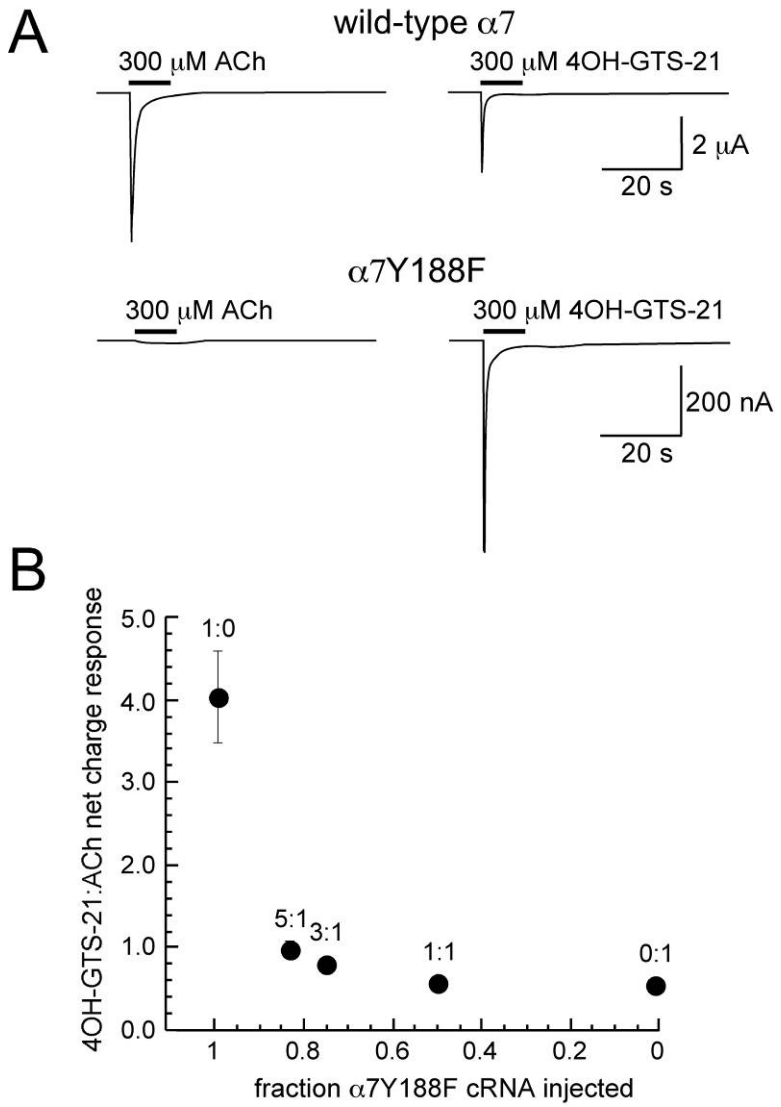

Figure 5-3. Probing the α7Y188F mutant receptor with selective and non-selective agonists. A) Mutation of the α7 tyrosine 188 to phenylalanine reduces sensitivity to low concentrations of ACh with little impact on sensitivity to the responses to the α7-selective agonist 4OH-GTS-21 [413]. The upper traces are representative responses of oocytes expressing wild type α7, for which 300 μM 4OH-GTS-21 evoked responses that are 57 ± 4 % the magnitude of the responses evoked by 300 μM ACh, in net charge. In contrast, for oocytes expressing α7Y188F, 300 μM 4OH-GTS-21-evoked net charge responses that are 405 ± 55 % the magnitude of the responses evoked by 300 μM ACh. B) Oocytes were injected with RNA for α7Y188F and wild type α7 at (mutant:wild type) 1:0, 5:1, 3:1, 1:1, and 0:1 ratios and then tested for their relative responses to 300 μM ACh and 300 μM 4OH-GTS-21. The values are plotted in relation to the fraction of α7Y188F RNA injected at each ratio and are the means ± SEM of at least 4 oocytes for every condition.

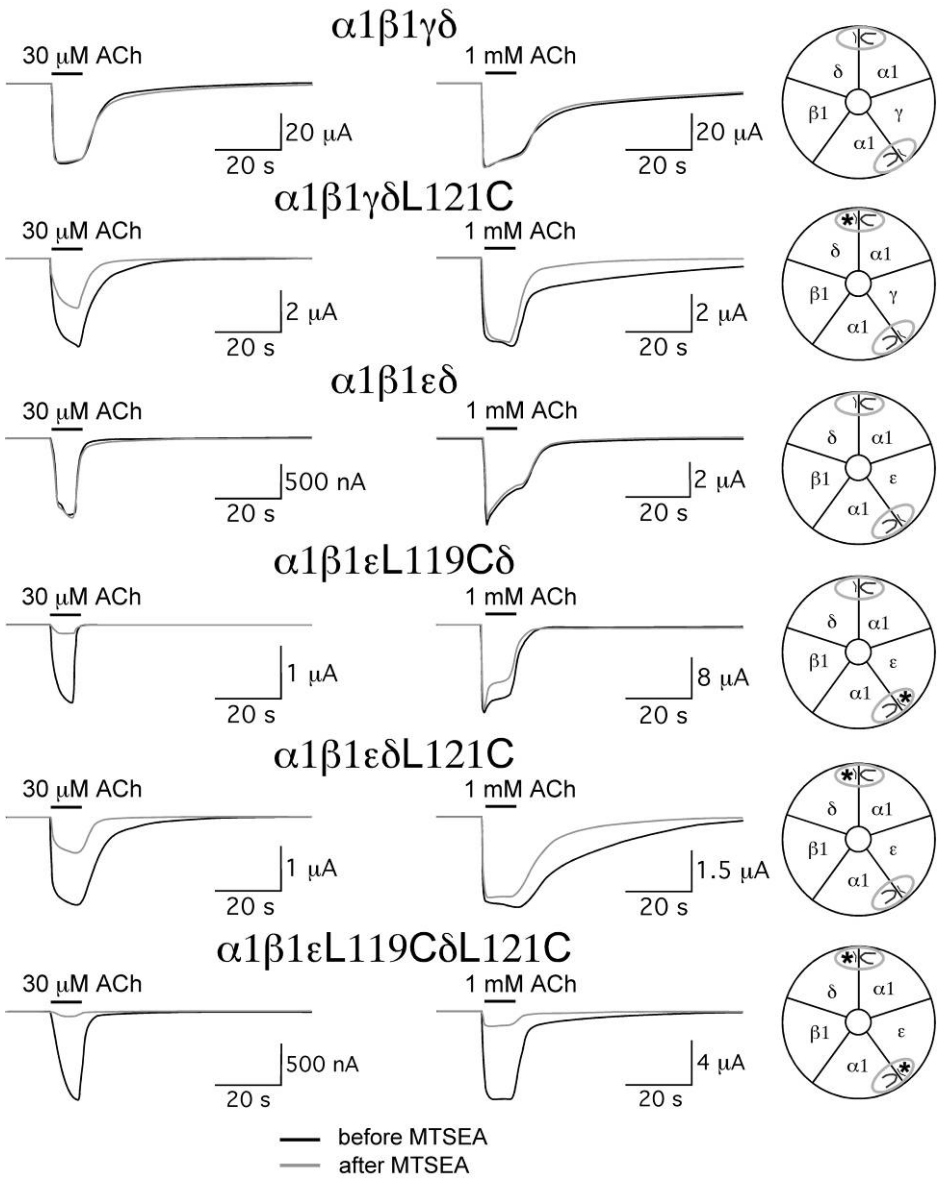

Figure 5-4. The effect of MTSEA on muscle-type receptors with mutations homologous to α7L119C in muscle δ, γ, and ε subunits. Representative responses obtained prior to MTSEA treatments are shown as black lines and responses obtained after MTSEA are gray lines. The schematics to the right of the traces represent the subunit composition and disposition of the ACh binding sites for the different receptor subtypes. The asterisks represent the location of the mutations in the complementary face of the agonist binding site.

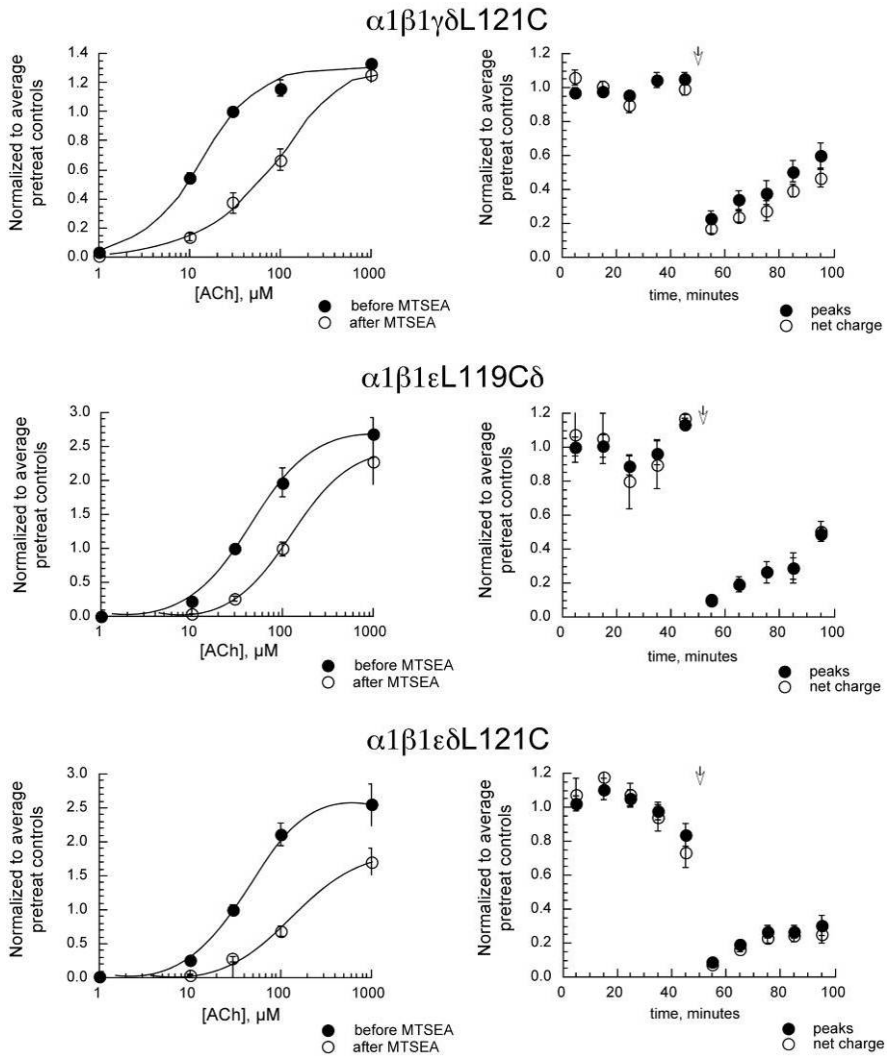

Figure 5-5. ACh concentration-response data for muscle-type single subunit mutants before and after MTSEA treatment. Oocytes were stimulated alternately with control applications of 30 μM ACh and ACh at increasing test concentrations. The oocytes were then treated with 2 mM MTSEA for 60 s before being tested with the same sequence of ACh applications. All of the data were normalized to the individual oocytes' average responses to the five 30 μM ACh applications given prior to the MTSEA treatment. The plots on the right represent the repeated 30 μM ACh responses obtained through the course of the entire experiments, normalized to the average pre-MTSEA 30 μM ACh responses from each cell. The arrowhead indicates the point at which MTSEA was applied. The values plotted are the means ± SEM of 5, 3, and 8 oocytes for α1β1γδL121C, α1β1εL119Cδ, α1β1εδL121C, respectively. Fit parameters are listed in Table 5-2.

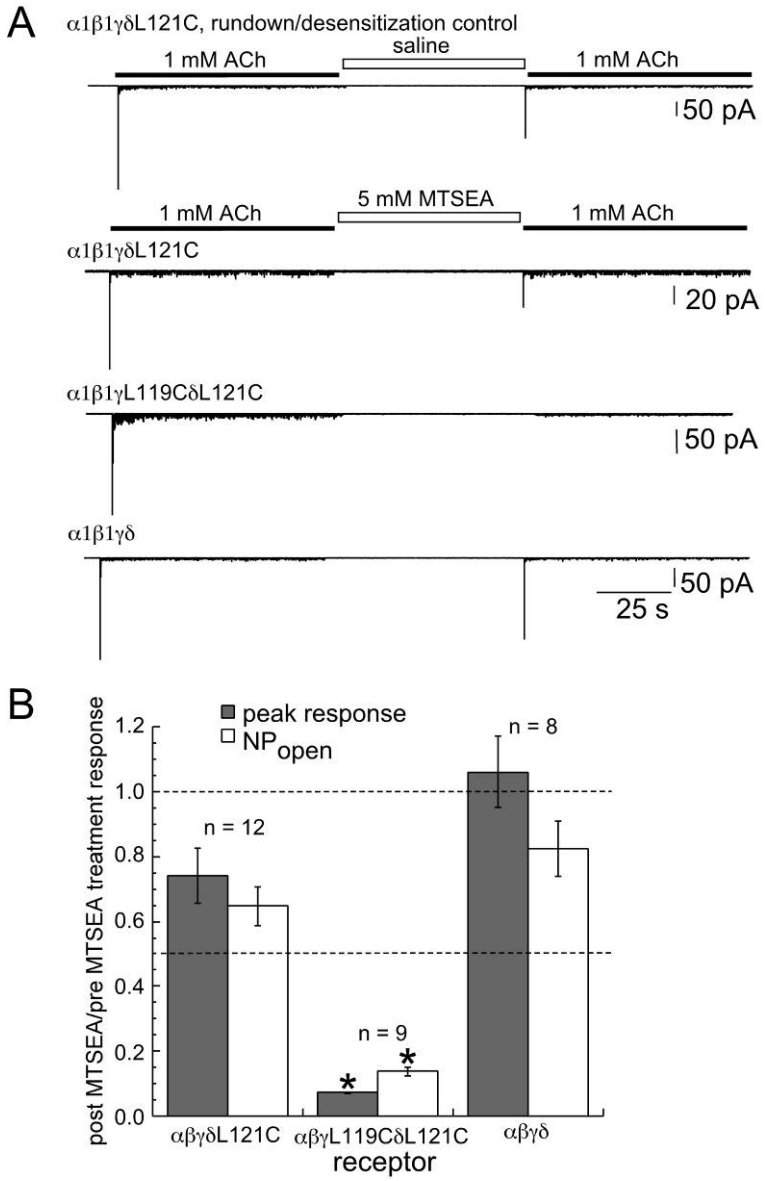

Figure 5-6. The effect of MTSEA treatment on peak and NP_{open} responses from receptors expressed in BOSC23 cells. A) Example traces of outside-out patches from each condition. A rapid (≤ 0.7 ms) drug application system was used to apply ACh and MTSEA. B) Summary of the effect of MTSEA treatment (5 mM, 60 s) on peak current and NP_{open} responses to 1 mM ACh shown as the average of post-MTSEA measurements relative to the pre-MTSEA measurements of each patch. The measurements are normalized to the average peak curent and NP_{open} responses from 8 rundown control patches. Asterisks above the values for $\alpha 1\beta 1\gamma$L119CδL121C indicate statistical significance ($p < 0.01$) when compared with values from either $\alpha 1\beta 1\gamma\delta$L121C or wild type. See Table 5-3 for values.

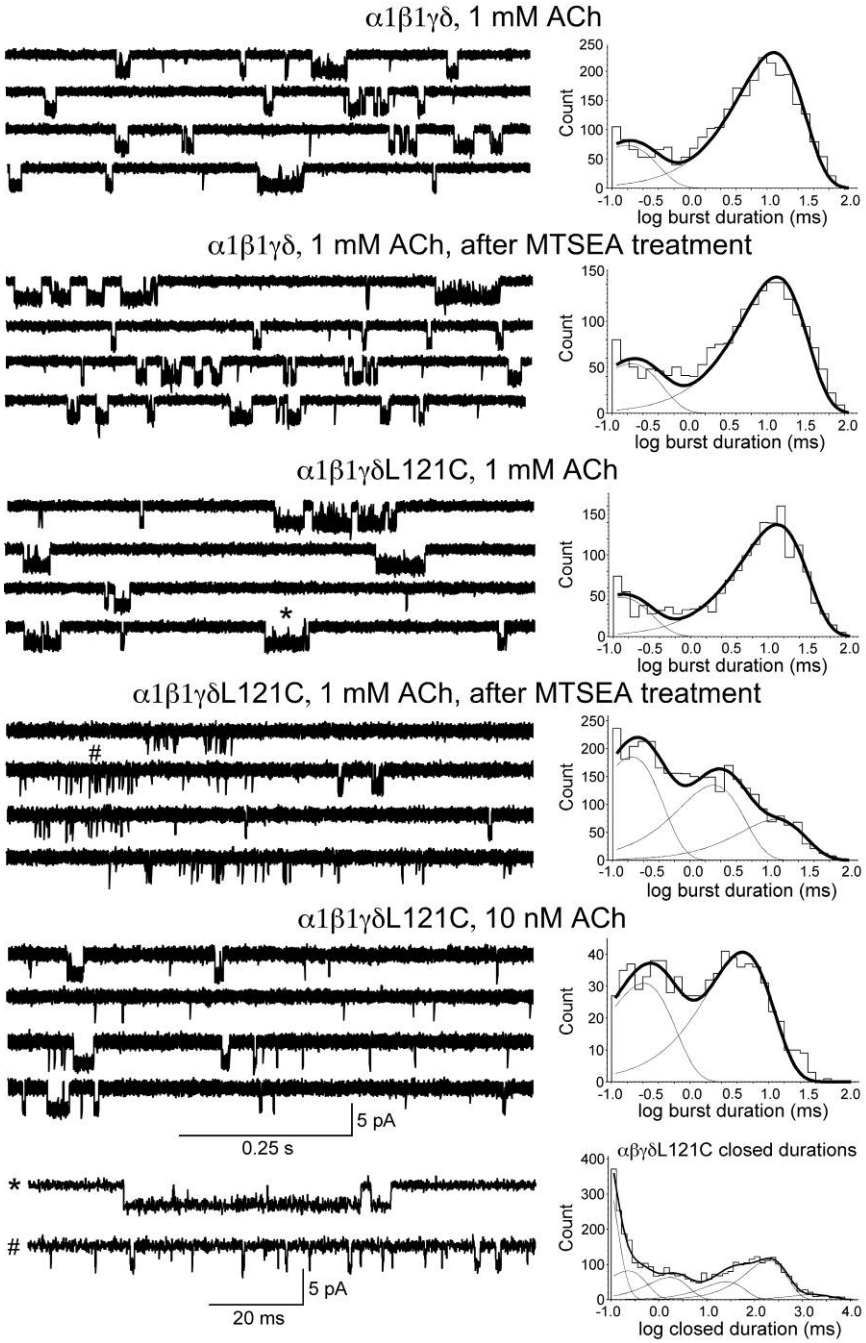

Figure 5-7. Single-channel traces and fit burst-duration histograms from wild type $\alpha1\beta1\gamma\delta$ and $\alpha1\beta1\gamma\delta$L121C receptors before and after MTSEA treatment (5 mM, 60 s) as indicated. Bursts from $\alpha1\beta1\gamma\delta$L121C receptors before and after MTSEA treatment (indicated * or #) are shown on the bottom row in higher time resolution together with the closed duration histogram from $\alpha1\beta1\gamma\delta$L121C (before MTSEA treatment) used to define bursts. Currents were sampled at 100 kHz and ultimately low-pass filtered to 5 kHz. Each histogram represents the data pooled from at least individual 4 patches recorded under identical conditions, except for the 10 nM ACh concentration histogram, where data were pooled from 3 patches. Fit parameters are listed in Table 5-4.

Table 5-1. α7L119C ratio experiments net charge data after MTSEA treatment

mut:wt ratio	I_{max}[a]	EC_{50}, μM
1:1	1.16 ± 0.05	30 ± 4
3:1	0.83 ± 0.04	31 ± 4
5:1	0.78 ± 0.01	72 ± 3

[a]Measured relative to ACh maximum before MTSEA treatment.
Note: Values are the means ± SEM of at least 5 oocytes.

Table 5-2. MTSEA effects on muscle mutants expressed in *Xenopus* oocytes

	Before MTSEA		After MTSEA	
Muscle mutant	I_{max}[a]	EC_{50}, μM	I_{max}[a]	EC_{50}, μM
α1β1γδL121C (n = 5)	1.30 ± 0.05	12.7 ± 1.5	1.41 ± 0.03	111 ± 8
α1β1εL119Cδ (n = 3)	2.72 ± 0.08	48.0 ± 4.0	2.40 ± 0.02	126 ± 4
α1β1εδL121C (n = 8)	2.56 ± 0.01	39.1 ± 0.4	1.84 ± 0.04	145 ± 9
α1β1γδ (n = 5)	1.15 ± 0.03	4.52 ± 0.39	1.35 ± 0.05	3.24 ± 0.41
α1β1εδ (n = 7)	1.28 ± 0.003	16.1 ± 0.1	1.53 ± 0.004	22.0 ± 0.11

[a]Measured relative to average 30 μM ACh control before MTSEA treatment.

Table 5-3. Peak current and NP_{open} measurements from the outside-out patch clamp experiments

	α1β1γδL121C (control) (n = 8)	α1β1γδL121C (n = 12)	α1β1γL119CδL121C (n = 9)	α1β1γδ (n = 8)
avg. post/pre NP_{open}[a]	0.44 (1)	0.28 (0.65)	0.060 (0.14)	0.36 (0.83)
SEM	0.13	0.059	0.015	0.085
range	0.078 – 1.13	0.066 – 0.69	0.0088 – 0.11	0.14 – 0.65
median	0.38	0.25	0.066	0.36
avg. post/pre peak[a]	0.41 (1)	0.31 (0.74)	0.030 (0.073)	0.44 (1.06)
SEM	0.081	0.084	0.0027	0.11
range	0.11 – 0.74	0.051 – 1.10	0.020 – 0.045	0.14 – 0.78
median	0.42	0.23	0.026	0.44

[a]Normalized values are indicated in parenthesis.
Note: 1 mM ACh applied before and after 5 mM ACh treatment.

Table 5-4. Fit time-constants from the burst-duration histograms

condition	τ_1 ± sem	P_1 ± sem	τ_2 ± sem	P_2 ± sem	τ_3 ± sem	P_3 ± sem
α1β1γδ; 1 mM Ach	0.15 ± 0.17	0.24 ± 0.03	12.2 ± 0.04	0.76 ± 0.02	n/a	n/a
α1β1γδ after MTSEA	0.18 ± 0.15	0.26 ± 0.03	13.3 ± 0.04	0.74 ± 0.02	n/a	n/a
α1β1γδL121C; 1 mM ACh	0.13 ± 0.2	0.26 ± 0.04	12.9 ± 0.05	0.74 ± 0.02	n/a	n/a
α1β1γδL121C after MTSEA	0.18 ± 0.08	0.47 ± 0.02	2.02 ± 0.12	0.34 ± 0.03	12.6 ± 0.2	0.19 ± 0.03
α1β1γδL121C; 10 nM ACh	0.26 ± 0.07	0.43 ± 0.02	4.66 ± 0.04	0.57 ± 0.02	n/a	n/a

Note: τ values are indicated in ms and P values indicate fraction of total events from histogram fits.

CHAPTER 6
INVESTIGATION OF THE MOLECULAR MECHANISM OF THE ALPHA7 NICOTINIC ACETYLCHOLINE RECEPTOR POSITIVE ALLOSTERIC MODULATOR PNU-120596 PROVIDES EVIDENCE FOR TWO DISTINCT DESENSITIZED STATES

Introduction

Alpha7 nAChRs are considered potentially important therapeutic targets, but the development of selective agonists has been hindered by the concern that endogenous cholinergic function will be disrupted by an agonist-based therapeutic approach. Therapeutic strategies utilizing PAMs may allow this issue to be avoided [322]. The α7 nAChR is a good candidate for allosteric potentiation due to its intrinsically low P_{open}. PNU-120596 is one of the most well known α7 PAMs due to its ability to profoundly enhance the amplitude and dramatically prolong agonist-evoked responses. In addition, application of PNU-120596 evokes currents α7 receptors that have been desensitized by previous exposure to agonist [318, 325]. Here, the potentiation of α7-mediated responses by PNU-120596 was studied via receptors expressed in *Xenopus* oocytes and outside-out patches from BOSC23 cells. Two distinct forms of α7 desensitization are identified; one form of desensitization is destabilized by PNU-120596 (D_s) and the other form of desensitization is insensitive (D_i) to reversal by the PAM and is, in fact, promoted by strong activation. The onset of D_i is so pronounced that large macroscopic currents from outside-out patches decay to the point that PNU-120596 potentiated bursts from individual α7 channels are observed, enabling the properties of PNU-120596 potentiated single-channel bursts to be measured. The outside-out patch clamp experiments demonstrate that PNU-120596 has a remarkable effect on α7 single-channel currents, prolonging the duration of an average single-channel opening bursts by approximately 100,000-fold.

Results

My contribution to the following results was the patch-clamp experiments, which were performed in parallel with the *Xenopus* oocyte experiments conceived by Dr. Roger Papke. Only the oocyte experiments that are most relevant to the experiments I performed are considered here, for the complete body of published work see [376].

ACh-Evoked Responses of α7 nAChR Expressed in *Xenopus* Oocytes

The concentration-response relationships of heteromeric nAChR macroscopic responses determined from peak currents and net charge are superimposable (Figure 6-1A). During a typical application of ACh the response profile closely matches the rate of agonist applications. The processes of activation and desensitization equilibrate to from a phase of relatively steady current, or a plateau, that decays as agonist is removed [213]. In contrast to heteromeric nAChRs, the concentration-response relationships of the homomeric α7 nAChR for peak currents and net charge are non-superimposable. This occurs because the responses of α7 nAChR evoked by high concentrations of agonist (Figure 6-1B) reach a peak before solution exchange is complete [213]. The application of high agonist concentrations produce large peak currents, which are indicative of synchronous channel activation, but do not increase total receptor activation measured by net charge because high agonist concentrations rapidly promote the entry of the receptor into a non-conducting desensitized state. A documented effect of the type II α7 PAM PNU-120596 is to reverse or destabilize one or more forms of α7 receptor desensitization. As shown in Figure 6-1C, the concentration-response relationships for peak current and net charge evoked by ACh and recorded in the presence of PNU-120596 were superimposable, as is the case with heteromeric

nAChR. This observation is consistent with the hypothesis that PNU-120596 destabilizes the rapid form of desensitization that is unique to α7.

ACh-Evoked Responses of α7 nAChR Expressed in BOSC23 Cells in the Absence and Presence of PNU-120596

A typical response of an outside-out patch expressing α7 to rapid application (≤0.7 ms) of 60 μM ACh is shown in Figure 6-2A. Channel openings occur with highest frequency immediately after application of ACh and then quickly disappear despite continued application of agonist. Individual α7 channel openings are extraordinarily brief, and appear primarily as isolated events rather than bursts of openings. At a bandwidth of 10 kHz, the average duration of the apparent α7 single-channel openings evoked by 60 μM ACh is 113 ± 7 μs (n = 187 openings, 13 patches). Considering that this short duration approaches the temporal resolution limit of 40 μs, many openings probably occurred that were too short to be reliably detected, and the average α7 open duration is over-estimated. Figure 6-2B displays a histogram of the apparent channel openings fit by a single exponential function. Assuming the distribution of the missed openings follows the fit exponential function to the ordinate, the corrected average α7 single-channel open duration is 59 ± 5 μs. At a holding potential of -70 mV, the average single-channel amplitude of the apparent α7 openings was -6.22 ± 0.08 pA. Given that individual α7 openings were so short in duration, this value may be an under-estimate of the true single-channel amplitude. A scatter plot of channel amplitude versus open duration showed no clear overall relationship. However, all openings > 300 μs in duration had single-channel amplitudes between -6.8 pA and -7.6 pA (not shown).

The type II PAM PNU-120596 had a profound impact on responses evoked by 60 μM ACh from outside-out patches (Figure 6-2C). In the absence of PNU-120596, responses evoked by 12 second applications of 60 μM ACh are limited due to the low P_{open} intrinsic to α7 and may lead one to believe the patch contains few channels. A follow-up application of 60 μM ACh with 10 μM PNU-120596 to the same patch revealed that in reality the patch contained a multitude of channels, demonstrating the massive potential for enhancement of α7 responses by PNU-120596. The net-charge response evoked by co-application of 60 μM ACh and 10 μM PNU-120596 was on average 1.35 ± 0.42 x 10^5-fold larger than the net-charge response evoked by 60 μM ACh alone (n = 4).

The peak current of the response evoked by ACh and PNU-120596 co-application, divided by the unitary current amplitude of PNU-120596-potentiated currents, provides a lower-limit estimate of the number of channels in a patch (N). The number of channels in each patch is unknown, but is a parameter of interest since it is required to calculate P_{open}. The ACh and PNU-120596 concentration combination that evokes maximal peak responses is important to know in order to obtain a lower-limit estimate of N that is as accurate as possible. Several experiments were performed with *Xenopus* oocytes expressing α7 to test various concentration combinations of ACh and PNU-120596 and found that a range of ACh (10 μM – 100 μM) concentrations with 10 μM PNU-120596 provided comparable maximal peak currents (data not shown). Based on the detected α7 openings in the absence of PNU-120596 and the lower-limit of N provided by peak currents in response to 60 μM ACh and 10 μM PNU-120596 co-application, an upper-limit estimate of α7 P_{open} in response to a 12 second application of

60 μM ACh of $7.4 \times 10^{-6} \pm 3.0 \times 10^{-6}$ (n = 4) was calculated. It is important to understand that this estimate is strictly an upper-limit estimate since N is unknown and potentially greatly underestimated. Also, it is equally important to appreciate that this estimate includes the non-stationary portion of the 60 μM ACh-evoked responses, immediately after application of ACh when channel activation occurs with highest probability, and that under true steady-state conditions the upper-limit α7 P_{open} will be much less.

Factors Limiting the Potentiating Effects of PNU-120596 on α7-Mediated Currents

The time and concentration-dependence of PNU-120596 potentiation of wild type human α7 nAChR responses was investigated by making repeated applications of 60 μM ACh in the presence of varying bath concentrations of PNU-120596 over the course of one hour. With ACh fixed at 60 μM, maximal potentiation of peak current amplitude was achieved with 10 μM PNU-120596 (Figure 6-3A). Interesting concentration-dependent effects were seen on the onset and decline of potentiation with varying concentrations of PNU-120596 (Figure 6-3B). In the presence of 0.3 μM PNU-120596, potentiation increased throughout the entire 64 minutes and never reached a plateau; potentiation was significantly ($p < 0.01$) larger at 64 minutes than at 12 minutes. In the presence of 1 μM PNU-120596, potentiation increased during the first 40 minutes and then began to decrease. Potentiation was greater at 40 minutes than at 12 minutes ($p < 0.05$), but not significantly greater at 64 minutes than at 12 minutes. For all concentrations of PNU-120596 ≥ 3 μM, potentiation reached a peak within 12 minutes and then decayed; potentiation at 64 minutes was significantly less than that at 12 minutes ($p < 0.05$). These data suggest that increasing concentrations of PNU-120596,

and by inference occupancy of the PAM binding sites, promote forms of desensitization that are insensitive (D_i) to PNU-120596 and that accumulate over time.

Likewise, the ability of increasing agonist concentrations, and by inference increasing agonist occupancy, to promote D_i is demonstrated by first applying 1 μM ACh and then applying 100 μM ACh to the same outside-out patch expressing α7 with a fixed concentration of PNU-120596 (Figure 6-4). Neither the peak current nor the net charge were different between responses evoked by 1 μM ACh or 100 μM ACh in the presence of 10 μM PNU-120596 on the time scale of these experiments. However, the onset and decay of the potentiated responses were different. Responses evoked by 1 μM ACh in the presence of 10 μM PNU-120596 had significantly ($p < 0.05$) slower 10%-90% rise-times than responses evoked by 100 μM ACh and 10 μM PNU-120596 (12.3 ± 5.1 s versus 1.4 ± 0.5 s; n = 4). Responses evoked by 100 μM ACh tended to peak relatively rapidly and then decay despite the continued application of ACh and PNU-120596, while responses evoked by 1 μM ACh generally showed little-to-no decay on the time scale of these recordings. The ratio of the net charge during the last quarter of the response relative to the first quarter of the response was 1.35 ± 0.28 with 1 μM ACh, whereas the ratio was 0.39 ± 0.08 in the 100 μM ACh condition. The average 90%-10% decay time of 100 μM ACh and 10 μM PNU-120596 responses was 26.14 ± 3.52 s (n = 4).

In order to test the hypothesis that the induction of D_i is dependent on receptor activation, oocytes were treated with one of two different stimulus protocols (Figure 6-5). In the continued presence of 3 μM PNU-120596, oocytes were either repeatedly stimulated with 10 μM ACh or with 10 μM ACh applications in alternation with stronger

stimulation by 300 μM ACh. As shown in Figure 6-5B, the 10 μM ACh-evoked responses of cells stimulated alternately with 300 μM ACh reached a level of maximal potentiation relatively quickly and then showed a decline, consistent with the induction of D_i. In contrast, the 10 μM ACh-evoked responses of oocytes that did not receive alternating application of 300 μM ACh were slower to reach the same level of maximal potentiation, but also no decline in potentiation occurred over the course of an hour. Together these results suggest that both agonist and PNU-120596 concentrations affect the time course of potentiated responses, with faster onset of potentiation and subsequent decay occurring at high concentrations, and low concentrations producing relatively slow rising, but longer-lasting currents.

Although α7 nAChRs desensitize rapidly in response to high concentrations of agonist, the desensitization is also rapidly reversible once agonist has dissociated from the receptor [229]. As shown in Figure 6-6A, if repeated co-applications of 60 μM ACh and 10 μM PNU-120596 to oocytes were stopped during the period of time when D_i was developing and later reinitiated, the receptors became resensitized to the effects of the PAM. Likewise, recovery from D_i occurred in outside-out patches in experiments performed on a much shorter timescale (Figure 6-6B), suggesting that PNU-120596-insensitive forms of desensitization are reversible.

Single-Channel Bursts of α7 nAChR Promoted by PNU-120596

Because the potentiation of responses by PNU-120596 is so profound, the probability of observing single-channel currents potentiated by PNU-120596 was initially hypothesized to be low. However, the decay of current was so pronounced with prolonged long applications of 300 μM ACh and 10 μM PNU-120596 that single-channel

bursts potentiated by PNU-120596 were revealed once the majority of channels entered the D_i state(s) (Figure 6-7A). From three patches with sections of continuous data > 60 seconds lacking simultaneous channel openings, the steady-state NP_{open} in 300 μM ACh and 10 μM PNU-120596 was 0.40 ± 0.04. Given the length of the single-channel bursts and the lack of simultaneous openings in these traces, it seems that the number of activatible channels at any time is greatly limited by D_i. It is unknown whether the openings in these traces all arise from one resilient channel that escaped and remained resistant to D_i, or whether the openings arose from multiple channels as they temporarily escaped D_i.

There appeared to be two qualitatively distinct groups of single-channel openings in the presence of PNU-120596 (Figure 6-7A). One class of PNU-120596-potentiated opening appeared as relatively brief events that primarily occurred in isolation, and the other, more common, type of PNU-120596-potentiated openings appeared to occur as long bursts of openings separated by very short closures to either fully closed or subconductance states (see below). Most of the brief openings observed in the presence of PNU-120596 were <1 m in duration, occasionally lasting approximately 8 ms (Table 6-1). A major component of the isolated openings evoked in the presence of PNU-120596 was fit with a time constant of 120 ± 6 μs, which is similar to the average apparent open duration in the absence of PNU-120596.

On average, the protracted bursts of openings potentiated by 10 μM PNU-120596 persisted for 5.48 ± 0.40 s (n = 217, 26 patches). The majority of the apparent intraburst closures were approximately 100 μs-200 μs; however, occasionally intraburst closures longer than approximately 10 ms were observed. The subconductance events

were approximately 400 μs or less in duration and were interrupted by many fast full channel closures (Figure 6-7A inset, Table 6-1). There appeared to be two distinct classes of the long PNU-120596-potentiated bursts; the distinction was made based on the duration of the intraburst openings (Figure 6-7B, Table 6-1). Approximately 27% of the bursts analyzed exclusively contained intraburst openings of approximately 5 ms in duration (class I bursts) and 73% of the bursts exclusively contained intraburst openings of approximately 30 ms in duration (class II bursts); no clear relationship was apparent between burst length and average intraburst open durations (Figure 6-7B). The apparent closed and subconductance duration intervals were similar between the two classes of bursts (Table 6-1). The reason for the two types of bursts is unclear, but may be related to occupancy of ACh and/or PNU-120596 at their respective binding sites during the burst of openings.

At a holding potential of -70 mV, the single-channel amplitude of openings potentiated by PNU-120596 was -7.76 ± 0.08 pA, and the subconductance level amplitude was -3.59 ± 0.02 pA. The current-voltage relationship of currents evoked in the presence of PNU-120596 showed strong inward rectification, a reversal potential of -6.93 ± 1.01 mV, and a single-channel chord conductance of 129 ± 3 pS through the linear section of the relationship (n = 6, data not shown). Given that PNU-120596 appears to have little, if any, effect on channel conductance [318], the conductance measured in the presence of PNU-120596 is likely to be a reasonable estimate of single-channel $\alpha 7$ conductance in the absence of PNU-120596. This measurement of 129 ± 3 pS is higher than the previously published values of 60-90 pS [215, 216], but

the difference is probably related to the limited ability to accurately measure $\alpha 7$ open channel amplitude, since non-potentiated $\alpha 7$ openings are so brief.

A phenomenon observed with currents from the outside-out patches that have been activated with ACh and potentiated by PNU-120596 was a postponed return to baseline after the removal of external ACh (Figure 6-8A). For single-channel bursts activated in the presence of 300 μM ACh and 10 μM PNU-120596, currents persisted for 2.57 ± 0.2 s following the removal of external ACh (n = 143, 15 patches). There was no detectable change of intraburst open durations, nor was there an apparent trend toward change in intraburst open duration over time after ACh removal. The protracted currents were not an artifact of slow or incomplete solution exchange based on three arguments. First, following data collection each patch was blown off the tip of the pipette and solution exchange profiles were determined by measuring changes in holding current upon moving diluted saline over the open pipette tip with the piezoelectric stepper (Figure 6-8B). Data were analyzed only if the solution exchange profile measured in this way was clean and occurred rapidly, within ~700 μs (10%-90% rise-time). Typical solution exchange times measured with this method were between 400 μs and 700 μs. Second, there was a sharp reduction in current noise that was intimately associated with the removal of external ACh (Figure 6-8B). This reduction in noise was likely due to relief of channel block by ACh, given that a relatively high concentration was used as the stimulating agonist [412]. This reduction in current noise was highly significant ($p < 3 \times 10^{-15}$), as measured by changes in the standard deviation from the mean open current before and after removal of external ACh (σ = 0.44 ± 0.008 versus 0.31 ± 0.003). Third, replacement of external ACh with the competitive $\alpha 7$

antagonist MLA greatly attenuated the duration of the protracted currents (see below). The currents that persisted long after the removal of external ACh were consistent with prolonged retention of ACh at the binding sites when PNU-120596 is applied. However, this observation could also be explained by maintenance of the channel in a reverberating conducting condition by PNU-120596 after dissociation of ACh on termination of external ACh application.

An attempt to test the hypothesis that PNU-120596 prolongs the retention of ACh to its binding site was made by removing external ACh and replacing it with 3 μM MLA. The initial reasoning behind this experiment was if the affinity of the agonist binding site for ACh were increased by PNU-120596, application of the high MLA concentration would have little effect on the duration of protracted currents given that the channel was both occupied by ACh and in an activated condition on application of MLA. However, when ACh was replaced with MLA, the currents persisted for 0.22 ± 0.03 s (n = 25, 3 patches) after removal of external ACh, a significant ($p < 1 \times 10^{-5}$) reduction of the protracted current duration (Figure 6-8C). It is noteworthy that the effect of MLA, which is normally considered a competitive antagonist, had the appearance of an inverse agonist in these experiments, given that channels were active when MLA was applied, and MLA shortened burst activity under conditions when no external ACh was available for competition. Prior to moving the patches out of the solution containing 300 μM ACh, it is reasonable to assume that the five agonist binding sites of $\alpha 7$ were occupied by ACh at high probability. Further, it seems likely that after the removal of external ACh, agonist molecules began to dissociate one-by-one until the last ACh molecule dissociated, perhaps resulting in termination of the burst. When external ACh was

removed, and individual ACh molecules began to dissociate, MLA may have had the opportunity to bind the receptor in the vacant binding sites and terminate the burst before all ACh molecules had dissociated. The data suggest that binding of only one or two molecules of MLA may be sufficient to inactivate the entire receptor and that MLA may actively inhibit channel gating, perhaps by stabilizing non-conducting receptor conformations, rather than simply occupying the cavity where ACh binds to produce channel activation.

Discussion

The initial characterizations of the type II PAMs PNU-120596, TQS, and A-867744 reported that these agents reverse or eliminate desensitization [434]. This finding was supported by observations that potentiated currents did not substantially decay on the time scale of the experiments and that previously desensitized receptors could be de-desensitized with application of a type II PAM [318, 325, 326]. The results presented here show that at least two distinct forms of $\alpha 7$ desensitization exist; these are distinguished by their stability in the presence of PNU-120596. The published literature lacks a formal description of D_i, but there are some published observations from other research groups that are interpreted as consistent with the existence of PAM-insensitive D_i states. First, when agonist concentrations are increased in the presence of a fixed PAM concentration, responses are generally enhanced over the full agonist concentration ranges, but the magnitude of potentiation often tends to peak at intermediate concentrations and actually decrease at the higher agonist concentrations [318, 321, 325]. A similar phenomenon is sometimes observed when modulator concentrations are increased in the presence of a constant agonist concentration [320,

321]. Second, applications of TQS [325] or A-867744 [326] were shown to re-activate receptors that had been desensitized by a high concentration of agonist and produced a non-decaying current on the time scale of the experiments, consistent with reversal of D_s states to conducting states. However, the peak of the potentiated current in the presence of either TQS or A-867744 was only ~50% of the peak response recorded in the absence of PAM, indicating that only a fraction of the receptor populations were actually conducting current at any given moment. Third, several applications of 30 μM nicotine, with short inter-stimulus intervals, in the continued presence of PNU-120596 produced successively smaller responses [316], indicative of the accumulation of modulator-insensitive D_i states. Fourth, an α-bungarotoxin-sensitive and PNU-120596-dependent increase in calcium response from bovine chromaffin cells was only observed when low (1 μM) concentrations of nicotine were used to stimulate the cells. At concentrations of ≥ 3 μM nicotine, neither PNU-120596 nor α-bungarotoxin had an effect on the response, indicating that the α7 component was lost by the higher nicotine concentrations [435]. In addition, when the α7 component of the total calcium response was isolated, increased concentrations of the α7 agonist PNU-282987, with a fixed PNU-120596 concentration, resulted in decreased α7-dependent calcium responses [435].

The strong apparent induction of D_i in the outside-out patches, yet extremely long bursting activity of individual channels, suggests PNU-120596 is capable of having very large effects on just a few channels at a time. While the net charge of an oocyte whole-cell current is increased as much as 500-fold by PNU-120596, the net charge of a single-channel burst for a PNU-120596-primed channel is approximately 100,000 times

greater than that of a non-potentiated $\alpha 7$ single-channel opening. These two numbers are resolved if only 1 in 200 receptors are active in the bursting states at any moment during a PNU-120596 treatment. While the data suggest that high levels of agonist occupancy generally disfavor channel opening through stabilization of D_i, the mode by which a few resilient PNU-120596-primed channels escape D_i and enter the hyper-bursting state, despite high agonist and PAM occupancy, is less clear. These observations indicate that PNU-120596-primed currents should be used with caution for setting a lower-limit on N, meaning the $\alpha 7$ P_{open} estimate following application of 60 μM ACh could be much less than 7.4×10^{-6}. Even if this upper-limit is greatly overestimated, the data in Figure 6-2 argue strongly against the assumption that $\alpha 7$ P_{open} is high immediately following rapid exposure to agonist, as previously proposed [436].

The observation that bursting activity of single-channels in the presence of PNU-120596 persist for approximately 2.5 seconds after removal of external ACh is consistent with the prolonged retention of ACh once channels enter the PNU-120596-primed bursting mode. This observation, in combination with the finding that the onset of potentiation by PNU-120596 is dependent on channel activity, suggests the possibility that agonist and PAM binding sites mutually interact. This possibility is supported by a recent report that the potency of the agonist PNU-282987 to evoke calcium responses in IMR-32 cells was increased with higher PNU-120596 concentrations, and, vice versa, the potency of PNU-120596 to potentiate responses was increased with higher PNU-282987 concentrations [437]. In addition, computer docking simulations predicted that binding of PNU-120596 to the proposed

transmembrane cavity has higher affinity in an “open” channel model than in a “closed” channel model [344].

Other experiments presented in Williams *et al*., 2011 that were designed by Dr. Papke and performed by other members of the laboratory further support the existence of D_i states [376]. The peaks of potentiated currents were shown to occur faster with stronger stimulation. However, the height of the peak currents and sustained equilibrium currents over time were smallest when higher concentrations of agonist and PNU-120596 were applied, consistent with the induction of D_i states under conditions of strong stimulation. In addition, the competitive antagonists MLA and dihydro-β-erythroidine were shown to be able to modulate the equilibrium between D_s and D_i states. Notably, competitive antagonists appeared to actually have the effect of increasing currents evoked by choline and PNU-120596 in a manner that was dependent on the agonist and antagonist concentrations. Furthermore, benzylidene anabaseine agonists of α7 were shown to stabilize PNU-120596 sensitive states to varying degrees, despite structural similarity, agonists can preferentially stabilize D_s or D_i states. The ability of agonists to preferentially stabilize receptor states may be important in the rational design of α7 agonists if one type of state mediates a desired therapeutic effect. Interestingly, α7-mediated signal transduction has been observed under conditions when ion channel activation is not apparent [438], leaving the intriguing possibility open that α7 desensitized states are not inactive, but functionally meaningful.

Activation of α7 can have either protective or toxic effects depending on the mode of stimulation [227] and the potential for enormous potentiation of α7 responses by type

II PAMs invites the concern that potentiation of α7 with type II PAMs may bring receptor activation to dangerously high levels [434]. There are contradicting reports in the published literature regarding the *in vitro* cytotoxicity profile of PNU-120596; in the two cases where PNU-120596 was found to be toxic [316, 321], the stimulating agonist was the weakly potent α7 agonist choline at a concentration of ~100 μM, which is well below the published EC_{50} value [214] and potentially falls within the window of strong α7 potentiation where D_i is avoided. In contrast, PNU-120596 was reported to lack a significant cytotoxicity profile when co-applied with 10 μM of the potent α7 agonist PNU-282987 [374]. Given that the published EC_{50} value of PNU-282987 in the presence of 3 μM PNU-120596 is only 200 nM [325], and D_i induced by high PNU-282987 concentrations is apparent in bovine chromaffin cells [435], the existence of D_i states may provide an intrinsic safety mechanism and might account for the discrepancy in the published literature regarding type II PAM toxicity profiles.

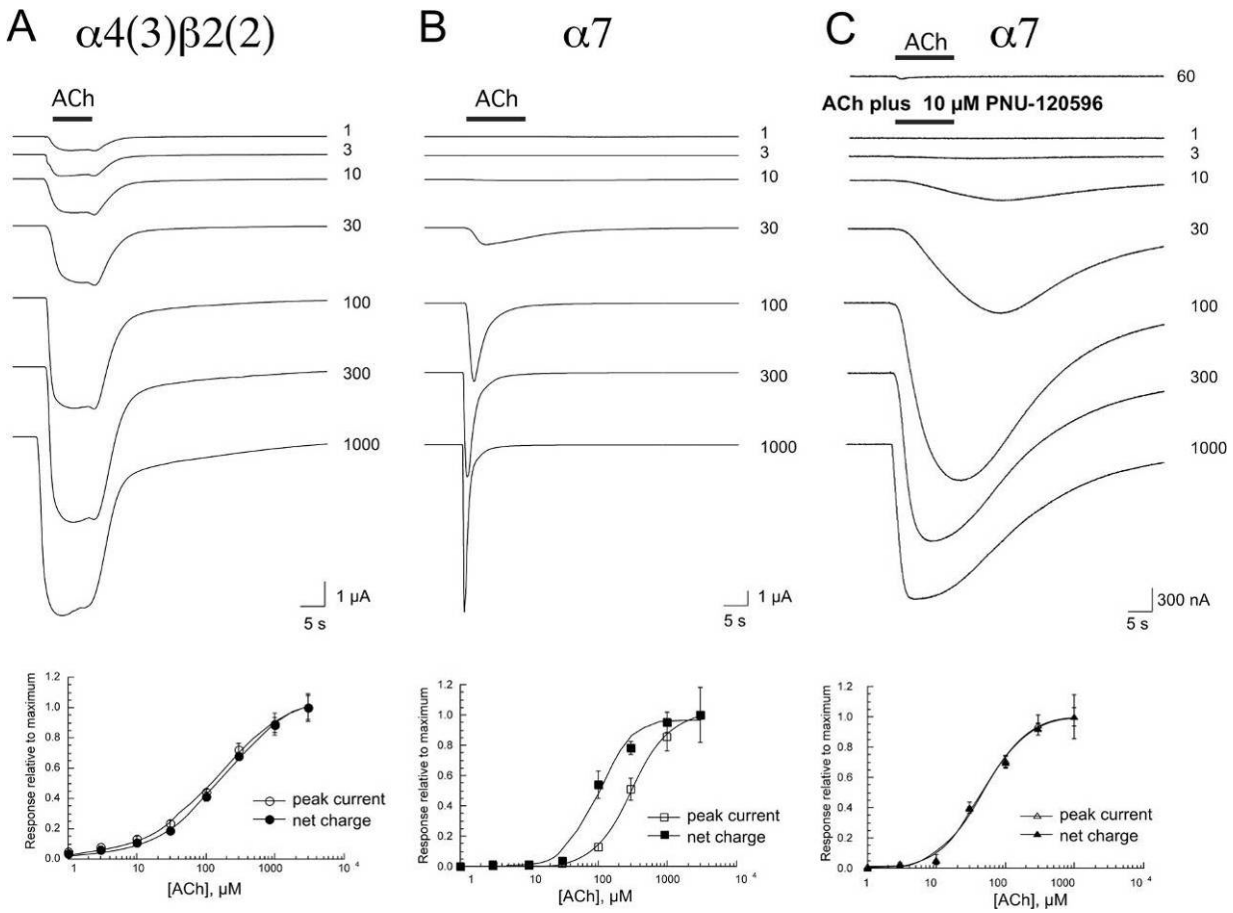

Figure 6-1. The basic characterization of $\alpha 7$ macroscopic currents, comparison to currents from heteromeric $\alpha 4\beta 2$ nAChR, and the effects of PNU-120596. The data in this figure were collected by OpusXpress technicians and were analyzed by Dr. Roger Papke. A) ACh concentration-response relationships for peak currents and net charge from *Xenopus* oocytes expressing human $(\alpha 4)_3(\beta 2)_2$ nAChR. B) ACh concentration-response relationships for peak currents and net charge from *Xenopus* oocytes expressing human $\alpha 7$ nAChR. C) ACh concentration-response relationships in the presence of 10 µM PNU-120596 for peak currents and net charge from *Xenopus* oocytes expressing human $\alpha 7$ nAChR. After obtaining two initial control responses to the application of 60 µM ACh alone, the bath perfusion system was switched to a solution containing 10 µM PNU-120596. ACh and PNU-120596 co-applications were made with the pipette delivery system. Net-charge responses were calculated for a period of 120 s following drug applications. Each data point is the average of at least 4 cells ± SEM.

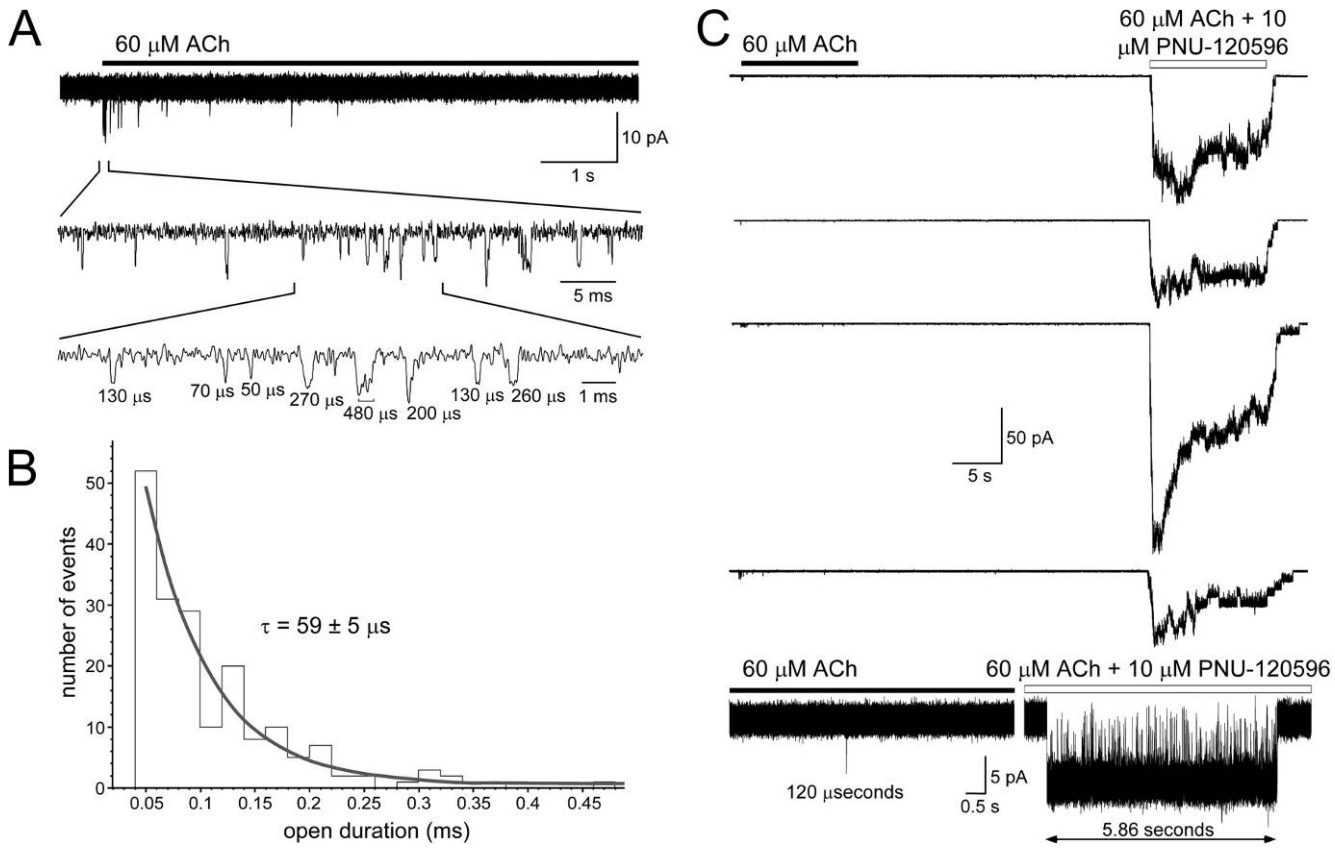

Figure 6-2. The low intrinsic P_{open} of $\alpha 7$ is enhanced by PNU-120596. Data were obtained from outside-out patches pulled from BOSC23 cells transiently expressing human $\alpha 7$ and ric3. A) A typical response evoked by rapid (≤0.7 ms) application of 60 μM ACh showing the short-lived openings that are characteristic of $\alpha 7$. Notice that the frequency of channel openings quickly diminished following exposure of the patch to ACh. B) A histogram of the apparent single-channel $\alpha 7$ open durations evoked by 60 μM ACh (n = 187 open events from 13 patches; 10 kHz bandwidth). Putative openings that could not be clearly distinguished from brief, random noise spikes were excluded from the histogram. The histogram is described by a single exponential function, which predicts that $\alpha 7$ single-channel openings are, on average, approximately 60 μs in duration assuming the distribution of openings too short to be detected (<40 μs) reasonably follows the fit exponential function. C) Responses produced by 60 μM ACh and relative increases produced with co-application of with 60 μM ACh and 10 μM PNU-120596. Drug applications and inter-stimulus intervals were 12 s and 30 s in duration, respectively.

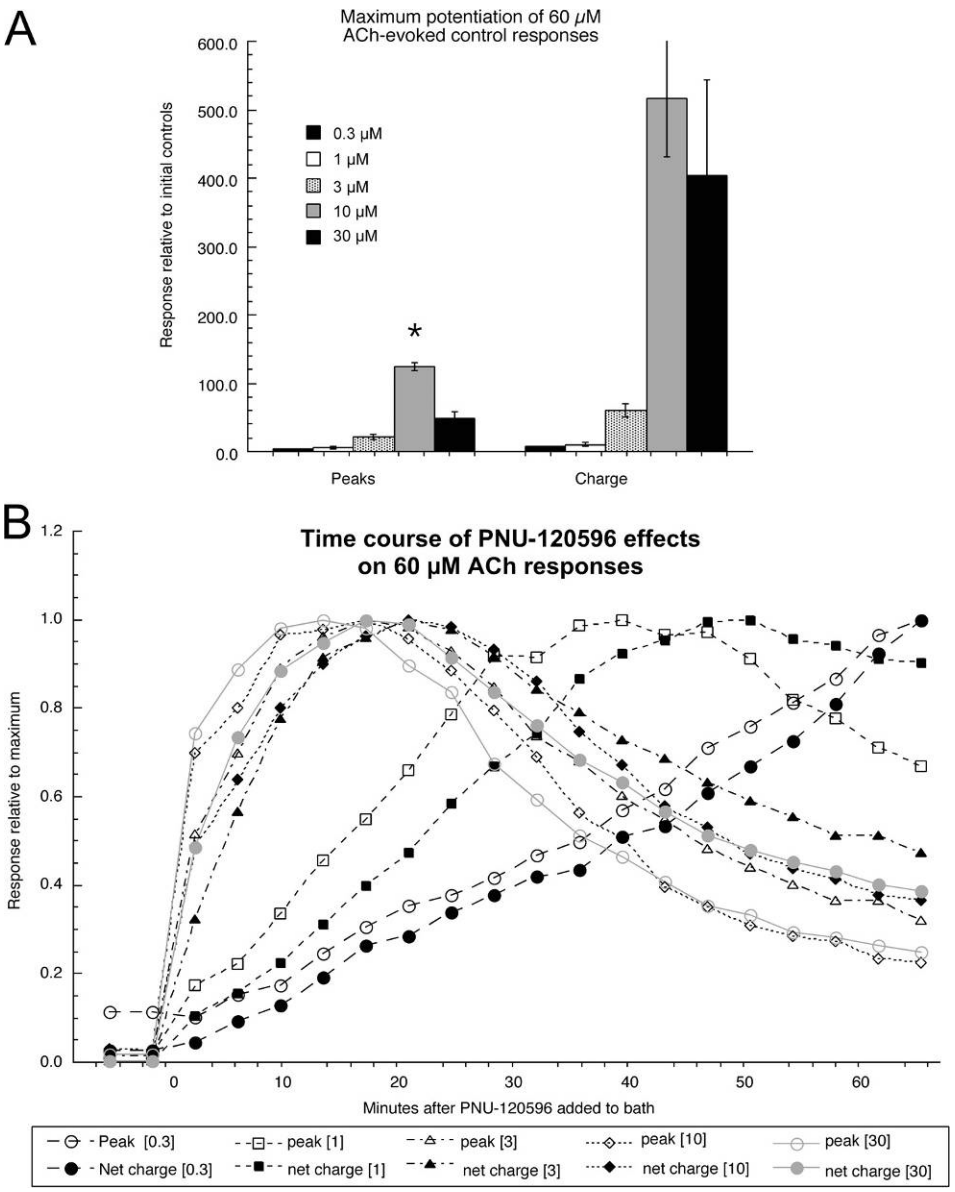

Figure 6-3. Factors defining and limiting the potentiating effects of PNU-120596 on $\alpha 7$ nAChR expressed in *Xenopus* oocytes. The data in this figure were collected by OpusXpress technicians and were analyzed by Dr. Roger Papke. A) Maximum potentiation of 60 μM ACh-evoked responses obtained with different concentrations of bath-applied PNU-120596 applied repeatedly at 4 minute intervals for over 60 minutes. B) The time course of the potentiation of 60 μM ACh-evoked responses by varying concentrations of bath-applied PNU-120596. Note that although each point represents the average of at least four oocytes, error bars have been omitted for clear presentation of the kinetic differences.

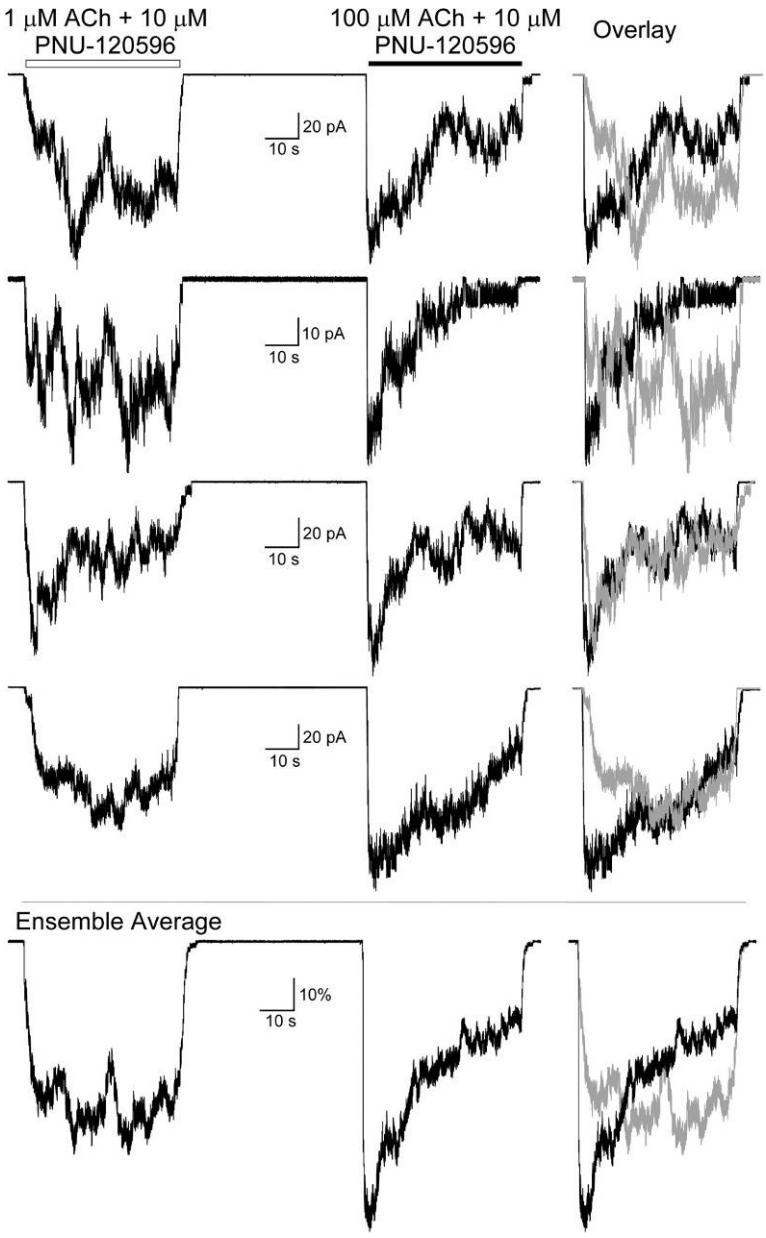

Figure 6-4. Agonist concentration-dependence on the onset and decline of potentiation by PNU-120596 in outside-out patches containing α7 receptors. Comparison of responses from the same patch potentiated by 10 μM PNU-120596 and evoked by 1 or 100 μM ACh. Drug applications and interstimulus intervals were 45 and 55 s in duration, respectively. The ensemble average of all four current traces was created by first normalizing each data point of an individual trace to the peak current of that trace. Then, the average value of the normalized currents was calculated for each data point.

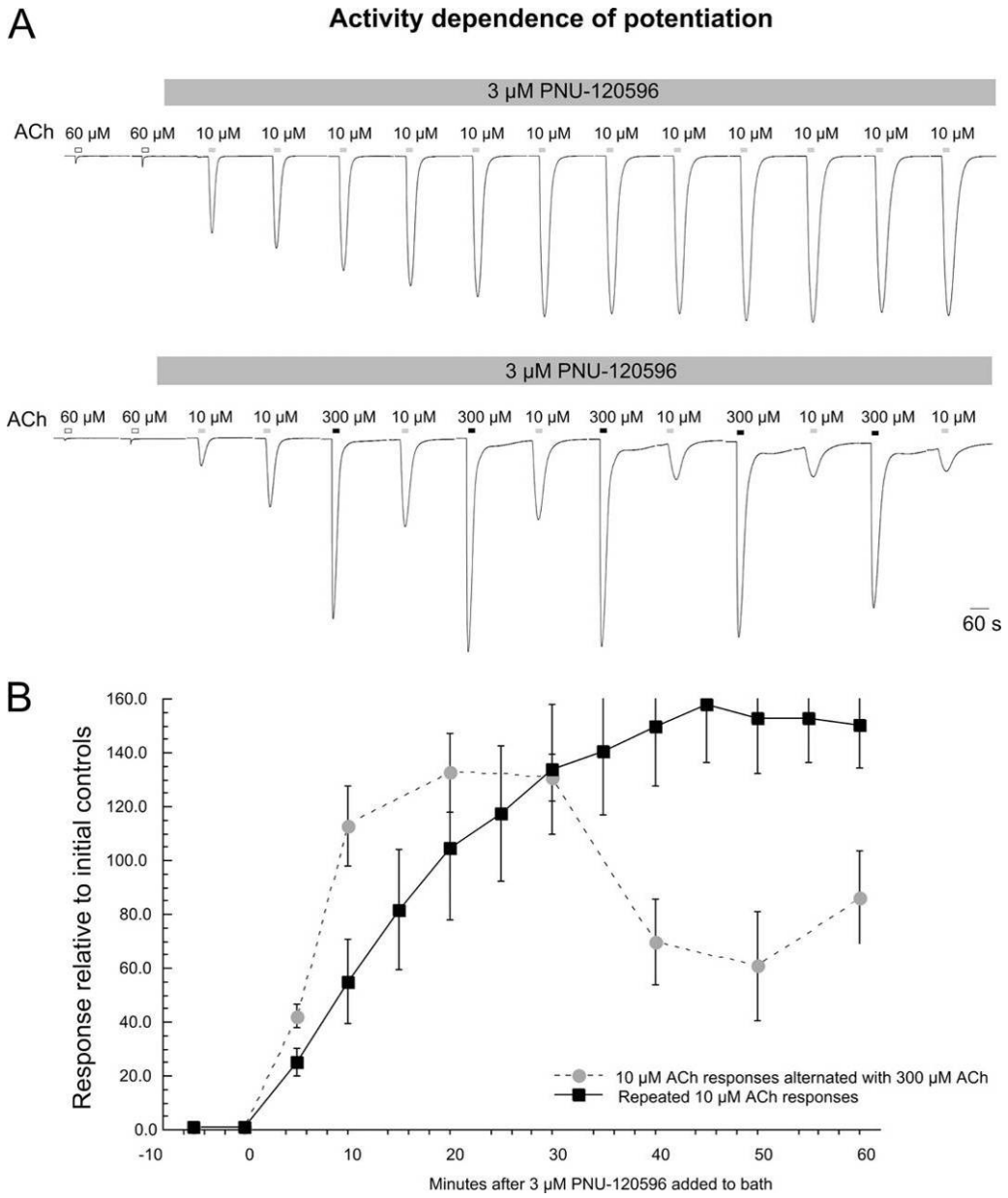

Figure 6-5. Activity dependence of PNU-120596 potentiation onset and decline. The data in this figure were collected by OpusXpress technicians and analyzed by Dr. Roger Papke. A) Representative data traces showing the repeated stimulation of $\alpha 7$ expressing oocytes in the presence of 3 μM PNU-120596. Cells were either stimulated repeatedly with 10 μM ACh (upper trace), or 10 μM ACh alternating with applications of 300 μM ACh (lower trace). B) Average data ± SEM for 10 μM ACh-evoked responses obtained with the two protocols illustrated in panel A. Note that maximal potentiation was achieved more rapidly when there were alternating applications of the high concentration of ACh; however, potentiation subsequently declined.

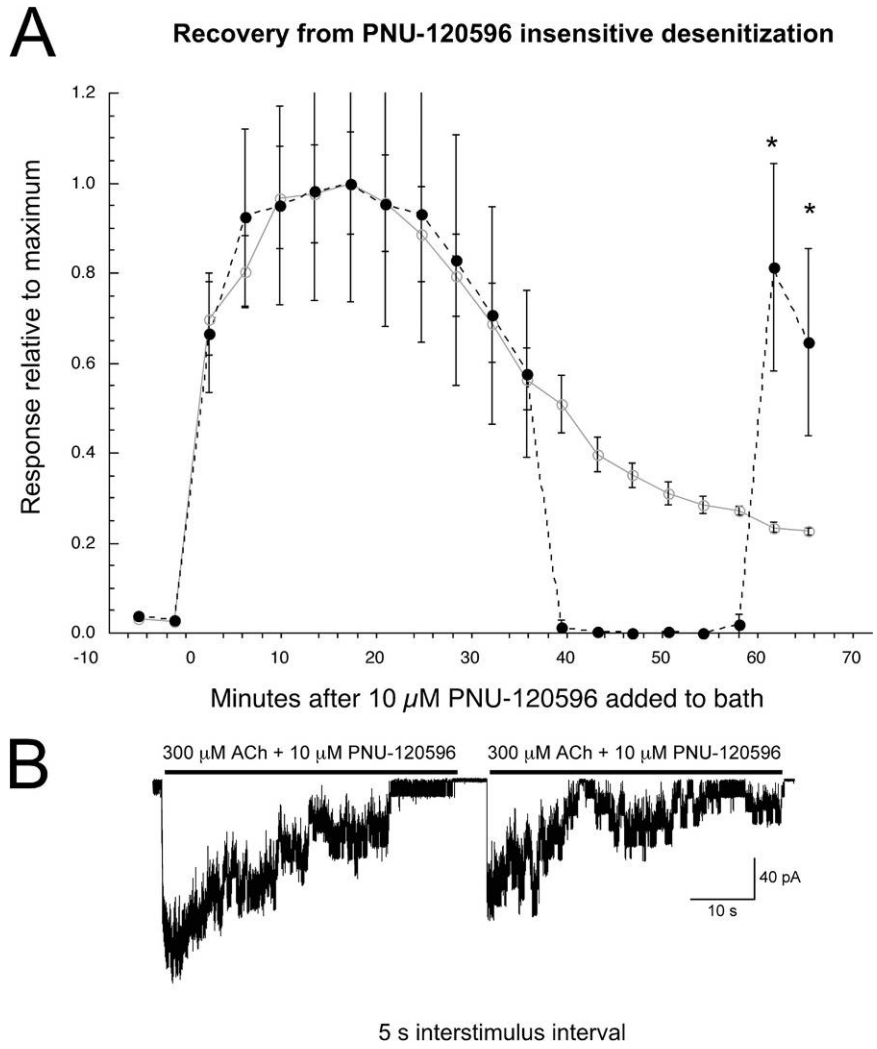

Figure 6-6. Recovery from PNU-120596-insensitive desensitization. A) These data were collected by OpusXpress technicians and were analyzed by Dr. Roger Papke. *Xenopus* oocytes expressing human $\alpha 7$ were stimulated repeatedly with 60 μM ACh in the presence of 10 μM PNU-120596. To determine if the decline in ACh-evoked responses represented a reversible form of PNU-120596 desensitization, some cells (solid points) received 6 applications of PNU-120596 solution alone rather than repeated co-applications of ACh plus PNU-120596. Subsequent application of ACh plus PNU-120596 to the cells that had received a respite from the repeated ACh stimulations returned to a level that was not different the previously maximal level of potentiation, and significantly greater than ($p < 0.01$) that of the cell receiving continuous stimulation. B) Responses potentiated by 10 μM PNU-120596 and evoked by 300 μM ACh show a rapid rise and subsequent decay despite the continued presence of ACh and PNU-120596, indicative of stabilized D_i states. Recovery from D_i induced by co-application of 300 μM ACh and 10 μM PNU-120596 occurs rapidly. Identical 45 s drug applications were separated by 5 s inter-stimulus intervals.

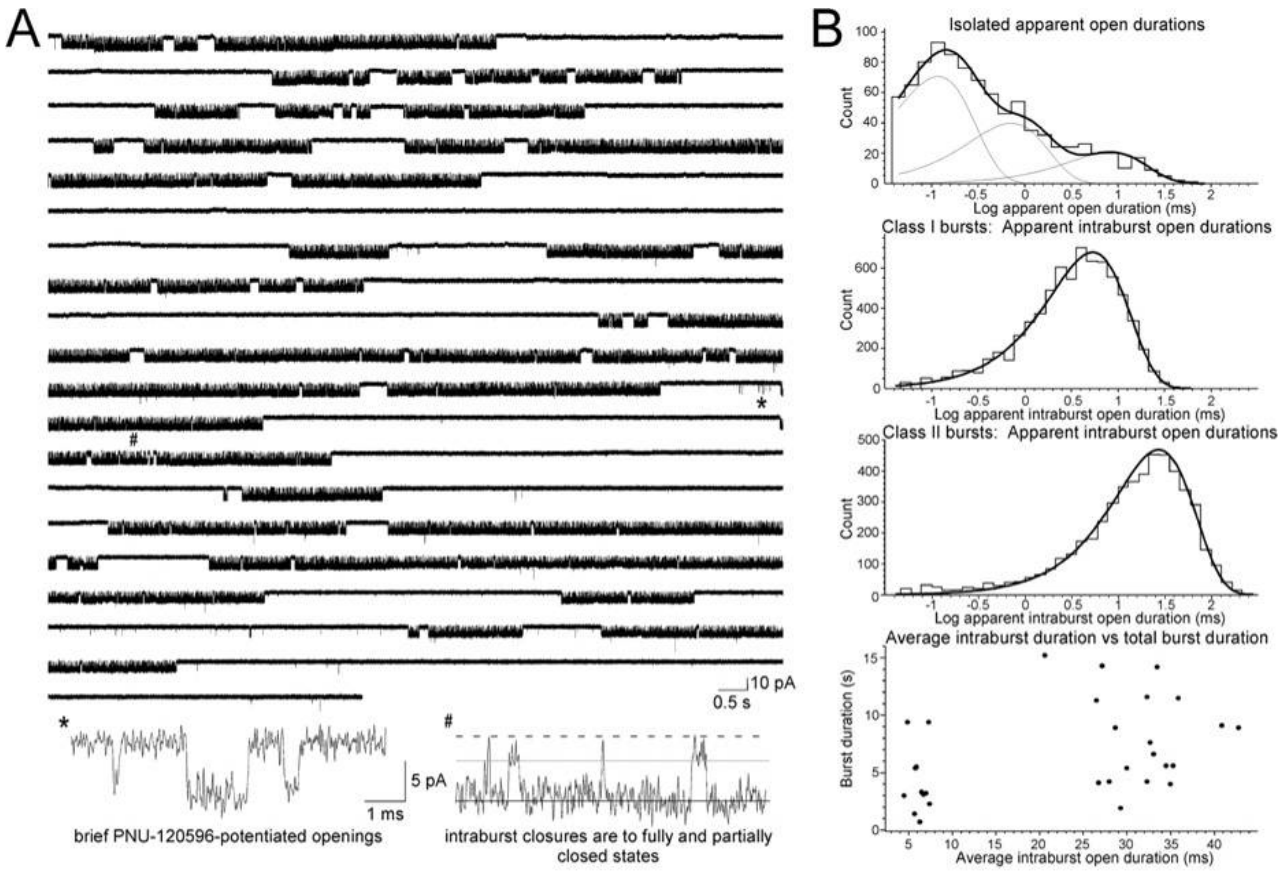

Figure 6-7. Single-channel $\alpha 7$ bursts evoked by 300 μM ACh and potentiated by 10 μM PNU-120596. Data were obtained from outside-out patches pulled from BOSC23 cells transiently expressing human $\alpha 7$ and ric3. A) Continuous data demonstrating the bursting characteristics and high steady-state P_{open} of single-channel openings potentiated by PNU-120596. B) Fit histograms displaying apparent open durations from $\alpha 7$ channels activated by 300 μM ACh and potentiated by 10 μM PNU-120596. Shown are histograms compiled from currents potentiated by PNU-120596 that occur as brief events in isolation, and in long groups of openings as bursts. Two classes of bursts are distinguished based on the average intraburst open duration, which is demonstrated below with a scatter plot of average intraburst duration versus total burst length.

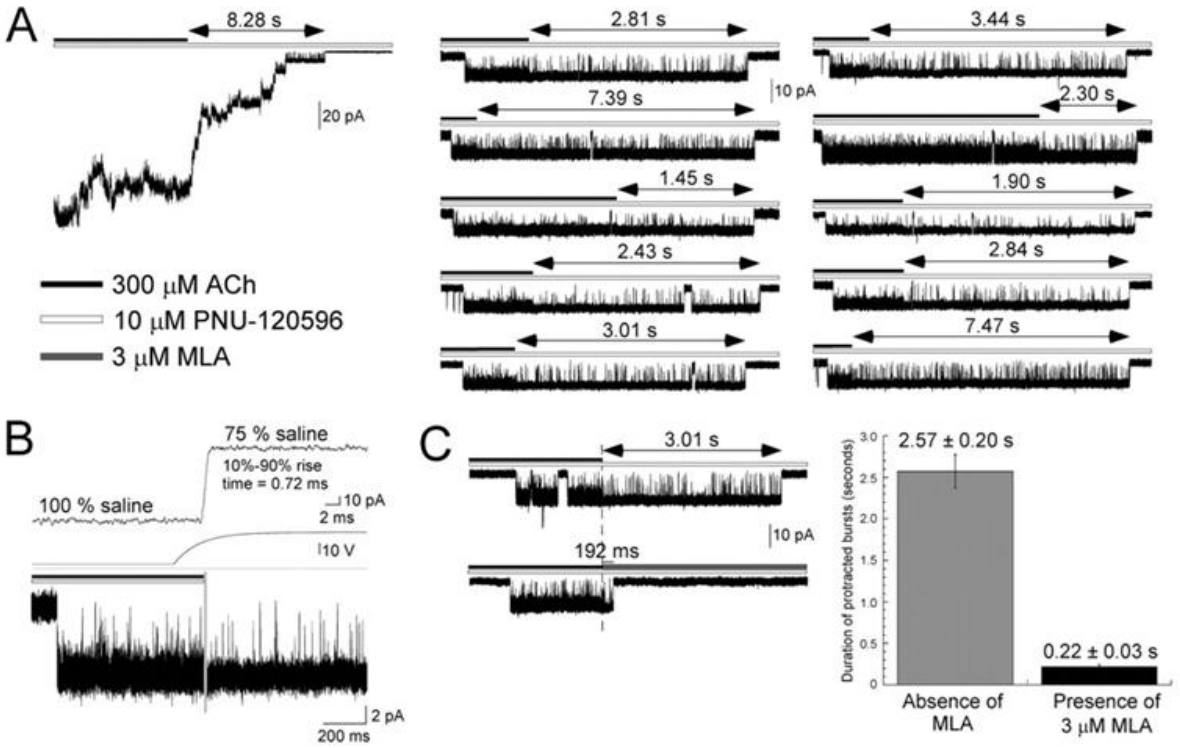

Figure 6-8. Single-channel $\alpha 7$ bursts evoked by 300 μM ACh and potentiated by 10 μM PNU-120596 persist despite the removal of ACh and in a MLA-sensitive manner. Data were obtained from outside-out patches pulled from BOSC23 cells transiently expressing human $\alpha 7$ and ric3. A) PNU-120596-potentiated channel openings persist for seconds after removal of external ACh. Left, an example of a protracted macroscopic current that persisted for approximately 8.3 seconds after external ACh removal. Right, single-channel bursts showing protracted currents of various durations after external ACh removal. B) The protracted currents were not an artifact of solution exchange. Above, solution exchanges typically occurred within 400 μs - 700 μs, as measured by open-tip recordings performed following data collection from each patch. Below, a sharp reduction in current noise was associated with the removal of external ACh. The noise was likely due to channel block by agonist, which disappeared as external agonist was removed. C) Application of the competitive antagonist MLA following removal of external ACh shortened the duration of protracted currents. All currents were obtained from the same patch.

Table 6-1. Fit time-constants from event duration histograms in the presence of 300 μM ACh and 10 μM PNU-120596

	Isolated openings		Class I bursts		Class II bursts	
Type of event	P ± sem	τ ± sem	P ± sem	τ ± sem	P ± sem	τ ± sem
Intraburst closures	n/a	n/a	0.91 ± 0.06	0.07 ± 0.10	0.77 ± 0.14	0.16 ± 0.18
	n/a	n/a	0.07 ± 0.04	0.51 ± 0.82	0.21 ± 0.15	0.57 ± 0.6
	n/a	n/a	0.02 ± 0.03	9.16 ± 4.52	0.02 ± 0.04	13.2 ± 2.5
Intraburst subcond	n/a	n/a	0.80 ± 0.12	0.08 ± 0.09	0.82 ± 0.07	0.14 ± 0.09
	n/a	n/a	0.20 ± 0.04	0.40 ± 0.20	0.18 ± 0.09	0.37 ± 0.24
Intraburst openings	0.54 ± 0.02	0.12 ± 0.06	n/a	n/a	n/a	n/a
	0.30 ± 0.02	0.71 ± 0.11	n/a	n/a	n/a	n/a
	0.16 ± 0.02	8.23 ± 0.14	1	5.35 ± 0.02	1	27.25 ± 0.02

Note: τ values are indicated in ms and P values indicate fraction of total events from fit Histograms.

CHAPTER 7
A NOVEL CELL LINE STABLY EXPRESSING HUMAN ALPHA7 NICOTINIC ACETYLCHOLINE RECEPTORS REVEALS THAT PNU-120596 POTENTIATION AND CYTOXICITY ARE ATTENUATED AT PHYSIOLOGICAL TEMPERATURES

Introduction

Within the last 20 years both academic and industrial labs have discovered numerous agonists with selectively for α7 [314]. These efforts have been justified by large amounts of pre-clinical *in vitro* and *in vivo* behavioral data from several independent laboratories suggesting that activation of α7 may provide cytoprotection, enhances performance in a variety of behavioral tasks thought to be related to cognitive function, and reduces auditory gating deficits modeled after those seen in schizophrenia [294, 295]. An alternative therapeutic approach based on allosteric modulation has gained momentum in recent years with the discovery many structurally diverse PAMs of α7 nAChR [322].

In cases where activation of α7 is necessary for a desired effect [291], a PAM-based therapeutic approach offers several potential advantages over agonist-based strategies. For example, PAMs may be able to offer increased selective targeting of a desired receptor subtype since PAM binding sites presumably have less evolutionary pressure than agonist binding sites, which must accommodate the endogenous ligand. In addition, the temporal firing dynamics of native cholinergic signaling may be better conserved since PAMs would theoretically only augment the response provided by the natural release of ACh. However, a PAM-based strategy is also subject to some important limitations that need to be appreciated. First, PAMs will require sufficient endogenous neurotransmitter release, which could be an issue in neurodegenerative disorders. Second, desensitized states have been identified that are stable in the

presence of PNU-120596 (see chapter 6 and [376]). This type of desensitization (D_i) appears to be promoted by strong channel activation and high fractional occupancy of both agonist and modulator binding sites. Although the implications of such states have not been addressed *in vivo,* it is conceivable that D_i states may accumulate over time with the prolonged presentation of a PAM. Third, toxicity poses a real threat due to excess activation of the calcium-permeable pore. Indeed, strong activation of α7 channels has been previously shown to be cytotoxic [371, 373]. The issue of PAM-induced toxicity *in vitro* has been evaluated by three independent groups and while the data agree that type I PAMs appear to lack *in vitro* cytotoxicity, the data are contradicting regarding the toxicity of the type II PAM PNU-120596. Fourth, the ability of α7 PAMs to potentiate α7-mediated responses may be significantly reduced at physiological temperature [439]. This has obvious implications for understanding basic science questions about how these compounds work and, more importantly, for their development as human therapeutics. These results also raise questions regarding the relevance of *in vitro* electrophysiological experiments performed at non-physiological temperatures, which are preferentially performed due to technical reasons including the fact that patches are less stable at higher temperatures and the requirement for additional equipment in order to precisely control the temperature of experimental solutions.

Here, a novel HEK293 cell line stably expressing the human α7 nAChR was created and used to characterize the *in vitro* temperature dependence of and cytotoxicity profile of PNU-120596. The findings suggest that the potentiating activity of PNU-120596 is reduced at physiological temperature, but that some endogenous

factors such as serum albumins may partially restore the ability of PNU-120596 to potentiate responses at 37°C.

Results

Expression of hric3 and hα7 mRNA in Hygromycin- and G418- Resistant Clones

Total mRNA was isolated from each hygromycin- and G418-resistant clone and tested for the presence of hric3 and hα7 mRNA through RT-PCR. As expected, untransfected HEK293 was negative for hric3 and for hα7, but bands corresponding to the expected nucleotide length were observed for both hric3 and hα7 from the antibiotic-resistant cell lines (Figure 7-1A). Messenger RNA for GAPDH, a common housekeeping gene, was probed as a positive control to verify that the RT-PCR protocol was successful in the case that hric3 and hα7 bands were absent.

Identification of the hα7 Protein via Western Blot in Antibiotic- Resistant Clones

Immunoprecipitation and western blots for α7 protein from whole cell lysates were performed by Clare Stokes and Monica Santisteban. As expected, no labeling was observed from untransfected cells and cells stably expressing hric3. In contrast, some labeling was observed from cells transfected with hα7 while stronger labeling was seen in cells stably expressing both hα7 and hric3 (Figure 7-1B). The α7 protein detected in this Western Blot is an aggregation with a molecular weight > 220 kDa; the expected molecular weight of an α7 pentamer is 280 kDa.

Labeling of HEK-hα7/hric3 Cells with Alexa488-Conjugated α-Bungarotoxin

Intact cells were labeled with Alexa488-conjugated α-bungarotoxin to qualitatively verify surface expression of α7 nAChR and to illustrate the distribution of receptor expression in this cell line. As expected, the untransfected HEK293, HEK-hα7, and

HEK-hric3 cell lines were not labeled with the fluorescent toxin. In contrast, the HEK-hα7/hric3 cell line was labeled by the fluorescent α-bungarotoxin, and in a competitive manner with 1 mM nicotine (Figure 7-2). The labeling appears in non-continuous clusters, suggesting that surface expression of α7 in this cell line may be non-uniform. Similar patterns of labeling by fluorescent dye-conjugated ligands of α7 have been seen in other cell lines and in cultured neurons [440, 441].

Specific Binding of [^{125}I]-α-Bungarotoxin to Intact HEK-hα7/hric3 Cells

Specific labeling with 3 nM [^{125}I]-α-bungarotoxin was observed in intact HEK-hα7/hric3 cells while no specific labeling was detected in untransfected HEK293 cells treated in parallel (Figure 7-3A). From three saturation binding experiments to intact cells, the K_d of α-bungarotoxin is 991 ± 67 pM and the B_{max} is 7.71 x 10^{-8} ± 1.28 x 10^{-8} pmol/cell (Figure 7-3B). This B_{max} translates to an average of 9,284 ± 1,544 receptors expressed/cell assuming that 5 molecules of radiolabeled α-bungarotoxin bind each α7 receptor. From 34 HEK-hα7/hric3 cells, the average peak current and net-charge (during one second) evoked by 300 μM ACh was 163 ± 26 pA and 9,775 ± 1,458 pA x ms, respectively. The single-channel amplitude of α7 channels (potentiated by PNU-120596) was determined to be approximately 7.8 pA [376]; this means that ~21 α7 channels were open at the peak of an average current. If an average cell expresses 9,300 α7 ion channels, and all of those ion channels are equally activatible just prior to the agonist stimulation, the maximal α7 P_{open} at the peak of the current is approximately 0.0023. Assuming an average single-channel open lifetime of 0.1 ms [376], an average net-charge response to a one second application of 300 μM ACh contains ~12,532 channel openings. Based on these numbers, the average number of times an individual

channel opened during the one second of 300 μM ACh application is 1.35. These numbers are certainly rough estimates, but they suggest that the instantaneous P_{open} of α7 is never high, not even immediately after the presentation of a strong agonist stimulus, and that an individual α7 channel probably opens 3 times or less before becoming desensitized in response to 300 μM ACh. Under steady-state conditions where ACh is presented for prolonged periods of time, the α7 P_{open} will be substantially less than the estimated maximum of 0.0023 due to desensitization. The peak current of PNU-120596 potentiated responses from outside-out patches was previously used to obtain a lower-limit of the number of channels (N) in the patch. This lower-limit of N was used to estimate that the upper-limit of the α7 P_{open} during a 12-second application of 60 μM ACh is $7.4 \times 10^{-6} \pm 3.0 \times 10^{-6}$ (see Chapter 6).

ACh-Evoked Responses from HEK-hα7/hric3 Cells and Inhibition of those Currents with MLA in a Concentration-Dependent Manner

ACh-evoked whole-cell currents were recorded from HEK-hα7/hric3 cells with patch clamp electrophysiology. The ACh concentration-response relationship resulted in non-superimposable curves for peak current and net charge measurements, as expected for α7 receptors (Figure 7-4A and B). The EC_{50} values determined from peak currents and net charge were 167 ± 20 μM and 26 ± 6 μM, respectively. These values are very similar to those previously reported for human α7 nAChRs expressed in *Xenopus* ooctyes [214]. The curve for net charge was fit between the 1 μM ACh and 300 μM ACh points since the net charge was reduced from the maximum at ACh concentrations above 300 μM. A unique feature of the α7 receptor is the concentration-dependent desensitization that rapidly occurs with applications of high agonist

concentrations. In fact, this form of desensitization occurs more rapidly than solution exchanges can be practically made [213]. The reductions in net charge at high concentrations seen in this experiment were more pronounced than normally occurs in oocyte experiments. This was likely due to differences in the presentation of agonist; drug applications were made with a system that provided solution exchanges on the order of several milliseconds versus the drug delivery that occurs on a time scale of 3-4 seconds in a typical oocyte experiment. The rapid application of high agonist concentrations produced synchronous activation and desensitization of the α7 receptor population, resulting in extremely sharp macroscopic responses with minimal area (Figure 7-4B). This is also demonstrated by comparing the rise-times and rise-slopes with increasing concentrations of ACh; the 10-90% rise-times became shorter and the 10-90% rise-slopes became steeper as ACh concentrations increased (Table 7-1).

The ACh-evoked responses recorded from HEK-hα7/hric3 cells were sensitive to inhibition by the α7 selective antagonist MLA in a concentration-dependent manner (Figure 7-4C and D). In this experiment, the ACh concentration was fixed at 170 μM (the EC_{50} for peak currents determined above), with increasing co-applications of MLA. No preincubation with MLA was made in these experiments. The IC_{50} of MLA measured in this paradigm was 2.7±0.4 μM. At first glance this may seem like a rather high value for MLA, but when one considers that IC_{50} values are dependent on variables such as agonist concentration, timing, and duration of antagonist applications, this value is reasonable. For example, high affinity inhibition of α7-mediated responses is obtained only when MLA is pre-incubated prior to the application of agonist [133, 442]. In addition, the IC_{50} value of MLA in an oocyte experiment utilizing a similar paradigm to

the one used here (no MLA pre-incubation) was determined to be 1.2±0.2 μM with an ACh concentration of 60 μM [443]. Given that the ACh concentration used here was 170 μM, or roughly 3-fold higher, the IC_{50} of 2.7±0.4 μM for MLA inhibition of responses evoked by 170 μM ACh is consistent with previously published data.

In Vitro Cytotoxicity Profile of PNU-120596 in HEK-hα7/hric3 Cells

The *in vitro* cytotoxocity profile of PNU-120596 was evaluated in the HEK-hα7/hric3 cell line. In contrast to previous studies, which tested limited agonist and/or PAM concentrations, the toxicity profile of PNU-120596 was assessed over a range of agonist (choline) and PNU-120596 concentrations. Based on the recent finding that high concentrations of agonist and PNU-120596 promote non-conducting desensitized states that are insensitive to reversal by PNU-120596 [376], maximal cytotoxicity was hypothesized to occur upon treatment with relatively low concentrations of both agonist and PNU-120596 since this condition produces the greatest degree of ion channel activation over time. In addition, the existence of D_i states were hypothesized to account for the discrepancy in the literature regarding the toxicity of PNU-120596, given that the two studies reporting PNU-120596 toxicity used 100 μM choline as the agonist while the one study that reported a lack of PNU-120596 toxicity used a very strong agonist stimulus that potentially stabilized D_i states (explained in Chapter 6). The hypothesis that temperature might account for the discrepancy is unlikely given that all of the previously published studies were performed at 37ºC. Nonetheless, there was great interest in determining if the apparent temperature dependence of PNU-120596 from electrophysiology experiments might translate into measurable differences in cytotoxic effects when PNU-120596 treatments were incubated at different

temperatures. In these experiments choline, rather than ACh, was used as the stimulating agonist to avoid issues that may accompany the labile nature of ACh. Choline has been shown to selectively activate α7 nAChRs with similar efficacy to ACh, although with approximately 10-fold lower potency [444].

Initial cytotoxicity experiments were performed in full rich DMEM media containing 10% FBS with treatments incubated at 37ºC. A range of choline concentrations between 0 and 3 mM were co-applied with 10 μM PNU-120596 and in these experiments cell viabilities were reduced to approximately 15-25% of the controls whenever PNU-120596 was applied (data not shown). Two observations were immediately obvious from the initial experiments. First, PNU-120596 produced a great deal of toxicity even at 37ºC despite the electrophysiological evidence that PNU-120596 potentiates poorly at this temperature (this is addressed below). This finding was in agreement with Dinklo *et al.*, 2011 and Ng *et al.*, 2007. Second, PNU-120596 applied alone without agonist caused the same degree of toxicity as when applied with agonist. Evaluation of the ingredients in DMEM revealed that the medium contains approximately 30 μM choline. In addition, FBS is undefined, and very likely contains an unknown (but probably relatively low) concentration of choline. Experiments were performed to evaluate the onset of toxicity produced by the choline + PNU-120596 treatments, which was determined to occur to a full extent with less than 2 hours of treatment (data not shown). Due to the short incubation time required to produce the toxic effect, it was reasoned that the experiments could be performed in HBSS, a simple buffered solution containing glucose, without FBS supplementation. When experiments

were performed in HBSS, treatments with PNU-120596 alone failed to produce cytotoxicity and all future experiments were performed in HBSS.

Significant toxicity was observed when treatments were incubated at 28°C in HBSS in a manner that was dependent on the concentration of PNU-120596, and to a lesser extent the choline concentration (Figure 7-5A). In contrast, when choline and PNU-120596 treatments were incubated at 37°C in HBSS, no significant degree of toxicity was observed for any of the choline/PNU-120596 combinations (Figure 7-5B). As a control, all treatments were made in parallel to untransfected HEK293 cells and no treatment of choline and/or PNU-120596 at 28°C or 37°C produced significant toxicity (data not shown). Applications of choline alone or PNU-120596 alone did not reduce cell viabilities. No significant toxicity was produced with 1 μM PNU-120596 over the range of choline concentrations tested. At 3 μM PNU-120596 statistically significant toxicity was observed with 1 mM and 3 mM choline co-applications. The greatest degree of toxicity was observed when choline was applied with 10 μM PNU-120596, with all concentrations of choline tested producing approximately 50% reductions in cell viability relative to the controls. With 30 μM PNU-120596, significant reductions in cell viability were observed when co-applications were made with 100 μM and 1 mM choline, but the magnitude of toxicity in this case was less than was observed when treatments included 10 μM PNU-120596. Overall, there was no clear relationship between agonist concentration and degree of toxicity as predicted *a priori.* However, the observation that the magnitude of toxicity is actually decreased with 30 μM PNU-120596 treatments relative to 10 μM PNU-120596 treatments is consistent with the induction of D_i states when modulator concentrations are high, and by inference high

occupancy of PNU-120596 binding sites. In addition, the temperature-dependent cytotoxicity effects of PNU-120596 correlate well to the temperature-dependent potentiating activity of PNU-120596 observed in the whole-cell electrophysiology experiments of Sitzia *et al*., 2011 and Dr. Can Peng (see below).

To confirm whether the observed toxicity occurred via α7 nAChRs, the competitive antagonist MLA was given at varying time points with 100 μM choline + 10 μM PNU-120596 treatments and incubated at 28°C. As seen in Figure 7-6, neither a 10 minute pre-application nor co-application of 10 nM MLA were able to block the choline + PNU-120596 toxicity. However, this is consistent with the recent observation that 10 nM applications of MLA on top of steady-state currents elicited by choline + 3 μM PNU-120596 actually transiently increase current rather than inhibit current, suggesting that low concentrations of MLA may alter the equilibrium between D_s and D_i towards D_s [376]. Application of a 10-fold higher MLA concentration either 10 minutes before or with 100 μM choline + 10 μM PNU-120596 was able to completely block the toxic effect, suggesting the toxicity is mediated by α7 receptors. In contrast, 100 nM MLA was unable to block the effect if it was applied 10 minutes or more after the toxic choline + 10 PNU-120596 treatment. This suggests that the onset of PNU-120596 induced toxicity in these cells occurs rapidly, in less than 10 minutes.

Bovine Serum Albumin Eliminates the Temperature Dependence of PNU-120596 Toxicity and, to a Lesser Degree, Potentiation Activity

As stated above, an observation made with the initial experiments is that choline and 10 μM PNU-120596 treatments were toxic at 37ºC when the solutions were prepared in DMEM with 10% FBS. This result was curious and led to additional experiments in which choline + 10 μM PNU-120596 solutions were prepared in HBSS

supplemented with 10% FBS. As seen in Figure 7-7A and B, the presence of FBS eliminated the temperature dependence of the PNU-120596 toxicity. Bovine serum albumin is the primary constituent of FBS and serum albumins have previously been shown to potentiate α7 nAChR-mediated responses [445]. Therefore, the experiments were repeated in HBSS solutions containing 30 μM BSA, the approximate concentration of BSA found in solutions containing 10% FBS [446, 447]. Again, the temperature dependence of cytotoxicity induced by PNU-120596 was eliminated (Figure 7-7C and D), suggesting that BSA is the constituent of FBS primarily responsible for the effect. Given that BSA is a non-specific carrier of hormones and fatty acids in blood plasma, it is possible that a substance bound to the BSA is responsible for the effect, rather than BSA itself. Nonetheless, this observation suggests that although, the ability of PNU-120596 to potentiate α7 mediated current at physiological temperature is reduced, some intrinsic factors may exist that confer activity to PNU-120596 under conditions when it would otherwise be inactive. The toxic effect of 100 μM choline + 10 μM PNU-120596 treatment at 37°C in HBSS with 30 μM BSA was tested for sensitivity to the competitive antagonist MLA, and also the non-competitive antagonist mecamylamine to confirm this effect is mediated by α7 nAChR and whether it requires activation of the ion channel (Figure 7-8). As before, 10 nM MLA was unable to completely block the toxic effect of the treatment, but 10 minute pre-applications and co-applications of 100 nM MLA completely reversed the toxicity while applications of MLA 10 minutes or more after the choline and PNU-120596 treatment were ineffective. In addition, ten minute pre-treatment and co-treatment with 100 μM mecamylamine was able to partially block the toxicity of choline and PNU-120596 treatment while mecamylamine treatments 10

minutes or more after the treatment had no effect. The IC_{50} for mecamylamine was approximately 10 μM in experiments performed in oocytes where mecamylamine was co-applied with 300 μM ACh [448]. In addition, 100 μM mecamylamine appears to fully block steady-state currents generated by choline and PNU-120596 co-application in recent experiments [376]. Although the 100 μM concentration of mecamylamine was unable to completely block the toxic effect in these studies, the partial block that was observed combined with the rapid onset of the toxicity in less than 10 minutes is consistent with direct ion channel activity. The observation that 100 nM MLA completely blocked the toxic effect of choline + PNU-120596 treatment at 37°C in the presence of 30 μM BSA suggests the effect is mediated by the α7 nAChR.

The Temperature-Dependence of PNU-120596 is Confirmed through Whole-Cell Patch Clamp Recordings

The whole-cell electrophysiology data presented below were collected and analyzed by Dr. Can Peng. Only her data with PNU-120596 that are relevant to the cytotoxicity experiments will be shown here. The basic protocol used in these experiments was to obtain three responses at room temperature (23.5°C), record three responses at 37°C, and then reduce the temperature back down to 23.5°C over a period of 20 minutes. Acetylcholine was co-applied with PAM for 3 seconds with 57 second inter-stimulus intervals. Prior to presenting the data, it is important to note that above ~30ºC the quality of the whole-cell recordings almost always deteriorated. Because of this, the parameters used to define an acceptable whole-cell recording at 37ºC were more relaxed than they would be for a typical whole-cell recording made at room temperature. Whole-cell seals with access resistance < 40 megaOhms, input resistance > 100 megaOhms, and holding current < 700 pA at 37°C were deemed

acceptable. Prior to the increase in temperature, access resistances were < 15 megaOhms, input resistances were > 1 gigaOhm, and the holding current was between -50 pA and 0 pA. In most cases, if the patch survived the time at 37ºC, the whole-cell parameters improved as temperatures returned near room temperature. In rundown control experiments performed over a period of 20 minutes with no temperature adjustments, the amplitude of the responses at the end of the experiment were ~70% of the responses at the beginning (Figure 7-9A and B).

When 1 mM ACh was applied without a PAM, peak currents at 37°C were 44±4% of the initial baseline currents recorded at 23.5°C and they recovered to ~75% upon temperature reduction back to 23.5°C, a full recovery based on the rundown control (Figure 7-9C and D). Thus, it is important to note that in these experiments currents evoked by ACh alone were reduced by approximately 56% at 37°C. When evaluating the effect of temperature on PNU-120596 potentiation, the ACh-evoked responses at 37°C are used as the baseline for comparison. The deterioration in whole-cell recording properties at 37°C could lead to a reduction in the fidelity of the voltage-clamp. It is feasible that the currents evoked in the presence of PNU-120596, given their size, could contribute to a greater loss of voltage-clamp fidelity than may have occurred with ACh alone. However, the increased temperature had less of an effect on the responses evoked with TQS than on the responses evoked with PNU-120596, relative to the initial baseline responses (44 ± 3% vs 11 ± 3%; TQS data not shown here, but will be included in Williams *et al*., in preparation). This is despite the fact that the absolute magnitude of the responses recorded with TQS was larger than those with PNU-120596 (3,080 ± 484 pA vs. 1,333 ± 414 pA at 23.5°C and 1,438 ± 229 vs. 104 ± 31 pA at

37°C). These data suggest that temperature has a unique effect on potentiation by PNU-120596 and that voltage-clamp errors are probably not responsible for the diminished currents with PNU-120596 at 37°C. In addition, the toxicity data provide another form of evidence that PNU-120596 potentiation is reduced at 37°C.

When 10 μM PNU-120596 was co-applied with 1 mM ACh, potentiated responses at 37°C were reduced to a greater extent than the response reduction that occurred when ACh was applied alone (Figure 7-10A and B). At 37ºC PNU-120596 potentiated responses were only 11±3% (~89% reduction) of the baseline responses obtained initially at 23.5°C, but recovered fully when the temperature was returned to 23.5°C. This result is consistent with the findings of Sitzia *et al*., 2011 and also correlates well with the temperature dependence of the PNU-120596 cytotoxicity seen above. One hypothesis to explain this phenomenon is that entry into PNU-120596-insensitive desensitized states occurs more readily at 37°C than at room temperature. Since recently published work suggests that D_i states are stabilized by high PNU-120596 concentrations, this hypothesis was tested by repeating the temperature experiment with a 10-fold lower concentration of PNU-120596. However, the result with 1 μM PNU-120596 was similar to that with 10 μM PNU-120596 (Figure 7-10C and D). When 1 μM PNU-120596 was co-applied with 1 mM ACh, potentiated responses at 37C were 9±3% (~91% reduction) of the initial responses at 23.5°C, and then fully recovered when the temperature was returned to room temperature.

Since 30 μM BSA appeared to eliminate the temperature dependence of PNU-120596 cytotoxicity in a manner that was dependent on α7 nAChR signaling, whole-cell electrophysiology experiments were performed in the presence of 30 μM BSA. When

the responses recorded with 30 μM BSA at 37°C were expressed relative to the initial responses obtained at 23.5°C, the effect of BSA on the normalized peak currents was not statistically significant (Figure 7-11A; $p>0.05$). However, when the same data were plotted based on the absolute magnitude of the recorded peak currents, the responses recorded in the presence of 30 μM BSA at 23.5°C and 37°C were significantly larger than responses recorded in the absence of BSA (Figure 7-11B; $p<0.05$; see Chapter 3 for statistical methods). On average, the peak currents evoked by 1 mM ACh and 10 μM PNU-120596 co-application at 23.5°C in the absence and presence of 30 μM BSA were 1,333 ± 414 pA and 2,951 ± 307 pA, respectively. The average peak currents recorded at 37°C in the absence and presence of 30 μM BSA were 104 ± 31 pA and 422 ± 117, respectively. These data suggest that 30 μM BSA potentiates α7-mediated responses, and does so in an additive manner with PNU-120596.

Discussion

Numerous lines of *in vitro* evidence from independent labs suggest that potentiators of α7-mediated signals may produce signals with relevance to living biological systems. Although the available *in vivo* data are relatively limited at the present time, α7 PAMs have been shown to produce measurable effects through behavioral measures of cognitive function and has been shown to reverse auditory gating deficits in drug-induced or DBA/2 models when administered to living animals [322]. These studies suggest that the α7 PAMs possess sufficient pharmacokinetic properties to modulate brain α7 receptors *in vivo*, and suggest that the PAMs are pharmacologically active at physiological temperature. The finding that PNU-120596 administration improved auditory gating deficits induced by amphetamine [318] and

deficits in the set-shifting tasks induced by phencyclidine [449] may be seen as inconsistent with the temperature dependence of PNU-120596 originally reported by Sitzia *et al*., 2011. However, the viability assays and electrophysiology experiments performed in solutions containing BSA suggest that some intrinsic factor may partially preserve the pharmacological activity of PNU-120596 at 37°C, and may preserve the activity sufficiently well to continue producing biologically relevant signals (in this case, toxic signals). Given that $\alpha 7$ nAChR has an intrinsically low P_{open} and PNU-120596 is such a profoundly powerful potentiator, it seems conceivable that even a modest preservation of PNU-120596 potentiation may be sufficient to produce significant *in vitro* cytotoxicity at 37°C and effects *in vivo*. More pre-clinical *in vivo* data regarding the activity of PNU-120596 and other $\alpha 7$ PAMs are needed to fully evaluate their potential utility as therapeutics. At any rate, the data presented here suggest that experiments performed at room temperature should be applied with extreme caution in the interpretation of data generated *in vivo*.

At this point it would be entirely speculative to state a mechanism for the apparent temperature dependence of PNU-120596. Therefore, only one brief comment will be made regarding this matter until further information is available. The putative binding site for PNU-120596, and other PAMs, is in the intrasubunit cavity formed by the four membrane-spanning helices [322, 344]. The increased kinetic energy at 37°C may alter the protein conformation, fluidity of the membrane and/or the composition of the membrane at the receptor-membrane interface in a manner that disrupts the mechanism of PNU-120596. The functional properties of nAChRs have been shown to be affected by interactions with lipids [450].

One of the purposes of the cytotoxicity experiments was to characterize the *in vitro* cytotoxicity profile of PNU-120596 over a wide range of agonist and modulator concentrations. In HBSS-based experimental solutions and 28°C incubations, the data suggest that PNU-120596 is toxic in a concentration-dependent manner and the observation that the magnitude of toxicity decreased between treatments with 10 μM PNU-120596 and 30 μM PNU-120596 is consistent with the induction of D_i states. In contrast, there was no clear dependence of toxicity on choline concentration over a given PNU-120596 concentration. The experiments performed with the α7 antagonists MLA and mecamylamine suggest that the onset of PNU-120596 toxicity is rapid. The rapid onset of toxicity could conceivably account for the lack of a clear choline concentration-dependence in the toxicity experiments with PNU-120596. Even if D_i did eventually accumulate when choline concentrations were high, the cells may have died before a significant accumulation of D_i could occur to prevent the toxicity.

The finding that co-application of 30 μM-3mM choline with 10 μM PNU-120596 produces toxicity at 37°C in the presence of FBS is consistent with the findings of Dinklo *et al*., 2011 and Ng *et al*., 2007 and inconsistent with the results of Hu *et al*., 2009. Both of the published studies that show evidence in favor of in vitro PNU-120596 toxicity were incubated at 37°C in media containing FBS for 24 hours. Unfortunately, the methods used by Hu *et al*., 2009 to show the lack of PAM cytotoxicity are vague. In addition, the fact that Hu *et al*., 2009 failed to directly demonstrate functional α7 receptors in their undifferentiated PC12 cells and cultured cortical neurons is a severe limitation of their study. Furthermore, the fact that there is no dependence on modulator concentration for any of the PAMs tested in this study is curious. However, the

possibility that induction of D_i states accounted for the lack of toxicity in these studies still cannot be completely ruled out.

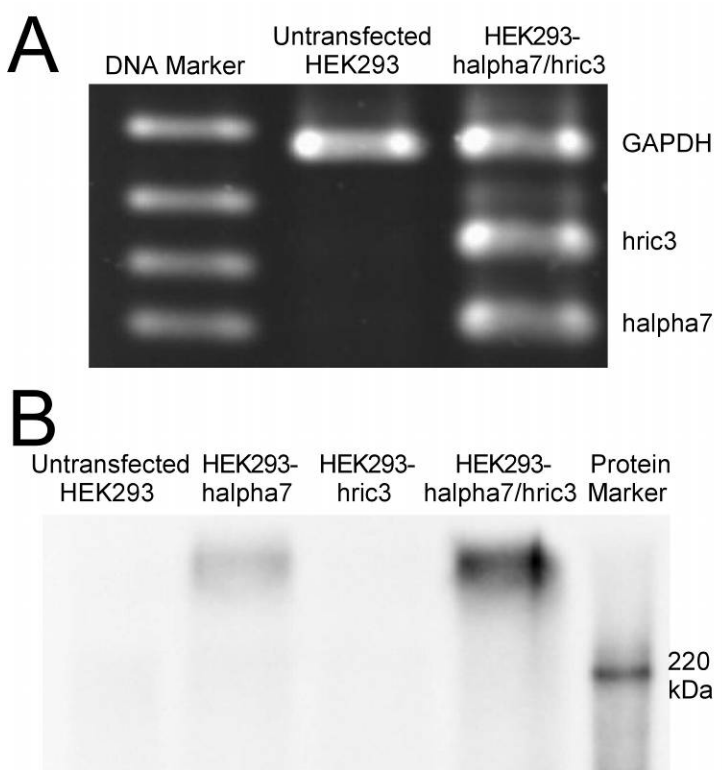

Figure 7-1. Expression of human α7 and ric3 by the HEK-hα7/hric3 cell line. A) Expression of human α7 and ric3 mRNA is verified by RT-PCR. The observed bands for GAPDH, hric3, and hα7 are 516 bp, 346 bp, and 414 bp, as expected based on the primers used. B) Immunoprecipitation and western blot from cell lysates performed by Clare Stokes and Monica Santisteban. Untransfected HEK293 and HEK-hric3 cells were negative for hα7 protein. The labeled protein from HEK-hα7 and HEK-hα7/hric3 cell lysates is an aggregate with molecular weight > 220 kDa. The primary antibodies for α7 were generously provided by Dr. Cecilia Gotti (University of Milan, Italy).

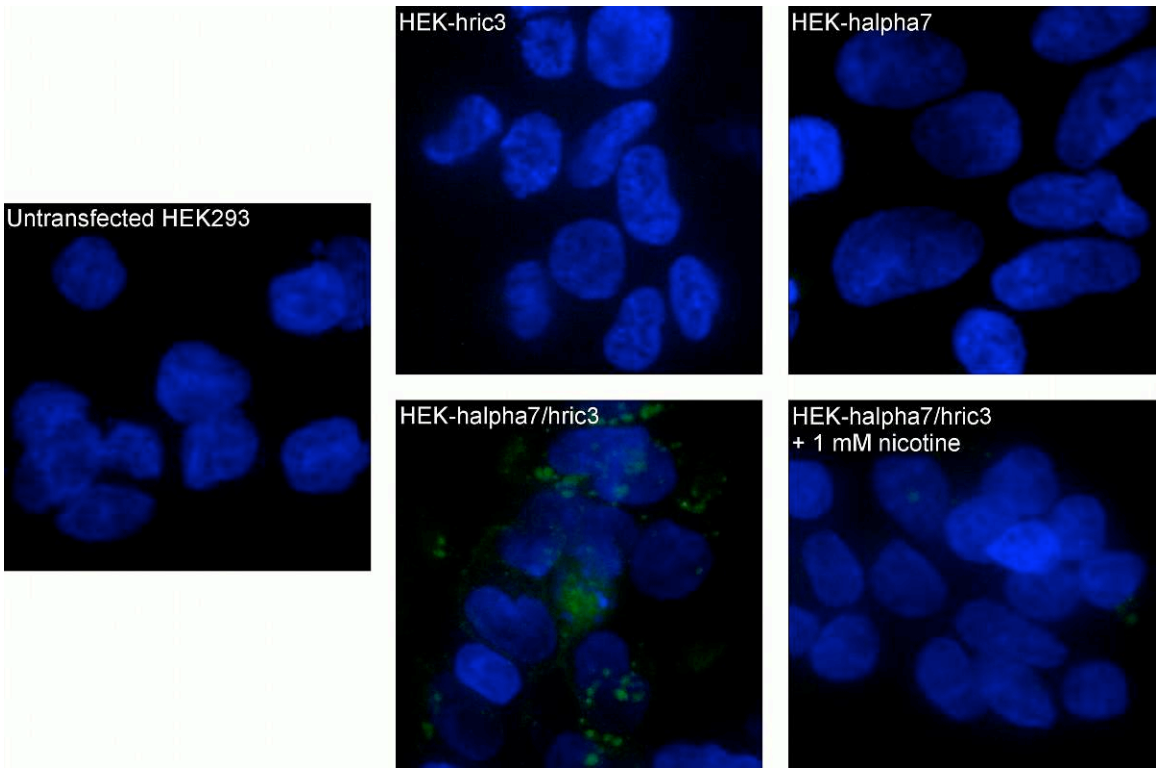

Figure 7-2. Labeling of intact HEK-hα7/hric3 cells with Alexa Fluor488-α-bungarotoxin. No labeling was observed for untransfected HEK293, HEK-hric3, or HEK-hα7 cell lines. In contrast, labeling was observed on HEK-hα7/hric3 cells in a competitive manner with 1 mM nicotine. Cellular nuclei are stained in blue with DAPI and the Alexa Fluor488-α-bungarotoxin label is green.

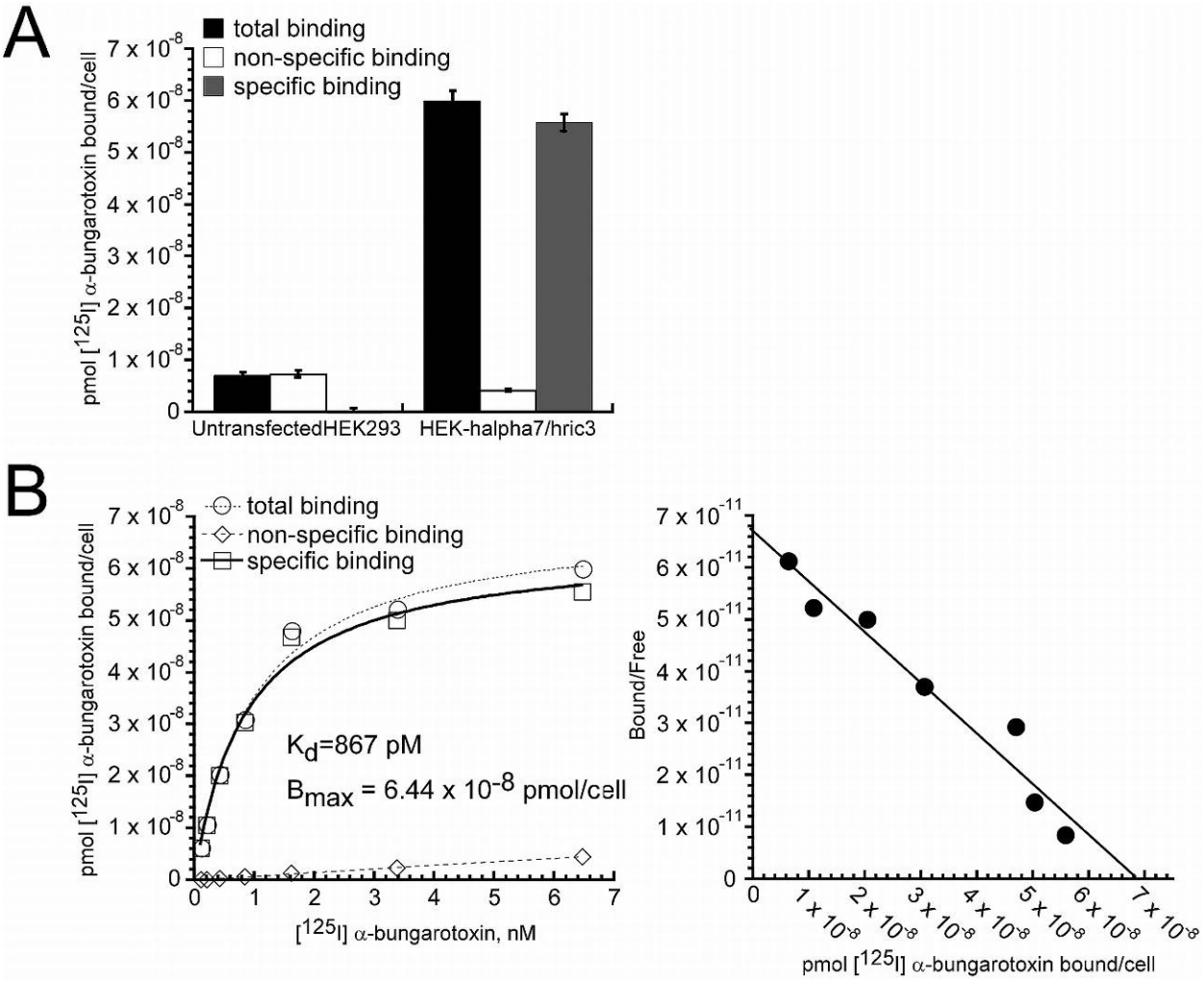

Figure 7-3. Saturation binding of [^{125}I] α-bungarotoxin binding to intact HEK-hα7/hric3 cells. A) No specific binding is detected with untransfected HEK293. Values are the mean ± SEM of 5-6 replicates. B) A saturation binding curve from one representative experiment is shown on the left and the Scatchard transformation of the same data is shown on the right. The average K_d and B_{max} values from three independent saturation binding experiments are 991 ± 67 pM and 7.71 x 10^{-8} ± 1.28 x 10^{-8} pmol/cell, respectively. Specific binding is defined as the difference between total binding and non-specific binding. Non-specific binding was determined using 1 μM unlabelled α-bungarotoxin.

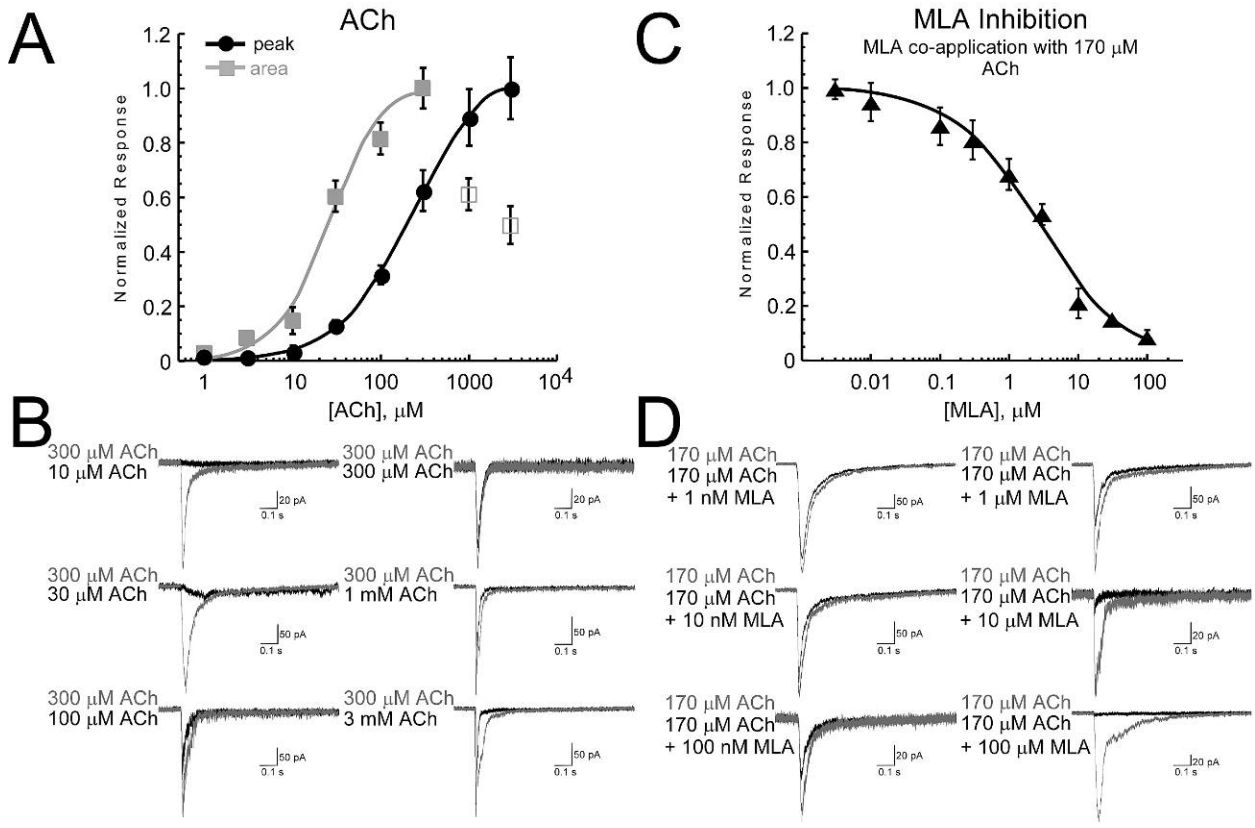

Figure 7-4. ACh concentration-response relationship and inhibition of currents by MLA from HEK-hα7/hric3 cells. A) Concentration-response relationship for whole-cell peak currents and net charge responses evoked by ACh. The curve for net charge was fit between 1 μM ACh and 300 μM ACh, denoted by the solid grey boxes. Each point represents the mean ± SEM from 4-8 cells. Net charge responses were calculated for a period of 1 s following ACh application. B) Inhibition of responses by MLA determined from peak responses. In these experiments increasing MLA concentrations were co-applied with 170 μM ACh, the EC_{50} for peak currents determined in part A. Each point represents the mean ± SEM determined from 4-6 cells. The holding potential was -70 mV.

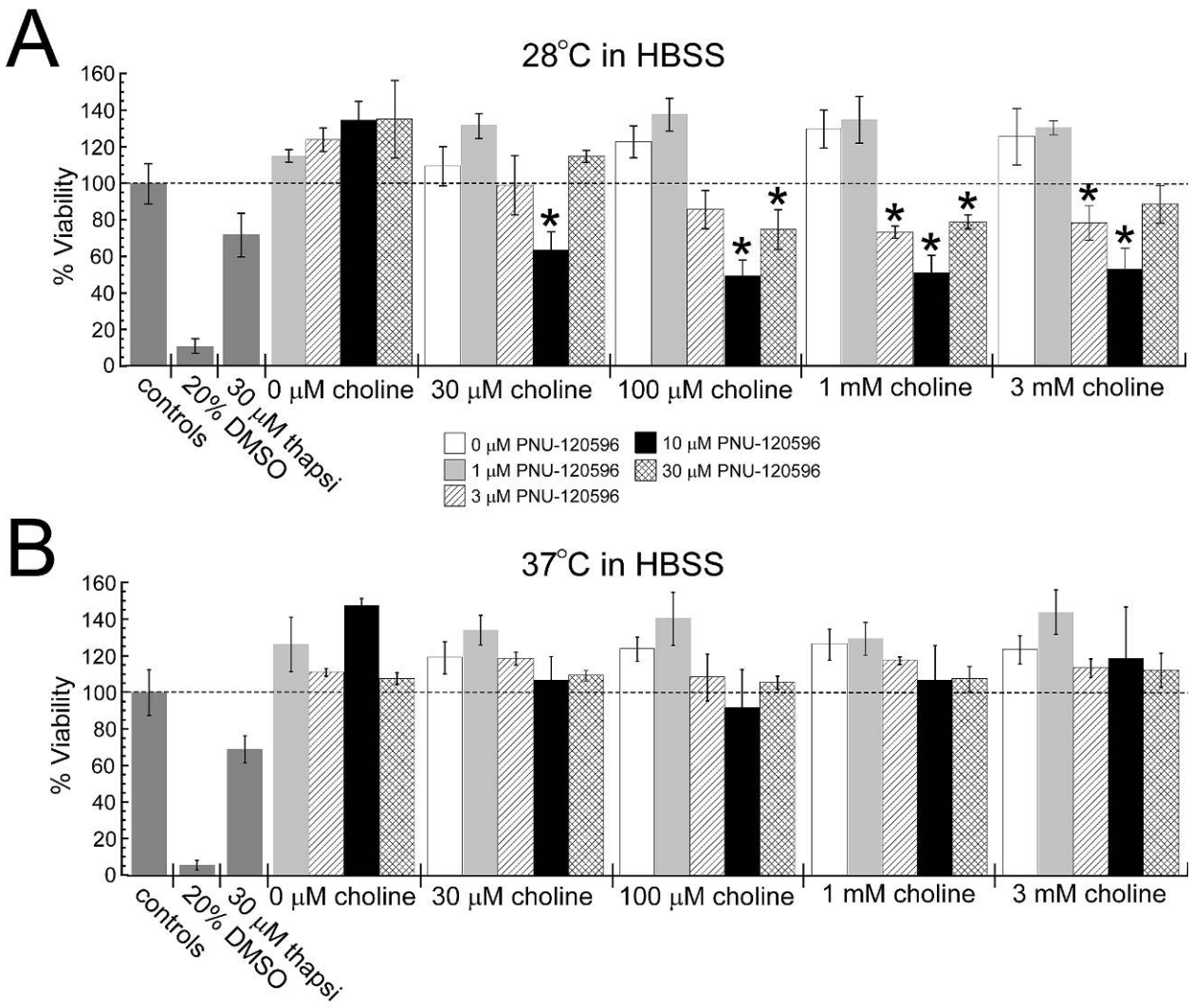

Figure 7-5. Temperature- and concentration-dependence of PNU-120596 cytotoxicity with treatments prepared in HBSS solutions. A) Cytotoxicity profile of 0-30 μM PNU-120596 with 0-3 mM choline when treatments were incubated at 28°C/5%CO_2. B) Cytotoxicity profile of 0-30 μM PNU-120596 with 0-3 mM choline when treatments were incubated at 37°C/5% CO_2. The * indicates a two-tailed p-value < 0.05. Each value is the average ± SEM of 3-5 independent experiments. Two sets of cells were plated from the same passage one day prior to experiments. The two sets of cells were treated identically with the same experimental solutions and then one set of cells was immediately placed in a CO_2 incubator set to 28°C and the other set of cells in an incubator set to 37°C for 2 hours. Untransfected HEK293 cells were treated in parallel and were unaffected by all choline and PNU-120596 treatments at 28°C and 37°C (data not shown).

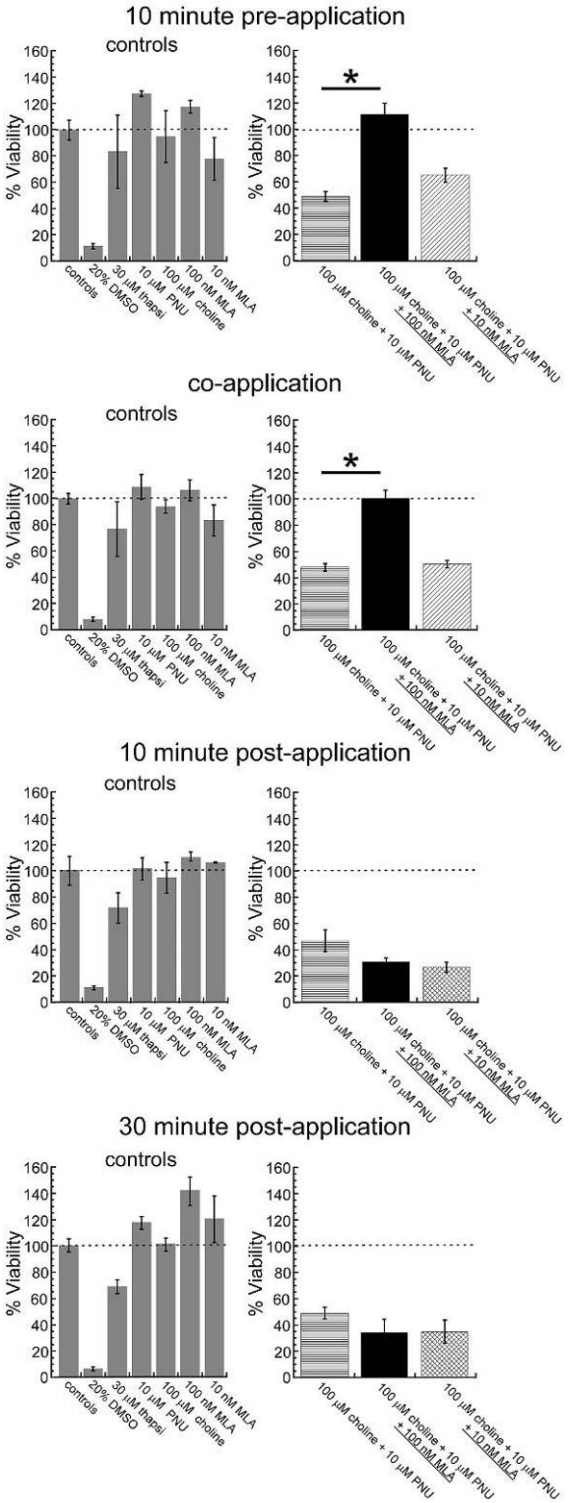

Figure 7-6. Sensitivity of the cytotoxic effect of 100 μM choline + 10 μM PNU-120596 treatment in HBSS at 28°C to the competitive antagonist MLA. Either 10 nM or 100 nM MLA was added at the time indicated, relative to the toxic 100 μM choline + 10 μM PNU-120595 treatment. The * indicates a two-tailed p-value < 0.05. Values are averages ± SEM from 3 independent experiments.

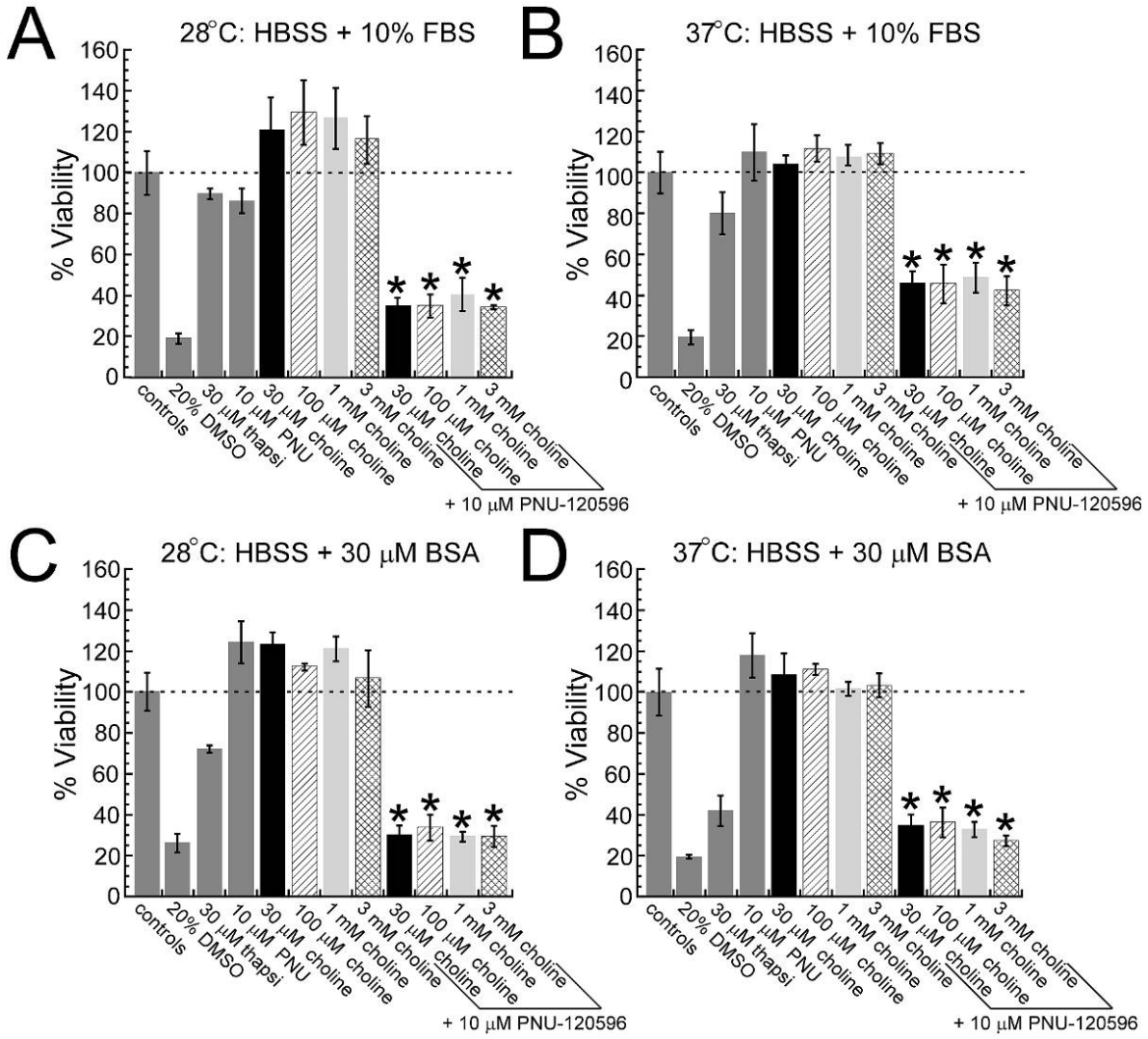

Figure 7-7. Elimination of the temperature dependence of PNU-120596 cytotoxicity. A) Cytotoxicity of 0 – 3 mM choline and 10 μM PNU-120596 co-applications at 28°C in HBSS solutions with 10% FBS. B) Cytotoxicity of 0 – 3 mM choline and 10 μM PNU-120596 co-applications at 37°C in HBSS solutions with 10% FBS. Notably, a factor in FBS appears to remove the temperature-dependent cytotoxicity seen in Figure 7-5. C) Cytotoxicity of 0 – 3 mM choline and 10 μM PNU-120596 co-applications at 28°C in HBSS solutions with 30 μM BSA. D) Cytotoxicity of 0 – 3 μM choline and 10 μM PNU-120596 co-applications at 37°C in HBSS solutions with 30 μM BSA. The effect of 30 μM BSA appears to be very similar to that of FBS. The * indicates a two-tailed p-value < 0.05. Values are averages ± SEM from 3 independent experiments.

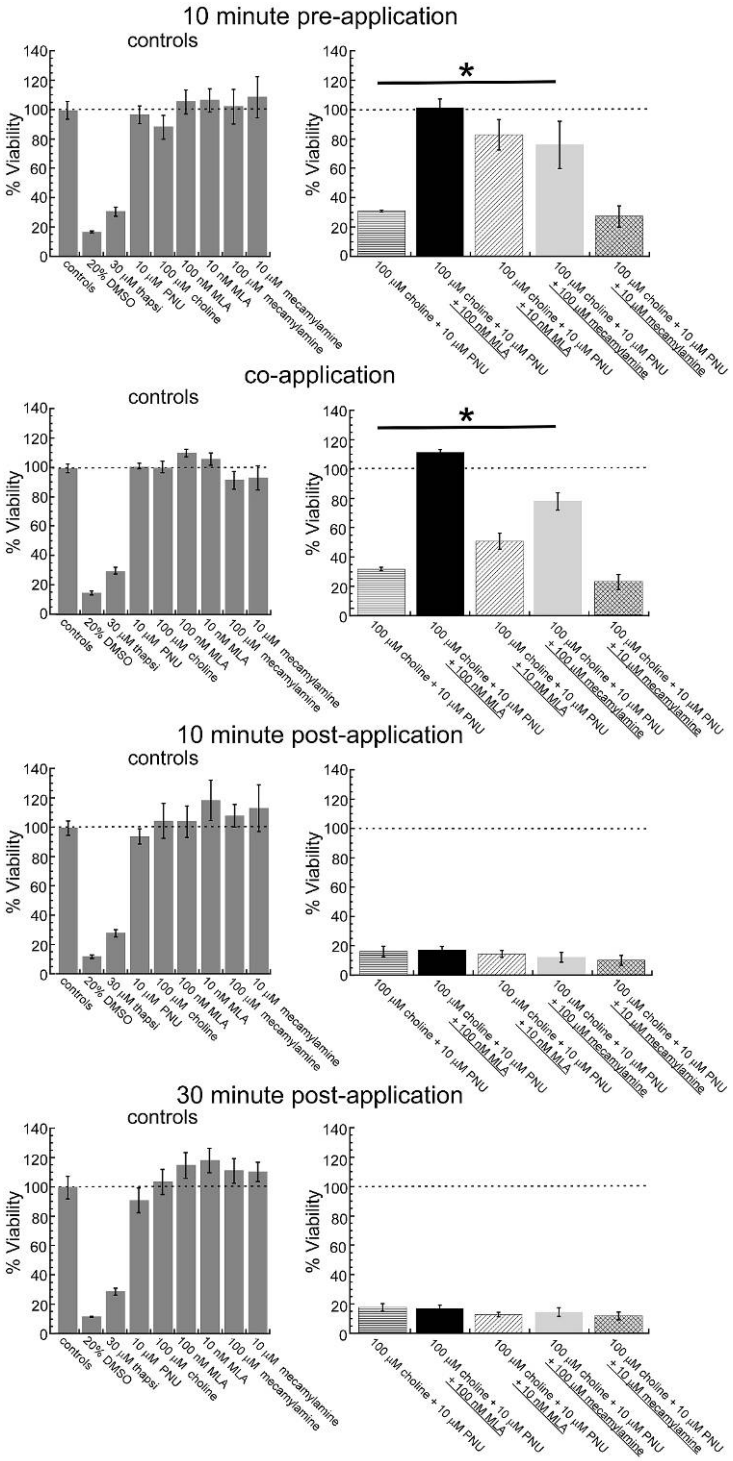

Figure 7-8. Sensitivity of the cytotoxic effect of 100 μM choline + 10 μM PNU-120596 treatment in HBSS with 30 μM BSA at 37°C to the competitive antagonist MLA and the non-competitive antagonist memamylamine. 10 nM and 100 nM MLA or 10 μM and 100 μM mecamylamine were added at the time indicated, relative to the toxic treatment. The * indicates a two-tailed p-value < 0.05. Values are averages ± SEM from 3 independent experiments.

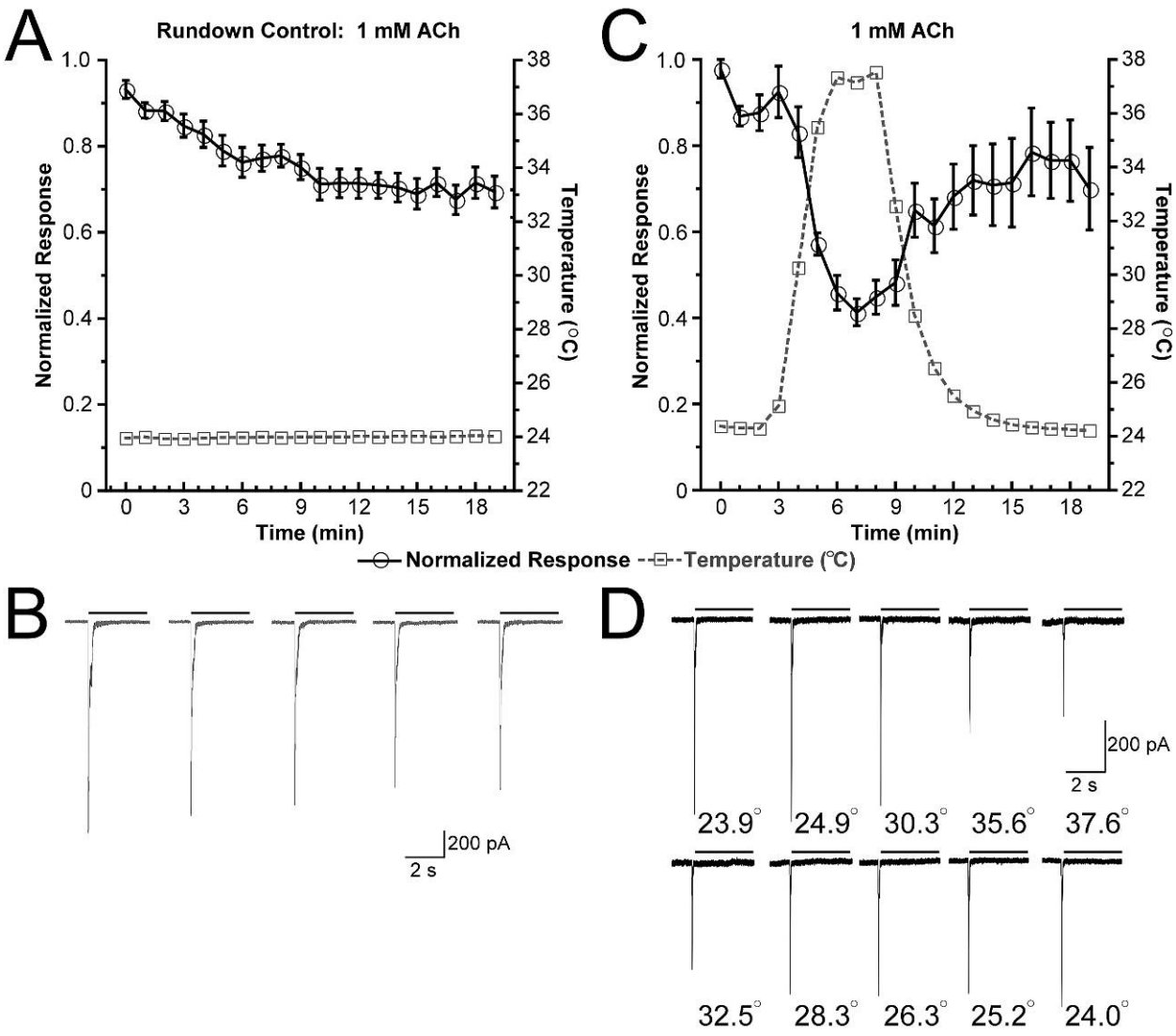

Figure 7-9. Controls for the whole-cell patch clamp recordings illustrating the temperature-dependence of PNU-120596 potentiation. These data were collected and analyzed by Dr. Can Peng. A) Rundown control performed at 23.5°C. Peak responses to 3 second applications 1 mM ACh were recorded every 60 seconds over a period of 20 minutes. Each point is the average ± SEM of 15 cells. B) Temperature-dependent effects of peak responses evoked by 1 mM ACh. Each point is the average ± SEM of 6 cells.

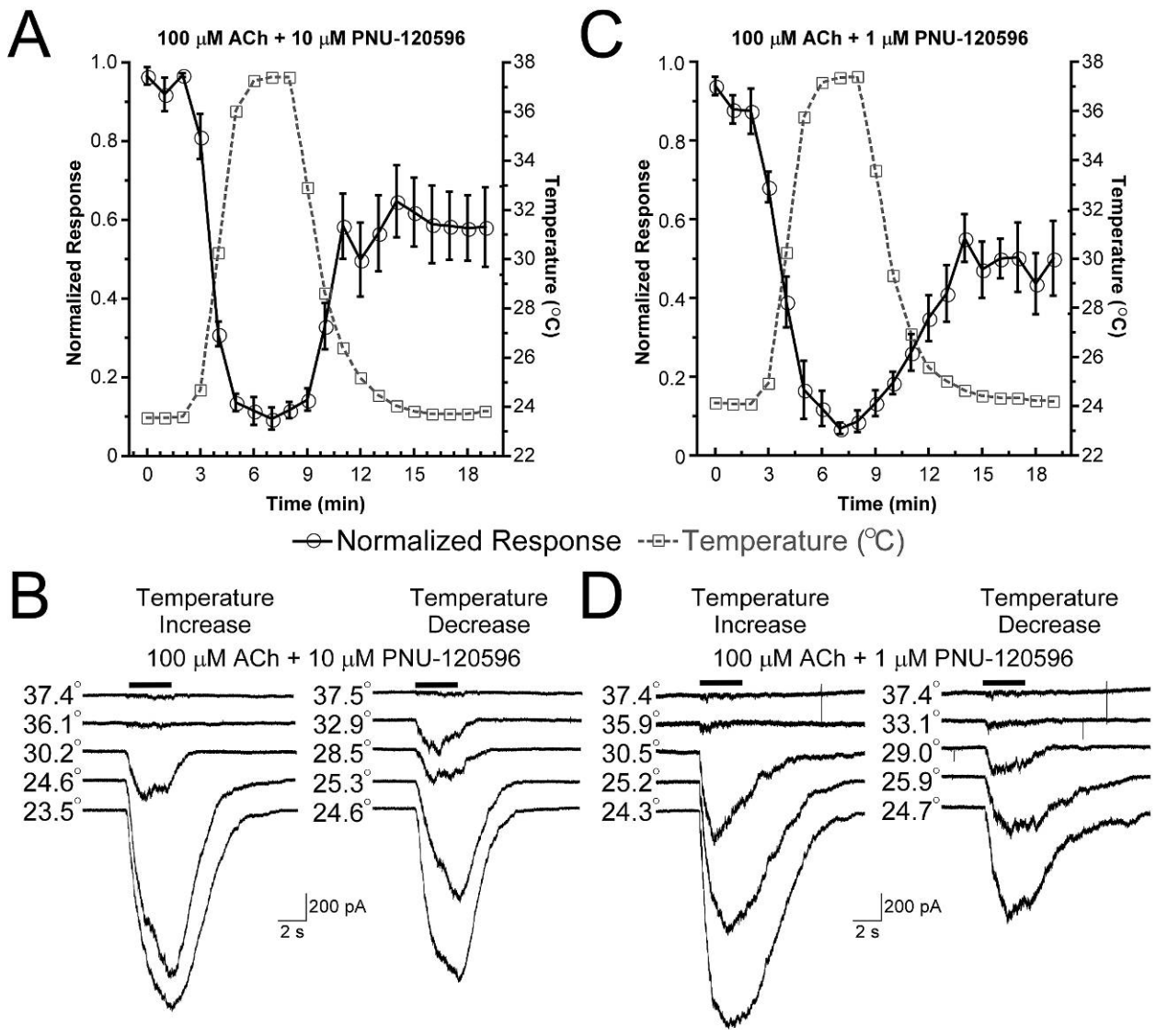

Figure 7-10. Temperature-dependence of PNU-120596 potentiation of α7-mediated responses. These data were collected and analyzed by Dr. Can Peng. A) Whole-cell recordings from HEK-hα7/hric3 cells evoked by 3 second co-applications of 100 μM ACh and 10 μM PNU-120596 every 60 seconds over a period of 20 minutes with varied temperatures between 23.5°C and 37°C. Each point represents the average ± SEM of 8 cells. B) Sample data traces recorded at the indicated temperature. C) Whole-cell recordings from HEK-hα7/hric3 cells evoked by 3 second co-applications of 100 μM ACh and 1 μM PNU-120596 every 60 seconds over a period of 20 minutes with varied temperatures between 23.5°C and 37°C. Each point represents the average ± SEM of 6 cells. D) Sample data traces recorded at the indicated temperature. Responses were measured as peak currents. The responses are normalized to the three initial responses obtained at 23.5°C.

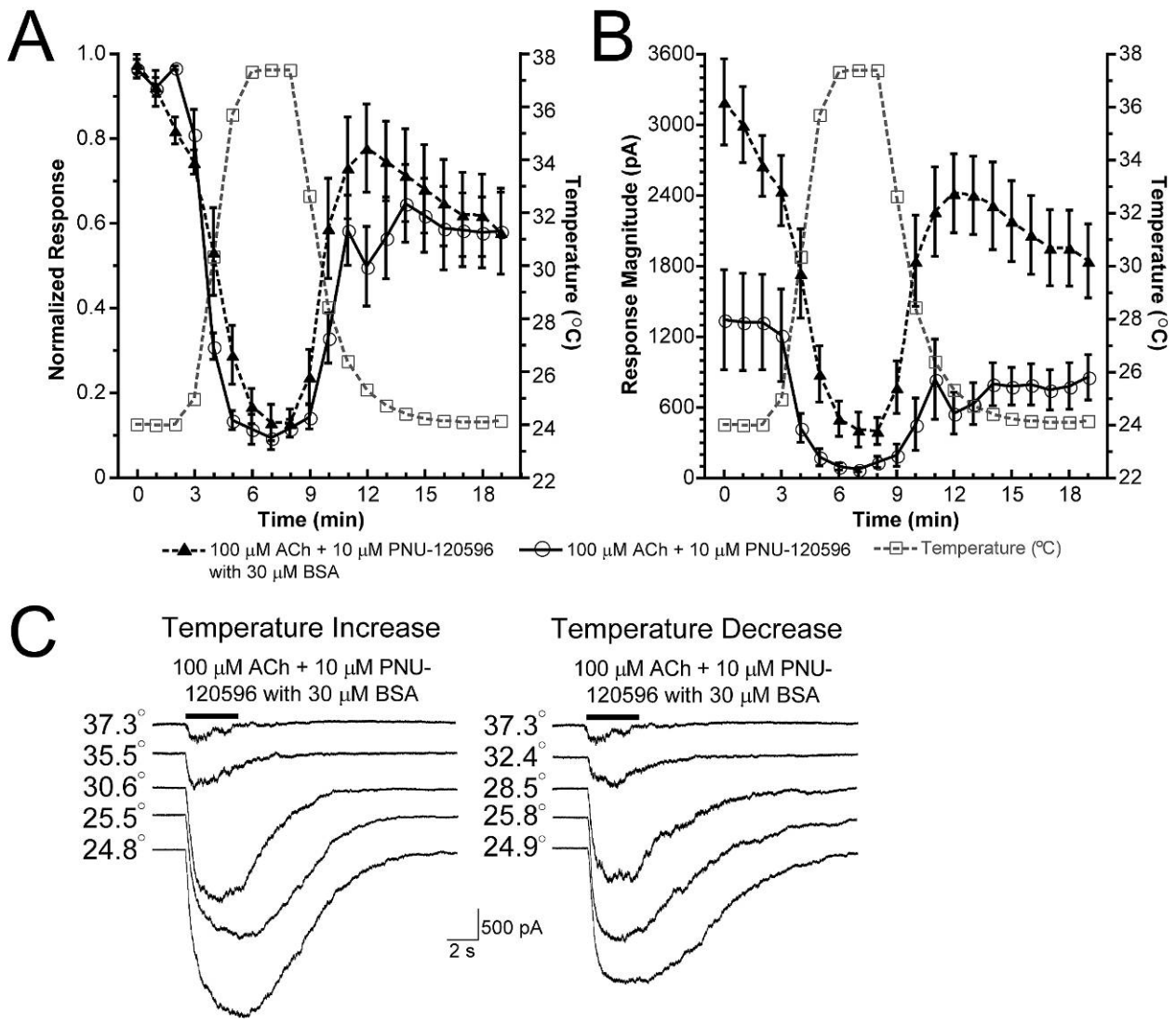

Figure 7-11. Modest preservation of PNU-120596 potentiation at 37°C in solutions containing 30 μM BSA. These data were collected and analyzed by Dr. Can Peng. A) Whole-cell recordings from HEK-hα7/hric3 cells evoked by 3 second co-applications of 100 μM ACh and 10 μM PNU-120596 in the absence or presence of 30 μM BSA with varied temperatures between 23.5°C and 37°C. The data plotted in the absence of BSA are the same data shown in Figure 7-10A. Responses were normalized to the initial responses obtained at 23.5°C. Each point in the presence of 30 μM BSA represents the average ± SEM of 9 cells. Responses were measured as peak currents. B) The same data shown in panel A expressed as peak current magnitude rather than normalized responses. C) Sample data traces recorded at the indicated temperature.

Table 7-1. 10-90% rise-times and rise-slopes with increasing concentrations of ACh

[ACh], μM	10-90% Rise-time (ms)	10-90% Rise-slope (pA/ms)
30	74.6 ± 30.8	0.195 ± 0.081
100	22.3 ± 7.20	1.34 ± 0.465
300	9.86 ± 1.45	22.7 ± 6.90
1000	2.61 ± 0.26	47.2 ± 12.4
3000	1.84 ± 0.53	294 ± 105

CHAPTER 8
SUMMARY AND CONCLUSIONS

The work presented in this dissertation has provided insights regarding the activation, desensitization, and potentiation of α7 nAChRs that will hopefully be useful in optimizing the therapeutic targeting of this receptor. Though α7W149 and α7W55 are both highly conserved aromatic residues found within the agonist binding sites, they appear to play different roles in receptor activation by agonist. The W55 residue is important for regulating the subtype selectivity of benzylidene anabaseine compounds, whereas the W149 residue is less able to tolerate mutation. Although the α7 nAChR has five agonist binding sites, effective activation occurs with low fractional occupancy. In contrast, occupancy of all five binding sites appears to actually promote inactivation of the receptor, rather than activation. Characterization of the α7 PAM PNU-120596 has revealed that at least two forms of α7 desensitization exist: the well-known rapid and concentration-dependent desensitization that is characteristic of α7, and desensitized states that are stable in the presence of the modulator PNU-120596. The *in vivo* implications of D_i states have not been investigated. On one hand, these states may prove to be a real limitation to the usefulness of PAMs like PNU-120596. On the other hand, D_i states may provide an intrinsic safety mechanism against over-stimulation. The reported temperature dependence of PNU-120596 potentiation has been confirmed through electrophysiology and *in vitro* cytotoxicity experiments with a novel cell line stably expressing human α7 and ric3. However, the presence of certain factors, such as BSA, may partially preserve the activity of PNU-120596 at physiological temperature to an extent that the temperature dependence of PNU-120596-induced *in vitro* cytotoxicity is eliminated.

A general qualitative model for the α7 nAChR is suggested based on the data presented here and years of work performed in Dr. Roger Papke's laboratory. The early single-channel studies of muscle-type nAChR first identified two distinct open states; isolated short-lived openings and longer-lived openings that occurred in groups or "bursts". As agonist concentrations were increased, the probability of long-lived openings also increased. However, short-lived openings continued to occur even under conditions that would saturate the agonist binding sites [412]. Under normal conditions, α7 nAChRs may only open to the short-lived open state (O*) that is analogous to the short-lived type of open state observed predominately with singly liganded heteromeric nAChR; the longer-lived open state (O') is replaced by the D_s state. The effect of high agonist occupancy is to stabilize the D_s state, similar to the way high agonist occupancy stabilizes the long-lived open state in heteromeric nAChRs. This explains the observation that high fractional occupancy of the α7 agonist binding sites appears to be functionally negative (see Figure 7-4; [229]). The modulation of the α7 D_s state by PNU-120596 appears to be through stabilization of intrinsic states of the channel, rather than creation of new conducting states, since PNU-120596 has no effect on ion selectivity and little, if any, effect on channel conductance [318].

Basic models of nAChRs are required to account for closed states, open states, and desensitized states, as well as the effects of agonist binding and the relative occupancy of these states. The model in Figure 8-1 describes the functional states of the receptor based on hypothetical relative free energy levels and intervening energy barriers through a matrix of increasing occupancies at both agonist and PAM binding sites. Vertical distances represent absolute differences in free energy, or stability, of the

various states under equilibrium conditions. The relative energy levels and heights of the energy barriers are proportionate to the logs of the transition rate constants in standard Markov models. It is important to emphasize that the model is intended to only represent qualitative characteristics of the data obtained with the agonist ACh. To simplify comparisons between the schematics for the various levels of agonist occupancy, the resting closed states were set to the same level. However, it should be appreciated that the average free energy of the resting bound state for each schematic probably increases (becomes less stable) in a step-wise manner as agonist occupancy increases.

The shallow energy well assigned to the short-lived open state characteristic of $\alpha 7$ (O*) is consistent with the brief opening observed in single-channel recordings, and the high energy barriers into the O* state are consistent with the low P_{open} of $\alpha 7$. Transition from C to O* will never occur with high probability, but is most likely prior to saturation of the agonist binding sites. The stability (represented by vertical displacements) of the D_s and D_i states relative to C increases with agonist occupancy, and the equilibrium between D_s and D_i will most strongly favor D_i at the highest levels of agonist and PAM occupancy. Single-channel openings evoked by ACh in the presence of PNU-120596 can occur as extremely long bursts or groups of openings separated by very short closures. The D_s state represents the rapid concentration-dependent form of desensitization unique to $\alpha 7$, and the effect of PNU-120596 may be to convert or connect the D_s state into the longer-lived open state(s) (O'). The short intraburst closures, many of which appear as subconductances, may represent the reverberation between D_s and O' in the presence of PNU-120596. The O' state(s) may be analogous

to the long-lived open states of doubly liganded heteromeric receptors so that conversions between D_s to O' are the primary mechanism through which PNU-120596 reconciles the peak current and net charge ACh concentration-response curves of $\alpha 7$ receptors (see Figure 6-1). Entry into D_i states primarily occurs through activated channel states, and the barrier heights between O'/D_s and D_i states are reduced at high occupancy levels. Therefore, strong ion channel activation promotes D_i, and a primary effect of high PAM occupancy is to stabilize D_i. The stabilization of D_i by high levels of both agonist and PAM occupancy results in a window where maximal potentiation occurs within the low-intermediate range of both agonist and PAM occupancy.

The $\alpha 7$ nAChR has been hotly pursued as a therapeutic target in the last 20 or so years. Tremendous progress has been made in identifying ligands that selectively activate and potentiate the receptor, yet the optimal approach to pharmacologically target the receptor for specific therapeutic purposes is still not understood. Using structurally related agonists that activate the receptor with varying efficacy, it was shown that channel activation is important for improving performance in inhibitory avoidance behavioral tasks in rodents [291]. However, the most efficacious $\alpha 7$ agonists are not always the most effective at producing protective or cognitive-enhancing effects in a number of studies. For example, GTS-21 is a partial agonist of $\alpha 7$, yet it has been documented to protect PC12 cells from trophic factor deprivation [227, 275, 451], cultured neurons from glutamate-induced cytotoxicity [276], and $\alpha 7$-expressing cell lines from amyloid beta fragments [452, 453]. In addition, GTS-21 has been shown to reduce neuronal cell loss in vivo after ischemic injury or lesions to the nucleus basalis [451] and has been shown to preserve functional responses of $\alpha 7$ function in hippocampal

interneurons following disruption of cholinergic input by lesioning the fimbria-fornix [454]. Furthermore, GTS-21 has been shown to improve attention- and memory-related tasks in humans [455]. Interestingly, GTS-21 is effective at stabilizing the α7 receptor in non-conducting desensitized states [327, 376]. Together these observations lead to the hypothesis that there may be more to α7 than activation of the ion channel. Perhaps α7 is capable of transmitting intracellular metabotropic signals from non-conducting, but nonetheless functional states. A proteomics study has indicated that many proteins co-assemble in complexes with nAChR, including numerous mediators of intracellular signal transduction [456].

This idea is still very much in its infancy and others have in fact declared desensitized states of ligand-gated ion channels to be “more of an experimental nuisance than a physiologically interesting phenomenon” [65], but there have been some observations that α7-mediated signal transduction occurs in non-neuronal cells even though ion channel activity is not detectable [457, 458]. We have shown that different agonists preferentially stabilize specific conformations (i.e. D_s, or D_i) using PNU-120596 as a probe for functional states [376]. Furthermore, the same ligand may be able to preferentially stabilize specific functional states depending on its binding orientation [380]. Given that the stability of the non-conducting conformations appears to be much greater than the stability of the activated ion conducting states, the design and discovery of ligands that specifically stabilize desired receptor conformations could be important to α7 drug development efforts in the future. However, figuring out exactly what the desired conformational states are in order to produce a desired effect is a monumental task that lies ahead.

Despite the identification and initial characterizing of $\alpha 7$ PAMs including PNU-120596, the current knowledge of the limiting factors for PAM-based therapy and the most desirable functional characteristics of PAMs as therapeutic agents is incomplete. Indeed there are more questions than answers. For example, are there different conditions when either a type I or type II PAM might be most advantageous? To what degree might a type II PAM disturb native temporal characteristics of a neuronal circuit? Can a PAM alter the native channel kinetics and still provide an acceptable therapeutic index? Are the most efficacious PAMs most desirable? Can $\alpha 7$ PAMs induce cytotoxicity due to high levels of channel-mediated calcium flux? What are the limiting factors of allosteric potentiation, and under what condition is the potentiation optimized? Does the ability of a PAM to modulate responses change over significant amounts of time? Are the known $\alpha 7$ PAMs sufficiently selective to avoid undesired effects? Would sufficient endogenous acetylcholine be present in patients with degenerated cholinergic neurons for effective positive allosteric modulation? Will PAMs retain sufficient pharmacological activity at physiological temperature to be useful? Some of these questions have begun to be answered, but clearly, the search for understanding and identifying characteristics of an ideal $\alpha 7$ PAM continues.

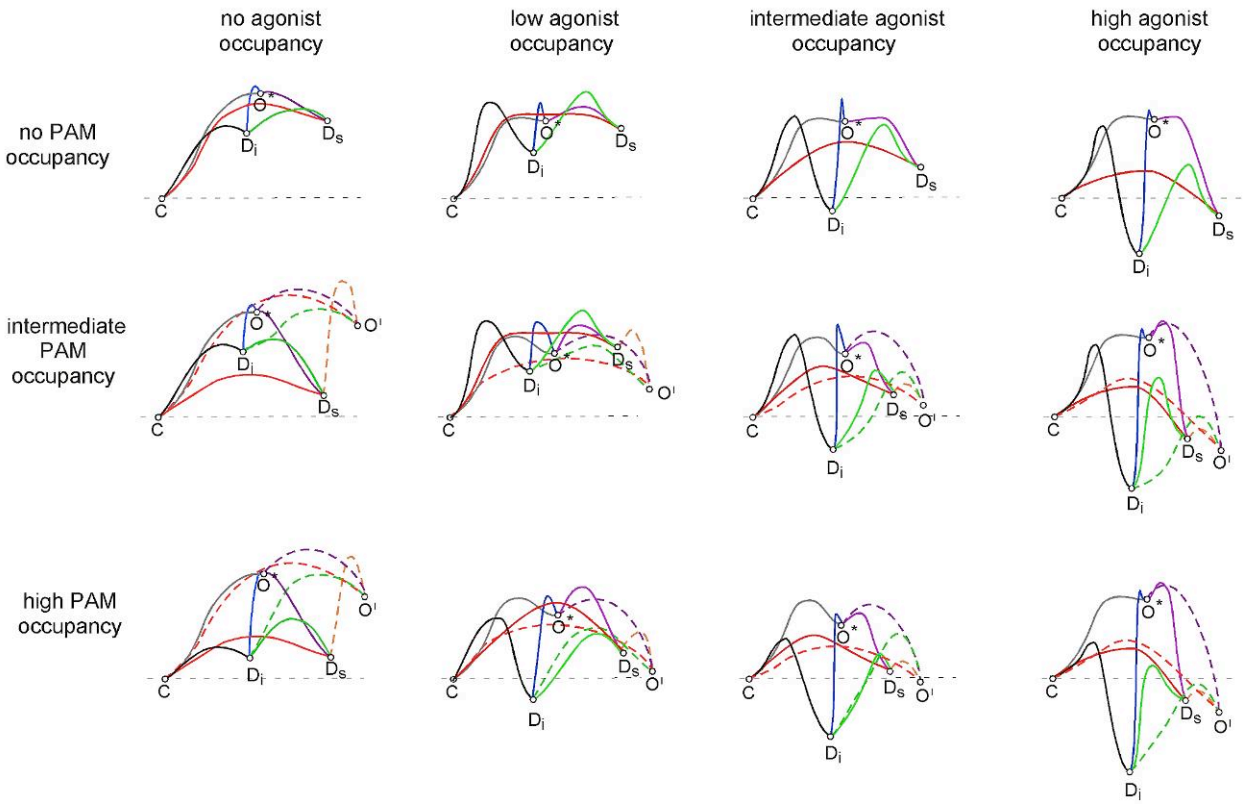

Figure 8-1. Proposed qualitative models for the activation, desensitization, and modulation of $\alpha 7$ nAChR. This figure was prepared together with Dr. Roger Papke. In the absence of any PNU-120596 binding, the primary effect of agonist binding is to shift the equilibrium between the conformational states from the resting closed state toward the desensitized states, D_s, which is sensitive to destabilization by PNU-120596, and D_i, which is insensitive to the activating effects of PNU-120596. The lower two rows include a new long-lived open state O', promoted by the binding of PNU-120596 and possibly connected to a modified form of the D_s state. Both agonist and PAM binding dynamically regulate the balance between D_s and D_i. Maximal ion channel activity occurs with intermediate levels of both agonist and PAM occupancy.

REFERENCES

[1] Schuetze SM. The discovery of the action potential. Trends Neurosci 1983;6:164-8.

[2] Lopez-Munoz F, Alamo C. Historical evolution of the neurotransmission concept. J Neural Transm 2009;116:515-33.

[3] Bennett MR. The early history of the synapse: from Plato to Sherrington. Brain Res Bull 1999;50:95-118.

[4] Cobb M. Timeline: exorcizing the animal spirits: Jan Swammerdam on nerve function. Nat Rev Neurosci 2002;3:395-400.

[5] Verkhratsky A, Krishtal OA, Petersen OH. From Galvani to patch clamp: the development of electrophysiology. Pflugers Arch 2006;453:233-47.

[6] Cajavilca C, Varon J, Sternbach GL. Resuscitation great. Luigi Galvani and the foundations of electrophysiology. Resuscitation 2009;80:159-62.

[7] Piccolino M. Animal electricity and the birth of electrophysiology: the legacy of Luigi Galvani. Brain Res Bull 1998;46:381-407.

[8] Goldensohn ES. Animal electricity from Bologna to Boston. Electroencephalogr Clin Neurophysiol 1998;106:94-100.

[9] Kettenmann H. Alexander von Humboldt and the concept of animal electricity. Trends Neurosci 1997;20:239-42.

[10] Hoff HE, Geddes LA. The rheotome and its prehistory: a study in the historical interrelation of electrophysiology and electromechanics. Bull Hist Med 1957;31:327-47.

[11] Seyfarth EA. Julius Bernstein (1839-1917): pioneer neurobiologist and biophysicist. Biol Cybern 2006;94:2-8.

[12] Piccolino M. Fifty years of the Hodgkin-Huxley era. Trends Neurosci 2002;25:552-3.

[13] Edidin M. Lipids on the frontier: a century of cell-membrane bilayers. Nat Rev Mol Cell Biol 2003;4:414-8.

[14] Nilius B. Pflugers Archiv and the advent of modern electrophysiology. From the first action potential to patch clamp. Pflugers Arch 2003;447:267-71.

[15] Gorter E, Grendel F. On Bimolecular Layers of Lipoids on the Chromocytes of the Blood. J Exp Med 1925;41:439-43.

[16] Grant G. The 1932 and 1944 Nobel Prizes in physiology or medicine: rewards for ground-breaking studies in neurophysiology. J Hist Neurosci 2006;15:341-57.

[17] Langmoen IA, Apuzzo ML. The brain on itself: Nobel laureates and the history of fundamental nervous system function. Neurosurgery 2007;61:891-907.

[18] Gasser HS, Erlanger J. The cathode ray oscilliograph as a means of recording nerve action currents and induction shocks. Am J Physiol 1921;59:473-5.

[19] Huxley A. From overshoot to voltage clamp. Trends Neurosci 2002;25:553-8.

[20] Young JZ, Keynes R. The Functioning of the Giant Nerve Fibres of the Squid. 1938 - J.Z. and the discovery of squid giant nerve fibres. J Exp Biol 2005;208:179-80.

[21] Cole KS, Curtis HJ. Electric Impedance of the Squid Giant Axon during Activity. J Gen Physiol 1939;22:649-70.

[22] Hodgkin AL, Katz B. The effect of sodium ions on the electrical activity of giant axon of the squid. J Physiol 1949;108:37-77.

[23] Huxley AF. Hodgkin and the action potential 1935-1952. J Physiol 2002;538:2.

[24] Hodgkin AL, Huxley AF. A quantitative description of membrane current and its application to conduction and excitation in nerve. J Physiol 1952;117:500-44.

[25] Elliott TR. The action of adrenalin. J Physiol 1905;32:401-67.

[26] Valenstein ES. The discovery of chemical neurotransmitters. Brain Cogn 2002;49:73-95.

[27] Dale HH. The action of certain esters and ethers of choline, and their relation to muscarine. J Pharmacol Exp Ther 1914;6:147-90.

[28] Dale H. Chemical Transmission of the Effects of Nerve Impulses. Br Med J 1934;1:835-41.

[29] Dale HH, Dudley HW. The presence of histamine and acetylcholine in the spleen of the ox and the horse. J Physiol 1929;68:97-123.

[30] Dale HH, Feldberg W, Vogt M. Release of acetylcholine at voluntary motor nerve endings. J Physiol 1936;86:353-80.

[31] Dale HH, Feldberg W. The chemical transmission of secretory impulses to the sweat glands of the cat. J Physiol 1934;82:121-8.

[32] Shepherd GM, Erulkar SD. Centenary of the synapse: from Sherrington to the molecular biology of the synapse and beyond. Trends Neurosci 1997;20:385-92.

[33] Todman D. John Eccles (1903-97) and the experiment that proved chemical synaptic transmission in the central nervous system. J Clin Neurosci 2008;15:972-7.

[34] Eccles C, Fatt P, Koketsu K. Cholinergic and inhibitory synapses in a central nervous pathway. Aust J Sci 1953;16:50-4.

[35] Fatt P, Katz B. Spontaneous subthreshold activity at motor nerve endings. J Physiol 1952;117:109-28.

[36] Del Castillo J, Katz B. Quantal components of the end-plate potential. J Physiol 1954;124:560-73.

[37] De Robertis ED, Bennett HS. Some features of the submicroscopic morphology of synapses in frog and earthworm. J Biophys Biochem Cytol 1955;1:47-58.

[38] Katz B, Miledi R. The Effect of Calcium on Acetylcholine Release from Motor Nerve Terminals. Proc R Soc Lond B Biol Sci 1965;161:496-503.

[39] Prull CR. Part of a scientific master plan? Paul Ehrlich and the origins of his receptor concept. Med Hist 2003;47:332-56.

[40] Klotz IM. Ligand-receptor complexes: origin and development of the concept. J Biol Chem 2004;279:1-12.

[41] Langley JN. On the Physiology of the Salivary Secretion: Part II. On the Mutual Antagonism of Atropin and Pilocarpin, having especial reference to their relations in the Sub-maxillary Gland of the Cat. J Physiol 1878;1:339-69.

[42] Langley JN. On the reaction of cells and of nerve-endings to certain poisons, chiefly as regards the reaction of striated muscle to nicotine and to curari. J Physiol 1905;33:374-413.

[43] Hill AV. The mode of action of nicotine and curari, determined by the form of the contraction curve and the method of temperature coefficients. J Physiol 1909;39:361-73.

[44] Hill AV. The possible effect of the aggregation of the molecules of haemoglobin on its dissociation curves. J Physiol 1910;40:4-7.

[45] Clark AJ. The mode of action of drugs on cells. London: E Arnold Company, 1933.

[46] Black J. Heinz Otto Schild - 18 May 1906-15 June 1984. Biogr Mem Fellows R Soc 1994;39:383-415.

[47] Arunlakshana O, Schild HO. Some quantitative uses of drug antagonists. Br J Pharmacol Chemother 1959;14:48-58.

[48] Gaddum JH. Theories of drug antagonism. Pharmacol Rev 1957;9:211-8.

[49] Schild HO. pAx and competitive drug antagonism. Br J Pharmacol Chemother 1949;4:277-80.

[50] Stephenson RP. A modification of receptor theory. Br J Pharmacol Chemother 1956;11:379-93.

[51] Del Castillo J, Katz B. Interaction at end-plate receptors between different choline derivatives. Proc R Soc Lond B Biol Sci 1957;146:369-81.

[52] Karlin A. On the application of "a plausible model" of allosteric proteins to the receptor for acetylcholine. J Theor Biol 1967;16:306-20.

[53] Changeux JP, Edelstein S. Conformational selection or induced fit? 50 years of debate resolved. F1000 Biol Rep 2011;3:19.

[54] Shanes AM, Berman MD. Kinetics of ion movement in the squid giant axon. J Gen Physiol 1955;39:279-300.

[55] Tasaki I, Hagiwar AS. Demonstration of two stable potential states in the squid giant axon under tetraethylammonium chloride. J Gen Physiol 1957;40:859-85.

[56] Narahashi T, Moore JW, Scott WR. Tetrodotoxin Blockage of Sodium Conductance Increase in Lobster Giant Axons. J Gen Physiol 1964;47:965-74.

[57] Takeuchi A, Takeuchi N. On the permeability of end-plate membrane during the action of transmitter. J Physiol 1960;154:52-67.

[58] Mueller P, Rudin DO, Tien HT, Wescott WC. Reconstitution of cell membrane structure in vitro and its transformation into an excitable system. Nature 1962;194:979-80.

[59] Hladky SB, Haydon DA. Discreteness of conductance change in bimolecular lipid membranes in the presence of certain antibiotics. Nature 1970;225:451-3.

[60] Hladky SB, Haydon DA. Ion transfer across lipid membranes in the presence of gramicidin A. I. Studies of the unit conductance channel. Biochim Biophys Acta 1972;274:294-312.

[61] Hille B. The hydration of sodium ions crossing the nerve membrane. Proc Natl Acad Sci U S A 1971;68:280-2.

[62] Hille B. The permeability of the sodium channel to organic cations in myelinated nerve. J Gen Physiol 1971;58:599-619.

[63] Katz B, Miledi R. Membrane noise produced by acetylcholine. Nature 1970;226:962-3.

[64] Katz B, Miledi R. The statistical nature of the acetycholine potential and its molecular components. J Physiol 1972;224:665-99.

[65] Colquhoun D, Sakmann B. From muscle endplate to brain synapses: a short history of synapses and agonist-activated ion channels. Neuron 1998;20:381-7.

[66] Neher E, Lux HD. Voltage clamp on Helix pomatia neuronal membrane; current measurement over a limited area of the soma surface. Pflugers Arch 1969;311:272-7.

[67] Neher E, Sakmann B. Single-channel currents recorded from membrane of denervated frog muscle fibres. Nature 1976;260:799-802.

[68] Hamill OP, Marty A, Neher E, Sakmann B, Sigworth FJ. Improved patch-clamp techniques for high-resolution current recording from cells and cell-free membrane patches. Pflugers Arch 1981;391:85-100.

[69] Colquhoun D, Sakmann B. Fluctuations in the microsecond time range of the current through single acetylcholine receptor ion channels. Nature 1981;294:464-6.

[70] Colquhoun D, Sakmann B. Fast events in single-channel currents activated by acetylcholine and its analogues at the frog muscle end-plate. J Physiol 1985;369:501-57.

[71] Green T, Heinemann SF, Gusella JF. Molecular neurobiology and genetics: investigation of neural function and dysfunction. Neuron 1998;20:427-44.

[72] Armstrong CM, Hille B. Voltage-gated ion channels and electrical excitability. Neuron 1998;20:371-80.

[73] Toyoshima C, Unwin N. Ion channel of acetylcholine receptor reconstructed from images of postsynaptic membranes. Nature 1988;336:247-50.

[74] Doyle DA, Morais Cabral J, Pfuetzner RA, Kuo A, Gulbis JM, Cohen SL, et al. The structure of the potassium channel: molecular basis of K+ conduction and selectivity. Science 1998;280:69-77.

[75] Sui H, Han BG, Lee JK, Walian P, Jap BK. Structural basis of water-specific transport through the AQP1 water channel. Nature 2001;414:872-8.

[76] Jiang Y, Lee A, Chen J, Cadene M, Chait BT, MacKinnon R. Crystal structure and mechanism of a calcium-gated potassium channel. Nature 2002;417:515-22.

[77] Ortells MO, Lunt GG. Evolutionary history of the ligand-gated ion-channel superfamily of receptors. Trends in Neurosciences 1995;18:121-7.

[78] Karlin A, Akabas MH. Toward a structural basis for the function of nicotinic acetylcholine receptors and their cousins. Neuron 1995;15:1231-44.

[79] Grenningloh G, Rienitz A, Schmitt B, Methfessel C, Zensen M, Beyreuther K, et al. The strychnine-binding subunit of the glycine receptor shows homology with nicotinic acetylcholine receptors. Nature 1987;328:215-20.

[80] Schofield PR, Darlison MG, Fujita N, Burt DR, Stephenson FA, Rodriguez H, et al. Sequence and functional expression of the GABA A receptor shows a ligand-gated receptor super-family. Nature 1987;328:221-7.

[81] Levitan ES, Schofield PR, Burt DR, Rhee LM, Wisden W, Kohler M, et al. Structural and functional basis for GABAA receptor heterogeneity. Nature 1988;335:76-9.

[82] Eisele JL, Bertrand S, Galzi JL, Devillers-Thiery A, Changeux JP, Bertrand D. Chimaeric nicotinic-serotonergic receptor combines distinct ligand binding and channel specificities. Nature 1993;366:479-83.

[83] Galzi J-L, Devillers-Thiery A, Hussy N, Bertrand S, Changeux J-P, Bertrand D. Mutations in the channel domain of a neuronal nicotinic receptor convert ion selectivity from cationic to anionic. Nature 1992;359:500-5.

[84] Devillers-Thiery A, Galzi JL, Eisele JL, Bertrand S, Bertrand D, Changeux JP. Functional architecture of the nicotinic acetylcholine receptor: a prototype of ligand-gated ion channels. J Membr Biol 1993;136:97-112.

[85] Miledi R, Molinoff P, Potter LT. Isolation of the cholinergic receptor protein of Torpedo electric tissue. Nature 1971;229:554-7.

[86] Karlin A, Cowburn D. The affinity-labeling of partially purified acetylcholine receptor from electric tissue of Electrophorus. Proceedings of the National Academy of Sciences of the United States of America 1973;70:3636-40.

[87] Reynolds JA, Karlin A. Molecular weight in detergent solution of acetylcholine receptor from *Torpedo californica*. Biochemistry 1978;17:2035-8.

[88] Lindstrom J, Merlie J, Yogeeswaran G. Biochemical properties of acteylcholine receptor subunits from Torpedo californica. Biochemistry 1979;18:4465-70.

[89] Raftery MA, Hunkapiller MW, Strader CD, Hood LE. Acetylcholine receptor: complex of homologous subunits. Science 1980;208:1454-7.

[90] Ballivet M, Patrick J, Lee J, Heinemann S. Molecular cloning of cDNA coding for the gamma subunit of *Torpedo* acetylcholine receptor. Proc Natl Acad Sci USA 1982;79:4466-70.

[91] Noda M, Takahashi H, Tanabe T, Toyosato M, Kikyotani S, Furutani Y, et al. Structural homology of *Torpedo californica* acetylcholine receptor subunits. Nature 1983;302:528-32.

[92] Claudio T, Ballivet M, Patrick J, Heinemann S. Nucleotide and deduced amino acid sequences of *Torpedo californica* acetylcholine receptor gamma-subunit. Proc Natl Acad Sci USA 1983;80:1111-5.

[93] Boulter J, Luyten W, Evans K, Mason P, Ballivet M, Goldman D, et al. Isolation of a clone coding for the alpha-subunit of a mouse acetylcholine receptor. J Neurosci 1985;5:2545-52.

[94] Mishina M, Takai T, Imoto K, Noda M, Takahashi T, Numa S, et al. Molecular distinction between fetal and adult forms of muscle acetylcholine receptor. Nature 1986;321:406-11.

[95] Unwin N. The nicotinic acetylcholine receptor at 9A resolution. J Mol Biol 1993;229:1101-24.

[96] Unwin N. Refined structure of the nicotinic acetylcholine receptor at 4A resolution. J Mol Biol 2005;346:967-89.

[97] Devillers-Thiery A, Giraudat J, Bentaboulet M, Changeux JP. Complete mRNA coding sequence of the acetylcholine binding alpha-subunit of Torpedo marmorata acetylcholine receptor: a model for the transmembrane organization of the polypeptide chain. Proceedings of the National Academy of Sciences of the United States of America 1983;80:2067-71.

[98] Chavez RA, Hall ZW. Expression of fusion proteins of the nicotinic acetylcholine receptor from mammalian muscle identifies the membrane-spanning regions in the α and δ subunits. J Cell Biol 1992;116:385-93.

[99] Sine S, Taylor P. Functional consequences of agonist-mediated state transitions in the cholinergic receptor. Studies in cultured muscle cells. The Journal of biological chemistry 1979;254:3315-25.

[100] Sine S, Taylor P. The relationship between agonist occupation and the permeability response of the cholinergic receptor revealed by bound cobra alpha-toxin. J Biol Chem 1980;255:10144-56.

[101] Dionne VE, Steinbach JH, Stevens CF. An analysis of the dose-response relationship at voltage-clamped frog neuromuscular junctions. The Journal of physiology 1978;281:421-44.

[102] Cash DJ, Hess GP. Molecular mechanism of acetylcholine receptor-controlled ion translocation across cell membranes. Proceedings of the National Academy of Sciences of the United States of America 1980;77:842-6.

[103] Blount P, Merlie JP. Molecular basis of the two nonequivalent ligand binding sites of the muscle nicotinic acetylcholine receptor. Neuron 1989;3:349-57.

[104] Pedersen SE, Cohen JB. *d*-tubocurarine binding sites are located at α-γ and α-δ subunit interfaces of the nicotinic acetylcholine receptor. Proc Natl Acad Sci USA 1990;87:2785-9.

[105] Sine SM, Claudio T. Gamma- and delta-subunits regulate the affinity and the cooperativity of ligand binding to the acetylcholine receptor. The Journal of biological chemistry 1991;266:19369-77.

[106] Hansen SB, Sulzenbacher G, Huxford T, Marchot P, Taylor P, Bourne Y. Structures of Aplysia AChBP complexes with nicotinic agonists and antagonists reveal distinctive binding interfaces and conformations. Embo J 2005;24:3635-46.

[107] Zhong W, Gallivan JP, Zhang Y, Li L, Lester HA, Dougherty DA. From ab initio quantum mechanics to molecular neurobiology: a cation-pi binding site in the nicotinic receptor. Proc Natl Acad Sci U S A 1998;95:12088-93.

[108] Sine SM. The nicotinic receptor ligand binding domain. J Neurobiol 2002;53:431-46.

[109] Machold J, Weise C, Utkin Y, Tsetlin V, Hucho F. The handedness of the subunit arrangement of the nicotinic acetylcholine receptor from *Torpedo Californica*. Eur J Biochem 1995;234:427-30.

[110] Keller SH, Taylor P. Determinants responsible for assembly of the nicotinic acetylcholine receptor. The Journal of general physiology 1999;113:171-6.

[111] Karlin A, Holtzman E, Yodh N, Lobel P, Wall J, Hainfeld J. The arrangement of the subunits of the acetylcholine receptor of *Torpedo Californica*. J Biol Chem 1983;258:6678-81.

[112] Francis MM, Choi KI, Horenstein BA, Papke RL. Sensitivity to voltage-independent inhibition determined by pore-lining region of ACh receptor. Biophys J 1998;74:2306-17.

[113] Downing JEG, Role LW. Activators of protein kinase C enhance acetylcholine receptor desensitization in sympathetic ganglion neurons. Proc Natl Acad Sci USA 1987;84:7739-43.

[114] Swope SL, Moss SJ, Blackstone CD, Huganir RL. Phosphorylation of ligand-gated ion channels: a possible mode of synaptic plasticity. Faseb J 1992;6:2514-23.

[115] Moss SJ, McDonald BJ, Rudhard Y, Schoepfer R. Phosphorylation of the predicted major intracellular domains of the rat and chick neuronal nicotinic acetylcholine receptor alpha 7 subunit by cAMP-dependent protein kinase. Neuropharmacology 1996;35:1023-8.

[116] Cho CH, Song W, Leitzell K, Teo E, Meleth AD, Quick MW, et al. Rapid upregulation of alpha7 nicotinic acetylcholine receptors by tyrosine dephosphorylation. J Neurosci 2005;25:3712-23.

[117] Charpantier E, Wiesner A, Huh KH, Ogier R, Hoda JC, Allaman G, et al. Alpha7 neuronal nicotinic acetylcholine receptors are negatively regulated by tyrosine phosphorylation and Src-family kinases. J Neurosci 2005;25:9836-49.

[118] Brejc K, van Dijk WJ, Klaassen RV, Schuurmans M, van Der Oost J, Smit AB, et al. Crystal structure of an ACh-binding protein reveals the ligand-binding domain of nicotinic receptors. Nature 2001;411:269-76.

[119] Celie PH, van Rossum-Fikkert SE, van Dijk WJ, Brejc K, Smit AB, Sixma TK. Nicotine and carbamylcholine binding to nicotinic acetylcholine receptors as studied in AChBP crystal structures. Neuron 2004;41:907-14.

[120] Hansen SB, Sulzenbacher G, Huxford T, Marchot P, Bourne Y, Taylor P. Structural characterization of agonist and antagonist-bound acetylcholine-binding protein from Aplysia californica. Journal of molecular neuroscience : MN 2006;30:101-2.

[121] Smit AB, Celie PH, Kasheverov IE, Mordvintsev DY, van Nierop P, Bertrand D, et al. Acetylcholine-binding proteins: functional and structural homologs of nicotinic acetylcholine receptors. Journal of molecular neuroscience : MN 2006;30:9-10.

[122] Boulter J, Evans K, Goldman D, Martin G, Treco D, Heinemann S, et al. Isolation of a cDNA clone coding for a possible neural nicotinic acetylcholine receptor alpha-subunit. Nature 1986;319:368-74.

[123] Heinemann SF, Boulter J, Connolly J, Deneris E, Duvoisin R, Hartley M, et al. Brain nicotinic receptor genes. NIDA Res Monogr 1991;111:3-23.

[124] Goldman D, Simmons D, Swanson LW, Patrick J, Heinemann S. Mapping of brain areas expressing RNA homologous to two different acetylcholine receptor alpha-subunit cDNAs. Proceedings of the National Academy of Sciences of the United States of America 1986;83:4076-80.

[125] Shytle RD, Mori T, Townsend K, Vendrame M, Sun N, Zeng J, et al. Cholinergic modulation of microglial activation by alpha 7 nicotinic receptors. J Neurochem 2004;89:337-43.

[126] Wang H, Yu M, Ochani M, Amella CA, Tanovic M, Susarla S, et al. Nicotinic acetylcholine receptor alpha7 subunit is an essential regulator of inflammation. Nature 2003;421:384-8.

[127] Kao PN, Karlin A. Acetylcholine receptor binding site contains a disulfide cross-link between adjacent half-cystinyl residues. J Biol Chem 1986;261:8085-8.

[128] Papke RL, Stokes C, Williams DK, Wang J, Horenstein NA. Cysteine accessibility analysis of the human alpha7 nicotinic acetylcholine receptor ligand-binding domain identifies L119 as a gatekeeper. Neuropharmacology 2011;60:159-71.

[129] Conroy WG, Vernallis AB, Berg DK. The alpha 5 gene product assembles with multiple acetylcholine receptor subunits to form distinctive receptor subtypes in brain. Neuron 1992;9:679-91.

[130] Gerzanich V, Wang F, Kuryatov A, Lindstrom J. alpha 5 Subunit alters desensitization, pharmacology, Ca++ permeability and Ca++ modulation of human neuronal alpha 3 nicotinic receptors. J Pharmacol Exp Ther 1998;286:311-20.

[131] Nelson ME, Kuryatov A, Choi CH, Zhou Y, Lindstrom J. Alternate stoichiometries of alpha4beta2 nicotinic acetylcholine receptors. Mol Pharmacol 2003;63:332-41.

[132] Gotti C, Zoli M, Clementi F. Brain nicotinic acetylcholine receptors: native subtypes and their relevance. Trends Pharmacol Sci 2006;27:482-91.

[133] Palma E, Bertrand S, Binzoni T, Bertrand D. Neuronal nicotinic alpha 7 receptor expressed in Xenopus oocytes presents five putative binding sites for methyllycaconitine. J Physiol 1996;491:151-61.

[134] Murray TA, Bertrand D, Papke RL, George AA, Pantoja R, Srinivasan R, et al. alpha7beta2 Nicotinic Acetylcholine Receptors Assemble, Function, and Are Activated Primarily via Their alpha7-alpha7 Interfaces. Molecular pharmacology 2012;81:175-88.

[135] Liu Q, Huang Y, Xue F, Simard A, DeChon J, Li G, et al. A novel nicotinic acetylcholine receptor subtype in basal forebrain cholinergic neurons with high sensitivity to amyloid peptides. J Neurosci 2009;29:918-29.

[136] Khiroug SS, Harkness PC, Lamb PW, Sudweeks SN, Khiroug L, Millar NS, et al. Rat nicotinic ACh receptor alpha7 and beta2 subunits co-assemble to form functional heteromeric nicotinic receptor channels. J Physiol 2002;540:425-34.

[137] Gotti C, Hanke W, Maury K, Moretti M, Ballivet M, Clementi F, et al. Pharmacology and biophysical properties of alpha 7 and alpha 7-alpha 8 alpha-bungarotoxin receptor subtypes immunopurified from the chick optic lobe. The European journal of neuroscience 1994;6:1281-91.

[138] Keyser KT, Britto LR, Schoepfer R, Whiting P, Cooper J, Conroy W, et al. Three subtypes of alpha-bungarotoxin-sensitive nicotinic acetylcholine receptors are expressed in chick retina. The Journal of neuroscience : the official journal of the Society for Neuroscience 1993;13:442-54.

[139] Lips KS, Pfeil U, Kummer W. Coexpression of alpha 9 and alpha 10 nicotinic acetylcholine receptors in rat dorsal root ganglion neurons. Neuroscience 2002;115:1-5.

[140] Severance EG, Zhang H, Cruz Y, Pakhlevaniants S, Hadley SH, Amin J, et al. The alpha7 nicotinic acetylcholine receptor subunit exists in two isoforms that contribute to functional ligand-gated ion channels. Mol Pharmacol 2004;66:420-9.

[141] Gault J, Robinson M, Berger R, Drebing C, Logel J, Hopkins J, et al. Genomic organization and partial duplication of the human alpha7 neuronal nicotinic acetylcholine receptor gene (CHRNA7). Genomics 1998;52:173-85.

[142] Katz B, Miledi R. The binding of acetylcholine to receptors and its removal from the synaptic cleft. Journal of Physiology (London) 1973;231:549-74.

[143] Paton WDA, Zaimis EJ. The pharmacological actions of polymethylene bis-trimethylammonium salts. 1949;Brit. J. Pharm.:381-400.

[144] Gurney AM, Rang HP. The channel blocking action of methonium compounds on rat submandibular ganglion cells. Br J Pharmacol 1984;82:623-42.

[145] Papke RL, Wecker L, Stitzel JA. Activation and inhibition of mouse muscle and neuronal nicotinic acetylcholine receptors expressed in Xenopus oocytes. J Pharmacol Exp Ther 2010;333:501-18.

[146] Mulle C, Choquet D, Korn H, Changeux J-P. Calcium influx through nicotinic receptor in rat central neurons: its relevance to cellular regulation. Neuron 1992;8:135-43.

[147] Vernino S, Amador M, Luetje CW, Patrick J, Dani JA. Calcium modulation and high calcium permeability of neuronal nicotinic acetylcholine receptors. Neuron 1992;8:127-34.

[148] Vernino S, Rogers M, Radcliffe KA, Dani JA. Quantitative measurement of calcium flux through muscle and neuronal nicotinic acetylcholine receptors. J Neurosci 1994;14:5514-24.

[149] Costa AC, Patrick JW, Dani JA. Improved technique for studying ion channels expressed in *Xenopus* oocytes, including fast superfusion. Biophys J 1994;67:395-401.

[150] Mathie A, Colquhoun D, Cull-Candy SG. Rectification of currents activated by nicotinic acetylcholine receptors in rat sympathetic ganglion neurones. J Physiol (Lond) 1990;427:625-55.

[151] Ifune CK, Steinbach JH. Rectification of acetylcholine-elicited currents in PC12 pheochromocytoma cells. Proc Natl Acad Sci USA 1990;87:4794-8.

[152] Haghighi AP, Cooper E. Neuronal nicotinic acetylcholine receptors are blocked by intracellular spermine in a voltage-dependent manner. J Neurosci 1998;18:4050-62.

[153] Krashia P, Moroni M, Broadbent S, Hofmann G, Kracun S, Beato M, et al. Human alpha3beta4 neuronal nicotinic receptors show different stoichiometry if they are expressed in Xenopus oocytes or mammalian HEK293 cells. PloS one 2010;5:e13611.

[154] Whiting PJ, Lindstrom JM. Characterization of bovine and human neuronal nicotinic acetylcholine receptors using monoclonal antibodies. J Neurosci 1988;8:3395-404.

[155] Ullian EM, McIntosh JM, Sargent PB. Rapid synaptic transmission in the avian ciliary ganglion is mediated by two distinct classes of nicotinic receptors. The Journal of neuroscience : the official journal of the Society for Neuroscience 1997;17:7210-9.

[156] Clarke PBS, Schwartz RD, Paul SM, Pert CB, Pert A. Nicotinic binding in rat brain: autoradiographic comparison of [^{3}H] acetylcholine [$_{3}$H] nicotine and [^{125}I]-alpha-bungarotoxin. J Neurosci 1985;5:1307-15.

[157] Deneris ES, Connolly J, Boulter J, Wada E, Wada K, Swanson LW, et al. Primary structure and expression of β2: a novel subunit of neuronal nicotinic acetylcholine receptors. Neuron 1988;1:45-54.

[158] Couturier S, Bertrand D, Matter JM, Hernandez M-C, Bertrand S, Millar N, et al. A neuronal nicotinic acetylcholine receptor subunit (α7) is developmentally regulated and forms a homo-oligomeric channel blocked by α-btx. Neuron 1990;5:847-56.

[159] Schoepfer R, Conroy WG, Whiting P, Gore M, Lindstrom J. Brain alpha-bungarotoxin binding protein cDNAs and MAbs reveal subtypes of this branch of the ligand-gated ion channel gene superfamily. Neuron 1990;5:35-48.

[160] Seguela P, Wadiche J, Dinely-Miller K, Dani JA, Patrick JW. Molecular cloning, functional properties and distribution of rat brain alpha 7: a nicotinic cation channel highly permeable to calcium. J Neurosci 1993;13(2):596-604.

[161] Zhou FM, Wilson CJ, Dani JA. Cholinergic interneuron characteristics and nicotinic properties in the striatum. Journal of neurobiology 2002;53:590-605.

[162] Umbriaco D, Watkins KC, Descarries L, Cozzari C, Hartman BK. Ultrastructural and morphometric features of the acetylcholine innervation in adult rat parietal cortex: an electron microscopic study in serial sections. The Journal of comparative neurology 1994;348:351-73.

[163] Descarries L, Gisiger V, Steriade M. Diffuse transmission by acetylcholine in the CNS. Prog Neurobiol 1997;53:603-25.

[164] Brown DA, Docherty RJ, Halliwell JV. Chemical transmission in the rat interpeduncular nucleus in vitro. The Journal of physiology 1983;341:655-70.

[165] McGehee DS, Role LW. Physiological diversity of nicotinic acetylcholine receptors expressed by vertebrate neurons. Annu Rev Physiol 1995;57:521-46.

[166] Brown DA. Acetylcholine. Br J Pharmacol 2006;147 Suppl 1:S120-6.

[167] Kawaja MD, Flumerfelt BA, Hrycyshyn AW. A comparison of the subnuclear and ultrastructural distribution of acetylcholinesterase and choline acetyltransferase in the rat interpeduncular nucleus. Brain research bulletin 1990;24:517-23.

[168] Nirogi R, Mudigonda K, Kandikere V, Ponnamaneni R. Quantification of acetylcholine, an essential neurotransmitter, in brain microdialysis samples by liquid chromatography mass spectrometry. Biomed Chromatogr 2010;24:39-48.

[169] Jones S, Sudweeks S, Yakel JL. Nicotinic receptors in the brain: correlating physiology with function. Trends in neurosciences 1999;22:555-61.

[170] Frazier CJ, Buhler AV, Weiner JL, Dunwiddie TV. Synaptic potentials mediated via alpha-bungarotoxin-sensitive nicotinic acetylcholine receptors in rat hippocampal interneurons. J Neurosci 1998;18:8228-35.

[171] Hatton GI, Yang QZ. Synaptic potentials mediated by alpha 7 nicotinic acetylcholine receptors in supraoptic nucleus. J Neurosci 2002;22:29-37.

[172] Fabian-Fine R, Skehel P, Errington ML, Davies HA, Sher E, Stewart MG, et al. Ultrastructural distribution of the alpha7 nicotinic acetylcholine receptor subunit in rat hippocampus. J Neurosci 2001;21:7993-8003.

[173] Jacob MH, Berg DK. The ultrastructural localization of alpha-bungarotoxin binding sites in relation to synapses on chick ciliary ganglion neurons. J Neurosci 1983;3:260-71.

[174] Wilson Horch HL, Sargent PB. Perisynaptic surface distribution of multiple classes of nicotinic acetylcholine receptors on neurons in the chicken ciliary ganglion. J Neurosci 1995;15:7778-95.

[175] Jones IW, Wonnacott S. Precise localization of alpha7 nicotinic acetylcholine receptors on glutamatergic axon terminals in the rat ventral tegmental area. The Journal of neuroscience : the official journal of the Society for Neuroscience 2004;24:11244-52.

[176] Wonnacott S. Presynaptic nicotinic ACh receptors. TINS 1997;20:92-8.

[177] Role L, Berg D. Nicotinic receptors in the development and modulation of CNS synapses. Neuron 1996;16:1077-85.

[178] Coggan JS, Paysan J, Conroy WG, Berg DK. Direct Recording of Nicotinic Responses in Presynaptic Nerve Terminals. J Neurosci 1997;17:5798-806.

[179] Soliakov L, Wonnacott S. Voltage-sensitive Ca2+ channels involved in nicotinic receptor-mediated [3H]dopamine release from rat striatal synaptosomes. Journal of neurochemistry 1996;67:163-70.

[180] McGehee DS, Heath MJS, Gelber S, Devay P, Role LW. Nicotine enhancement of fast excitatory synaptic transmission in CNS by presynaptic receptors. Science 1995;269:1692-6.

[181] Gray R, Rajan AS, Radcliffe KA, Yakehiro M, Dani JA. Hippocampal synaptic transmission enhanced by low concentrations of nicotine. Nature 1996;383:713-6.

[182] Levin ED, Rezvani AH. Nicotinic treatment for cognitive dysfunction. Curr Drug Targets CNS Neurol Disord 2002;1:423-31.

[183] Rezvani AH, Levin ED. Cognitive effects of nicotine. Biol Psychiatry 2001;49:258-67.

[184] Warburton DM. Nicotine as a cognitive enhancer. Progress in neuro-psychopharmacology & biological psychiatry 1992;16:181-91.

[185] Picciotto MR, Zoli M. Nicotinic receptors in aging and dementia. Journal of neurobiology 2002;53:641-55.

[186] Potter AS, Newhouse PA. Effects of acute nicotine administration on behavioral inhibition in adolescents with attention-deficit/hyperactivity disorder. Psychopharmacology 2004;176:182-94.

[187] Dani JA, Bertrand D. Nicotinic acetylcholine receptors and nicotinic cholinergic mechanisms of the central nervous system. Annu Rev Pharmacol Toxicol 2007;47:699-729.

[188] Levin ED, McClernon FJ, Rezvani AH. Nicotinic effects on cognitive function: behavioral characterization, pharmacological specification, and anatomic localization. Psychopharmacology (Berl) 2006;184:523-39.

[189] Levin ED, Simon BB. Nicotinic acetylcholine involvement in cognitive function in animals. Psychopharmacology 1998;138:217-30.

[190] Swanson L, Simmons D, Whiting P, Lindstrom J. Immunohistochemical localization of neuronal nicotinic receptors in the rodent central nervous system. J Neurosci 1987;7:3334-42.

[191] Picciotto MR, Zoli M, Lena C, Bessis A, Lallemand Y, LeNovere M, et al. Abnormal avoidance learning in mice lacking functional high-affinity nicotine receptor in the brain. Nature 1995;374:65-7.

[192] Zoli M, Lena C, Picciotto MR, Changeux JP. Identification of four classes of brain nicotinic receptors using beta2 mutant mice. J Neurosci 1998;18:4461-72.

[193] Flores CM, Rogers SW, Pabreza LA, Wolfe BB, Kellar KJ. A subtype of nicotinic cholinergic receptor in rat brain is composed of $\alpha 4$ and $\beta 2$ subunits and is up-regulated by chronic nicotine treatment. Mol Pharm 1992;41:31-7.

[194] Han ZY, Le Novere N, Zoli M, Hill JA, Jr., Champtiaux N, Changeux JP. Localization of nAChR subunit mRNAs in the brain of Macaca mulatta. Eur J Neurosci 2000;12:3664-74.

[195] Mulle C, Vidal C, Benoit P, Changeux J-P. Existence of different subtypes of nicotinic acetylcholine receptors in the rat habenulo-interpeduncular system. J Neurosci 1991;11:2588-97.

[196] Grady SR, Salminen O, Laverty DC, Whiteaker P, McIntosh JM, Collins AC, et al. The subtypes of nicotinic acetylcholine receptors on dopaminergic terminals of mouse striatum. Biochem Pharmacol 2007;74:1235-46.

[197] Zhou FM, Liang Y, Dani JA. Endogenous nicotinic cholinergic activity regulates dopamine release in the striatum. Nat Neurosci 2001;4:1224-9.

[198] Marshall DL, Redfern PH, Wonnacott S. Presynaptic nicotinic modulation of dopamine release in the three ascending pathways studied by in vivo microdialysis: comparison of naive and chronic nicotine-treated rats. Journal of neurochemistry 1997;68:1511-9.

[199] Corrigall WA. Nicotine self-administration in animals as a dependence model. Nicotine & tobacco research : official journal of the Society for Research on Nicotine and Tobacco 1999;1:11-20.

[200] Fagen ZM, Mansvelder HD, Keath JR, McGehee DS. Short- and long-term modulation of synaptic inputs to brain reward areas by nicotine. Annals of the New York Academy of Sciences 2003;1003:185-95.

[201] Olale F, Gerzanich V, Kuryatov A, Wang F, Lindstrom J. Chronic nicotine exposure differentially affects the function of human α3, α4, and α7 neuronal nicotinic receptor subtypes. J Pharm Exp Ther 1997;283:675-83.

[202] Li P, Steinbach JH. The neuronal nicotinic alpha4beta2 receptor has a high maximal probability of being open. Br J Pharm 2010;160:1906-15.

[203] Dani JA, Radcliffe KA, Pidoplichko VI. Variations in desensitization of nicotinic acetylcholine receptors from hippocampus and midbrain dopamine areas. Eur J Pharmacol 2000;393:31-8.

[204] Quick MW, Lester RA. Desensitization of neuronal nicotinic receptors. J Neurobiol 2002;53:457-78.

[205] Wooltorton JR, Pidoplichko VI, Broide RS, Dani JA. Differential desensitization and distribution of nicotinic acetylcholine receptor subtypes in midbrain dopamine areas. J Neurosci 2003;23:3176-85.

[206] Govind AP, Walsh H, Green WN. Nicotine-induced upregulation of native neuronal nicotinic receptors is caused by multiple mechanisms. The Journal of neuroscience : the official journal of the Society for Neuroscience 2012;32:2227-38.

[207] Tribollet E, Bertrand D, Marguerat A, Raggenbass M. Comparative distribution of nicotinic receptor subtypes during development, adulthood and aging: an autoradiographic study in the rat brain. Neuroscience 2004;124:405-20.

[208] Cimino M, Marini P, Fornasari D, Cattabeni F, Clementi F. Distribution of nicotinic receptors in cynomolgus monkey brain and ganglia: localization of alpha 3 subunit mRNA, alpha-bungarotoxin and nicotine binding sites. Neuroscience 1992;51:77-86.

[209] Spurden DP, Court JA, Lloyd S, Oakley A, Perry R, Pearson C, et al. Nicotinic receptor distribution in the human thalamus: autoradiographical localization of [3H]nicotine and [125I] alpha- bungarotoxin binding. J Chem Neuroanat 1997;13:105-13.

[210] Breese CR, Adams C, Logel J, Drebing C, Rollins Y, Barnhart M, et al. Comparison of the regional expression of nicotinic acetylcholine receptor alpha7 mRNA and [125I]-alpha-bungarotoxin binding in human postmortem brain. J Comp Neurol 1997;387:385-98.

[211] Albuquerque EX, Pereira EF, Alkondon M, Rogers SW. Mammalian nicotinic acetylcholine receptors: from structure to function. Physiological reviews 2009;89:73-120.

[212] Le Novere N, Changeux JP. Molecular evolution of the nicotinic acetylcholine receptor: an example of multigene family in excitable cells. J Mol Evol 1995;40:155-72.

[213] Papke RL, Thinschmidt JS. The correction of alpha7 nicotinic acetylcholine receptor concentration-response relationships in *Xenopus* oocytes. Neurosci Let 1998;256:163-6.

[214] Papke RL, Papke JKP. Comparative pharmacology of rat and human alpha7 nAChR conducted with net charge analysis. Br J of Pharm 2002;137:49-61.

[215] Mike A, Castro NG, Albuquerque EX. Choline and acetylcholine have similar kinetic properties of activation and desensitization on the alpha7 nicotinic receptors in rat hippocampal neurons. Brain Res 2000;882:155-68.

[216] McNerney ME, Pardi D, Pugh PC, Nai Q, Margiotta JF. Expression and channel properties of alpha-bungarotoxin-sensitive acetylcholine receptors on chick ciliary and choroid neurons. J Neurophysiol 2000;84:1314-29.

[217] Kalappa BI, Gusev AG, Uteshev VV. Activation of functional alpha7-containing nAChRs in hippocampal CA1 pyramidal neurons by physiological levels of choline in the presence of PNU-120596. PLoS One 2010;5:e13964.

[218] Uteshev VV, Meyer EM, Papke RL. Regulation of neuronal function by choline and 4OH-GTS-21 through alpha7 nicotinic receptors. J Neurophysiol 2003;89:33-46.

[219] Scremin OU, Jenden DJ. Time-dependent changes in cerebral choline and acetylcholine induced by transient global ischemia in rats. Stroke 1991;22:643-7.

[220] Sands SB, Barish ME. Calcium permeability of neuronal nicotinic acetylcholine receptor channels in PC12 cells. Br Res 1991;560:38-42.

[221] Bertrand D, Galzi JL, Devillers-Thiery A, Bertrand S, P. CJ. Mutations at two distinct sites within the channel domain M2 alter calcium permeability of neuronal alpha 7 nicotinic receptor. Proc Natl Acad Sci USA 1993;90:6971-5.

[222] Dickinson JA, Hanrott KE, Mok MH, Kew JN, Wonnacott S. Differential coupling of alpha7 and non-alpha7 nicotinic acetylcholine receptors to calcium-induced calcium release and voltage-operated calcium channels in PC12 cells. J Neurochem 2007;100:1089-96.

[223] Ren K, Puig V, Papke RL, Itoh Y, Hughes JA, Meyer EM. Multiple calcium channels and kinases mediate alpha7 nicotinic receptor neuroprotection in PC12 cells. J Neurochem 2005;94:926-33.

[224] Dajas-Bailador F, Wonnacott S. Nicotinic acetylcholine receptors and the regulation of neuronal signalling. Trends Pharmacol Sci 2004;25:317-24.

[225] Sabban EL, Gueorguiev VD. Effects of short- and long-term nicotine treatment on intracellular calcium and tyrosine hydroxylase gene expression. Ann N Y Acad Sci 2002;971:39-44.

[226] Gueorguiev VD, Zeman RJ, Meyer EM, Sabban EL. Involvement of alpha7 nicotinic acetylcholine receptors in activation of tyrosine hydroxylase and dopamine beta-hydroxylase gene expression in PC12 cells. J Neurochem 2000;75:1997-2005.

[227] Li Y, Papke RL, He Y-J, Millard B, Meyer EM. Characterization of the neuroprotective and toxic effects of $\alpha 7$ nicotinic receptor activation in PC12 cells. Brain Res 1999;81:218-25.

[228] Guan ZZ, Yu WF, Nordberg A. Dual effects of nicotine on oxidative stress and neuroprotection in PC12 cells. Neurochem Int 2003;43:243-9.

[229] Papke RL, Meyer E, Nutter T, Uteshev VV. Alpha7-selective agonists and modes of alpha7 receptor activation. Eur J Pharmacol 2000;393:179-95.

[230] Choi DW. Calcium and excitotoxic neuronal injury. Annals of the New York Academy of Sciences 1994;747:162-71.

[231] Deutsch JA. The cholinergic synapse and the site of memory. Science 1971;174:788-94.

[232] Drachman DA, Leavitt J. Human memory and the cholinergic system. A relationship to aging? Arch Neurol 1974;30:113-21.

[233] Bartus RT. On neurodegenerative diseases, models, and treatment strategies: lessons learned and lessons forgotten a generation following the cholinergic hypothesis. Exp Neurol 2000;163:495-529.

[234] Terry AV, Jr., Buccafusco JJ. The cholinergic hypothesis of age and Alzheimer's disease-related cognitive deficits: recent challenges and their implications for novel drug development. J Pharmacol Exp Ther 2003;306:821-7.

[235] Davis KL, Mohs RC, Marin D, Purohit DP, Perl DP, Lantz M, et al. Cholinergic markers in elderly patients with early signs of Alzheimer disease. JAMA 1999;281:1401-6.

[236] DeKosky ST, Ikonomovic MD, Styren SD, Beckett L, Wisniewski S, Bennett DA, et al. Upregulation of choline acetyltransferase activity in hippocampus and frontal cortex of elderly subjects with mild cognitive impairment. Ann Neurol 2002;51:145-55.

[237] Gilmor ML, Erickson JD, Varoqui H, Hersh LB, Bennett DA, Cochran EJ, et al. Preservation of nucleus basalis neurons containing choline acetyltransferase and the vesicular acetylcholine transporter in the elderly with mild cognitive impairment and early Alzheimer's disease. J Comp Neurol 1999;411:693-704.

[238] Morris JC. Challenging assumptions about Alzheimer's disease: mild cognitive impairment and the cholinergic hypothesis. Ann Neurol 2002;51:143-4.

[239] Decker MW, McGaugh JL. The role of interactions between the cholinergic system and other neuromodulatory systems in learning and memory. Synapse 1991;7:151-68.

[240] Gibson GE, Peterson C. Aging decreases oxidative metabolism and the release and synthesis of acetylcholine. J Neurochem 1981;37:978-84.

[241] Gibson GE, Peterson C, Sansone J. Neurotransmitter and carbohydrate metabolism during aging and mild hypoxia. Neurobiol Aging 1981;2:165-72.

[242] Wu CF, Bertorelli R, Sacconi M, Pepeu G, Consolo S. Decrease of brain acetylcholine release in aging freely-moving rats detected by microdialysis. Neurobiol Aging 1988;9:357-61.

[243] Burk JA, Herzog CD, Porter MC, Sarter M. Interactions between aging and cortical cholinergic deafferentation on attention. Neurobiol Aging 2002;23:467-77.

[244] Zemishlany Z, Thorne AE. Anticholinergic challenge and cognitive functions: a comparison between young and elderly normal subjects. Isr J Psychiatry Relat Sci 1991;28:32-41.

[245] Flicker C, Ferris SH, Serby M. Hypersensitivity to scopolamine in the elderly. Psychopharmacology (Berl) 1992;107:437-41.

[246] Sunderland T, Tariot PN, Cohen RM, Weingartner H, Mueller EA, 3rd, Murphy DL. Anticholinergic sensitivity in patients with dementia of the Alzheimer type and age-matched controls. A dose-response study. Arch Gen Psychiatry 1987;44:418-26.

[247] Kuhl DE, Koeppe RA, Minoshima S, Snyder SE, Ficaro EP, Foster NL, et al. In vivo mapping of cerebral acetylcholinesterase activity in aging and Alzheimer's disease. Neurology 1999;52:691-9.

[248] Nordberg A. Nicotinic receptor abnormalities of Alzheimer's disease: therapeutic implications. Biol Psychiatry 2001;49:200-10.

[249] Zubieta JK, Koeppe RA, Frey KA, Kilbourn MR, Mangner TJ, Foster NL, et al. Assessment of muscarinic receptor concentrations in aging and Alzheimer disease with [11C]NMPB and PET. Synapse 2001;39:275-87.

[250] Kuhl DE, Minoshima S, Fessler JA, Frey KA, Foster NL, Ficaro EP, et al. In vivo mapping of cholinergic terminals in normal aging, Alzheimer's disease, and Parkinson's disease. Ann Neurol 1996;40:399-410.

[251] Arciniegas DB. The cholinergic hypothesis of cognitive impairment caused by traumatic brain injury. Curr Psychiatry Rep 2003;5:391-9.

[252] Sponheim SR, Jung RE, Seidman LJ, Mesholam-Gately RI, Manoach DS, O'Leary DS, et al. Cognitive deficits in recent-onset and chronic schizophrenia. J Psychiatr Res 2009.

[253] Terry AV, Jr. Role of the central cholinergic system in the therapeutics of schizophrenia. Curr Neuropharmacol 2008;6:286-92.

[254] Francis PT, Perry EK. Cholinergic and other neurotransmitter mechanisms in Parkinson's disease, Parkinson's disease dementia, and dementia with Lewy bodies. Mov Disord 2007;22 Suppl 17:S351-7.

[255] Hauser TA, Kucinski A, Jordan KG, Gatto GJ, Wersinger SR, Hesse RA, et al. TC-5619: an alpha7 neuronal nicotinic receptor-selective agonist that demonstrates efficacy in animal models of the positive and negative symptoms and cognitive dysfunction of schizophrenia. Biochem Pharmacol 2009;78:803-12.

[256] Olincy A, Stevens KE. Treating schizophrenia symptoms with an alpha7 nicotinic agonist, from mice to men. Biochem Pharmacol 2007;74:1192-201.

[257] Leiser SC, Bowlby MR, Comery TA, Dunlop J. A cog in cognition: how the alpha7 nicotinic acetylcholine receptor is geared towards improving cognitive deficits. Pharmacol Ther 2009;122:302-11.

[258] Shimohama S. Nicotinic receptor-mediated neuroprotection in neurodegenerative disease models. Biol Pharm Bull 2009;32:332-6.

[259] Egea J, Rosa AO, Sobrado M, Gandia L, Lopez MG, Garcia AG. Neuroprotection afforded by nicotine against oxygen and glucose deprivation in hippocampal slices is lost in alpha7 nicotinic receptor knockout mice. Neuroscience 2007;145:866-72.

[260] Rosa AO, Egea J, Gandia L, Lopez MG, Garcia AG. Neuroprotection by nicotine in hippocampal slices subjected to oxygen-glucose deprivation: involvement of the alpha7 nAChR subtype. J Mol Neurosci 2006;30:61-2.

[261] Akaike A, Tamura, Y., Takeharu, Y., Shimohama, S., and Kimura, J. Nicotine-induced protection of cultured cortical neurons against N-methyl-D-aspartate receptor-mediated glutamate cytotoxicity. Brain Res 1994;644:181-7.

[262] Donnelly-Roberts DL, Xue IC, Arneric SP, Sullivan JP. In vitro neuroprotective properties of the novel cholinergic channel activator (ChCA), ABT-418. Brain Res 1996;719:36-44.

[263] Carlson NG, Bacchi A, Rogers SW, Gahring LC. Nicotine blocks TNF-alpha-mediated neuroprotection to NMDA by an alpha-bungarotoxin-sensitive pathway. J Neurobiol 1998;35:29-36.

[264] Kaneko S, Maeda T, Kume T, Kochiyama H, Akaike A, Shimohama S, et al. Nicotine protects cultured cortical neurons against glutamate-induced cytotoxicity via alpha7-neuronal receptors and neuronal CNS receptors. Brain Res 1997;765:135-40.

[265] Jonnala RR, Buccafusco JJ. Relationship between the increased cell surface alpha7 nicotinic receptor expression and neuroprotection induced by several nicotinic receptor agonists. J Neurosci Res 2001;66:565-72.

[266] Gahring LC, Meyer EL, Rogers SW. Nicotine-induced neuroprotection against N-methyl-D-aspartic acid or beta-amyloid peptide occur through independent mechanisms distinguished by pro-inflammatory cytokines. J Neurochem 2003;87:1125-36.

[267] Li XD, Buccafusco JJ. Effect of Beta-Amyloid Peptide 1-42 on the Cytoprotective Action Mediated by {alpha}7 Nicotinic Acetylcholine Receptors in Growth Factor-deprived Differentiated PC-12 Cells. J Pharmacol Exp Ther 2003;11:11.

[268] Meyer EM, Tay ET, Zoltewicz JA, Papke RL, Meyers C, King M, et al. Neuroprotective and memory-related actions of novel $\alpha 7$ nicotinic agents with different mixed agonist/antagonist properties. J Pharmacol Exp Ther 1998;284:1026-32.

[269] Li Y, King MA, Grimes J, Smith N, de Fiebre CM, Meyer EM. Alpha7 nicotinic receptor mediated protection against ethanol-induced cytotoxicity in PC12 cells. Brain research 1999;816:225-8.

[270] Li Y, King MA, Meyer EM. alpha7 nicotinic receptor-mediated protection against ethanol-induced oxidative stress and cytotoxicity in PC12 cells. Brain Res 2000;861:165-7.

[271] Sun X, Liu Y, Hu G, Wang H. Protective effects of nicotine against glutamate-induced neurotoxicity in PC12 cells. Cell Mol Biol Lett 2004;9:409-22.

[272] Shaw S, Bencherif M, Marrero MB. Janus kinase 2, an early target of alpha 7 nicotinic acetylcholine receptor-mediated neuroprotection against Abeta-(1-42) amyloid. J Biol Chem 2002;277:44920-4.

[273] Tohgi H, Utsugisawa K, Nagane Y. Protective effect of nicotine through nicotinic acetylcholine receptor alpha 7 on hypoxia-induced membrane disintegration and DNA fragmentation of cultured PC12 cells. Neurosci Lett 2000;285:91-4.

[274] Utsugisawa K, Nagane Y, Obara D, Tohgi H. Overexpression of alpha7 nicotinic acetylcholine receptor prevents G1-arrest and DNA fragmentation in PC12 cells after hypoxia. J Neurochem 2002;81:497-505.

[275] Martin EJ, Panikar KS, King MA, Deyrup M, Hunter B, Wang G, et al. Cytoprotective actions of 2,4-dimethoxybenzylidene anabaseine in differentiated PC12 cells and septal cholinergic cells. Drug Dev Res 1994;31:134-41.

[276] Shimohama S, Greenwald DL, Shafron DH, Akaike A, Maeda T, Kaneko S, et al. Nicotinic $\alpha 7$ receptors protect against glutamate neurotoxicity and neuronal ischemic damage. Brain Res 1998;779:359-63.

[277] Socci DJ, Arendash GW. Chronic nicotine treatment prevents neuronal loss in neocortex resulting from nucleus basalis lesions in young adult and aged rats. Mol Chem Neuropathol 1996;27:285-305.

[278] Nanri M, Miyake H, Murakami Y, Matsumoto K, Watanabe H. GTS-21, a nicotinic agonist, attenuates multiple infarctions and cognitive deficit caused by permanent occlusion of bilateral common carotid arteries in rats. Jpn J Pharmacol 1998;78:463-9.

[279] Pugh PC, Margiotta JF. Nicotinic acetylcholine receptor agonists promote survival and reduce apoptosis of chick ciliary ganglion neurons. Molecular and cellular neurosciences 2000;15:113-22.

[280] Picciotto MR, Zoli M. Neuroprotection via nAChRs: the role of nAChRs in neurodegenerative disorders such as Alzheimer's and Parkinson's disease. Front Biosci 2008;13:492-504.

[281] Dajas-Bailador FA, Lima PA, Wonnacott S. The alpha7 nicotinic acetylcholine receptor subtype mediates nicotine protection against NMDA excitotoxicity in primary hippocampal cultures through a Ca(2+) dependent mechanism. Neuropharmacology 2000;39:2799-807.

[282] Arendash GW, Sengstock GJ, Sanberg PR, Kem WR. Improved learning and memory in aged rats with chronic administration of the nicotinic receptor agonist GTS-21. Brain Res 1995;674:252-9.

[283] Briggs CA, Anderson DJ, Brioni JD, Buccafusco JJ, Buckley MJ, Campbell JE, et al. Functional characterization of the novel nicotinic receptor ligand GTS-21 in vitro and in vivo. Pharm Biochem and Behav 1997;57:231-41.

[284] Meyer EM, King MA, Meyers C. Neuroprotective effects of 2,4-dimethoxybenzylidene anabaseine (DMXB) and tetrahydroaminoacridine (THA) in neocortices of nucleus basalis lesioned rats. Brain Res 1998;786:252-4.

[285] Bjugstad KB, Mahnir VM, Kem WR, Socci DJ, Arendash GW. Long-term treatment with GTS-21 or nicotine enhances water maze performance in aged rats without affecting the density of nicotinic receptor subtypes in neocortex. Drug Dev Res 1996;39:19-28.

[286] Tatsumi R, Fujio M, Takanashi S, Numata A, Katayama J, Satoh H, et al. (R)-3'-(3-methylbenzo[b]thiophen-5-yl)spiro[1-azabicyclo[2,2,2]octane-3,5' -oxazolidin]-2'-one, a novel and potent alpha7 nicotinic acetylcholine receptor partial agonist displays cognitive enhancing properties. J Med Chem 2006;49:4374-83.

[287] Van Kampen M, Selbach K, Schneider R, Schiegel E, Boess F, Schreiber R. AR-R 17779 improves social recognition in rats by activation of nicotinic alpha7 receptors. Psychopharmacol (Berl) 2004;172:375-83.

[288] Wishka DG, Walker DP, Yates KM, Reitz SC, Jia S, Myers JK, et al. Discovery of N-[(3R)-1-azabicyclo[2.2.2]oct-3-yl]furo[2,3-c]pyridine-5-carboxamide, an agonist of the alpha7 nicotinic acetylcholine receptor, for the potential treatment of cognitive deficits in schizophrenia: synthesis and structure-activity relationship. J Med Chem 2006;49:4425-36.

[289] Woodruff-Pak DS, Li Y, Kem WR. A nicotinic agonist (GTS-21), eyeblink classical conditioning, and nicotinic receptor binding in rabbit brain. Brain Res 1994;645:309-17.

[290] Woodruff-Pak DS, Green JT, Coleman-Valencia C, Pak JT. A nicotinic cholinergic agonist (GTS-21) and eyeblink classical conditioning: acquisition, retention, and relearning in older rabbits. Exp Aging Res 2000;26:323-36.

[291] Briggs CA, Gronlien JH, Curzon P, Timmermann DB, Ween H, Thorin-Hagene K, et al. Role of channel activation in cognitive enhancement mediated by alpha7 nicotinic acetylcholine receptors. Br J Pharmacol 2009;158:1486-94.

[292] Roncarati R, Scali C, Comery TA, Grauer SM, Aschmi S, Bothmann H, et al. Procognitive and neuroprotective activity of a novel alpha7 nicotinic acetylcholine receptor agonist for treatment of neurodegenerative and cognitive disorders. J Pharmacol Exp Ther 2009;329:459-68.

[293] Marighetto A, Valerio S, Desmedt A, Philippin JN, Trocme-Thibierge C, Morain P. Comparative effects of the alpha7 nicotinic partial agonist, S 24795, and the cholinesterase inhibitor, donepezil, against aging-related deficits in declarative and working memory in mice. Psychopharmacology (Berl) 2008;197:499-508.

[294] Haydar SN, Dunlop J. Neuronal nicotinic acetylcholine receptors - targets for the development of drugs to treat cognitive impairment associated with schizophrenia and Alzheimer's disease. Curr Top Med Chem 2010;10:144-52.

[295] Thomsen MS, Hansen HH, Timmerman DB, Mikkelsen JD. Cognitive improvement by activation of alpha7 nicotinic acetylcholine receptors: from animal models to human pathophysiology. Curr Pharm Des 2010;16:323-43.

[296] Wallace TL, Porter RH. Targeting the nicotinic alpha7 acetylcholine receptor to enhance cognition in disease. Biochemical pharmacology 2011;82:891-903.

[297] van Haaren F, Anderson KG, Haworth SC, Kem WR. GTS-21, a mixed nicotinic receptor agonist/antagonist, does not affect the nicotine cue. Pharmacol Biochem Behav 1999;64:439-44.

[298] Grottick AJ, Trube G, Corrigall WA, Huwyler J, Malherbe P, Wyler R, et al. Evidence that nicotinic alpha(7) receptors are not involved in the hyperlocomotor and rewarding effects of nicotine. J Pharmacol Exp Ther 2000;294:1112-9.

[299] Adler LE, Olincy A, Waldo M, Harris JG, Griffith J, Stevens K, et al. Schizophrenia, sensory gating, and nicotinic receptors. Schizophr Bull 1998;24:189-202.

[300] Gopalaswamy AK, Morgan R. Smoking in chronic schizophrenia. The British journal of psychiatry : the journal of mental science 1986;149:523.

[301] Leonard S, Adams C, Breese CR, Adler LE, Bickford P, Byerley W, et al. Nicotinic receptor function in schizophrenia. Schizophr Bull 1996;22:431-45.

[302] Cullum CM, Harris JG, Waldo MC, Smernoff E, Madison A, Nagamoto HT, et al. Neurophysiological and neuropsychological evidence for attentional dysfunction in schizophrenia. Schizophr Res 1993;10:131-41.

[303] Olincy A, Harris JG, Johnson LL, Pender V, Kongs S, Allensworth D, et al. Proof-of-concept trial of an alpha7 nicotinic agonist in schizophrenia. Arch Gen Psychiatry 2006;63:630-8.

[304] Freedman R, Coon H, Myles-Worsley M, Orr-Urtreger A, Olincy A, Davis A, et al. Linkage of a neurophysiological deficit in schizophrenia to a chromosome 15 locus. Proceedings of the National Academy of Sciences USA 1997;94:587-92.

[305] Freedman R, Leonard S, Gault JM, Hopkins J, Cloninger CR, Kaufmann CA, et al. Linkage disequilibrium for schizophrenia at the chromosome 15q13-14 locus of the alpha7-nicotinic acetylcholine receptor subunit gene (CHRNA7). Am J Med Genet 2001;105:20-2.

[306] Hajos M, Rogers BN. Targeting alpha7 nicotinic acetylcholine receptors in the treatment of schizophrenia. Curr Pharm Des 2010;16:538-54.

[307] Leonard S, Gault J, Hopkins J, Logel J, Vianzon R, Short M, et al. Association of promoter variants in the alpha7 nicotinic acetylcholine receptor subunit gene with an inhibitory deficit found in schizophrenia. Arch Gen Psychiatry 2002;59:1085-96.

[308] Freedman R, Leonard S, Olincy A, Kaufmann CA, Malaspina D, Cloninger CR, et al. Evidence for the multigenic inheritance of schizophrenia. American journal of medical genetics 2001;105:794-800.

[309] Monod J, Jacob F. Teleonomic mechanisms in cellular metabolism, growth, and differentiation. Cold Spring Harb Symp Quant Biol 1961;26:389-401.

[310] Monod J, Changeux JP, Jacob F. Allosteric proteins and cellular control systems. J Mol Biol 1963;6:306-29.

[311] Monod J, Wyman J, Changeux JP. On the Nature of Allosteric Transitions: A Plausible Model. J Mol Biol 1965;12:88-118.

[312] Changeux JP, Edelstein SJ. Allosteric receptors after 30 years. Neuron 1998;21:959-80.

[313] Changeux JP, Edelstein SJ. Allosteric mechanisms of signal transduction. Science 2005;308:1424-8.

[314] Horenstein NA, Leonik FM, Papke RL. Multiple pharmacophores for the selective activation of nicotinic alpha7-type acetylcholine receptors. Mol Pharmacol 2008;74:1496-511.

[315] Ortells MO, Lunt GG. Evolutionary history of the ligand-gated ion-channel superfamily of receptors. Trends Neurosci 1995;18:121-7.

[316] Ng HJ, Whittemore ER, Tran MB, Hogenkamp DJ, Broide RS, Johnstone TB, et al. Nootropic alpha7 nicotinic receptor allosteric modulator derived from GABAA receptor modulators. Proc Natl Acad Sci U S A 2007;104:8059-64.

[317] Timmermann DB, Gronlien JH, Kohlhaas KL, Nielsen EO, Dam E, Dyhring T, et al. An allosteric modulator of the {alpha}7 nicotinic acetylcholine receptor possessing cognition enhancing properties in vivo. J Pharmacol Exp Ther 2007;323:294-307.

[318] Hurst RS, Hajos M, Raggenbass M, Wall TM, Higdon NR, Lawson JA, et al. A novel positive allosteric modulator of the alpha7 neuronal nicotinic acetylcholine receptor: in vitro and in vivo characterization. J Neurosci 2005;25:4396-405.

[319] Faghih R, Gopalakrishnan SM, Gronlien JH, Malysz J, Briggs CA, Wetterstrand C, et al. Discovery of 4-(5-(4-chlorophenyl)-2-methyl-3-propionyl-1H-pyrrol-1-yl)benzenesulfonami de (A-867744) as a novel positive allosteric modulator of the alpha7 nicotinic acetylcholine receptor. J Med Chem 2009;52:3377-84.

[320] Dunlop J, Lock T, Jow B, Sitzia F, Grauer S, Jow F, et al. Old and new pharmacology: positive allosteric modulation of the alpha7 nicotinic acetylcholine receptor by the 5-hydroxytryptamine(2B/C) receptor antagonist SB-206553 (3,5-dihydro-5-methyl-N-3-pyridinylbenzo[1,2-b:4,5-b']di pyrrole-1(2H)-carboxamide). J Pharmacol Exp Ther 2009;328:766-76.

[321] Dinklo T, Shaban H, Thuring JW, Lavreysen H, Stevens KE, Zheng L, et al. Characterization of 2-[[4-fluoro-3-(trifluoromethyl)phenyl]amino]-4-(4-pyridinyl)-5-thiazoleme thanol (JNJ-1930942), a novel positive allosteric modulator of the {alpha}7 nicotinic acetylcholine receptor. J Pharmacol Exp Ther 2011;336:560-74.

[322] Williams DK, Wang J, Papke RL. Positive allosteric modulators as an approach to nicotinic acetylcholine receptor-targeted therapeutics: advantages and limitations. Biochemical pharmacology 2011;82:915-30.

[323] Faghih R, Gopalakrishnan M, Briggs CA. Allosteric modulators of the alpha7 nicotinic acetylcholine receptor. J Med Chem 2008;51:701-12.

[324] Gill JK, Dhankher P, Sheppard TD, Sher E, Millar NS. A Series of alpha7 Nicotinic Acetylcholine Receptor Allosteric Modulators with Close Chemical Similarity but Diverse Pharmacological Properties. Molecular pharmacology 2012.

[325] Gronlien JH, Haakerud M, Ween H, Thorin-Hagene K, Briggs CA, Gopalakrishnan M, et al. Distinct profiles of {alpha}7 nAChR positive allosteric modulation revealed by structurally diverse chemotypes. Mol Pharmacol 2007;72:715-24.

[326] Malysz J, Gronlien JH, Anderson DJ, Hakerud M, Thorin-Hagene K, Ween H, et al. In vitro pharmacological characterization of a novel allosteric modulator of alpha 7 neuronal acetylcholine receptor, 4-(5-(4-chlorophenyl)-2-methyl-3-propionyl-1H-pyrrol-1-yl)benzenesulfonami de (A-867744), exhibiting unique pharmacological profile. J Pharmacol Exp Ther 2009;330:257-67.

[327] Papke RL, Kem WR, Soti F, López-Hernández GY, Horenstein NA. Activation and desensitization of nicotinic alpha7-type acetylcholine receptors by benzylidene anabaseines and nicotine. J Pharmacol Exp Ther 2009;329:791-807.

[328] Gill JK, Savolainen M, Young GT, Zwart R, Sher E, Millar NS. Agonist activation of {alpha}7 nicotinic acetylcholine receptors via an allosteric transmembrane site. Proc Natl Acad Sci U S A 2011;108:5867-72.

[329] Malysz J, Gronlien JH, Timmermann DB, Hakerud M, Thorin-Hagene K, Ween H, et al. Evaluation of alpha7 nicotinic acetylcholine receptor agonists and positive allosteric modulators using the parallel oocyte electrophysiology test station. Assay Drug Dev Technol 2009;7:374-90.

[330] Olsen RW, Chang CS, Li G, Hanchar HJ, Wallner M. Fishing for allosteric sites on GABA(A) receptors. Biochem Pharmacol 2004;68:1675-84.

[331] Chang Y, Huang Y, Whiteaker P. Mechanism of Allosteric Modulation of the Cys-loop Receptors. Pharmaceuticals 2010;3:2592-609.

[332] Forman SA, Miller KW. Anesthetic sites and allosteric mechanisms of action on Cys-loop ligand-gated ion channels. Can J Anaesth 2011;58:191-205.

[333] Baenziger JE, Corringer PJ. 3D structure and allosteric modulation of the transmembrane domain of pentameric ligand-gated ion channels. Neuropharmacology 2011;60:116-25.

[334] Nury H, Van Renterghem C, Weng Y, Tran A, Baaden M, Dufresne V, et al. X-ray structures of general anaesthetics bound to a pentameric ligand-gated ion channel. Nature 2011;469:428-31.

[335] Eisele JL, Bertrand S, Galzi JL, Devillers-Thiery A, Changeux JP, Bertrand D. Chimaeric nicotinic-serotonergic receptor combines distinct ligand binding and channel specificities. Nature 1993;366:479-83.

[336] Galzi JL, Bertrand S, Corringer PJ, Changeux JP, Bertrand D. Identification of calcium binding sites that regulate potentiation of a neuronal nicotinic acetylcholine receptor. EMBO J 1996;15:5824-32.

[337] Hansen SB, Taylor P. Galanthamine and non-competitive inhibitor binding to ACh-binding protein: evidence for a binding site on non-alpha-subunit interfaces of heteromeric neuronal nicotinic receptors. J Mol Biol 2007;369:895-901.

[338] Ludwig J, Hoffle-Maas A, Samochocki M, Luttmann E, Albuquerque EX, Fels G, et al. Localization by site-directed mutagenesis of a galantamine binding site on alpha7 nicotinic acetylcholine receptor extracellular domain. J Recept Signal Transduct Res 2010;30:469-83.

[339] Luttmann E, Ludwig J, Hoffle-Maas A, Samochocki M, Maelicke A, Fels G. Structural model for the binding sites of allosterically potentiating ligands on nicotinic acetylcholine receptors. ChemMedChem 2009;4:1874-82.

[340] Dey R, Chen L. In Search of Allosteric Modulators of a7-nAChR by Solvent Density Guided Virtual Screening. J Biomol Struct Dyn 2011;28:695-715.

[341] Ernst M, Brauchart D, Boresch S, Sieghart W. Comparative modeling of GABA(A) receptors: limits, insights, future developments. Neuroscience 2003;119:933-43.

[342] Bertrand D, Bertrand S, Cassar S, Gubbins E, Li J, Gopalakrishnan M. Positive allosteric modulation of the alpha7 nicotinic acetylcholine receptor: ligand interactions with distinct binding sites and evidence for a prominent role of the M2-M3 segment. Mol Pharmacol 2008;74:1407-16.

[343] Gronlien JH, Ween H, Thorin-Hagene K, Cassar S, Li J, Briggs CA, et al. Importance of M2-M3 loop in governing properties of genistein at the alpha7 nicotinic acetylcholine receptor inferred from alpha7/5-HT3A chimera. Eur J Pharmacol 2010;647:37-47.

[344] Young GT, Zwart R, Walker AS, Sher E, Millar NS. Potentiation of alpha7 nicotinic acetylcholine receptors via an allosteric transmembrane site. Proc Natl Acad Sci U S A 2008;105:14686-91.

[345] Collins T, Millar NS. Nicotinic acetylcholine receptor transmembrane mutations convert ivermectin from a positive to a negative allosteric modulator. Mol Pharmacol 2010;78:198-204.

[346] Mihic SJ, Ye Q, Wick MJ, Koltchine VV, Krasowski MD, Finn SE, et al. Sites of alcohol and volatile anaesthetic action on GABA(A) and glycine receptors. Nature 1997;389:385-9.

[347] Hosie AM, Wilkins ME, da Silva HM, Smart TG. Endogenous neurosteroids regulate GABAA receptors through two discrete transmembrane sites. Nature 2006;444:486-9.

[348] Ye Q, Koltchine VV, Mihic SJ, Mascia MP, Wick MJ, Finn SE, et al. Enhancement of glycine receptor function by ethanol is inversely correlated with molecular volume at position alpha267. J Biol Chem 1998;273:3314-9.

[349] Lobo IA, Trudell JR, Harris RA. Accessibility to residues in transmembrane segment four of the glycine receptor. Neuropharmacology 2006;50:174-81.

[350] Sattelle DB, Buckingham SD, Akamatsu M, Matsuda K, Pienaar IS, Jones AK, et al. Comparative pharmacology and computational modelling yield insights into allosteric modulation of human alpha7 nicotinic acetylcholine receptors. Biochem Pharmacol 2009;78:836-43.

[351] Malysz J, Anderson DJ, Gronlien JH, Ji J, Bunnelle WH, Hakerud M, et al. In vitro pharmacological characterization of a novel selective alpha7 neuronal nicotinic acetylcholine receptor agonist ABT-107. J Pharmacol Exp Ther 2010;334:863-74.

[352] Gubbins EJ, Gopalakrishnan M, Li J. Alpha7 nAChR-mediated activation of MAP kinase pathways in PC12 cells. Brain Res 2010;1328:1-11.

[353] El Kouhen R, Hu M, Anderson DJ, Li J, Gopalakrishnan M. Pharmacology of alpha7 nicotinic acetylcholine receptor mediated extracellular signal-regulated kinase signalling in PC12 cells. Br J Pharmacol 2009;156:638-48.

[354] Utsugisawa K, Nagane Y, Obara D, Tohgi H. Over-expression of alpha7 nicotinic acetylcholine receptor induces sustained ERK phosphorylation and N-cadherin expression in PC12 cells. Brain Res Mol Brain Res 2002;106:88-93.

[355] Bitner RS, Bunnelle WH, Anderson DJ, Briggs CA, Buccafusco J, Curzon P, et al. Broad-spectrum efficacy across cognitive domains by alpha7 nicotinic acetylcholine receptor agonism correlates with activation of ERK1/2 and CREB phosphorylation pathways. J Neurosci 2007;27:10578-87.

[356] Atkins CM, Selcher JC, Petraitis JJ, Trzaskos JM, Sweatt JD. The MAPK cascade is required for mammalian associative learning. Nat Neurosci 1998;1:602-9.

[357] Selcher JC, Atkins CM, Trzaskos JM, Paylor R, Sweatt JD. A necessity for MAP kinase activation in mammalian spatial learning. Learn Mem 1999;6:478-90.

[358] Sweatt JD. The neuronal MAP kinase cascade: a biochemical signal integration system subserving synaptic plasticity and memory. J Neurochem 2001;76:1-10.

[359] Adams JP, Sweatt JD. Molecular psychology: roles for the ERK MAP kinase cascade in memory. Annu Rev Pharmacol Toxicol 2002;42:135-63.

[360] Lopez-Hernandez G, Placzek AN, Thinschmidt JS, Lestage P, Trocme-Thibierge C, Morain P, et al. Partial agonist and neuromodulatory activity of S 24795 for alpha7 nAChR responses of hippocampal interneurons. Neuropharmacology 2007;53:134-44.

[361] López-Hernández GY, Thinschmidt JS, Morain P, Trocme-Thibierge C, Kem WR, Soti F, et al. Positive modulation of alpha7 nAChR responses in rat hippocampal interneurons to full agonists and the alpha7-selective partial agonists, 4OH-GTS-21 and S 24795. Neuropharm 2009;56:821-30.

[362] Velez-Fort M, Audinat E, Angulo MC. Functional alpha 7-containing nicotinic receptors of NG2-expressing cells in the hippocampus. Glia 2009;57:1104-14.

[363] Arnaiz-Cot JJ, Gonzalez JC, Sobrado M, Baldelli P, Carbone E, Gandia L, et al. Allosteric modulation of alpha 7 nicotinic receptors selectively depolarizes hippocampal interneurons, enhancing spontaneous GABAergic transmission. Eur J Neurosci 2008;27:1097-110.

[364] Mok MHS, Kew JN. Excitation of rat hippocampal interneurons via modulation of endogenous agonist activity at the alpha7 nicotinic ACh receptor. J Physiol 2006;574:699-710.

[365] de Filippi G, Mogg AJ, Phillips KG, Zwart R, Sher E, Chen Y. The subtype-selective nicotinic acetylcholine receptor positive allosteric potentiator 2087101 differentially facilitates neurotransmission in the brain. Eur J Pharmacol 2010;643:218-24.

[366] Zwart R, De Filippi G, Broad LM, McPhie GI, Pearson KH, Baldwinson T, et al. 5-Hydroxyindole potentiates human alpha 7 nicotinic receptor-mediated responses and enhances acetylcholine-induced glutamate release in cerebellar slices. Neuropharm 2002;43:374-84.

[367] Livingstone PD, Dickinson JA, Srinivasan J, Kew JN, Wonnacott S. Glutamate-dopamine crosstalk in the rat prefrontal cortex is modulated by Alpha7 nicotinic receptors and potentiated by PNU-120596. J Mol Neurosci 2010;40:172-6.

[368] Welsby PJ, Rowan MJ, Anwyl R. Intracellular mechanisms underlying the nicotinic enhancement of LTP in the rat dentate gyrus. Eur J Neurosci 2009;29:65-75.

[369] Gusev AG, Uteshev VV. Physiological concentrations of choline activate native alpha7-containing nicotinic acetylcholine receptors in the presence of PNU-120596 [1-(5-chloro-2,4-dimethoxyphenyl)-3-(5-methylisoxazol-3-yl)-urea]. J Pharmacol Exp Ther 2010;332:588-98.

[370] Johnstone TB, Gu Z, Yoshimura RF, Villegier AS, Hogenkamp DJ, Whittemore ER, et al. Allosteric modulation of related ligand-gated ion channels synergistically induces long-term potentiation in the hippocampus and enhances cognition. J Pharmacol Exp Ther 2011;336:908-15.

[371] Lukas RJ, Lucero L, Buisson B, Galzi JL, Puchacz E, Fryer JD, et al. Neurotoxicity of channel mutations in heterologously expressed alpha7-nicotinic acetylcholine receptors. Eur J Neurosci 2001;13:1849-60.

[372] Orrenius S, Zhivotovsky B, Nicotera P. Regulation of cell death: the calcium-apoptosis link. Nat Rev Mol Cell Biol 2003;4:552-65.

[373] Orr-Urtreger A, Broide RS, Kasten MR, Dang H, Dani JA, Beaudet AL, et al. Mice homozygous for the L250T mutation in the alpha7 nicotinic acetylcholine receptor show increased neuronal apoptosis and die within 1 day of birth. J Neurochem 2000;74:2154-66.

[374] Hu M, Gopalakrishnan M, Li J. Positive allosteric modulation of alpha7 neuronal nicotinic acetylcholine receptors: lack of cytotoxicity in PC12 cells and rat primary cortical neurons. Br J Pharmacol 2009;158:1857-64.

[375] Halevi S, McKay J, Palfreyman M, Yassin L, Eshel M, Jorgensen E, et al. The C. elegans ric-3 gene is required for maturation of nicotinic acetylcholine receptors. EMBO J 2002;21:1012-20.

[376] Williams DK, Wang J, Papke RL. Investigation of the molecular mechanism of the alpha7 nicotinic acetylcholine receptor positive allosteric modulator PNU-120596 provides evidence for two distinct desensitized states. Molecular pharmacology 2011;80:1013-32.

[377] Halevi S, Yassin L, Eshel M, Sala F, Sala S, Criado M, et al. Conservation within the RIC-3 gene family. Effectors of mammalian nicotinic acetylcholine receptor expression. J Biol Chem 2003;278:34411-7.

[378] Kuryatov A, Onksen J, Lindstrom J. Roles of accessory subunits in alpha4beta2(*) nicotinic receptors. Mol Pharmacol 2008;74:132-43.

[379] Papke RL, Stokes C. Working with OpusXpress: methods for high volume oocyte experiments. Methods 2010;51:121-33.

[380] Wang J, Horenstein NA, Stokes C, Papke RL. Tethered agonist analogs as site-specific probes for domains of the human alpha7 nicotinic acetylcholine receptor that differentially regulate activation and desensitization. Mol Pharmacol 2010;78:1012-25.

[381] Press WH. Numerical Recipies in C: The art of Scientific Computing. Cambridge, United Kingdom: Cambridge University Press, 1988.

[382] Franke C, Hatt H, Dudel J. Liquid filament switch for ultra-fast exchanges of solutions at excised patches of synaptic membrane of crayfish muscle. Neurosci Lett 1987;77:199-204.

[383] Jonas P. Fast application of agonists to isolated membrane patches. In: Sakmann B, Neher E, editors. Single-Channel Recording. New Yory, NY: Plenum Press, 1995. p. 231-43.

[384] Kabakov AY, Papke RL. Ultra fast solution applications for prolonged gap-free recordings: Controlling a Burleigh piezo-electric positioner with Clampex7. Axobits 1998;January:6-9.

[385] Mortensen M, Smart TG. Single-channel recording of ligand-gated ion channels. Nat Protoc 2007;2:2826-41.

[386] Jackson MB, Wong BS, Morris CE, Lecar H, Christian CN. Successive openings of the same acetylcholine receptor channel are correlated in open time. Biophys J 1983;42:109-14.

[387] Colquhoun D, Sakmann B. Fitting and statistical analysis of single-channel records. In: Sakmann B, Neher E, editors. Single-Channel Recording. New York, NY: Plenum Press, 1995. p. 483-585.

[388] Qin F. Restoration of single-channel currents using the segmental k-means method based on hidden Markov modeling. Biophys J 2004;86:1488-501.

[389] Tasneem A, Iyer LM, Jakobsson E, Aravind L. Identification of the prokaryotic ligand-gated ion channels and their implications for the mechanisms and origins of animal Cys-loop ion channels. Genome Biol 2005;6:R4.

[390] Chiara DC, Cohen JB. Identification of amino acids contributing to high and low affinity d-tubocurarine sites in the Torpedo nicotinic acetylcholine receptor. J Biol Chem 1997;272:32940-50.

[391] Chiara DC, Middleton RE, Cohen JB. Identification of tryptophan 55 as the primary site of [3H]nicotine photoincorporation in the gamma-subunit of the Torpedo nicotinic acetylcholine receptor. FEBS Lett 1998;423:223-6.

[392] Galzi JL, Changeux JP. Neuronal nicotinic receptors: molecular organization and regulations. Neuropharmacology 1995;34:563-82.

[393] Cohen JB, Sharp SD, Liu WS. Structure of the agonist-binding site of the nicotinic acetylcholine receptor. [3H]acetylcholine mustard identifies residues in the cation-binding subsite. J Biol Chem 1991;266:23354-64.

[394] Tomaselli GF, McLaughlin JT, Jurman ME, Hawrot E, Yellen G. Mutations affecting the agonist sensitivity of the nicotinic acetylcholine receptor. Biophys J 1991;60:721-7.

[395] Aylwin ML, White MM. Ligand-receptor interactions in the nicotinic acetylcholine receptor probed using multiple substitutions at conserved tyrosines on the alpha subunit. FEBS Lett 1994;349:99-103.

[396] Xiu X, Puskar NL, Shanata JA, Lester HA, Dougherty DA. Nicotine binding to brain receptors requires a strong cation-pi interaction. Nature 2009.

[397] Sine SM, Quiram P, Papanikolaou F, Kreienkamp HJ, Taylor P. Conserved tyrosines in the alpha subunit of the nicotinic acetylcholine receptor stabilize quaternary ammonium groups of agonists and curariform antagonists. J Biol Chem 1994;269:8808-16.

[398] O'Leary ME, White MM. Mutational analysis of ligand-induced activation of the Torpedo acetylcholine receptor. J Biol Chem 1992;267:8360-5.

[399] Galzi JL, Bertrand D, Devillers-Thiery A, Revah F, Bertrand S, Changeux JP. Functional significance of aromatic amino acids from three peptide loops of the alpha 7 neuronal nicotinic receptor site investigated by site-directed mutagenesis. FEBS Lett 1991;294:198-202.

[400] Xie Y, Cohen JB. Contributions of Torpedo nicotinic acetylcholine receptor gamma Trp-55 and delta Trp-57 to agonist and competitive antagonist function. J Biol Chem 2001;276:2417-26.

[401] Horenstein NA, McCormack TJ, Stokes C, Ren K, Papke RL. Reversal of agonist selectivity by mutations of conserved amino acids in the binding site of nicotinic acetylcholine receptors. The Journal of biological chemistry 2007;282:5899-909.

[402] Kalamida D, Poulas K, Avramopoulou V, Fostieri E, Lagoumintzis G, Lazaridis K, et al. Muscle and neuronal nicotinic acetylcholine receptors. Structure, function and pathogenicity. Febs J 2007;274:3799-845.

[403] Gay EA, Giniatullin R, Skorinkin A, Yakel JL. Aromatic residues at position 55 of rat alpha7 nicotinic acetylcholine receptors are critical for maintaining rapid desensitization. J Physiol 2008;586:1105-15.

[404] Papke RL. Estimation of both the potency and efficacy of alpha7 nAChR agonists from single-concentration responses. Life Sci 2006;78:2812-9.

[405] Papke RL. Tricks of Perspective: Insights and limitations to the study of macroscopic currents for the analysis of nAChR activation and desensitization. Journal of Molecular Neuroscience 2009;40:77-86.

[406] Mu TW, Lester HA, Dougherty DA. Different binding orientations for the same agonist at homologous receptors: a lock and key or a simple wedge? J Am Chem Soc 2003;125:6850-1.

[407] Pettersen EF, Goddard TD, Huang CC, Couch GS, Greenblatt DM, Meng EC, et al. UCSF Chimera--a visualization system for exploratory research and analysis. J Comput Chem 2004;25:1605-12.

[408] Higgins DG, Thompson JD, Gibson TJ. Using CLUSTAL for multiple sequence alignments. Methods Enzymol 1996;266:383-402.

[409] Jope RS, Gu X. Seizures increase acetylcholine and choline concentrations in rat brain regions. Neurochem Res 1991;16:1219-26.

[410] Takeda K, Trautmann A. A patch-clamp of the partial agonist actions of tubocurarine on rat myotubes. Journal of Physiology (London) 1984;349:353-74.

[411] Labarca P, Montal MS, Lindstrom JM, Montal M. The occurrence of long openings in the purified cholinergic receptor channel increases with acetylcholine concentration. J Neurosci 1985;5:3409-13.

[412] Colquhoun D, Sakmann B. Fast events in single-channel currents activated by acetylcholine and its analogues at the frog muscle end-plate. Journal of Physiology (London) 1985;369:501-57.

[413] Horenstein NA, McCormack TJ, Stokes C, Ren K, Papke RL. Reversal of agonist selectivity by mutations of conserved amino acids in the binding site of nicotinic acetylcholine receptors. J Biol Chem 2007;282:5899-909.

[414] Jackson MB. Spontaneous openings of the acetylcholine receptor channel. Proc Natl Acad Sci U S A 1984;81:3901-4.

[415] Jackson MB. Kinetics of unliganded acetylcholine receptor channel gating. Biophys J 1986;49:663-72.

[416] Jha A, Auerbach A. Acetylcholine receptor channels activated by a single agonist molecule. Biophys J 2010;98:1840-6.

[417] Amin J, Weiss DS. Insights into the activation mechanism of rho1 GABA receptors obtained by coexpression of wild type and activation-impaired subunits. Proc Biol Sci 1996;263:273-82.

[418] Mott DD, Erreger K, Banke TG, Traynelis SF. Open probability of homomeric murine 5-HT(3A) serotonin receptors depends on subunit occupancy. Journal of Physiology (London) 2001;535:427-43.

[419] Beato M, Groot-Kormelink PJ, Colquhoun D, Sivilotti LG. The activation mechanism of alpha1 homomeric glycine receptors. J Neurosci 2004;24:895-906.

[420] Rayes D, De Rosa MJ, Sine SM, Bouzat C. Number and locations of agonist binding sites required to activate homomeric Cys-loop receptors. J Neurosci 2009;29:6022-32.

[421] Barron SC, McLaughlin JT, See JA, Richards VL, Rosenberg RL. An allosteric modulator of alpha7 nicotinic receptors, N-(5-Chloro-2,4-dimethoxyphenyl)-N'-(5-methyl-3-isoxazolyl)-urea (PNU-120596), causes conformational changes in the extracellular ligand binding domain similar to those caused by acetylcholine. Mol Pharmacol 2009;76:253-63.

[422] Sine SM, Steinbach JH. Activation of a nicotinic acetylcholine receptor. Biophys J 1984;45:175-85.

[423] Sine SM, Steinbach JH. Activation of acetylcholine receptors on clonal mammalian BC3H-1 cells by high concentrations of agonist. J Physiol 1987;385:325-59.

[424] Papke RL, Millhauser G, Lieberman Z, Oswald RE. Relationships of agonist properties to the single channel kinetics of nicotinic acetylcholine receptors. Biophys J 1988;53:1-10.

[425] Papke RL, Oswald RE. Mechanisms of noncompetitive inhibition of acetylcholine-induced single channel currents. J Gen Physiol 1989;93:785-811.

[426] Sine SM, Steinbach JH. Agonists block currents through acetylcholine receptor channels. Biophys J 1984;46:277-84.

[427] Jaramillo F, Schuetze SM. Kinetic differences between embryonic- and adult-type acetylcholine receptor in rat myotubes. Journal of Physiology (London) 1988;396:267-96.

[428] Schuetze SM, Role LW. Developmental regulation of nicotinic acetylcholine receptors. Annu Rev Neurosci 1987;10:403-57.

[429] Groebe DR, Dumm JM, Levitan ES, Abramson SN. alpha-Conotoxins selectively inhibit one of the two acetylcholine binding sites of nicotinic receptors. Mol Pharmacol 1995;48:105-11.

[430] Sine SM. Identification of equivalent residues in the gamma, delta, and epsilon subunits of the nicotinic receptor that contribute to alpha-bungarotoxin binding. J Biol Chem 1997;272:23521-7.

[431] Sivilotti L, Colquhoun D. Acetylcholine receptors: too many channels, two few functions. Science 1995;269:1681-2.

[432] Uteshev VV, Meyer EM, Papke RL. Activation and inhibition of native neuronal alpha-bungarotoxin-sensitive nicotinic ACh receptors. Brain Res 2002;948:33-46.

[433] Guex N, Peitsch MC. SWISS-MODEL and the Swiss-PdbViewer: an environment for comparative protein modeling. Electrophoresis 1997;18:2714-23.

[434] Williams DK, Wang J, Papke RL. Positive allosteric modulators as an approach to nicotinic acetylcholine receptor-targeted therapeutics: Advantages and limitations. Biochem Pharmacol 2011;In press.

[435] del Barrio L, Egea J, Leon R, Romero A, Ruiz A, Montero M, et al. Calcium signalling mediated through alpha7 and non-alpha7 nAChR stimulation is differentially regulated in bovine chromaffin cells to induce catecholamine release. Br J Pharmacol 2011;162:94-110.

[436] Bouzat C, Bartos M, Corradi J, Sine SM. The interface between extracellular and transmembrane domains of homomeric Cys-loop receptors governs open-channel lifetime and rate of desensitization. The Journal of neuroscience : the official journal of the Society for Neuroscience 2008;28:7808-19.

[437] Gopalakrishnan SM, Philip BM, Gronlien JH, Malysz J, Anderson DJ, Gopalakrishnan M, et al. Functional Characterization and High-Throughput Screening of Positive Allosteric Modulators of alpha7 Nicotinic Acetylcholine Receptors in IMR-32 Neuroblastoma Cells. Assay Drug Dev Technol 2011.

[438] Skok MV. To channel or not to channel? Functioning of nicotinic acetylcholine receptors in leukocytes. J Leukoc Biol 2009;86:1-3.

[439] Sitzia F, Brown JT, Randall AD, Dunlop J. Voltage- and Temperature-Dependent Allosteric Modulation of alpha7 Nicotinic Receptors by PNU120596. Front Pharmacol 2011;2:81.

[440] Hone AJ, Whiteaker P, Mohn JL, Jacob MH, McIntosh JM. Alexa Fluor 546-ArIB[V11L;V16A] is a potent ligand for selectively labeling alpha 7 nicotinic acetylcholine receptors. Journal of neurochemistry 2010;114:994-1006.

[441] Valles AS, Roccamo AM, Barrantes FJ. Ric-3 chaperone-mediated stable cell-surface expression of the neuronal alpha7 nicotinic acetylcholine receptor in mammalian cells. Acta pharmacologica Sinica 2009;30:818-27.

[442] Alkondon M, Pereira EF, Wonnacott S, Albuquerque EX. Blockade of nicotinic currents in hippocampal neurons defines methyllycaconitine as a potent and specific receptor antagonist. Molecular pharmacology 1992;41:802-8.

[443] Lopez-Hernandez GY, Thinschmidt JS, Zheng G, Zhang Z, Crooks PA, Dwoskin LP, et al. Selective inhibition of acetylcholine-evoked responses of alpha7 neuronal nicotinic acetylcholine receptors by novel tris- and tetrakis-azaaromatic quaternary ammonium antagonists. Mol Pharmacol 2009;76:652-66.

[444] Papke RL, Bencherif M, Lippiello P. An evaluation of neuronal nicotinic acetylcholine receptor activation by quaternary nitrogen compounds indicates that choline is selective for the $\alpha 7$ subtype. Neurosci Lett 1996;213:201-4.

[445] Conroy WG, Liu QS, Nai Q, Margiotta JF, Berg DK. Potentiation of alpha7-containing nicotinic acetylcholine receptors by select albumins. Mol Pharmacol 2003;63:419-28.

[446] Giles S, Czuprynski C. Novel role for albumin in innate immunity: serum albumin inhibits the growth of Blastomyces dermatitidis yeast form in vitro. Infect Immun 2003;71:6648-52.

[447] Granato A, Gores G, Vilei MT, Tolando R, Ferraresso C, Muraca M. Bilirubin inhibits bile acid induced apoptosis in rat hepatocytes. Gut 2003;52:1774-8.

[448] Papke RL, Sanberg PR, Shytle RD. Analysis of mecamylamine stereoisomers on human nicotinic receptor subtypes. J Pharmacol Exp Ther 2001;297:646-56.

[449] McLean SL, Idris N, Grayson B, Gendle D, Mackie C, Lesage A, et al. PNU-120596, a positive allosteric modulator of alpha7 nicotinic acetylcholine receptors, reverses a sub-chronic phencyclidine-induced cognitive deficit in the attentional set-shifting task in female rats. J Psychopharmacol 2011.

[450] Barrantes FJ. Structural basis for lipid modulation of nicotinic acetylcholine receptor function. Brain Res Brain Res Rev 2004;47:71-95.

[451] Meyer EM, Tay ET, Papke RL, Meyers C, Huang G, de Fiebre CM. Effects of 3-[2,4-dimethoxybenzylidene]anabaseine (DMXB) on rat nicotinic receptors and memory-related behaviors. Brain Res 1997;768:49-56.

[452] Kihara T, Shimohama S, Sawada H, Honda K, Nakamizo T, Shibasaki H, et al. alpha 7 nicotinic receptor transduces signals to phosphatidylinositol 3-kinase to block A beta-amyloid-induced neurotoxicity. J Biol Chem 2001;276:13541-6.

[453] Kihara T, Shimohama S, Sawada H, Kimura J, Kume T, Kochiyama H, et al. Nicotinic receptor stimulation protects neurons against β-amyloid toxicity. Ann Neurol 1997;42:159-63.

[454] Thinschmidt JS, Frazier CJ, King MA, Meyer EM, Papke RL. Septal innervation regulates the function of alpha7 nicotinic receptors in CA1 hippocampal interneurons. Exp Neurol 2005;195:342-52.

[455] Kitagawa H, Takenouchi T, Azuma R, Wesnes KA, Kramer WG, Clody DE, et al. Safety, pharmacokinetics, and effects on cognitive function of multiple doses of GTS-21 in healthy, male volunteers. Neuropsychopharm 2003;28:542-51.

[456] Paulo J, Brucker W, Hawrot E. Proteomic Analysis of an 7 Nicotinic Acetylcholine Receptor Interactome. J Proteome Res 2009;8:1849-58.

[457] de Jonge WJ, Ulloa L. The alpha7 nicotinic acetylcholine receptor as a pharmacological target for inflammation. Br J Pharmacol 2007;151:915-29.

[458] Chernyavsky AI, Arredondo J, Qian J, Galitovskiy V, Grando SA. Coupling of ionic events to protein kinase signaling cascades upon activation of alpha7 nicotinic receptor: cooperative regulation of alpha2-integrin expression and Rho kinase activity. J Biol Chem 2009;284:22140-8.

BIOGRAPHICAL SKETCH

Dustin Kyle Williams was born November 12, 1982 in Logan, Utah to Kevin and Kathy Williams. Dustin grew up in Boise, Idaho and graduated from Centennial High School in 2001. After high school, Dustin completed a two-year mission for the Church of Jesus Christ of Latter-day Saints in Rio Grande do Sul, Brazil from January 2002 to December 2003. Upon returning from Brazil, Dustin completed one year of college at Boise State University before transferring to Brigham Young University-Hawaii where he completed an undergraduate degree in Biochemistry in June 2007. Dustin met his wife, Julie, while they were both students in Laie, Hawaii. Dustin started graduate school at the University of Florida in August 2007 with an elementary interest in understanding how neuronal activity produces behavior. He joined the laboratory of Dr. Roger Papke, where he learned electrophysiological methods to study nAChRs, an important family of ion channels expressed in the central and peripheral nervous systems.